

Lehrstuhl für Steuerungs- und Regelungstechnik  
Technische Universität München

Univ.-Prof. Dr.-Ing./Univ. Tokio Martin Buss

# **Simulation, Control, and Evaluation of Actuated Car Doors**

**Michael Strolz**

Vollständiger Abdruck der von der Fakultät für Elektrotechnik und Informationstechnik der Technischen Universität München zur Erlangung des akademischen Grades eines

**Doktor-Ingenieurs (Dr.-Ing.)**

genehmigten Dissertation.

Vorsitzender: Univ.-Prof. Dr.-Ing. Thomas Eibert

Prüfer der Dissertation:

1. Univ.-Prof. Dr.-Ing./Univ. Tokio Martin Buss
2. Univ.-Prof. Dr.-Ing. Michael Zäh

Die Dissertation wurde am 22.06.2010 bei der Technischen Universität München eingereicht und durch die Fakultät für Elektrotechnik und Informationstechnik am 07.12.2010 angenommen.



# Foreword

This thesis is a result of three-and-a-half years of work in the group of Prof. Martin Buss at the Institute of Automatic Control Engineering (LSR) at TU München.

First of all, I would like to thank my thesis advisor Prof. Martin Buss for providing me with an excellent and stimulating working environment. It was a great experience to get this generous freedom for research and at the same time advice and encouragement.

I was privileged to work together with a lot of talented and interested researchers who helped me to develop and realize my ideas and projects. Many thanks go to my colleagues, especially Dr.-Ing. Angelika Peer, Raphaela Groten, Dr.-Ing. Marc Ueberle, Matthias Althoff, and Klaas Klasing for their theoretical and to Dr.-Ing. Ulrich Unterhinninghofen, Jens Hölldampf, and Nikolay Stefanov for their practical support and discussions. I also would like to thank Christian Scharfenberger, Adel Olaf Sabbah, and all other PhD students involved in the research project MechaTUM for the great collaboration and the successful realization of our versatile actuated door-seat system.

Thanks go also to Florian Soldner at BMW AG and to Dr.-Ing. Patrick Kuhl and Michael Gräf at BMW Forschung und Technik GmbH for their support in the realization and evaluation of hardware and controllers. Furthermore, I would like to thank the non-scientific staff of the LSR, especially Mr. Gradl, Mr. Kubick, Mr. Stöber and Mr. Lowitz for the realization of hardware and Mr. Jaschik for the software support.

Most of the work described in this thesis is a result of my intense collaboration and discussion with the students I supervised. Specifically, I would like to thank the ones who significantly contributed to my research:

- Hamza Ben Rached (controllers [209], SSD evaluation [149], working student)
- Yuxiang Chen (multi-threaded path planning [45], working student)
- Andreas Dömel (path planning [66, 67], working student)
- Claudia Ehinger (development of the one-DOF door simulator [74])
- Yueming Fan (VRP of the TLD [85])
- Anh Cuong Hoang (collision detection [119], SSD evaluation [149], working student)
- Kong Huang (controller for the TLD prototype [123])
- Alexander Mörtl (controller for the door prototype with one DOF [178])
- Quirin Mühlbauer (VR simulation, intention recognition [182])
- Mingjing Ren (evaluation of the one-DOF door simulator [212])
- Amir Solhjoo (further improvement and evaluation of the TLD [230])
- Tobias Stadler (multi-threaded collision detection [235])

Finally, I thank my family and friends for their tolerance and unconditional support.

Munich, June 2010

Michael Strolz



# Contents

|          |   |           |
|----------|---|-----------|
| <b>1</b> | <b>Introduction</b>   | <b>1</b>  |
| 1.1      | Problem Definitions and Challenges . . . . .                                | 3         |
| 1.2      | Main Contributions and Outline of this Thesis . . . . .                     | 4         |
| <b>2</b> | <b>Virtual Reality Prototyping (VRP) by Active Admittance Control (AAC)</b> | <b>6</b>  |
| 2.1      | History and State of the Art of Virtual Reality Prototyping (VRP) . . . . . | 6         |
| 2.1.1    | History of Virtual Reality Research . . . . .                               | 6         |
| 2.1.2    | Definition and Issues of VRP . . . . .                                      | 7         |
| 2.1.3    | State of the Art of VRP without Haptic Interaction . . . . .                | 9         |
| 2.1.4    | State of the Art of VRP with Haptic Interaction . . . . .                   | 10        |
| 2.2      | Modeling of Mechatronic Systems as Active Admittance (AA) . . . . .         | 12        |
| 2.2.1    | Structure of an AA . . . . .  | 12        |
| 2.2.2    | Overview of Potentially Relevant Elements and Properties . . . . .          | 13        |
| 2.2.3    | Reduced AA for VRP in Early Development Stages . . . . .                    | 15        |
| 2.3      | Haptic Rendering by Active Admittance Control (AAC) . . . . .               | 16        |
| 2.3.1    | General Structure of AAC . . . . .  | 16        |
| 2.3.2    | Controller Design and Stability Issues . . . . .                            | 17        |
| 2.3.3    | Exemplary Application of AAC to a Pivotal Sliding Door . . . . .            | 20        |
| 2.4      | Summary . . . . .   | 21        |
| <b>3</b> | <b>Generic Methods for the Haptic Support of Human-System-Interaction</b>   | <b>22</b> |
| 3.1      | Intention Recognition: Determination and Support of the Intended Motion     | 23        |
| 3.1.1    | State of the Art . . . . .  | 23        |
| 3.1.2    | Design of a Combination of Static and Dynamic Virtual Fixtures . . . . .    | 24        |
| 3.2      | Path Planning: Determination and Support of Collision-Free Motion . . . . . | 27        |
| 3.2.1    | State of the Art . . . . .  | 28        |
| 3.2.2    | SamPP, a New Sampling-Based Path Planning Library . . . . .                 | 29        |
| 3.2.3    | Benchmark Results for SamPP . . . . .                                       | 33        |
| 3.2.4    | Generalized OR Paradigm . . . . .   | 41        |
| 3.2.5    | Conclusion . . . . .  | 46        |
| 3.3      | Collision Avoidance: Reducing the Risk of a Collision . . . . .             | 48        |
| 3.3.1    | Performance Benchmark of Collision Detection Libraries . . . . .            | 49        |
| 3.3.2    | Multi-Threaded Collision Detection . . . . .                                | 50        |
| 3.3.3    | Collision Avoidance . . . . .   | 53        |
| 3.4      | Summary . . . . .   | 56        |

|          |  |            |
|----------|--|------------|
| <b>4</b> | <b>VRP of Actuated Car Doors: Control, Simulation, and Evaluation</b>          | <b>57</b>  |
| 4.1      | VRP of Actuated Car Doors with Several DOF . . . . .                           | 57         |
| 4.1.1    | Generic VRP Test Bed . . . . .   | 57         |
| 4.1.2    | Comparison of Five Different Car Door Kinematics . . . . .                     | 62         |
| 4.1.3    | Free-Flying Door (FFD): Preferred Guidance Depends on Person . . . . .         | 63         |
| 4.1.4    | Pivotable-Sliding Door (PSD): Dynamics Should be Adaptable . . . . .           | 66         |
| 4.1.5    | Two-Link Door (TLD): Haptic User Support is Beneficial . . . . .               | 68         |
| 4.1.6    | Summary . . . . .  | 75         |
| 4.2      | VRP of Car Doors with One Rotational DOF . . . . .                             | 77         |
| 4.2.1    | Modeling and Specification Issues . . . . .                                    | 77         |
| 4.2.2    | Performance Specification of the Haptic Device . . . . .                       | 84         |
| 4.2.3    | Design of the Haptic Device . . . . .  | 86         |
| 4.2.4    | Evaluation of the Transparency of the Haptic Rendering . . . . .               | 88         |
| 4.2.5    | Additional Evaluations and Results . . . . .                                   | 92         |
| 4.2.6    | Simulation and Evaluation of a Semi-Actuated Car Door . . . . .                | 94         |
| 4.2.7    | Summary . . . . .  | 97         |
| <b>5</b> | <b>Control and Evaluation of Two Physical Prototypes of Actuated Car Doors</b> | <b>99</b>  |
| 5.1      | Two-Link Door Prototype with Two Actuated DOF . . . . .                        | 99         |
| 5.1.1    | System Description . . . . .   | 100        |
| 5.1.2    | Closed-Loop Position Control . . . . .   | 104        |
| 5.1.3    | Transfer and Modification of the Controller Developed by VRP . . . . .         | 104        |
| 5.1.4    | Experimental Evaluation . . . . .  | 109        |
| 5.1.5    | Summary . . . . .  | 113        |
| 5.2      | Close-to-Series Door Prototype with One Actuated DOF . . . . .                 | 115        |
| 5.2.1    | Measurement of the User Interaction Force . . . . .                            | 116        |
| 5.2.2    | System Description . . . . .   | 120        |
| 5.2.3    | Automatic Door Operation . . . . .   | 124        |
| 5.2.4    | Manual Door Operation: Prearrangements . . . . .                               | 127        |
| 5.2.5    | Manual Door Operation: Control Schemes . . . . .                               | 131        |
| 5.2.6    | Manual Door Operation: Evaluation . . . . .                                    | 135        |
| 5.2.7    | Summary . . . . .  | 137        |
| <b>6</b> | <b>Conclusion and Future Work</b>  | <b>139</b> |
| 6.1      | Concluding Remarks . . . . .   | 139        |
| 6.2      | Future Work . . . . .  | 142        |
| <b>A</b> | <b>State of the Art of Unactuated Car Doors</b>                                | <b>145</b> |
| <b>B</b> | <b>Technical Details Related to the AAC of Car Doors</b>                       | <b>146</b> |
| B.1      | EOM of Several Simulated Car Doors . . . . .                                   | 146        |
| B.1.1    | Car Door Body and Free-Flying Door (FFD) . . . . .                             | 146        |
| B.1.2    | Pivotable Sliding Door (PSD) . . . . .   | 148        |
| B.1.3    | Two-Link Door (TLD) . . . . .  | 148        |
| B.2      | Typical Opening Paths of Some Car Doors . . . . .                              | 149        |

---

|          |  |            |
|----------|--|------------|
| B.3      | Autolev Code . . . . .   | 150        |
| B.3.1    | Autolev Code of the TLD VRP Simulation . . . . .                             | 150        |
| B.3.2    | Autolev Code of the TLD Prototype . . . . .                                  | 152        |
| B.4      | System Analysis of the TLD Prototype . . . . .                               | 155        |
| <b>C</b> | <b>Feedback-Linearized Position Controller for VISHARD10</b>                 | <b>156</b> |
| C.1      | Computed Torque (CT) Control . . . . .                                       | 156        |
| C.2      | Feedforward+PD (FFPD) Control . . . . .                                      | 158        |
| <b>D</b> | <b>Technical Details Related to Collision Avoidance and Path Planning</b>    | <b>159</b> |
| D.1      | Obstacle Detection System provided by RCS (TU München) . . . . .             | 159        |
| D.2      | Benchmark Scenarios for Obstacle Detection and Collision Avoidance . . . . . | 160        |
| D.2.1    | Scenarios for the Camera Mounted on the Door Mirror . . . . .                | 160        |
| D.2.2    | Scenarios for the Camera Mounted on the Inner Edge of the Door . . . . .     | 161        |
| D.3      | VRML Models of the Exemplary Car Door Body . . . . .                         | 162        |
| D.4      | SamPP: Representation of Kinematics . . . . .                                | 163        |
| <b>E</b> | <b>Notes on the QoS of the Communication Infrastructure</b>                  | <b>164</b> |
| E.1      | Selection of Ethernet and the UDP Protocol . . . . .                         | 164        |
| E.2      | Heuristic Evaluation of the UDP-Based Communication . . . . .                | 164        |
| E.2.1    | Evaluation in the Absence of Disturbances . . . . .                          | 165        |
| E.2.2    | Evaluation in the Presence of Disturbances . . . . .                         | 165        |
| <b>F</b> | <b>Detailed Evaluation Results</b>   | <b>167</b> |
| F.1      | Evaluation of the VRP Simulation of the PSD . . . . .                        | 167        |
| F.2      | Evaluation of the VRP Simulation of the TLD . . . . .                        | 170        |
| F.3      | Evaluation of the TLD Prototype . . . . .                                    | 175        |
| <b>G</b> | <b>Technical Details Related to the TLD Prototype</b>                        | <b>181</b> |
|          | <b>Bibliography</b>  | <b>187</b> |

# Notations

## Abbreviations

|         |   |
|---------|---|
| 3DD     | 3D data provided by the obstacle detection system |
| AA      | active admittance                                 |
| AAC     | active admittance control                         |
| C-space | configuration space of a robot                    |
| CT      | computed torque                                   |
| CAD     | computer aided design                             |
| COG     | center of gravity                                 |
| COS     | coordinate system                                 |
| CDL     | collision detection library                       |
| DD      | direct drive                                      |
| DFLD    | double-four-link door                             |
| DH      | Denavit-Hartenberg notation                       |
| DMU     | digital mock-up                                   |
| DOF     | degrees of freedom                                |
| DVF     | dynamic virtual fixture                           |
| EE      | end-effector                                      |
| EOM     | equations of motion                               |
| FFPD    | feedforward+pd control                            |
| fps     | frames per second                                 |
| FTS     | force-torque-sensor                               |
| HMD     | head-mounted display                              |
| HIP     | haptic interaction point                          |
| HSI     | human-system interaction                          |
| JND     | just noticeable difference                        |
| LTI     | linear, time-invariant                            |
| PMU     | physical mock-up                                  |
| PRM     | probabilistic road map                            |
| PSD     | pivotable-sliding door                            |
| PWM     | pulse width modulation                            |
| QoS     | quality of service                                |
| RP      | rapid prototyping                                 |
| RRT     | rapidly-exploring random tree                     |
| SSD     | swing-sliding door                                |
| SVF     | static virtual fixture                            |
| TLD     | two-link door                                     |

|           |   |
|-----------|---|
| UDP       | user datagram protocol  |
| VE        | virtual environment (also known as “virtual world”)           |
| VF        | virtual fixture   |
| ViSHARD10 | Virtual Scenario Haptic Rendering Device with 10 actuated DOF |
| VMU       | virtual mock-up   |
| VR        | virtual reality   |
| VRP       | virtual reality prototyping                                   |
| VW        | virtual wall  |

## Conventions

### Scalars, Vectors, and Matrices

*Scalars* are denoted by upper and lower case letters in italic type.

*Vectors* are denoted by bold lower case letters, as the vector  $\mathbf{x}$  is composed of elements  $x_i$ .

*Matrices* are denoted by bold upper case letters, as the matrix  $\mathbf{M}$  is composed of elements  $M_{ij}$  ( $i^{\text{th}}$  row,  $j^{\text{th}}$  column).

|                                       |   |
|---------------------------------------|---|
| $x, X$                                | scalar  |
| $\mathbf{x}$                          | vector  |
| $\mathbf{X}$                          | matrix  |
| $f(\cdot)$                            | scalar function   |
| $\mathbf{f}(\cdot)$                   | vector function   |
| $\dot{\mathbf{x}}, \ddot{\mathbf{x}}$ | equivalent to $\frac{d}{dt}\mathbf{x}$ and $\frac{d^2}{dt^2}\mathbf{x}$ |
| $\mathbf{X}^T$                        | transposed of $\mathbf{X}$  |
| $\mathbf{X}^{-1}$                     | inverse of $\mathbf{X}$   |

### Subscripts and Superscripts

|  |  |
|--|--|
| $\mathbf{x}_{\max}$                        | maximum value of $\mathbf{x}$                          |
| $\mathbf{x}_{\min}$                        | minimum value of $\mathbf{x}$                          |
| $\mathbf{x}_r$                             | reference, commanded, or desired value of $\mathbf{x}$ |
| $\hat{\mathbf{x}}$                         | estimated or predicted value of $\mathbf{x}$           |
| $\mathbf{x}^*$                             | measurement value of $\mathbf{x}$                      |
| $\ \mathbf{x}\ $                           | Euclidean norm of $\mathbf{x}$                         |
| $\ \mathbf{x}\ _p$                         | p-norm of $\mathbf{x}$                                 |
| $\mathbf{x}_x, \mathbf{x}_y, \mathbf{x}_z$ | component of $\mathbf{x}$ in x-, y- and z-direction    |

## Symbols

|  |  |
|--|--|
| $\mathbf{A}$                               | system matrix                              |
| $\mathbf{B}$                               | input matrix                               |
| $\mathbf{C}$                               | output matrix                              |
| $\mathbf{C}(\mathbf{q}, \dot{\mathbf{q}})$ | joint space Coriolis and centrifugal terms |
| $c$  | stiffness                                  |

|  |   |
|--|---|
| <b>D</b>                                   | feedthrough matrix  |
| $d$  | damping coefficient   |
| $E$  | energy  |
| <b>E</b>                                   | unity matrix  |
| <b>e</b>                                   | error   |
| $f$  | frequency   |
| <b>f</b>                                   | force (generalized Cartesian space force, i.e.<br>$\mathbf{f} = [F_x, F_y, F_z, T_x, T_y, T_z]^T$ )         |
| $\mathbf{f}_G$                             | force resulting from gravity  |
| $\mathbf{f}_F$                             | force resulting from friction   |
| $\mathbf{f}_u$                             | force exerted by user   |
| $\mathbf{f}_{u,r}$                         | reference for $\mathbf{f}_u$  |
| $\mathbf{f}_{as}$                          | assistive force for the haptic support of HSI   |
| $F_x, F_y, F_z$                            | Cartesian space force components in x-, y- and z-direction<br>around x-, y- and z-axis                      |
| $G(s)$                                     | transfer function   |
| <b>H</b> ( <b>q</b> )                      | joint space inertia matrix  |
| $I_c$                                      | 95% confidence interval   |
| $I_{zz}$                                   | Inertia with respect to the z-axis  |
| <b>I</b>                                   | Inertia   |
| <b>J</b>                                   | Jacobian  |
| $\mathbf{K}_p, \mathbf{K}_i, \mathbf{K}_d$ | matrices of proportional, integral and derivative control coefficients                                      |
| $k$  | control coefficient   |
| $l$  | link length   |
| <b>M</b> ( <b>x</b> )                      | Cartesian space inertia matrix  |
| $m$  | link mass   |
| <b>N</b> ( <b>x</b> , $\dot{\mathbf{x}}$ ) | Cartesian space Coriolis and centrifugal terms  |
| $n$  | number of rotational DOF of a robot   |
| $o$  | number of translational DOF of a robot  |
| $P$  | probability   |
| <b>q</b>                                   | joint position (generalized joint space position, i.e.<br>$\mathbf{q} = [q_1 \dots q_{n+o}]^T$ )            |
| $\dot{\mathbf{q}}, \ddot{\mathbf{q}}$      | joint velocity and acceleration   |
| $\mathbf{q}_r$                             | reference joint position  |
| $\dot{\mathbf{q}}_r, \ddot{\mathbf{q}}_r$  | reference joint velocity and acceleration   |
| $T$  | time constant   |
| $T_x, T_y, T_z$                            | Cartesian space torque components   |
| $t$  | time  |
| <b>u</b>                                   | control input vector  |
| <b>w</b>                                   | weighting factor for the robot joints   |
| <b>x</b>                                   | state vector  |
| <b>x</b>                                   | position (generalized Cartesian space position, i.e.<br>$\mathbf{x} = [x, y, z, \alpha, \beta, \gamma]^T$ ) |
| $\dot{\mathbf{x}}, \ddot{\mathbf{x}}$      | velocity and acceleration   |

---

|   |  |
|---|--|
| $\mathbf{x}^*$                            | measurement of $\mathbf{x}$  |
| $\mathbf{x}_u$                            | position of HIP  |
| $\mathbf{x}_r$                            | reference position   |
| $\dot{\mathbf{x}}_r, \ddot{\mathbf{x}}_r$ | reference velocity and acceleration  |
| $\mathbf{y}$                              | control output vector  |
| $\mu$                                     | friction coefficient   |
| $\sigma_{E,i}$                            | signals from external devices  |
| $\sigma_{E,o}$                            | signals to external devices  |
| $\sigma_{in}$                             | arbitrary input signals for the AA   |
| $\sigma_S$                                | simulated sensor signals   |
| $\boldsymbol{\tau}$                       | torque (generalized joint space torque, i.e.<br>$\boldsymbol{\tau} = [\tau_1 \dots \tau_n, f_{n+1} \dots f_{n+o}]^T$ ) |
| $\boldsymbol{\tau}_{as,c}$                | assistive torque based on collision avoidance  |
| $\boldsymbol{\tau}_{as,i}$                | assistive torque based on intention recognition  |
| $\boldsymbol{\tau}_{as,p}$                | assistive torque based on path planning  |
| $\boldsymbol{\tau}_A$                     | torque resulting from actuation  |
| $\boldsymbol{\tau}_F$                     | torque resulting from friction   |
| $\boldsymbol{\tau}_G$                     | torque resulting from gravity  |
| $\boldsymbol{\tau}_r$                     | reference actuator torque computed by the controller   |
| $\boldsymbol{\tau}_u$                     | torque given by $\mathbf{J}^T \mathbf{f}_u$  |
| $\boldsymbol{\tau}_u^*$                   | torque given by $\mathbf{J}^T \mathbf{f}_u^*$  |

## **Abstract**

This thesis describes the simulation, control, and evaluation of actuated car doors with one or more degrees of freedom (DOF). Virtual Reality Prototyping (VRP) with haptic feedback is proposed for the efficient development and evaluation of such doors. As universal framework for the haptic simulation and the controller development of actuated mechanisms, Active Admittance Control (AAC) is introduced. AAC enables an efficient and safe development of system functionalities, for instance support methods for a comfortable haptic interaction between a human user and the system. Generic interaction support methods such as intention recognition, path planning, and collision avoidance are developed. On this foundation, for a variety of novel actuated car doors simulation models and controllers are developed. They are evaluated by user studies at VRP test beds. Important findings are that the simulated dynamics of the doors should be adapted to the individual user, and that the proposed support methods are indeed effective. In consequence, the simulated car doors are rated positively by the participants. The VRP results are transferred to physical prototypes with one and two actuated DOF. The ease of this transfer highlights the advantages of the VRP approach. Comprehensive user studies reveal both the effectiveness of the proposed support methods in practice and the predominant appreciation of the two actuated car door prototypes.

## **Zusammenfassung**

Die vorliegende Arbeit beschreibt die Simulation, Regelung und Evaluation aktuierter Fahrzeugtüren mit einem oder mehreren Freiheitsgraden (FHG). Für deren effiziente Entwicklung und Untersuchung wird Virtual Reality Prototyping (VRP) mit haptischem Feedback vorgeschlagen. Dazu wird die Aktive Admittanzregelung (AAC) eingeführt, die einen universellen Ansatz zur haptischen Simulation und zur Reglerentwicklung aktuierter Mechanismen darstellt. Die AAC ermöglicht eine effiziente und sichere Entwicklung der Systemfunktionalitäten, beispielsweise von Unterstützungsmethoden, die eine komfortable haptische Interaktion zwischen Bediener und System ermöglichen. Es werden generische Unterstützungsmethoden entwickelt, z.B. Intentionserkennung, Pfadplanung und Kollisionsvermeidung. Auf dieser Grundlage werden für eine Vielzahl neuartiger, aktuierter Fahrzeugtüren Simulationsmodelle und Regler entwickelt. Sie werden durch Probandenstudien an zwei VRP-Versuchsständen evaluiert. Wichtige Erkenntnisse sind, dass die simulierte Türdynamik an den jeweiligen Benutzer angepasst werden sollte und dass die Unterstützungsmethoden tatsächlich effektiv sind. Entsprechend werden die simulierten Türen von den Probanden positiv bewertet. Die VRP-Ergebnisse werden auf Prototypen mit einem bzw. zwei FHG übertragen. Die Einfachheit dieses Transfers unterstreicht die Vorteile des VRP-Ansatzes. Umfangreiche Benutzerstudien belegen nicht nur die Effektivität der Unterstützungsmethoden in der Praxis, sondern auch ein hohes Maß an Wertschätzung der beiden aktuierten Fahrzeugtüren durch die Probanden.

# 1 Introduction

More and more actuated systems nowadays come with advanced functionality provided by software. The conventional development process for such mechatronic products exhibits “Build–Test–Refine” loops, see for example the design guideline VDI 2206 [263] for mechatronic systems which introduces the concept of iterating “macro cycles”. Each macro cycle includes the construction of a “physical mock-up” (prototype). This intermediate result serves as a means for the evaluation of the current design. Based on the evaluation results, potential for the improvement of basic elements, subsystems, or the overall system can be recognized and then realized in the next iteration of the product design.

The construction of a physical prototype is usually very time consuming, expensive, and prone to errors. A means to increase the quality of physical prototypes and to speed up the overall process is Rapid Prototyping (RP), which has become very popular in industry in the last 15 years [26]. RP comprises different technologies for generating prototypes from 3D CAD data, most of which are printing or selective laser-sintering of a specific material [161, 281]. However, this comes with sub-optimal mechanical properties, e.g. a significantly reduced stiffness when compared to a conventionally crafted prototype [161]. Furthermore, RP only provides mechanical parts or rather chunky mechatronic elements (“Molded Interconnect Devices”) [88]. Thus, it does not solve the problem of achieving a realistic physical setup of a mechatronic system *per se*. This holds especially for complex mechatronic systems which feature a lot of interdependencies between their mechanical, electrical, and electronic components. Finally, a very important shortcoming of RP is that it does not enable an interactive design approach, which means that design modifications necessitate further builds [46].

According to [206], up to 70% of the total life cycle costs of a product are committed by decisions made in the early stages of design. Thus, for the validation of functionalities and properties of mechatronic systems the use of computer simulation rather than physical prototypes is about to become the preferred choice [20, 281]. Furthermore, a substantial increase in productivity can be achieved with Virtual Reality Prototyping (VRP) [21]. Zachmann noted that the key advantage is “intuitive, direct manipulation of the digital mock-up by the human” [278] and added:

The vision and the goal [is to] be able to do without any physical prototypes at all. [278]

This motivates the investigation and enhancement of the VRP of mechatronic systems. One example of such a system is an actuated car door with more than one DOF, which may improve the comfort during ingress and egress even in narrow parking situations. Such doors pose considerable design issues when compared to conventional ones, which depend on the shape of both door and vehicle, the kinematic and dynamic properties, and ultimately on their control and operation. Thus, the design, control, and evaluation of

actuated car doors with one or more DOF using VRP technology was investigated. The research was performed within the *MechaTUM* project established by TU München and the BMW Group. This project aimed at decreasing the level of discomfort during car ingress and egress, respectively.

At the beginning of our studies, we conducted some preliminary experiments on car doors with two unactuated DOF [244] on a Virtual Reality (VR) test bed with haptic feedback. They revealed that users did not find the operation of unactuated car doors with several DOF to be intuitive and convenient. For instance, the dynamics of the links of a pivotable sliding door (PSD) led to a behavior that users were unable to fully anticipate. This showed the need for improving the haptic interaction between mechanism and user. The most promising modality to achieve such an improvement is haptics, specifically kinesthetic feedback, which requires the use of actuators and a controller. For car doors with more than one DOF, this universal configuration has been filed as a patent by us [242]. The corresponding controller should provide an intuitive and comfortable handling of the car door, paving the way for using any number of actuated DOF, which could be desirable in the future.

If a door is equipped with actuators, it is straightforward to use them for additional purposes. For instance, the actuation can be used to adapt the car door to meet the users' demands. This is a key advantage of an actuated car door in comparison to a conventional one as it enables an individually optimized behavior of the door for each user. However, the most important additional task of an actuated door might be to prevent collisions. This is especially true for a door with several DOF, because many kinematic configurations bear the possibility of self-collision (between door and car body) in addition to a collision with other objects. Hence, we suggest the use of path planning to prevent collisions a-priori as well as the use of a generic reactive collision avoidance. Thus, the following coarse specification of the functionality of actuated car doors could be derived:

1. Manual and automatic operation
2. Reactive support methods (collision avoidance)
3. Proactive support methods (haptic motion guidance)
4. Customizable, intuitive, and high-quality haptic sensation to users

These goals and specifications require an equipment which comprises force and position sensing capabilities as well as an obstacle detection system. VRP with haptic feedback was deemed to be essential for the development, simulation, and evaluation of such car doors and of complex actuated mechanisms in general – especially since the methods and controllers should be applied to a variety of different door concepts.

Our concept of the generic VRP of actuated car doors is shown in Fig. 1.1. The desired physical target system (left hand side) includes a car door with actuation, various sensors, obstacle detection, supportive methods, and an interaction controller. The car door should be operated automatically by a controller as well as manually by a human user within various realistic environments. The VRP system (right hand side) has to provide a realistic simulation of these scenarios, especially with respect to the interaction between user and car door.

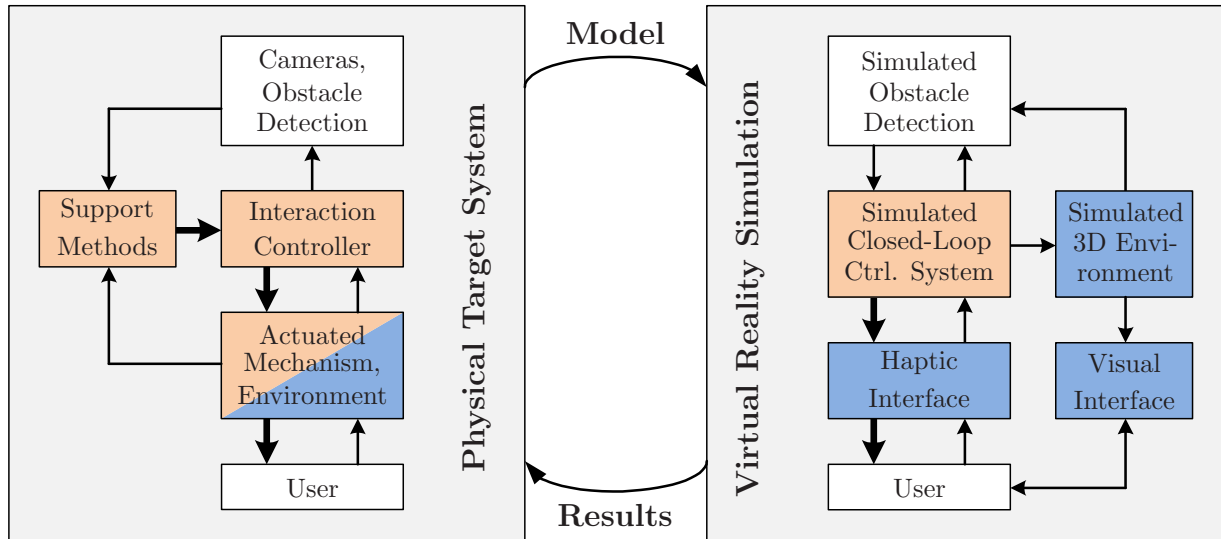


**Figure 1.1:** Virtual Reality Prototyping (VRP) of manually-operated actuated mechanisms: Based on a model of the physical target system, the actuated mechanism and its overall control are simulated in a virtual environment and iteratively improved. Finally, the results (methods, parameters, etc.) are transferred to the real system.

## 1.1 Problem Definitions and Challenges

**Actuated Car Doors:** The overwhelming majority of currently sold cars come with conventional car doors with one unactuated rotational or translational DOF (see Appendix A). Several actuated car doors with one (rotational or sliding) DOF have been filed as a patent and published. Most concepts focused on the automatic operation of such doors:

- Supervisory systems: Blocking of the movement of the car door in the event of an imminent collision [271, 87]
- Automatic systems: Automated procedure for unlocking the door [17] or for opening and closing the door [111, 143]

Only a few publications considered haptic interaction explicitly, e.g. [163, 234]. However, no comprehensive evaluation of these concepts was conducted. Thus, it is not known if they provide a handling of the car door which is significantly better for humans.

Lately, a two-DOF kinematic has been proposed to enable a sliding door movement without the necessity for exterior rails [19]. However, it also aimed at one-DOF movements, and it does not include interaction control. Actuated car doors with more than one DOF have initially been filed as patent [242] and introduced [244] by us. Beforehand, there were no kinematical concepts, no control schemes, and no evaluations for such car doors.

**Haptic Simulation of Actuated Mechanisms:** For developing and evaluating the support methods and the interaction controller for actuated mechanisms, the haptic and visual modalities are essential. A high-quality interactive visualization can be realized rather easily for example by using a commercially available head-mounted display with head tracking

as visual display. In contrast, a generic high-quality haptic simulation of the manual operation of a mechanism is more complicated, because many requirements have to be fulfilled:

1. Kinesthetic haptic device with a very large workspace ( $\geq 1 \text{ m}^2$  for the example of many car door kinematics)
2. End-effector that replicates the tactile properties expected by the user (e.g. the feel of a car door handle)
3. Closed-loop control bandwidth that is above the bandwidth of the typical user interaction with a car door
4. Force/torque and position sensors that acquire the HSI with a high resolution
5. Precise model of the car door, including its actuation

With respect to developing a framework for the VRP of actuated mechanisms, the most important issue was the generic modeling and representation of the desired physical target system. This is key for simulating and haptically rendering mechatronic systems.

Although several methods for the haptic rendering of large mechanisms have been proposed (compare [37, 49] for the simulation of conventional car doors), there were no haptic control schemes which explicitly take the actuation of a mechanism into account. However, a realistic haptic simulation must include the actuation effects. This would require the identification, modeling, and rendering of the elements that have a significant influence on the actuation.

**Haptic User Assistance:** A lot of publications in the vivid research area of haptic user assistance deal with providing haptic guidance by so-called Virtual Fixtures (VF). VF usually represent permitted motions in the workspace of a haptic device. Furthermore, methods have been introduced that estimate the intention of the user in a haptic interaction scenario. Finally, path planners have been utilized to enable the calculation of desired, collision-free motions. However, these methods have usually not been applied to actuated mechanisms in an interactive, real-time manner.

## 1.2 Main Contributions and Outline of this Thesis

The main goal of this thesis is to comprehensively investigate the simulation, control, and evaluation of actuated mechanisms with the example of car doors with one or more degrees of freedom (DOF). Following the concept of Virtual Reality Prototyping (VRP), concepts and functionalities are developed and evaluated based on simulations rather than on physical prototypes. Finally, the results are applied to real prototypes to validate the simulations in practice.

In Chap. 2, we describe our contribution of a generic, straightforward admittance control scheme for the haptic rendering of actuated mechanisms, introducing the concept of Active Admittance (AA). An AA extends the conventional admittance control by modeling the actuation and the movable parts of the mechanism separately. This allows for an efficient iterative design and evaluation of an actuated mechanism and its individual elements, specifically the controller and its functionalities/methods. The practicability of Active

Admittance Control (AAC) is demonstrated by haptically rendering a car door with two actuated DOF.

In Chap. 3, AAC is used as a framework for the integration of assistive functions into the simulation of actuated mechanisms. The development and implementation of intention recognition, path planning, and collision avoidance is described. They enable a haptic support of the user by force-feedback in real-time (response time  $< 30$  ms for typical scenarios), resulting in an intuitive and safe manual operation of actuated mechanisms. Furthermore, they can be utilized for their safe automatic operation as well.

The VRP of actuated car doors with more than one DOF is described in Chap. 4, including the development, simulation, control, and evaluation of such doors. The concept and corresponding technologies have been filed as a patent by us in [242]. We develop a generic VRP test bed for car doors with arbitrary kinematics as well as a specific high-fidelity door simulator with one rotational DOF. Using these tools, basic research is conducted for a variety of car doors to investigate which dynamics and controllers are preferred by human users.

To verify our results and to put them into practice, we developed the controller for the prototype of an actuated Two-Link Car Door (TLD) in the framework of MechaTUM. Its hardware setup, control of manual and automatic operation, and successful evaluation are described in Sec. 5.1. Furthermore, in Sec. 5.2 we developed and investigated force measurement concepts for car doors with one DOF, which also has been filed as patent by us [245]. Furthermore, we implemented a variety of controllers for the manual operation of a close-to-series actuated car door with one rotational DOF. The evaluation results show that a superior manual handling of the car door is achieved which is intuitive and convenient.

In Chap. 6, the main results of this thesis are summarized, and future directions of research are proposed.

## 2 Virtual Reality Prototyping (VRP) by Active Admittance Control (AAC)

Virtual Reality Prototyping (VRP) with haptic feedback offers great benefits in the development process of actuated systems. However, little research has yet been carried out in the field of haptic rendering of actuated mechanisms. Our contribution is a generic, straightforward admittance control scheme for the haptic rendering of actuated mechanisms, introducing the Active Admittance (AA). It extends the conventional admittance control by modeling the actuation and the movable parts of the mechanism separately. This allows for an efficient iterative design and evaluation of an actuated mechanism and its individual elements. The practicability of Active Admittance Control (AAC) is demonstrated by haptically rendering a car door with two actuated degrees of freedom (DOF).

### 2.1 History and State of the Art of Virtual Reality Prototyping (VRP)

#### 2.1.1 History of Virtual Reality Research

Two of the most important pioneers in the field of virtual reality (VR) are Douglas Engelbart and Ivan Sutherland. Engelbart became famous for inventing the computer mouse, which was a result of his visionary “bootstrapping” for innovation processes [76, 77] comprising a “strategic approach and set of organizing principles [...] designed to accelerate progress toward his goal” [68]. Sutherland published his idea of “The Ultimate Display” in 1965 [246, 248]. This advanced computer display interfaces human senses with a computer, enabling the experience of full immersion in a virtual (computer-generated) world – it even comprises a kinesthetic display with force-feedback capability [117]. His vision has been paraphrased by Brooks as follows:

Don’t think of that thing as a screen, think of it as a window, a window through which one looks into a virtual world. The challenge to computer graphics is to make that virtual world look real, sound real, move and respond to interaction in real time, and even feel real. [33]

However, it took more than 20 years to design the first hardware setups that enabled a reasonable degree of immersion, and an additional 10 years to establish industrial use of such tools. The rapid development of VR technology in the late 1990s is evident from the comparison of the states of the art in 1994 and 1999, given by Brooks [33]. Furthermore, it was supported by the huge variety of VR technology that already was available in the late 1990s [275]. The biggest driver of this process has been the computer and consumer

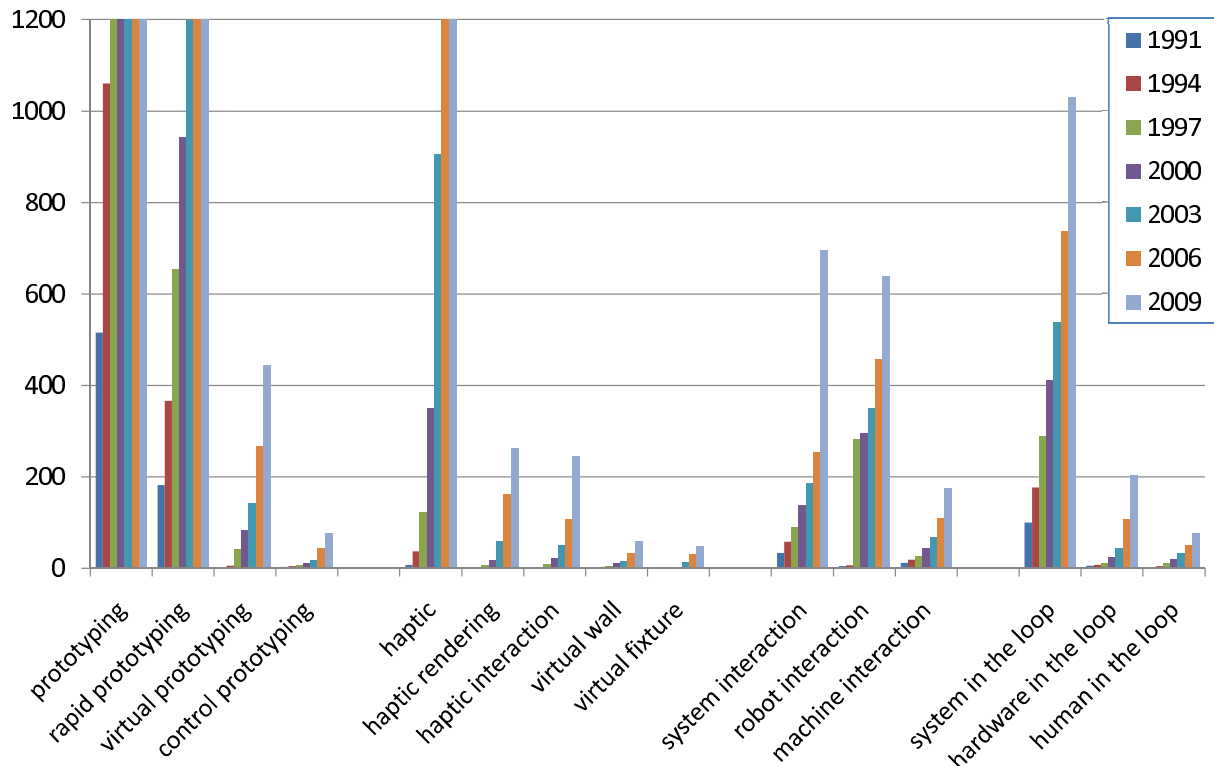


**Figure 2.1:** Number of results for various IEEEExplore [124] metadata search terms, where the number corresponds to a time range from 1950 until the respective year.

electronics market, which provided the technology for designing human-system interfaces that enable a highly realistic immersion into a VE. For instance, while the concept of Sutherland's original head-mounted display (HMD) [247] proposed in 1968 was very advanced already, it took almost 40 years until electronics hardware became fast enough to calculate photo-realistic images of complex VEs.

The tremendous increase of computing power and the advancement in computer science unlocked new fields and possibilities of VR research. The step, sometimes exponential increase of corresponding publications in recent years can clearly be seen in Fig. 2.1.

### 2.1.2 Definition and Issues of VRP

Nowadays, the field of virtual reality and virtual prototyping is broad, and a lot of different terms and definitions have been established. The most influential definitions of a virtual prototype and virtual prototyping were given in [61] and have been published by Garcia et al.:

**Virtual prototype:** A computer-based simulation of a system or subsystem with a degree of functional realism comparable to a physical prototype. [94]

**Virtual prototyping:** The process of using a virtual prototype, in lieu of a physical prototype, for index and evaluation of specific characteristics of a candidate design. [94]

Throughout this thesis, the more specific definition of Virtual Reality Prototyping by Kerttula et al. is used:

**Virtual Reality Prototyping (VRP):** A prototyping process in which a product or product concept, its behavior and usage situation is simulated as realistically as possible using computer models and virtual reality techniques. [135]

Ideally, VRP is so realistic that a human user gains a fully immersive experience and cannot discriminate it from reality (transparency that equals 1 [108]). Therefore, important aspects are the simulated features of the virtual prototype as well as the degree of realism of its rendering which depends on the quality of the employed interfaces [252].

### 2.1.2.1 Features of a Virtual Prototype

A physical prototype has a vast number of intrinsic and extrinsic features and properties which can be modeled and simulated by virtual prototyping techniques. Of special interest in VRP are features related to the interaction between the virtual prototype and its environment, which include one or more interacting humans. Thus, important features are [252]:

1. Functional behavior: The functional behavior of the virtual prototype can be modeled by implementing a functional description of the target product.
2. Mechanical properties: The virtual prototype will have a number of mechanical properties that can be modeled.
3. Haptic feedback: It is determined by object hardness, weight, surface, temperature, etc. and can be categorized as follows [35]:
  - a) force feedback
  - b) tactile feedback
  - c) proprioceptive feedback
4. Audio properties: A virtual prototype can have a number of audio properties (e.g. sound resulting from specific impact with another object).
5. Graphical qualities: The virtual prototype must resemble the appearance of the target product.
6. Virtual environment (VE): A virtual prototype can be simulated within a model of its (typical) environment, the VE.

### 2.1.2.2 Technological Issues

For general VR systems, four technologies have been identified as crucial [33, 72, 36]:

1. Interfaces (visual, aural, haptic) that immerse the user in the virtual world and that block out contradictory sensory impressions from the real world
2. Graphics rendering system for generating the visual feedback at  $f \geq 20$  fps
3. Tracking system for measuring the position and orientation of the head and limbs of the user

4. Database system for building and maintaining models of the virtual world

Furthermore, four auxiliary technologies are thought to be important [33]:

5. Synthesized sound, including directional sound and simulated sound fields
6. Display of synthesized forces and other haptic sensations to the kinesthetic senses
7. Devices by which the user specifies interactions with virtual objects
8. Interaction techniques that substitute for the real interactions possible with the physical world

In 1999, Brooks [33] pointed out a number of challenges that remain both in the enabling technologies and in the systems engineering and human factors disciplines. Four important ones are:

1. Getting latency down to acceptable levels
2. Producing satisfactory haptic augmentation for VR illusions
3. Interacting most effectively with virtual worlds (e.g. manipulation and wayfinding)
4. Measuring the illusion of presence and its operational effectiveness

This leads to the conclusion that current VR technology needs significant further improvement. Additionally, as noted by Zachmann,

it is understood that there is no single combination of devices which is best for all applications. Certain characteristics are inherent to the devices, at least they will prevail for a long time. These imply several different types of VR, distinguished mainly by the (characteristics of the) output device [...]. [278]

### 2.1.3 State of the Art of VRP without Haptic Interaction

A good overview of the state of the art of the non-haptic simulation of mechatronic systems is given in [75]. Initially, the simulation models were purely graphical representations. Later on, these “Digital Mock-Ups” (DMU) were enriched by additional product and engineering information, boosting Product Lifecycle Management [236]. Powerful Computer-Aided Design (CAD) tools such as CATIA V5 and COMSOL enabled the calculation and graphical rendering of many physical effects [280]. Furthermore, a variety of engineering software for the simulation of mechatronic systems (or parts of them) has been released, such as MATLAB/Simulink/Stateflow, SIMPACK, Dymola, etc. Multi Domain Simulation is a recent trend in VRP [86, 56, 90, 136, 153, 266], and therefore tools focused on only one engineering area are combined with others to enable the control and simulation of mechatronic systems, e.g. LabView (control, electronics) and SolidWorks (mechanics) [187]. However, often these tools and combinations are not used in an interactive fashion, but rather for the unidirectional simulation of certain predefined scenarios or functionalities (compare e.g. [277]). Examples of the application of VRP without haptic feedback include such diverse areas as electronics design [135, 136], active suspension in vehicles [175], the simulation of exoskeleton control [225], digital actors [130], robot motion control simulation [165, 151], and mechanism design [274]. For the latter, a generic methodology has been developed in [171].

There have been some attempts at and progress in creating interactive DMUs; see Sec. 2.1. This is generally known as Virtual (Reality) Prototyping (VRP) [94, 58], and accordingly the term “Virtual Mock-Up” (VMU) is used to distinguish its interactive simulation model from the conventional DMU approach.

In VRP, the user interface may feature a combination of different modalities. A straightforward approach for the interactive simulation of mechanisms is the use of haptic interaction. The haptic feedback enables the designers and engineers to explore the kinematic and the dynamic properties of the system, without requiring a physical prototype. This way, the effects of changing the system parameters can be perceived instantaneously.

As noted in [37], one major advantage of haptically-enhanced VRP is that already in the early stages of design comparable and repeatable user tests can be performed. In the following, we focus on haptic interaction and specifically on the kinesthetic haptic rendering of mechatronic systems.

### 2.1.4 State of the Art of VRP with Haptic Interaction

In Chap. 1 and Sec. 2.1, a short overview of the development of VR and VRP has been given. In the following, the history and state of the art of haptic rendering and of haptically-enhanced VRP is described.

The most important foundation of haptic interaction was laid by Hogan: In 1985, he introduced the impedance control paradigm [120], which he subsequently utilized for controlling the haptic interaction between a human and a robot [184, 121]. Since then, the haptic rendering of unactuated mechanisms has been investigated in detail. Besides impedance control, admittance control has become very popular. As it masks the natural dynamics of haptic devices to the user, it is often the preferred choice, especially when large haptic devices are needed to display a broad workspace [257]. Thereby, even industrial manipulators exhibiting high inertia can be used for haptic rendering [101, 37].

A generic framework for interactive simulation of physical systems was introduced in [270]. The key contribution was a modularized description of the constrained dynamics of a system. This enables an efficient combination and simulation of objects, constraints, and forces. Even its potential application to mechanism construction has been discussed.

In [100], a combined simulation and experimental apparatus for the haptic rendering and investigation of dynamical models has been proposed. Specifically, the consideration of changing kinematic constraints with numerical integration methods for mechanical system simulation has been advanced. Thereby, high-bandwidth haptic feedback for interaction with a keyboard was achieved.

In [185], the rendering problem is divided into two separate tasks: One is to prevent the violation of kinematic constraints, and the other is to display the dynamics only in the directions where motion is allowed. In order to satisfy these requirements, first (penalty) torques are calculated based on each requirement. These torques are summed up and applied to the haptic interface. To calculate the dynamic component of the overall torque, the use of the pseudo-inverse is proposed, which allows for a very elegant formulation for the case of an open kinematic chain [185]:

$$\boldsymbol{\tau} = \mathbf{J}(\mathbf{J}^T \mathbf{J})^{-1} [\mathbf{H}(\mathbf{q})\ddot{\mathbf{q}} + \mathbf{C}(\mathbf{q}, \dot{\mathbf{q}}) + \boldsymbol{\tau}_G] \quad (2.1)$$

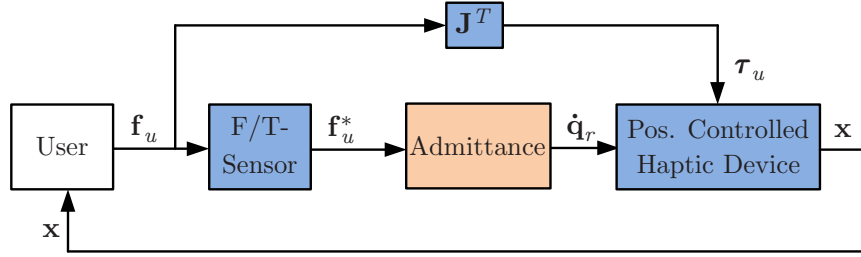


**Figure 2.2:** Conventional admittance control scheme where the measured user interaction force  $\mathbf{f}_u^*$  is input to the admittance (i.e. the simulated dynamics).

where  $\mathbf{J}$  and  $\mathbf{H}(\mathbf{q})$  are the Jacobian and the joint space inertial matrices of the open chain, and  $\mathbf{C}(\mathbf{q}, \dot{\mathbf{q}})$  and  $\boldsymbol{\tau}_G$  are vectors representing the joint space Coriolis, centrifugal, and gravity components.

A similar approach of task separation was used in [37] by distinguishing “Constrained Space” and “Mechanism Space”. The rendering of stiff virtual walls is improved with respect to [185] by switching from an admittance to an impedance control scheme when constraint violation in specified directions of the Mechanism Space occurs. Similarly, in [25] a virtual proxy is used to haptically display the kinematical constraint.

One of the first implementations of a system for accurately simulating the kinematic and dynamic properties of a large mechanism is known from Clover et al. [49]. The method they propose consists of mapping the measured user interaction  $\mathbf{f}_u^*$  from local sensor-based coordinates to generalized coordinates and applying them to the equations of motion of the mechanism. The desired motion is then mapped to the joint space of the haptic interfaces, and an independent joint controller finally provides an accurate position and velocity adjustment. This admittance control scheme is considered to be the most intuitive way of simulating the dynamics of a mechanism, because the user interaction  $\mathbf{f}_u$  results in a motion  $\mathbf{x}$  of the robot that is equivalent to the motion a physical instance of this mechanism would exhibit. The principal structure of the control scheme is given in Fig. 2.2.

Thus, haptic rendering of mechanisms has a long tradition and has been investigated in detail; compare also [11, 14, 100, 221, 69]. Even some applications to automotive mechanisms have been reported [37, 48, 16]. Besides the consideration of kinematic constraints, the identification of physical properties such as kinematics, inertia, and friction has been a central issue for deriving an accurate virtual model.

There have been some extensions to the haptic rendering of actuated mechanisms, especially in the area of steer-by-wire systems. However, they are mainly focused on considerations related to tele-operation [27, 193] and on HIL simulations, i.e. the hardware is included physically rather than model-based into the haptic rendering [28, 215, 24].

Summarizing, to the best of our knowledge there were no general applicable haptic control schemes which explicitly take into account the actuation of a simulated mechanism. By presenting the method of *Active Admittance Control* (AAC) [244], we bridge this gap.

## 2.2 Modeling of Mechatronic Systems as Active Admittance (AA)

Typically, mechatronic systems include actuated mechanisms. Thus, they can be characterized by their actuation on the one hand and all other properties on the other hand. We define “actuation” as follows:

Actuation: The entirety of all elements and properties of a system that are involved in the calculation and creation of forces and torques by actuators,  $\tau_A$ .

### 2.2.1 Structure of an AA

According to our definition of actuation, the actuator properties have to be separated carefully into two fields: Every property that only affects the creation of a  $\tau_A$  is part of the actuation, while all others are not. One example is the winding of an electrical drive: Its material, geometric layout, etc. define its inductivity, but only the latter is considered to be part of the actuation. Without limitation of generality, we term these actuation properties of a drive “electrical properties” in the following, while “mechanical properties” includes all other properties that might be of relevance for its modeling.

Thus, the main components of the actuation of a mechatronic system are

- Sensors
- Controller, including
  - I/O interfaces
  - Communication from and to external devices
  - Control algorithms
  - Computing platform and operating system
- Power electronics and power supply
- Actuators: “electrical properties” (force generation)

while other important components of the system include, but are not limited to

- Actuator: “mechanical properties”
- Transmissions
- Other mechanical parts of the mechanism

According to our definition, the physical properties of the movable parts of the mechatronic system are not part of the actuation. They are usually modeled in the form of equations of motion (EOM). The motion of the movable parts of the system is calculated by considering  $\tau_A$  and all other internal and external forces and torques as input to its EOM. Based on this, the overall model of the haptic properties of a mechatronic system can be built. This is called Active Admittance (AA), and its structure is displayed in Fig. 2.3.

Analogous to a conventional admittance (compare Fig. 2.2), the measurement of the user interaction  $\mathbf{f}_u^*$  is used as an input for the calculation of the motion of the simulated system,  $\dot{\mathbf{q}}_r$ . Another input is the actuation effect  $\tau_A$ , which may depend on a variety

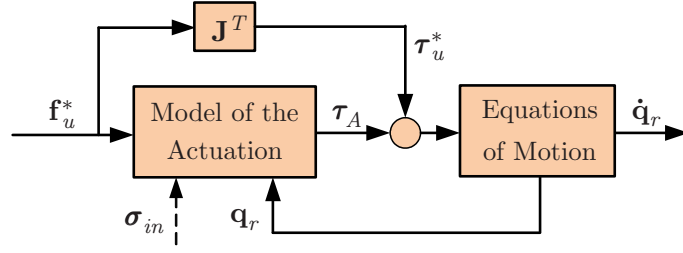


**Figure 2.3:** Active Admittance (AA): A generic model of the haptically relevant properties of a non-infinite-dimensional mechatronic system for use in a haptic simulation.

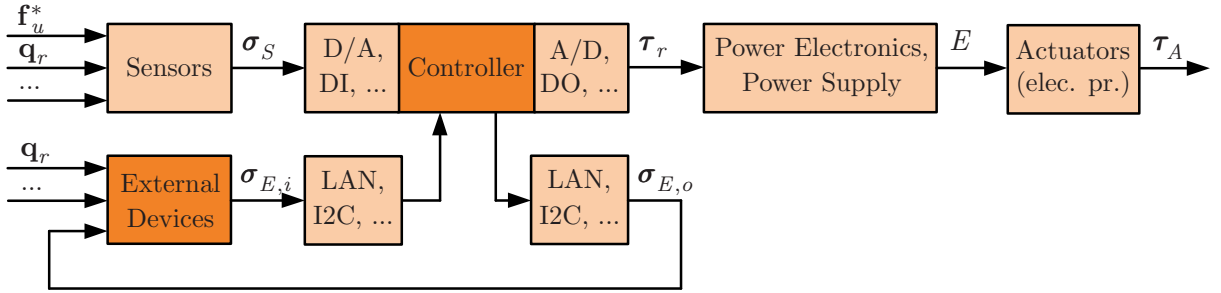


**Figure 2.4:** Model of the actuation of a mechatronic system: The actuation effect  $\tau_A$  is a result of a variety of properties of the interconnected system elements.

of sensor signals as well as on communication data exchanged with external devices. In Fig. 2.4, a comprehensive model of the actuation of a mechatronic system is given, which is generic with respect to its haptic properties. Main properties of its components are discussed in the following.

For a realistic simulation and haptic rendering of a mechatronic system it is vital to identify and model its actuation and EOM with sufficient accuracy. This necessitates the identification of the elements and properties that have a *significant* influence on the (haptic) behavior of the actuated mechanism. This knowledge about the “haptic contribution” of the individual elements enables the specification of a proper level of detail of the AA.

## 2.2.2 Overview of Potentially Relevant Elements and Properties

An ideal AA would contain all properties of the mechatronic system which affect its haptic simulation. Obviously, every property that affects the stability of the haptic interaction between a human user and the mechatronic system has influence on the haptic behavior. And this necessitates a comprehensive model of the human-system-interaction (HSI), because the user can vary for example a manual haptic interaction from moving the device with a very firm grip to unhanding it. Furthermore, all factors that potentially affect the closed-loop control bandwidth of the mechatronic device would have to be considered.

Some general rules for this assessment can be derived from the research in haptic rendering, especially from stability-related issues. An abundance of research in haptics has dealt with stability issues, and numerous sources of instability have been identified. For instance, it is well known that the stability of a haptic simulation depends on the sampling rate and

the sensor resolution [50]. Besides basically all factors that affect the closed-loop control bandwidth of a mechatronic device, they contain properties of the virtual environment (VE) as well as the interaction with the human user, which can vary greatly.

Based on [258] we try to give a comprehensive overview of the elements affecting the haptic rendering of a typical mechatronic system to a human user by a haptic device. The typically most important elements are marked in *italic bold font*.

1. Sensors:
  - ***Discretization/Quantization*** [50, 4, 65]
  - Accuracy
  - Noise
  - Bandwidth [105]
2. Process Interfaces:
  - ***A/D and D/A***: Conversion rate, noise, saturation [50, 102]
  - DIO and PWM: Timing
3. External devices: See “Process Interfaces”, “Communication”, and “Controller”
4. Communication via bus systems: Speed, buffering, packet loss [118]
5. Controller [172, 7, 65, 105]
  - Operating platform:
    - ***Sampling rate*** [4, 103]
    - Quality of “real-time” processing
  - Implementation of the control algorithm:
    - ***Filtering of input signals***:
      - \* Low-pass filtering [50]
      - \* Calculation of derivative
    - ***Dynamics defined by the controller***:
      - \* Simulated mass, damping, stiffness [207]
      - \* Simulated wrench [244]
    - Control signal saturation [102]
6. Power electronics: Bandwidth, saturation
7. Power supply: Voltage drop, ripple
8. Actuators (“electrical properties”) [80]:
  - ***Bandwidth*** (given by inductivity, resistance, and back-EMF)
  - Saturation
  - Output capability: Nominal, maximum
9. Mechanical properties:
  - Structural stiffness of joints and links, especially:
    - Stiffness between EE and force/torque sensor [200]
    - Stiffness between sensors and actuators [79]
  - Friction:

- *Coulomb friction* [207]
- Stiction [207, 254, 158]

10. **Haptic user interaction** as seen from device [39, 173, 121, 108]

- Mass, damping, stiffness
- Grasp force [205]

### 2.2.3 Reduced AA for VRP in Early Development Stages

Especially in an early stage of product development, there is no detailed model of the desired system – in fact, it is yet to be developed. Thus, only a part of the potentially haptically relevant properties listed in subsection 2.2.2 are given.

Based on the desired evidence of the haptic modality of the VRP, the individual properties that are thought to have the biggest impact on the haptic interaction have to be iteratively derived and added to the simulation model. In many cases the rather slow dynamics of the actuators dominate the overall dynamics of the system, while the time consumption of the data acquisition, signal processing, power electronics, and power supply may be negligible. For an early stage of product development, these considerations lead to a simplified and yet sufficient AA of typical mechatronic systems. Its actuation part is shown in Fig. 2.5, and the process of modeling its individual elements is briefly explained in the following:

- **Sensors:** Some of the sensor signals  $\sigma_S$  that are inputs for the controller may be derived from real sensors that are already part of the haptic interface or can be combined with it, e.g. position or force sensors. They are mapped onto the simulated system with respect to resolution, etc. The other sensor signals have to be simulated.
- **Controller, and its communication with external devices:** The control scheme of the actuated mechanism can usually be modeled very easily, as it typically already is a mathematical expression. The same holds for the signal processing of external devices. However, during the VRP process, an efficient, iterative refinement of controller and external software is desired. Thus, with respect to them and in contrast to hardware related issues, the primary concern of AAC in this stage is not a very detailed modeling but their efficient development. The interfacing electronics and bus systems are usually specified very well, so a thorough analysis can be performed to identify the elements which significantly limit the bandwidth of the overall system. These have to be subsequently included in the simulation model.
- **Electrical properties of the actuators:** Usually, the bandwidth of the power electronics and the actuators sufficiently describe the transfer function  $G(s) = \tau_A/\tau_r$ .
- **Equations of motion:** Typically, EOM are given as a set of differential equations of second order, corresponding to mass-spring-damper systems. Knowing the kinematic and dynamic parameters of the mechanism and its actuators, and having defined the user interaction ports, the EOM can be calculated using dedicated software packages [99]. However, non-linear effects require special consideration, compare e.g. the friction compensation used in [257].



**Figure 2.5:** Reduced model of the actuation for an early stage of product development: Communication delays are neglected, controller and external devices are simulated in one module, and the power supply is idealized.

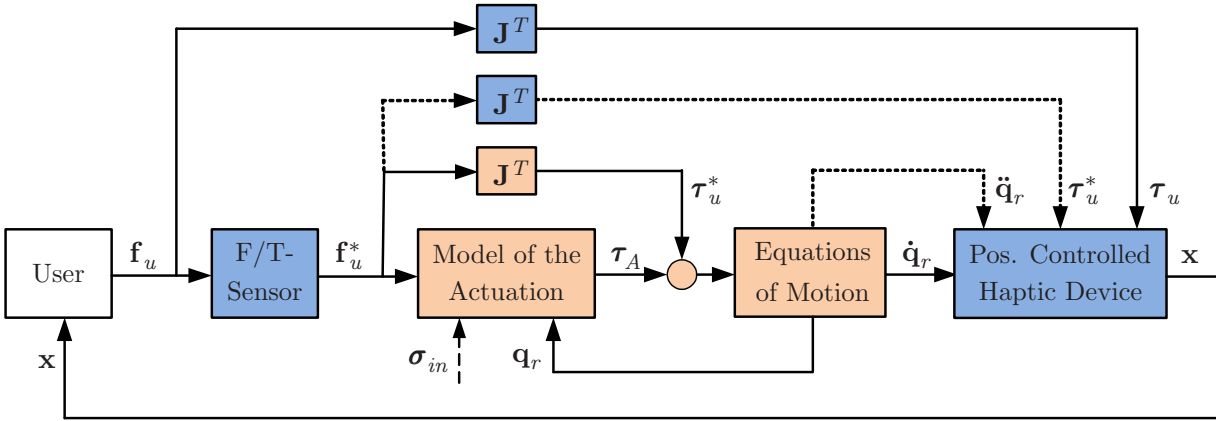


**Figure 2.6:** Active Admittance Control (AAC): Based on a model of the actuation (see Fig. 2.4) and the mechanical properties, a realistic haptic simulation of the mechatronic system is achieved.

After it has been modeled as an AA, the actuated mechanism can be haptically rendered by an admittance-type haptic device using Active Admittance Control. In combination with the gradually more detailed product information, this enables the iterative VRP and refinement of the mechatronic system.

## 2.3 Haptic Rendering by Active Admittance Control (AAC)

Active Admittance Control (AAC)<sup>1</sup> is the haptic rendering of mechatronic systems modeled by an Active Admittance (AA). After describing the general structure of AAC, we discuss the corresponding controller design as well as stability issues arising from it. Finally, we demonstrate its straightforward applicability by the example of a novel car door.

### 2.3.1 General Structure of AAC

We introduced the concept of the AA by separating the admittance into two parts, one which represents the actuation and therefore actively changes the energy of the overall system, and the other that represents the equations of motion of the actuated mechanism.

<sup>1</sup>Despite the similar wording, AAC is completely different to the “active impedance control” proposed 2009 in [54], which is simply an improved position controller.

Based on a model of the most relevant elements of the actuation,  $\boldsymbol{\tau}_A$  can be calculated. It is acting in parallel with  $\mathbf{J}^T \mathbf{f}_u^*$  on the EOM of the simulated mechanism. In analogy to conventional admittance control, this results in a simulated motion  $\mathbf{q}_r$  which is displayed by a kinesthetic haptic device. The position-based rendering is achieved by an inner closed-loop position controller. To compensate for environmental forces and to reduce the apparent dynamics of the haptic device, force feedforward [103] and feedback linearization should be utilized. A thorough investigation of state of the art control schemes for admittance-type haptic devices is given in [257].

## 2.3.2 Controller Design and Stability Issues

### 2.3.2.1 General Problem

One of the main reasons for the VRP of mechatronic systems is the possibility to implement and test the controller of the system iteratively. An important aspect is that both the simulated system itself *and* the haptic device which is used to render this system to the user have to be stable. This is the reason why all properties that are crucial for the stability of haptic rendering have to be considered in AAC.

In addition to sources of instability (“energy leaks”) that admittance control implementations exhibit in general, AAC can increase the energy of the overall haptic control system or parts of it by applying the actuation wrench  $\boldsymbol{\tau}_A$ . For example, if one task of the controller was to prevent a mechanism from colliding with other objects, the controller would calculate a wrench counteracting such a collision. The wrench results in a change in the motion of the mechanism and is thereby indirectly displayed to the user at the haptic interaction point (HIP). It can be useful as a haptic support in many applications, ranging from giving only partial information to the user (via a small and temporary signal) to determining the motion of the system (by applying  $\boldsymbol{\tau}_A \gg \boldsymbol{\tau}_{u,max}$ ).

At first sight, one might argue that there is no big difference in adding an additional term  $\boldsymbol{\tau}_A$  to the user interaction  $\boldsymbol{\tau}_u$  before applying it to a “conventional” passive admittance/impedance/VE in terms of stability. Unfortunately, this does not hold true in general: Given a simulation that contains a very dynamical and/or powerful actuator and a suitable controller, it is obvious that the bandwidth and/or the magnitude of  $\boldsymbol{\tau}_A$  can be dominating over any possible interaction of a human. Thus, two fundamental problems of AAC control design become evident:

1. Functionality: How to develop a suitable controller within the AAC framework?
2. Stability: How to achieve and ensure a robust, stable haptic interaction?

### 2.3.2.2 Functionality: Derived from Shared and Supervisory Control

The AAC structure is similar to some shared or supervisory control schemes; compare for example [159, 22, 251, 8, 237, 224] in which a human user and a controller are interacting with a common intermediary object. A difference lies in the point of view and the goal: While shared control directly deals with the control design of a physical system (intermediary object is real), AAC is used as a framework for the control design (intermediary object

is a simulation model). In other words, AAC can be used to develop a system commanded by a shared control scheme, but not vice versa.

Anyway, the theory of shared and supervisory control may be used to derive control algorithms for the controller of the mechatronic system. An example are haptic support functionalities, which are investigated in detail in Chap. 3.

After the functionality-driven control design, the controller has to be examined with respect to its applicability for both the desired target system and for its haptic rendering by AAC with a haptic device.

### 2.3.2.3 Stability: Based on Haptic Control Methodology

A lot of research has been carried out to examine the influence of the hardware and the control law of haptic devices on the stability of haptic rendering; see for example [6, 65]. Most of it considers the admittance to be a linear, time-invariant (LTI) set of differential equations, which definitely does not hold true in general for AAC. An extension to nonlinear VEs can be found in [172, 109].

One popular way is to connect the simulation model to the haptic rendering via a so-called virtual coupling; compare for instance [5]. In 2009, Griffith stated:

Traditional frequency-domain techniques that assess stability robustness in terms of gain margin and phase margin are not sufficient to address human-in-the-loop stability problems. This problem is more appropriately treated in the framework of coupled stability [...]. An effective, commonly employed approach that ensures coupled stability is to design the controller such that the closed-loop dynamics rendered to the user through the haptic device remain passive for all user interactions. Then if the human user also remains passive, the coupled system is guaranteed to be stable. [105]

This statement is based on a remarkable result which was achieved by Colgate in 1988 [51]: He found a “necessary and sufficient condition to ensure the stability of a linear manipulator coupled at a single interaction port to a linear, passive environment”. Based on this, he showed that it “is possible to extend this stability result to include active linear systems provided that the active terms are not state-dependent”. This means that any state-independent controller can stably be simulated by AAC – provided, that the haptic rendering loop itself is stable for conventional admittance control.

However, for the overwhelming majority of closed-loop control systems, one or more measured or estimated system states are an integral part of the controller. For instance, to achieve a reactive collision avoidance or to calculate a trajectory for actuated mechanisms, the kinematical configuration of the mechanism has inevitably to be considered. Thus, to the best of our knowledge there is no rule or paradigm that generically guarantees stability while not restricting the functionality of the system.

For limiting the effect of the active haptic support, bounds for the effective torque acting on the EOM, the simulated motion, and/or the total energy of the EOM may be introduced. A promising approach seems to be the utilization of elements similar to passivity observers [110, 109, 216]. Furthermore, output limiters could be utilized [150],

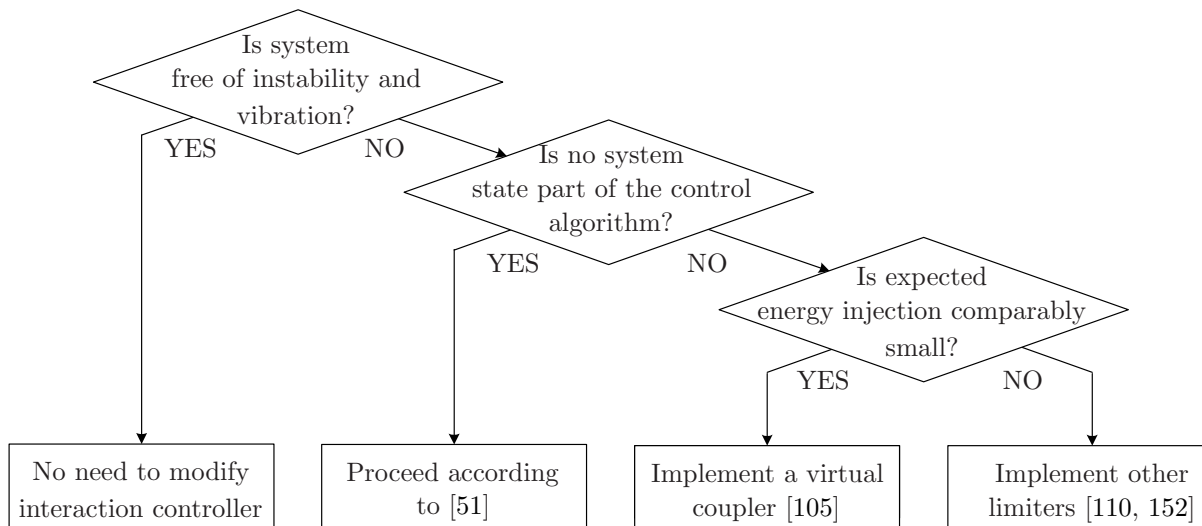


**Figure 2.7:** Flowchart describing the selection of appropriate controller restrictions for a simulated, actuated mechanism.

which for instance limit force and velocity simultaneously [152]. Another option is to adjust dissipating parameters as described in [70]. However, all of these approaches rely on bounding or “passifying” the influence of the active user support to some extent, which counteracts the desired functionality.

Thus, none of these approaches is suited or desired for the generic control design of actuated systems. Rather, the control design has to carefully consider the specific goals and restrictions of the mechatronic system to choose the appropriate control structure. In the following, we propose a guideline for this process.

#### 2.3.2.4 Guideline for the AAC Controller Design

In control design, it is a common goal to avoid overly conservative restrictions. Thus, the goal is to select the least conservative approach for the stability of the haptically rendered simulated mechanism based on the current state of the art (see subsection 2.3.2.3).

We propose a selection procedure for the overall controller structure and implementation of the simulated mechanism according to the flowchart given in Fig. 2.7: Changes may be necessary if instabilities or vibrations occur. If the controller of the desired system does not include any system state, the approach described by [51] is the best choice (see its stability proof). Otherwise, either a virtual coupling as for example described by [105] or limiting elements such as adjustable dampers [70], energy observers in analogy to [110], or limiters for both effort and flow [152] should be utilized to achieve a stable haptic interaction.

Both the coarse test and the fine-tuning of the control parameters can be efficiently performed by VRP based on the AAC. This is commonly an iterative process, especially since during the product development process the model described by the AA is gradually refined. The interactive haptic simulation supports this concurrent engineering of mechanical, electrical, and control design, resulting in an efficient and effective product design of actuated systems.

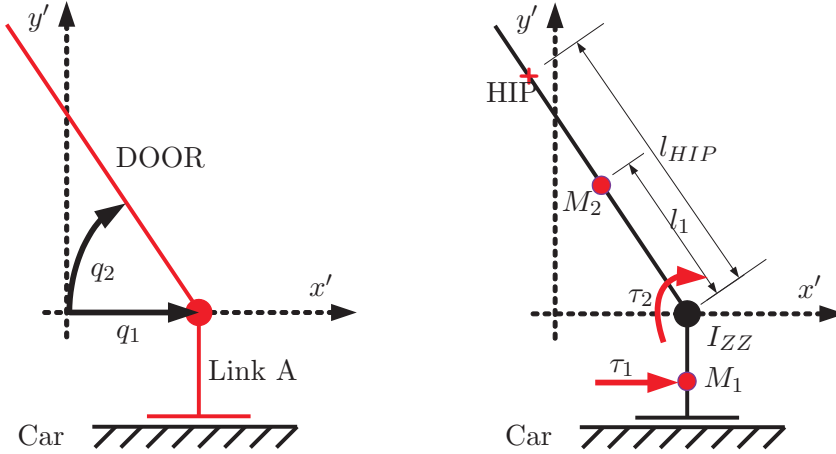


**Figure 2.8:** Sketch of the kinematics (l.) and dynamics (r.) of an Pivotal Sliding Car Door (PSD) described in generalized coordinates.

### 2.3.3 Exemplary Application of AAC to a Pivotal Sliding Door

Active admittance control (AAC) is exemplarily applied to the control and haptic rendering of a novel car door concept, the Actuated Pivotal Sliding Car Door (PSD). This door concept is expected to be desirable for car drivers as it combines the convenience of a sliding door with the general customer acceptance of a swing door [244].

The proposed PSD consists of an actuated slider (Link A) on which an actuated “conventional” car door (DOOR) is mounted; see Fig. 2.8. Thus, the system can be described by the generalized coordinates  $q_1$  and  $q_2$ . To keep the example simple, only the outer door handle is used as an interaction port. Thus, the location of the haptic interaction point (HIP) in Fig. 2.8 determines the mapping of the measured user force  $\mathbf{f}_u^*$  into the mechanism space given by  $q_1$  and  $q_2$ .

A simple functionality is defined for the controller of the door: It should react with a torque  $\tau_{coll}$  if an upper or lower border of  $q_1$  and/or  $q_2$  is violated. Thereby, a collision between the car door and the car bodywork must be prevented. According to the guideline described in subsection 2.3.2.4, one or more limiting elements have to be inserted. We decide to limit the reaction torque to  $\tau_{coll} \leq \tau_{coll,max}$ . In combination with the system-inherent damping, this will ensure a BIBO stable behavior no matter whether in contact with the human operator or not.

DC drives with time constants  $T_1$  and  $T_2$  have been chosen as actuators. We assume that the dimensionless transfer function of the encoders, the power electronics, and the transmissions equals  $\approx 1$ . Furthermore, we assume that the friction effects of both joints are dominated by Coulomb friction, which can be described by the coefficients  $\mu_1$  and  $\mu_2$ . The equations of motion of the PSD are given below.

$$\begin{aligned} \begin{pmatrix} m_1 + m_2 & m_2 l_2 \sin \phi \\ m_2 l_2 \sin \phi & m_2 l_2^2 + I_{ZZ} \end{pmatrix} \begin{pmatrix} \ddot{x} \\ \ddot{\phi} \end{pmatrix} + \begin{pmatrix} \mu_1 \dot{x} & + m_2 l_2 \cos \phi \dot{\phi}^2 \\ \mu_2 \dot{\phi} \end{pmatrix} \\ = \begin{pmatrix} f_1 + f_{I_x} \\ \tau_2 + \tau_{I_z} + l_{IP}(f_{I_x} \sin \phi + f_{I_y} \cos \phi) \end{pmatrix} \end{aligned} \quad (2.2)$$

Solving these equations for  $\mathbf{q}$ , the simulated states of the mechanism can be calculated. Finally, these states are mapped to the joint space of the haptic device (ViSHARD10 [259]) and fed to its position controller.

The implementation of an active admittance representing the PSD turned out to be straightforward. Some preliminary experiments have been conducted using the parameters noted in Tab. B.4. Both the kinematic and dynamic properties were displayed correctly, and the simulated controller effectively prevented a violation of the predefined joint limits. A detailed description of the VRP framework that has been used is given in Sec. 4.1.

During the evaluation of the PSD, the system-inherent coupling between the two DOF which can be seen from Eq. (2.2) posed a problem: Users were not able to fully anticipate the behavior of the car door. Thus, an assistance function should be developed to improve the usability of the car door. This is described in detail in Chap. 3.

## 2.4 Summary

In this chapter a comprehensive review of the history and state of the art of Virtual Reality Prototyping (VRP) has been given. VRP with haptic feedback offers great benefits in the development process of actuated systems. The importance of haptic feedback for the VRP of mechatronic mechanisms has been made clear. A comprehensive overview of the haptically relevant properties of mechatronic systems has been compiled.

Conventionally in haptic rendering, passive VEs are used which represent mechanical mass-spring-damper systems without consideration of actuation. We proposed an extended admittance model, the *Active Admittance* (AA). It includes models of all significant elements of the actuation loop, particularly the sensors, the controller, the actuators, and the transmission. Based on this, the actuation wrench  $\boldsymbol{\tau}_A$  is calculated. Both the actuation and the user wrench  $\boldsymbol{\tau}_u$  act on the model of the mechanical body of the mechatronic system, which is given in generalized coordinates. This leads to motion of the simulated actuated mechanism that can be displayed by a haptic device.

The controller design and stability issues of AAC were discussed. Two central issues have been identified: The development of the functionality of the interaction controller, and its robust, stable behavior and haptic rendering. Due to the analogy of human and controller affecting the same object, functionality aspects and methodologies can be derived from shared and supervisory control. Stability considerations are based on the abundant research on the control of haptic interfaces. However, no common approach is suited or desired for the generic control design of actuated systems. Rather, the control design has to carefully consider the specific goals and restrictions of the mechatronic system to choose the appropriate control structure. Therefore, a guideline is proposed to help in the identification of the least conservative control structure.

The active admittance control has successfully been demonstrated by modeling and haptically rendering a novel actuated car door with two DOF.

### 3 Generic Methods for the Haptic Support of Human-System-Interaction

Haptic feedback enables the support of human users during the interaction with a virtual, shared, and/or remote environment. In 2009, Abbink stated in [2]:

Compared with unassisted control, subjects can significantly and substantially improve their manual control task performance with haptic feedback.

This is desirable for a broad range of applications, where the limited capabilities of humans should be improved. Successful applications include training of students and employees, robotic surgery, and tele-operation in general; compare [83, 183, 195].

A variety of concepts have been developed to achieve an effective haptic support for the human-system-interaction (HSI) in specific scenarios. Currently, the most influential and important one is the concept of Virtual Fixtures (VF). Initially it has been proposed by Rosenberg as a static, rail-like support to reduce the DOF of human motion [213, 214]; see Fig. 3.1. Since then, a lot of extensions and variations of this concept have been developed, some of which even provide a dynamic, situation-dependent haptic support:

- Static Virtual Fixtures (SVF) [213]
  - Kinematic constraint: Simulated position equals VF [3, 60]
  - Kinematic pseudo-constraint: Virtual Wall (VW) [138]
- Dynamic Virtual Fixtures (DVF) [211, 97]
  - Based on intention recognition [160]
  - Based on path planning [13, 34, 132]

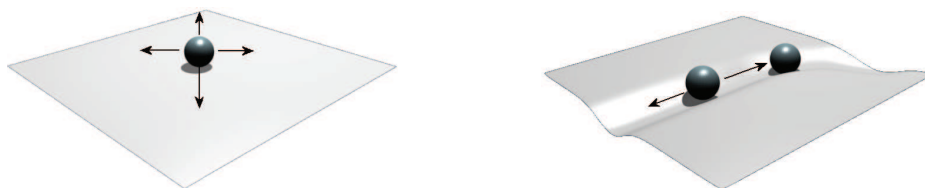


**Figure 3.1:** Illustration of the effect of an output-limited virtual fixture (on the right) on the haptic interaction with a virtual object [182].

In order to achieve an advanced support of the haptic interaction between a human user and an actuated mechanism, based on the VF technique, generic methods should be developed and investigated. At the example of simulated and real actuated car doors, they should provide a significant improvement of the usability. Thus, even for unconventional door kinematics and a demanding environment with obstacles, no significant level of discomfort should arise during the manual operation. The best way to achieve this goal was seen in a combination of proactive and reactive haptic support functionalities:

1. Intention Recognition (proactive): Based on static or online computed preferred goal configurations or motions, intention recognition can be utilized. On this foundation, the user can be supported haptically in a proactive manner.
2. Path Planning (proactive): In dynamic environments, the use of predefined paths/VF such as described in [154] is potentially dangerous. The remedy is to utilize an online path planner to determine possible collision-free motions. Haptic guidance could be based on path guidance of other domains; see for example [31].
3. Collision Avoidance (reactive): Even if a path planner determined collision-free trajectories for the haptic support, there is a risk of collision between the user, the interaction object, and the environment. Reactive real-time collision avoidance can prevent this from happening.

The combination of these different approaches can easily be realized using the active admittance control structure described in Chap. 2: All assistance functionalities contribute to the general actuation effect  $\tau_A$  which is displayed to the human user via haptic feedback. This is described with the implementation of the overall system in Sec. 4.1. In this chapter, our methods, implementations and results in the areas of intention recognition (Sec. 3.1), path planning (Sec. 3.2), and collision avoidance (Sec. 3.3) are described.

## 3.1 Intention Recognition: Determination and Support of the Intended Motion

As stated in subsection 2.3.3, the mechanics of a car door with more than one DOF caused a high level of discomfort during the manual operation of the door. Therefore, active haptic support that recognizes the user's intent and assists his or her movements is expected to be beneficial. We developed an approach which combines intention recognition with Static Virtual Fixtures (SVF) and Dynamic Virtual Fixtures (DVF). It is described in the following, while its evaluation by a user study is described in subsection 4.1.3.

### 3.1.1 State of the Art

Intention recognition has a tradition in artificial intelligence research [125]. In recent years, the focus shifted from natural language processing to image analysis. In haptics, intention recognition is about to become well-established.

Some approaches utilized Hidden Markov Models (HMM), a probabilistic technique designed to recognize transitions between different predefined states. In [89], the frequency spectrum of the measured user interaction force  $\mathbf{f}_u^*$  was used as input signal of an HMM, which enabled a coarse distinction between some intended motions. [276] trained an HMM with velocity information to be able to discriminate whether a certain path was intended to be followed or left by the user. Similarly, [1] proposed a Layered HMM to model human skill. After a training of this model, it enabled the support of repetitive tasks.

In [47],  $\mathbf{f}_u^*$  was directly used to derive the desired motion of a user within a walking support system. [70] proposed using the derivative of  $\mathbf{f}_u^*$  for intention recognition, because the user will usually exert force in the direction of his or her intended motion. [55] found that

point-to-point motions are characterized by a bell-shaped velocity profile. They utilized this to support this motion after a triggering event, but did not propose a corresponding intention recognition. However, [227] for example utilized it for a minimum-jerk based intention recognition.

[62] used a probabilistic framework based on Bayes' rule to decide which one of a number of possible motions the user intended to choose. Its input is the motion of a wheelchair.

### 3.1.2 Design of a Combination of Static and Dynamic Virtual Fixtures

For each given mechanism model, ergonomic and usability studies can be conducted to determine the most suitable, intuitive, and comfortable opening and closing motions (configurations, paths, or trajectories). Without loss of generality, we term these motions in the following "paths"; the proposed methodology could also be applied to trajectories.

Evidently, the actuated mechanism should support the human user in choosing and performing one of these favorable motions. To achieve this for the example of an actuated car door, its controller has to comprise different functionalities:

1. Favorable paths have to be known. They can be directly derived from a *teach in* at the actuated car door. Alternatively, they have to be computed online.
2. If the user is already on a favorable path, he or she should be supported in staying on it (respectively in following it). This is the common idea of Virtual Fixtures (VF).
3. However, the user should also be enabled to leave the VF if he or she intends this.
4. If the user is not on a favorable path, he or she should be supported in reaching the best one with respect to his or her current state.
5. Additionally, the transition from one favorable path to another should be supported.

An enabling technique for this is intention recognition. This can be based on measurements of the motion of the door ( $\dot{\mathbf{q}}, \mathbf{q}$ ) and the interaction force  $\mathbf{f}_u$ ; compare [1, 40]. Furthermore, predefined static paths have to be displayed, and situation-dependent dynamic paths have to be calculated.

In the following, we discriminate between two operational modes: Static VF, which are applied when the user is following one of the predefined favorable paths, and Dynamic VF, which are applied when the user is moving outside/between favorable paths.

#### 3.1.2.1 Static VF for the Support of Predefined Motion

It is assumed that two or more favorable paths are given by a list of subsequent nodes, which describe position and orientation  $\mathbf{x}$  of the haptic interaction point (HIP) in world coordinates. To achieve a VF-like haptic interaction and at the same time enable the transition from one static path to another at a crossing, static force fields are calculated for each path. To achieve a good trade-off between rigidity of the VF on the one hand and flexibility for desired deviating motions on the other hand, the force fields are composed of two terms: A Laplace distribution to achieve a sufficient fixation, and a normal distribution to nonetheless enable a smooth transition. These force fields are weighted using a

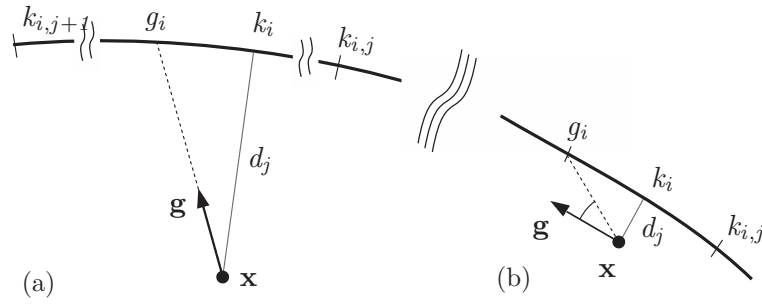


**Figure 3.2:** Target points for a user approaching a predefined path [182]. In (a) the user is moving towards a path, while in (b) the user’s movement is parallel to a path.

probabilistic approach, the Bayes’ theorem [62]:

$$P_k(\mathbf{x}_e | \mathbf{f}_{u,k}, \mathbf{x}_k) \propto P_{User}(\mathbf{f}_{u,k} | \mathbf{x}_e, \mathbf{x}_k) P_k(\mathbf{x}_e | \mathbf{x}_k) \quad (3.1)$$

where  $\mathbf{x}_k$  describes the HIP and  $\mathbf{f}_{u,k}$  the user signal (interaction force) at time step  $k$ . Three probabilities have to be considered:

- $P_k(\mathbf{x}_e | \mathbf{x}_k)$  is the a-priori distribution, based on the position and orientation of the door handle. From the controller’s point of view, it denotes the probability that a user aims to reach the configuration  $\mathbf{x}_e$  for a given  $\mathbf{x}_k$ . User signals and previous positions (e.g.  $\mathbf{x}_{k-1}$ ) are not taken into account.
- $P_{User}(\mathbf{f}_u | \mathbf{x}_e, \mathbf{x}_k)$  denotes the model of the user, which is the probability to observe the user signals  $\mathbf{f}_u$ , if the user really wants to approach the configuration  $\mathbf{x}_e$ .  $\mathbf{x}_k$  is taken into account for this calculation.
- $P_k(\mathbf{x}_e | \mathbf{f}_u, \mathbf{x}_k)$  is the a-posteriori distribution over all possible intentions of the user, after all user signals  $\mathbf{f}_u$  have been taken into account.

Thus, the static force fields are weighted based on their corresponding probability. For the SVF mode, the assistive effect  $\tau_{as,i}$  equals the sum of all these static force fields. It is haptically displayed to the user via AAC (compare Chap. 2).

### 3.1.2.2 Dynamic VF for the Support of Spontaneous Motion

The computation of weighting factors described in subsection 3.1.2.1 is suitable for the comfortable haptic rendering of predefined paths. However, it does not allow a path to be temporarily left in order to reach another one. Thus, dynamic guidance leading from one path to another should enhance the SVF.

To compute the intention of the user, a probability is assigned to each predefined path. This probability is described using a Gaussian distribution and depends on a distance measurement between the user and the path. For the distance measurement, the Euclidean distance between the two Cartesian points and the Euclidean distance between the two quaternions [59] describing the rotations is used. Quaternions are used to represent the orientation as they provide several advantages, such as exhibiting no singularities in

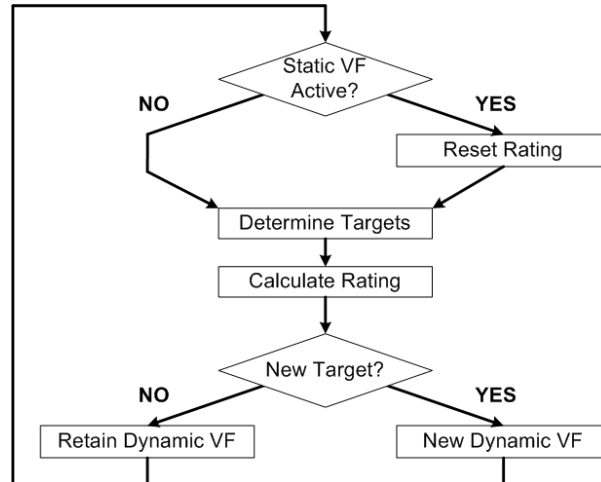


**Figure 3.3:** Algorithm for updating the Dynamic VF.

comparison to other representations like Euler angles. The intention recognition uses this probability and the movement of the door handle to estimate the aim of the user.

Fig. 3.2 shows how a possible target point  $g_i$  is computed. The distance  $d_j$  between the position  $\mathbf{x}$  of the user and a predefined path  $i$  is calculated, and a search window ( $k_{i,j}$  to  $k_{i,j+1}$ ) whose size corresponds to  $d_j$  is created on the path  $i$ . This can be seen in Fig. 3.2, where in (a) the window is larger than in (b).

The direction of the user's movement  $\mathbf{g}$  is used to compute the target  $g_i$  within the search window of the respective path  $i$ . In Fig. 3.2 (b), the movement is parallel to the path and consequently would lead to a point outside the window. However, instead the nearest point  $g_i$  on the path is chosen, such that the user will finally reach the path.

After the targets have been calculated for each path, a heuristic measure is applied to distinguish between the potential targets and the estimate of the user's desired target: If the user is moving towards a target, this target will be rewarded, otherwise it will be punished. Furthermore, the closest-point target, and the target whose distance is decreasing the quickest get a reward. After all possible targets have been rewarded or punished, the target with the highest rating is selected and a force field leading to the target is computed; compare Fig. 3.3. This computation is done in analogy to the static force field described in subsection 3.1.2.1.

Thus, the intention of the user is estimated from the "haptic signals"  $\mathbf{x}$  and  $\mathbf{f}_u^*$ . Based on this, the parameters for the creation of the force field as well as the weighting of each path are derived. Furthermore, it is used to adjust the parameters of the corresponding virtual walls (VW). The combination of all these results in the haptic intention support effect  $\tau_{as,i}$ . In fact, it represents a part of the actuation effect  $\tau_A$  of the AAC of the simulated door. Thus, it acts parallel to the user on the mechanical model of the door (compare subsection 2.2.3), and is thereby experienced as haptic support.

The evaluation of the haptic support based on intention recognition is described in subsection 4.1.3.

## 3.2 Path Planning: Determination and Support of Collision-Free Motion

A variety of concepts have been developed to achieve effective haptic support of the user in specific scenarios (see Chap. 3). However, most of these methods do not enable an adaptive support of the motion from a user within a (real or virtual) environment, which would be desirable in many situations. Especially when dynamical obstacles are involved or when the desired motion of the human is not known beforehand, an online computation of this support is essential, which should be based on a fast and effective determination of feasible motions.

In contrast to most other methods, sampling-based path planning is applicable to arbitrary scenarios and enables a solution to be found, providing one exists at all. Thus, it seems to be ideally suited for a generic framework that is able to deal with various kinematics, such as for instance a virtual prototyping test bed for the haptic evaluation of mechanisms requires. With such a test bed, the path planner could directly be coupled to the haptic rendering of a virtual scene to assist a user in approaching a target. Until the public release of OOPSMP [203, 204] in 2007, OpenRAVE [64, 63] in 2008, and of PP [140, 141] in 2009, there has been no easy-to-use<sup>1</sup>, powerful generic path planning software.

This motivated the development of SamPP, a sampling-based path planning library with implementations of the most important algorithms. It can be used for nearly arbitrary rigid robots and environments. By performing numerous benchmarks, we prove the effectiveness and efficiency of SamPP. It is shown that a single-threaded version of the path planning can be used for real-time support of the haptic interaction at actuated mechanisms. Note that we did not pursue a kinodynamic motion planning approach [168] due to the lack of obstacle-tracking at our hardware setups.

Furthermore, we enhance the path planning performance for unknown or dynamical environments significantly by the OR-Parallelization of different path planning programs. This Generalized OR Paradigm is a novel concept. We show by numeric simulation that for the case of dynamic environments the likelihood of a worst-case path planning result is lower with our approach. Thus, the quality of haptic interaction control based on path planning can be achieved and improved. When computational limitations vanish in the future, a brute-force application of the Generalized OR Paradigm will enable path planning within the global minimum of the response time.

For the near future, we highlight four promising research directions to exploit the concept of Generalized OR-Parallelization in current hardware setups:

1. Combination of different algorithms to achieve a synergy of their individual advantages
2. Concurrent use of different parameter sets of path planning algorithms
3. Online adaptation of these parameter sets
4. Online adaptation of the types and numbers of parallel executed planning threads

---

<sup>1</sup>This excludes the Motion Strategy Library [148] of Steve LaValle, which has not been updated since 2003.

### 3.2.1 State of the Art

Especially when (real or virtual) environments with dynamical obstacles are involved or when the desired motion of the human is not known beforehand, an online computation of a collision-free path is essential. In this area, path planning has been an active field of research especially in the past 15 years, and a variety of methods have been proposed.

A major drawback of many path planning algorithms is their lack of generality in terms of the existence of local minima. For instance, artificial potential fields which have been proposed for the assistance of haptic manipulation in the nano-scale [262, 34] are prone to produce local minima in many handling scenarios.

With the recent introduction of sampling-based methods [133, 146], these limitations have been overcome, and high-dimensional path planning problems have been solved efficiently. In general, in sampling-based path planning, the geometry of both robot and workspace is considered based on discrete samples of the configuration of a robot. Various methodologies exist for the creation of these samples, which greatly influence the properties of the path planner depending on a given scenario. For the generated samples, a collision check is performed, often by openly available collision detection libraries as for example the ones evaluated in [241]. The result is subsequently used by a path planning algorithm, which exclusively works in the configuration space (C-space) of the robot. To find a path for the robot, a local planner has to check whether two samples can be quasi-continuously connected without a collision.

Based on this, different strategies exist to find a path in the C-space: While single-query planners such as Rapidly-exploring Random Trees (RRT) [146] create a path specifically for a given start and goal configuration, multi-query planners such as Probabilistic Roadmaps (PRM) [133] proceed in two steps. In the processing step, a number of samples is connected to form a road map. In the query step, the given start and goal configurations have to be connected to the road map. If this succeeds and if the road map is connected, a solution surely exists and a suitable, optimized path can be found by a graph search. A very detailed introduction and state of the art of sampling-based path planning is given in [147].

It has been noted that some sampling-based path planning algorithms are (at least partially) embarrassingly parallel [12]. This means that the path planning time can be drastically reduced by implementing the algorithm in a parallel manner and running it on suitable hardware. Impressive demonstrations of this are given in [43, 202], where a nearly linear speedup for an increasing number of processors has been reported.

Recently, it has been shown that another way of speeding up sampling-based path planning is to run a number of path planning queries in parallel on suitable hardware [140]. It has been pointed out that with this OR paradigm the probability that none of the  $n$  queries finds a solution within a predefined time  $t$  is given by

$$1 - P_n(t) = (1 - P_1(t))^n \quad (3.2)$$

where  $P_1$  denotes the probability that one query finds a solution within  $t$  [43].

Obviously, this probability decreases rapidly with an increasing number of queries. However, as noted by Calisi [38], due to variations in the path planning environment there may be no single planner that will perform well in all possible situations. He added:

[A]n ideal motion planner would be a meta-planner using a suite of more specialized planners to cooperatively solve a motion planning problem. It would automatically apply the best-suited planner for each distinct region in the planning space and would produce regional solutions that could be composed to solve the overall motion planning instance. [38]

Furthermore, not only the choice of the algorithm itself but also its parameterization is a critical issue, because it drastically affects the performance of the path planning.

### 3.2.2 SamPP, a New Sampling-Based Path Planning Library

In this section, we introduce SamPP [66], a generic software library for sampling-based path planning for rigid robots within arbitrary environments. After describing the overall structure of the software and the representation of robot and environment, we present the implemented algorithms and experimental evaluations. Additionally, we compare SamPP with the recently released open source software library OpenRAVE [64, 63].

#### 3.2.2.1 Concept and Structure

SamPP has been intended to be part of a robotics control framework. Therefore, it was written in C++ (cross-platform) in an object-oriented manner as an API which is to be used in a client program. Using a specific parameter file which describes the path planning task at hand, a SAMPP object is instantiated there, and the path planning is executed. A path planning task is fully defined by the description of the robot and its environment as well as the start and goal configuration of the path.

To solve the task, an algorithm and its parameterization have to be chosen. The algorithm needs a 3D representation of the path planning scenario to perform collision checking, which is built based on the description of robot and environment. Accordingly, we structured the software architecture into the following components:

1. ROBOT: Parametrized description of the kinematics and the 3D shape of the robot
2. ENVIRONMENT: Parametrized description of the 3D shape of all potential obstacles within the path planning scenario
3. WORLD\_COLLISION and WORLD\_VISUALIZATION: Structure representing the 3D scenario for the collision checking and the visualization engine
4. PLANNER: Selection and parametrization of the path planning algorithm
5. SAMPP: Path planning object based on previous components

This way, a path planning query is performed by instantiating an SAMPP object, which will execute path planning based on a chosen parameter set.

#### 3.2.2.2 Representation of the Robot

The central consideration of sampling-based path planning is to find a collision-free path for the robot in the configuration space (C-space) of the robot. The C-space depends on the specific kinematics of the robot, i.e. the number, the type, and the limitations

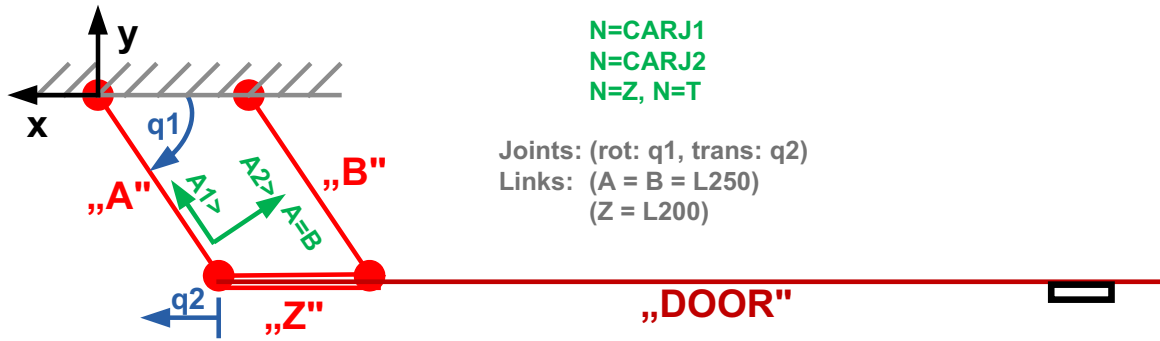


**Figure 3.4:** Swing-Sliding Car Door (SSD) exhibiting both a rotational and a translation DOF, parallel links, and a closed kinematic chain.

of its joints. The motion of every rigid kinematic can be described by a combination of rotational and translational DOF. Even if a mechanism possesses different joints, e.g. a non-prismatic translational one, the position and orientation of all links could be expressed using additional virtual rotational and/or translational joints. This also holds for parallel links, where fewer overall DOF exist than the single joints would exhibit in sum.

To give a better understanding of the problems involved with creating a scheme for the representation of arbitrary robots, consider the robotic application of a car door with the two DOF ( $q_1$ ,  $q_2$ ) depicted in Fig. 3.4. While the parts A and DOOR form an open tree-structured kinematic, due to the parallel mechanism the motion of the car door parts B and Z depend on ( $q_1$ ,  $q_2$ ). Thus, besides expressing rotational and translational DOF and their limitations, we need to express the potential dependencies inherent to parallel mechanisms.

By introducing dependent joints (dependent variables/dependent DOF), the problem of nonlinear and parallel kinematic configurations can be solved. For many real-world applications, a simple solution where the dependent joint configuration is calculated from the linear interpolation of predefined lookup table data is sufficient. This requires for every dependent joint the creation of a file that stores the lookup table. A common way to represent kinematic chains is to use the Denavit-Hartenberg notation (DH), where subsequently frames are created that describe a transformation from the base to the single links of the robot. This concept can be extended by introducing a parent for every frame, such that more than one child frame can be related to a frame. Thus, we build a tree structure, where each path represents a DH-like series of frames, which in combination with the dependent joints allows for the representation of parallel kinematics. This results in an intuitive tree-like robot description that can handle not only arbitrary open kinematic chains, but also kinematics with simple closed chains. A detailed specification of the representation of kinematics in SamPP is given in D.4.

Beside the kinematics, it is necessary to define parameters that take into account the influence of the single joints on the overall robot to ensure efficient and effective path planning. The path planner needs to rate motions of the robot. A common measure for this is the change of the kinematic configuration of the robot, which results from the single joint displacements. In serial kinematic structures, a displacement of a joint near to the base usually has a significantly bigger impact on the displacement of the overall

robot. This motivates the introduction of a cost function that punishes big displacements, thereby allowing the path planner to work efficiently. Right now, we use a simple constant weighting factor  $\mathbf{w}$  for the individual joints to achieve this goal. The weighting has to be chosen heuristically based on the scenario at hand.

Furthermore, a discretization has to be defined for the single DOF, because the path planning algorithm works in a discrete space, while the environment is continuous. The discretization  $\Delta\mathbf{q}$  defines a lower bound which enables planning that can be considered quasi-continuously. The distance of two states is calculated based on the simple L1 metric, thus all joint deviations are multiplied with their respective weight  $\mathbf{w}$  and summed up, such that  $\sum \mathbf{w}(\mathbf{q}_k - \mathbf{q}_{k-1})$  results. If this sum is smaller than the threshold  $\sum \mathbf{w}(\Delta\mathbf{q})$  (minimum cost), no collision is considered to be feasible when moving from state  $k - 1$  to state  $k$ , and thus no collision check is performed. This means that, if the discretization is too coarse, the calculated path may not be collision-free. However, if the discretization is very fine, the efficiency of the path planning is significantly reduced. Thus, it is crucial to provide a parametrization that is appropriate for the example at hand.

For enabling collision checks and visualization, besides the kinematics a graphical 3D representation of the single robot parts is also essential. Attention has to be paid to the handling of transformations and 3D data: The collision detection library and the visualization library may have different methods of handling files and transformations.

### 3.2.2.3 Representation of the Environment

In contrast to the usually rigid and fixed robot kinematics, the environment may have to be altered during runtime because of moving obstacles. If obstacles are detected by sensors, they are often handled without semantic knowledge, i.e. shape primitives are used to describe a convex hull over their respective 3D geometry; compare [241]. Based on the assumption that only such shape primitives would be important in the modification of the environment during runtime, we defined data structures and accordingly transformation matrices for them. Thus, the environment objects can be altered, removed, or new ones can be inserted during runtime. Sometimes it is more efficient to transform the objects than to create a new one.

### 3.2.2.4 Rapidly-Exploring Random Tree (RRT) Algorithms

Rapidly-exploring random Trees (RRTs, originally proposed in [146]) are the most popular Single Query planning algorithms. A particularly successful modification is the bidirectional RRT, which is pursued in our implementations: Instead of growing a tree from the start to the goal configuration, two trees are grown towards each other [145].

There exist several expansion strategies for growing the tree. In the “classical” approach, the RRT is grown exactly one discretization step towards a randomly generated sample. This can be extended by defining an upper bound for the expansion, for instance five discretization steps. In contrast, the “visibility” approach iterates discretization steps towards the sample as long as the sample is not reached and no collision has been detected. We implemented these strategies, denoted as RRT-cla and RRT-vis in the following. Both algorithms require the start and the goal state as inputs. An optional parameter timeout

enables the definition of a maximum duration for the path planning to quit the path planning for overly complex or even unsolvable problems. For an efficient handling of the search for nearest neighbors, we used kd-Trees and the open-source library ANN [180, 179].

### 3.2.2.5 Probabilistic Roadmap (PRM) Algorithms and their Parameterizations

PRM algorithms exhibit two phases: The processing step, where the probabilistic road map is built, and the query step, which consists of connecting the start and the goal state to the road map and a consecutive search for the optimal path between them. Analogous to the RRT implementations, we implemented algorithms with “classical” and “visibility” expansion strategies: PRM-cla and PRM-vis.

The goal of building the map (processing) is to get a road map that provides a good coverage of the C-space. This can be heavily influenced by several parameters, which will be introduced in the following.

**PrmMaxConnDist:** Maximum distance between two states. This parameter defines to which extent the path planner behaves classically (low values, near resolution) or visibility-based (high values) while building the map.

As mentioned in subsection 3.2.2.4, the efficacy strongly depends on the environment at hand. Thus, with this parameter the path planning can be tuned for a class of scenarios. For instance, when rather dense environments have to be considered, a low value would be a good choice.

**PrmInitialStates:** Number of initial states which are randomly sampled before the algorithm tries to connect them. If all initial states are connected (or if the timeout condition is triggered), the building of the map is stopped.

The higher the PrmInitialStates, the higher the probability of a dense road map. In turn, this makes it more likely that the start and goal states can be connected with the road map in the query stage. However, a high number leads to a more complex road map which inhibits the path search. One way of finding a good setting can be to start with a rather low value. If it turns out that the start and/or goal state cannot be connected with the map, this number can adaptively be increased. Note that this functionality would have to be provided by the client program.

**PrmMaxConnNumb:** Maximum number of connections between a new collision-free state and the road map. The higher this value, the better is the conjunction of the map, which tends to result in a smoother path and a longer path query. In many applications, a value of up to ten leads to good results.

**PrmCleanMapRate:** Rate of deletion of non-connected states. If a state is near an obstacle, it may be very difficult to connect it to the road map, which slows down the connection of the map. Therefore, the non-connected states are deleted with this rate. If this value is inappropriately low, it may be very difficult to build a map in a dense environment, because relevant states are deleted before being connected to the road map. Thus, this parameter is best only used if a relatively free C-space is assumed.

**PrmMapRateExam:** Rate of examination of the number of road maps. If the C-space is divided by obstacles such that not all states can be connected to one road map, some kind of timeout has to stop the attempt of the (infeasible) connection of the different road maps. This is done by examining the number of road maps at a constant rate. If the

number did not change within one time interval, it is assumed that the different road maps cannot be connected, and the processing stage is terminated.

**PrmMaxSampNumb:** Maximum number of random samples. If this value is set, the processing stage is terminated after this number of samples has been reached. After the road map has been built, path planning queries can be executed. This involves firstly connecting the start and the goal state to the (same) road map. If this succeeded, one is sure that the states are connected, and a graph search such as the famous A\* algorithm can be performed to find the optimal path. Otherwise, no path can be found, and an error is returned. Furthermore, a timeout results in an error, too.

### 3.2.3 Benchmark Results for SamPP

In the following, several benchmarks for SamPP are introduced and discussed. For all programs and scenarios, a PC with AMD Athlon™ 64 X2 Dual Core 5200+, 2 GB RAM and the operating system Linux Release 2.6.22-ipipe KDE 3.5.7 was used. Only one of the two cores was used, and all programs were run 20 times.

In the results, min and max denote the minimum and maximum, and  $\sigma$  and E the standard deviation and expectation values of the path planning duration and the path length of the 20 runs, respectively.

#### 3.2.3.1 Application to ViSHaRD10

Sampling-based path planning is superior to other path planning techniques especially if the number of DOF is high. To evaluate the efficiency of SamPP with respect to this, a scenario involving ViSHaRD10 [259] was developed. ViSHaRD10 is a robot with 10 rotational DOF, as shown in Fig. 3.5. Its special kinematic configuration does not allow a direct DH transformation from one joint to another for the joints 5, 8, and 9. Thus, for each of these joints two additional rigid joints were used such that the robot kinematics could be described. As VRML model of these pseudo joints, very small cubes were used, which are completely surrounded by neighboring joint models. Thus, they influence neither the path planning nor the visualization.

The single joints of ViSHaRD10 are constrained by the wiring. We considered a restriction to  $[-1.2\pi, 1.2\pi]$  as appropriate to avoid damage, and applied this to every joint description. Furthermore, we had to find a suitable weighting for the joints. We did this for every single joint by using the maximum absolute worst-case displacement of all robot parts caused by a movement of this joint. These displacements were further used to define the resolution for each joint.

The robot exhibits the highest versatility in the horizontal plane. Thus, a path planning scenario involving lots of motions in this plane was assumed to be most difficult, as it can constrain a high number of joints. For the evaluation, we used two scenarios.

Scenario 1 consisted of two narrow, parallel walls around the robot. The path planning task is to move the fully extended robot ( $q_{1..10} = 0$ ) to the opposite, fully stretched configuration ( $q_1 = \pi, q_{2..10} = 0$ ).

Scenario 2 is an extension of Scenario 1, where one additional short wall is placed exactly in the middle of the other two walls. This is shown in Fig. 3.5 (r.). The start configuration

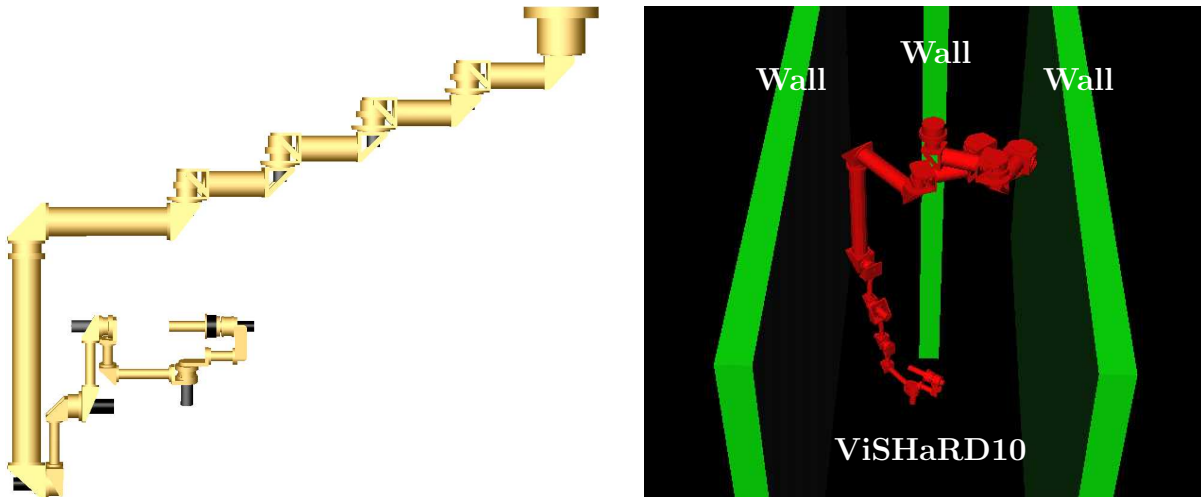


**Figure 3.5:** VRML model of ViSHaRD10 (l.) and path planning Scenario 2 with three walls (r.).

is given by  $(q_1 = \pi, q_2 = -\pi, q_{3..10} = 0)$ , the goal configuration by  $(q_1 = -\pi, q_2 = \pi, q_{3..10} = 0)$ .

Due to the high number of dimensions, PRM algorithms are not appropriate for a fast single-shot query, because a good coverage of the C-space would require a very large number of states, such that the graph search on the road map would be much slower than a single query method. Thus, we only consider the two RRT algorithms RRT-cla and RRT-vis for these scenarios. The benchmark results are given in Tab. 3.1.

**Table 3.1:** Path planning benchmark results for Scenario 1 and Scenario 2.

|                             |                       | Algorithm | min   | max    | $\sigma$ | E      |
|-----------------------------|-----------------------|-----------|-------|--------|----------|--------|
| Scenario 1<br>(two walls)   | Duration<br>[s]       | RRT-cla   | 0.471 | 6.435  | 1.475    | 2.618  |
|                             |                       | RRT-vis   | 0.086 | 1.309  | 0.422    | 0.387  |
|                             | Path length<br>[NORM] | RRT-cla   | 65.0  | 97.0   | 9.4      | 77.2   |
|                             |                       | RRT-vis   | 112.0 | 360.0  | 61.4     | 218.4  |
| Scenario 2<br>(three walls) | Duration<br>[s]       | RRT-cla   | 2.099 | 7.438  | 1.127    | 3.537  |
|                             |                       | RRT-vis   | 3.026 | 43.079 | 11.659   | 17.125 |
|                             | Path length<br>[NORM] | RRT-cla   | 92.0  | 188.0  | 35.1     | 125.9  |
|                             |                       | RRT-vis   | 164.0 | 432.0  | 62.0     | 290.9  |

The environment of the first scenario with two walls is not very narrow in joint space. Therefore, RRT-vis outperforms RRT-cla in the duration measures by a factor of approximately 3 to 6. The differences in the normalized path lengths clearly show that, despite the post-processing of the path the faster, RRT-vis produced costs whose average was three times higher than the RRT-cla. This shows one dilemma of sampling-based path planning: By choosing an appropriate algorithm and by tuning parameters, a trade-off has to be found for the scenario at hand.

In the second scenario, the third wall leads to a very narrow area in the C-space. This

limits the advantage of the RRT-vis, and consequently leads to a rather slow path planning when compared to RRT-cla. Again, the RRT-vis produces a much shorter path. For such an environment, the classic method is the best option.

Thus, by applying SamPP to a robot with 10 DOF, we have shown that the implementations RRT-vis and RRT-cla are able to plan a path in a relatively short time. In two complex scenarios, the RRT-cla exhibited a maximum planning time of 7.4 s. Furthermore, it found relatively short paths when compared to the visibility based method. This has also been visually observed when executing the planned path on the robot.

### 3.2.3.2 Preliminary Remarks on the Application to Different Car Doors

We apply SamPP to some car doors with two DOF and investigate the effect of different environments etc. As model of the car door, a VRML file with 31728 polygons was used (similar to Fig. D.6, the obstacles were represented as approximated spheres with 400 polygons each. The goal of the path planning is to provide a collision-free path from a fully closed position to a given open position. The following methods are investigated:

- RRT-vis: Visibility-based RRT implementation
- RRT-cla: Classic RRT implementation
- PRM-vis-P/Q: Processing/query stage of PRM-vis
- PRM-cla-5P/5Q: Processing/query stage of PRM-cla with five nearest neighbors
- PRM-cla-10P/10Q: Processing/query stage of PRM-cla with 10 nearest neighbors

### 3.2.3.3 Application to a Double-Four-Link Car Door (Two DOF)

In Scenario 3, a car door with two serial links named Double-Four-Link Door is considered. Its kinematics is depicted in Fig. 3.6 (r.). Though exhibiting four links and six joints, it only has two rotational DOF. Furthermore, due to the symmetry of the links, the door performs no rotation in world coordinates.

We consider three different environments which consist of three spheres as is shown in Fig. 3.6 (r.). The configuration space constrained by the environment is depicted in Fig. 3.6 (l., c.). The C-space consists of three non-connected areas. As both the start and the goal state are located in area B, a path can be found. Area A represents sphere 2 and, in combination with area C, forms a narrow corridor. This surely is the bottleneck for the path planning. If sphere 2 is varied only a little bit ( $\Delta x = 0.01$  m nearer to the car, which has a length of  $l = 1.30$  m), the corridor significantly narrows. In contrast, if sphere 2 is varied a little bit more ( $\Delta x = 0.10$  m further away from the car), it is out of the workspace of the door and thus has no influence on the path planning; see Fig. 3.6 (l., a.). Area B is now a very large free space, and path planning should accordingly be very fast. This example illustrates how extremely small variations in the configuration of the obstacles can affect path planning.

For all configurations of sphere 2 (“very narrow”, “narrow”, and “broad”), all path planning methods were evaluated. The results are summarized in Tab. 3.2. For configuration “very narrow”, RRT-cla performs best. The PRM methods are considerably slower in the processing stage, but excel in the variations PRM-cla-10Q and PRM-vis in the query

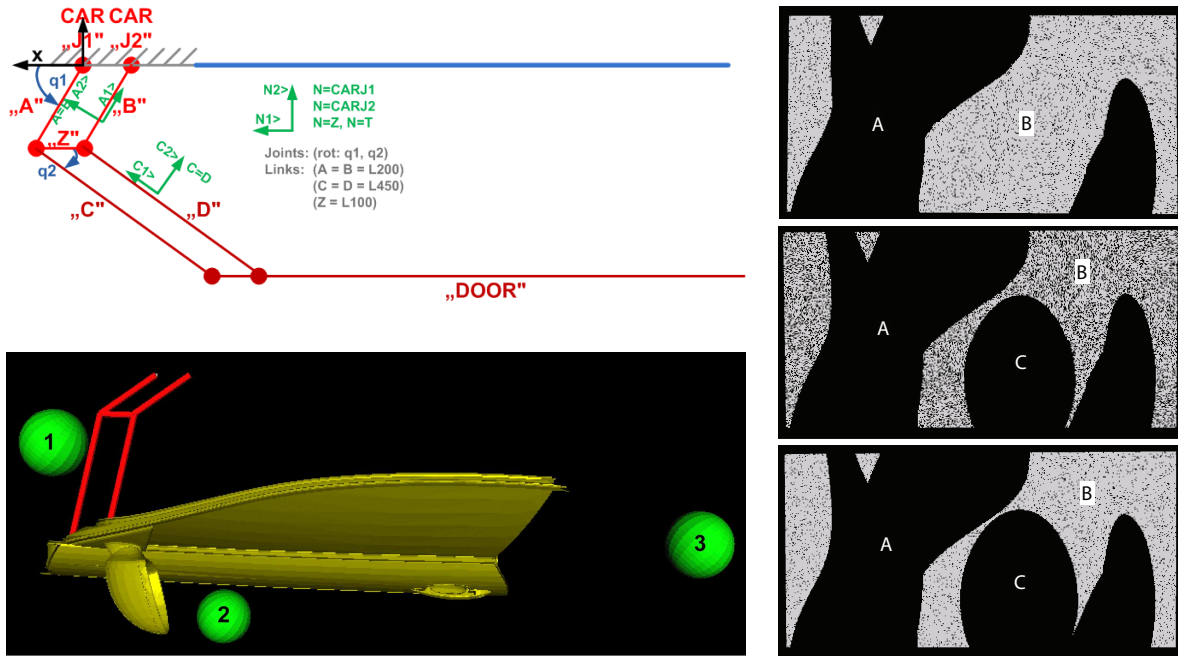


**Figure 3.6:** Scenario 3, given by a Double-Four-Link Door within three obstacles (l.). A slight variation of the position of obstacle 2 narrows the passage between start and goal configuration in the C-space significantly (r.): “broad”, “narrow” and “very narrow” configurations are depicted.

stage. If many queries are to be performed on such a kind of environment, PRM seems to be a good choice.

Interestingly, PRM-cla-10 is faster than PRM-cla-5 and PRM-vis. The reason for this must be that choosing five nearest neighbors leads to a road map which is too dense, while PRM-vis is too coarse. Thus, for every environment there is a range of connection lengths for which the planning performs best. In this particular case, by chance we found a good balance, as both a higher and a lower value perform worse.

With respect to the length (cost) of the paths, there is no great difference between the planners for all three scenarios – see the example given in Tab. 3.2, Scenario 3 “very narrow”. From the results for configuration “narrow”, one can see that the RRT methods give a similar expectancy value, while exhibiting a significantly different variance. The reason for this is that the RRT-vis sometimes “by chance” quickly finds a path through the narrow passage, but besides that works less efficiently in such a scenario. In contrast, from the PRM methods the PRM-vis performs best. This is due to the funnel-shaped C-space; if this was maze-like, the results most likely would have been much worse.

While there has been a strong improvement in the time duration, the path lengths seem not to significantly differ from the ones of the “very narrow” ones.

**Table 3.2:** Path planning benchmark results for Scenario 3 with variation of obstacle position.

|                            |                  | Algorithm   | min | max | $\sigma$ | E    |
|----------------------------|------------------|-------------|-----|-----|----------|------|
| Scenario 3<br>(broad)      | Duration<br>[ms] | RRT-cla     | 20  | 31  | 3        | 24   |
|                            |                  | RRT-vis     | 3   | 9   | 2        | 5    |
|                            |                  | PRM-cla-5P  | 22  | 48  | 8        | 35   |
|                            |                  | PRM-cla-5Q  | 7   | 17  | 3        | 11   |
|                            |                  | PRM-cla-10P | 25  | 49  | 7        | 34   |
|                            |                  | PRM-cla-10Q | 6   | 18  | 3        | 10   |
|                            |                  | PRM-vis-P   | 41  | 118 | 21       | 67   |
|                            |                  | PRM-vis-Q   | 4   | 13  | 2        | 6    |
| Scenario 3<br>(narrow)     | Duration<br>[ms] | RRT-cla     | 33  | 49  | 4        | 38   |
|                            |                  | RRT-vis     | 13  | 102 | 21       | 35   |
|                            |                  | PRM-cla-5P  | 198 | 396 | 54       | 266  |
|                            |                  | PRM-cla-5Q  | 17  | 48  | 8        | 25   |
|                            |                  | PRM-cla-10P | 117 | 160 | 31       | 231  |
|                            |                  | PRM-cla-10Q | 7   | 15  | 3        | 22   |
|                            |                  | PRM-vis-P   | 86  | 187 | 26       | 120  |
|                            |                  | PRM-vis-Q   | 4   | 17  | 4        | 9    |
| Scenario 3<br>(very narr.) | Duration<br>[ms] | RRT-cla     | 31  | 66  | 8        | 44   |
|                            |                  | RRT-vis     | 21  | 375 | 95       | 115  |
|                            |                  | PRM-cla-5P  | 314 | 517 | 80       | 404  |
|                            |                  | PRM-cla-5Q  | 27  | 60  | 24       | 114  |
|                            |                  | PRM-cla-10P | 240 | 382 | 40       | 275  |
|                            |                  | PRM-cla-10Q | 14  | 38  | 6        | 23   |
|                            |                  | PRM-vis-P   | 374 | 548 | 102      | 448  |
|                            |                  | PRM-vis-Q   | 10  | 23  | 4        | 16   |
|                            | Length<br>[NORM] | RRT-cla     | 39  | 42  | 0.9      | 40.5 |
|                            |                  | RRT-vis     | 39  | 46  | 2.0      | 41.1 |
|                            |                  | PRM-cla-5P  | 39  | 43  | 1.1      | 40.3 |
|                            |                  | PRM-cla-10P | 39  | 43  | 1.1      | 40.5 |
|                            |                  | PRM-vis     | 39  | 42  | 0.8      | 40.3 |

### 3.2.3.4 Application to a Two-Link Car Door (Two DOF)

In Scenario 4, SamPP has been applied to the Two-Link Door (TLD) which is depicted in Fig. 3.7 (l.). The environment consists of four spheres. The main problem in doing this is circumventing sphere 2 and reaching the state which is near the spheres 3 and 4. The C-space of this path planning problem is very narrow, as can be seen in Fig. 3.7 (r.). In area A both the start and the goal configuration is contained, thus a valid path can be found. The representation of sphere 2 forms a long and narrow passage from the start state.

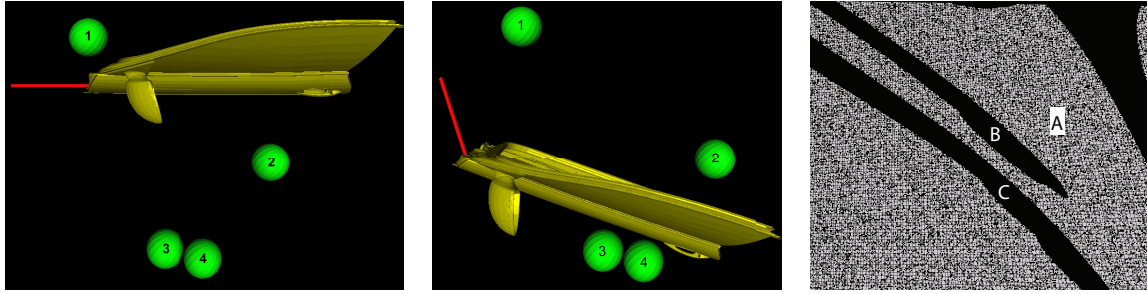


**Figure 3.7:** Scenario 4: Fully closed position (l.), fully opened position (m.) and depiction of narrow passage in the C-space of the Two-Link Car Door.

**Table 3.3:** Path planning benchmark results for Scenario 4

|                            |                  | Algorithm   | min | max | $\sigma$ | E    |
|----------------------------|------------------|-------------|-----|-----|----------|------|
| Scenario 4<br>(very narr.) | Duration<br>[ms] | RRT-cla     | 11  | 43  | 8        | 24   |
|                            |                  | RRT-vis     | 3   | 19  | 5        | 9    |
|                            |                  | PRM-cla-5P  | 75  | 168 | 23       | 103  |
|                            |                  | PRM-cla-5Q  | 6   | 17  | 3        | 11   |
|                            |                  | PRM-cla-10P | 87  | 169 | 29       | 130  |
|                            |                  | PRM-cla-10Q | 6   | 22  | 4        | 11   |
|                            |                  | PRM-vis-P   | 91  | 169 | 22       | 127  |
|                            |                  | PRM-vis-Q   | 4   | 19  | 4        | 9    |
|                            | Length<br>[NORM] | RRT-cla     | 19  | 44  | 7.5      | 36.8 |
|                            |                  | RRT-vis     | 36  | 62  | 7.2      | 54.0 |
|                            |                  | PRM-cla-5P  | 39  | 47  | 2.2      | 42.3 |
|                            |                  | PRM-cla-10P | 37  | 47  | 2.3      | 41.8 |
|                            |                  | PRM-vis     | 32  | 62  | 6.4      | 46.0 |

The RRT methods perform the path planning considerably faster than the PRM methods. The RRT-vis exhibits an expectation value of 9 ms, thereby even undercutting the expectation value of the PRM queries. If the corridor in the C-space had not been straight but curved, the PRM-cla would have been better. All PRM methods require a maximum of more than 150ms for building the map. This makes them unsuitable for real-time applications in scenarios like these. The path lengths exhibit a significant variance for all methods, which is a hint that the path post-processing performs very poorly for scenarios like these. Thus, it might be beneficial to improve this algorithm.

### 3.2.3.5 Application to Car Doors with Two DOF in the Presence of Many Obstacles

When interfacing the path planner with a sensor system [241], a much higher number of primitive objects will be used to represent obstacles in the workspace of the door. This motivated evaluating the influence of the number of obstacles on the path planner. We replaced the spheres of the environment (which represented vertical pillars) with 100 spheres each. This increase in the number of obstacles barely affects the C-space. From Tab. 3.4, it clearly can be seen that the RRT methods provide a much better performance than the PRMs for a single query. The reason is their reduced demand for collision checks: The PRMs suffer from the many collision queries that have to be performed when building the map. However, the maximum query time of the PRMs is significantly shorter than that of the RRT-vis. Thus, it is not possible to give a clear recommendation on whether to use PRMs or RRTs in a scenario with a high number of obstacles. In static scenarios, a combination might be a good choice: Two computers can be used, one running PRM-vis, the other RRT-vis. While the road map is built, only RRT-vis results are used for path planning. After that, as long as the environment does not change, both RRT-vis and a PRM-query are started simultaneously, and the faster result is used. For the evaluation scenarios, this would lead to a maximum time consumption for the “parallel query” of 68 ms, which is fast enough to be used in a haptic assistance task.

**Table 3.4:** Path planning benchmark results for modified Scenario 3 and Scenario 4 with 400 obstacles.

|                                    |                  | Algorithm | min  | max  | $\sigma$ | E    |
|------------------------------------|------------------|-----------|------|------|----------|------|
| Modified Scenario 3<br>(400 obst.) | Duration<br>[ms] | RRT-vis   | 39   | 548  | 117      | 190  |
|                                    |                  | PRM-vis-P | 142  | 2084 | 382      | 1704 |
|                                    |                  | PRM-vis-Q | 16   | 66   | 11       | 41   |
| Modified Scenario 4<br>(400 obst.) | Duration<br>[ms] | RRT-vis   | 20   | 117  | 21       | 42   |
|                                    |                  | PRM-vis-P | 2497 | 2926 | 106      | 2643 |
|                                    |                  | PRM-vis-Q | 31   | 68   | 8        | 41   |

### 3.2.3.6 Short Performance Comparison to OpenRAVE

We wanted to find out whether our implementation of sampling-based path planning algorithms had a performance that is comparable to implementations of other researchers. Recently, the professional, open-source path planning library OpenRAVE [64] was released. Its RRT algorithms seemed to be suitable for benchmarking our implementations of RRT-cla and RRT-vis. We initially installed OpenRAVE on the same Linux system that had been used for the evaluation of SamPP. We ran the same scenarios which we described in the previous sections. The performance was very poor when compared to SamPP: All time measures were by approximately one order of magnitude worse than the ones for SamPP. For instance, the average time of the bidirectional RRT was 32.04 s ( $\gg$  0.39 s of our RRT-vis) for Scenario 1 and 146 ms ( $\gg$  9 ms of our RRT-vis) for Scenario 4. We could not explain this discrepancy, so we installed OpenRAVE on a virtual Linux system (Ubuntu)

which was running on a Windows system (Windows XP, 2 GB RAM) and repeated the evaluation. Despite the fact that the virtual Linux most likely increases the computational overhead, the results here were much closer to the ones of SamPP. For instance, the average and minimum times of the bidirectional RRT was 2.45 s/0.53 s ( 0.39s/ 0.09s of our RRT-vis) for Scenario 1 and 12 ms/5 ms ( $> 9$  ms/ $> 3$  ms of our RRT-vis) for Scenario 4.

While these comparisons do not enable a fair overall judgment of the path planning performance (different system configuration, heavy dependence on specific scenarios), they nonetheless lead to the following conclusions:

1. We were not able to identify the reason for the poor performance of OpenRAVE on the first system. Thus, we advise potential users of OpenRAVE or other complex path planning libraries to benchmark the software on different systems to minimize the risk of running it in a very suboptimal configuration.
2. SamPP is comparable to professional state-of-the-art implementations of sampling-based path planning algorithms, such as OpenRAVE or PP.

#### 3.2.3.7 Remarks and Summary

We evaluated the performance of SamPP for executing path planning for a 10 DOF robot and for different two-DOF car doors within a (in terms of the configuration space) very demanding environment. Due to the RRT and PRM algorithms, SamPP is able to solve a variety of path planning problems efficiently. For the case of 300 to 400 obstacles, almost the “worst-case” placed in the workspace of these car doors, we found typical mean values for the path planning time in the area of 50 ms for RRTs, 1500 ms for building a PRM, and 30 ms for PRM queries. The evaluation results for Scenario 3 and Scenario 4 show that the performance of SamPP is indeed sufficient for the haptic real-time assistance of a human in various scenarios with two DOF. Independently of the planning algorithm, the path post-processing seems to work quite well if there are no overly narrow passages in the C-space of the robot. Note that the performance heavily depends on the environment at hand. The environments that we used for the evaluation often exhibited an uncluttered, rather free C-space. This promotes the visibility based methods.

However, it has been shown that there is no “one size fits all” solution: Depending on the environment at hand, variations of the parameter setting may decrease or increase the performance of the path planner. Furthermore, we observed that a comparison of the performance of PRM methods for fixed processing times showed that a larger road map leads to longer query response times, and that a reduction in the number of initial states proved to give better results for our scenario. It is relatively hard to find an appropriate number of initial sample states for simple environments of the robot. The road map has to sufficiently cover the C-space to provide a very high probability that the start and the end goal can be connected to the map. A large and complex road map, in turn, cannot quickly be evaluated by a graph search algorithm. This problem cannot occur when using an RRT method, because the planner is focused on connecting a start configuration as efficiently as possible with the goal configuration, such that no “overly complex” connection structure results. For rather simple scenarios, the total planning time of RRT-cla is faster than a query on a road map. For such cases, it does not make sense to use PRMs at all.

### 3.2.4 Generalized OR Paradigm

#### 3.2.4.1 Problem: There is no Best Algorithm

It was already highlighted that there is no overall best-performing path planning algorithm, because the kinematics of the robot and the structure of the environment have a huge impact on the level of difficulty of the path planning task. To clarify this, in Tab. 3.5 a composition of the fastest planners is given for slight modifications of Scenario 3.

**Table 3.5:** Composition of the fastest planners for modifications of Scenario 3.

|                                       |                  | Algorithm | min | max  | $\sigma$ | E    |
|---------------------------------------|------------------|-----------|-----|------|----------|------|
| Scenario 3<br>(broad)                 | Duration<br>[ms] | RRT-cla   | 20  | 31   | 3        | 24   |
|                                       |                  | RRT-vis   | 3   | 9    | 2        | 5    |
|                                       |                  | PRM-vis-P | 41  | 118  | 21       | 67   |
|                                       |                  | PRM-vis-Q | 4   | 13   | 2        | 6    |
| Scenario 3<br>(narrow)                | Duration<br>[ms] | RRT-cla   | 33  | 49   | 4        | 38   |
|                                       |                  | RRT-vis   | 13  | 102  | 21       | 35   |
|                                       |                  | PRM-vis-P | 86  | 187  | 26       | 120  |
|                                       |                  | PRM-vis-Q | 4   | 17   | 4        | 9    |
| Scenario 3<br>(very narr.)            | Duration<br>[ms] | RRT-cla   | 31  | 66   | 8        | 44   |
|                                       |                  | RRT-vis   | 21  | 375  | 95       | 115  |
|                                       |                  | PRM-vis-P | 374 | 548  | 102      | 448  |
|                                       |                  | PRM-vis-Q | 10  | 23   | 4        | 16   |
| Modified<br>Scenario 3<br>(400 obst.) | Duration<br>[ms] | RRT-vis   | 39  | 548  | 117      | 190  |
|                                       |                  | PRM-vis-P | 142 | 2084 | 382      | 1704 |
|                                       |                  | PRM-vis-Q | 16  | 66   | 11       | 41   |

To show that this problem also exists with other path planners and more complex scenarios, another series of benchmarks was performed for the path planning library PP [141]. We chose the corresponding standard scenario of a dual-arm robot within a kitchen. We added five spheres to the scenario and defined start and goal position such that the problem could not easily be solved; compare Fig. 3.8. We then iteratively performed benchmarks for a different number of parallel path planning threads and an increasing distance of sphere 1 to the robot ( $d = 1.0m$  to  $d = 1.5m$ ).

The result is depicted in Fig. 3.9. It can clearly be seen that for different threshold levels (l: 50th, m: 90th, r: 95th percentile) the relative performance of the different algorithms depends on the position of the “moving” sphere. For instance, while the RDT implementation performs worst for  $d = 1.0m$ , it performs best for  $d = 1.5m$ . This corresponds to a more significant decrease of the time  $t_{PRDT,90th}$  (90th percentile) in general and a lower value of  $t_{PRDT,1.4m,90th}$  than for instance the BiRDT implementation exhibits; see Fig. 3.10.

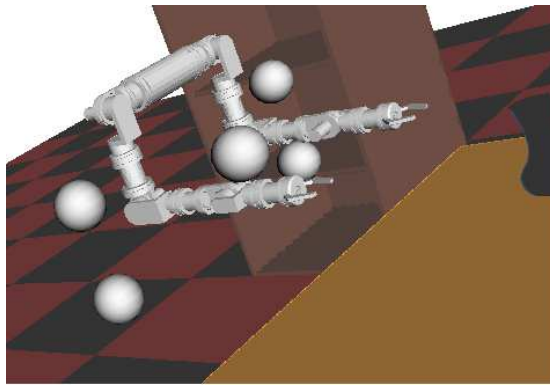


**Figure 3.8:** Screenshot of the benchmark scenario used for investigating the path planning performance of different algorithms of PP [141].

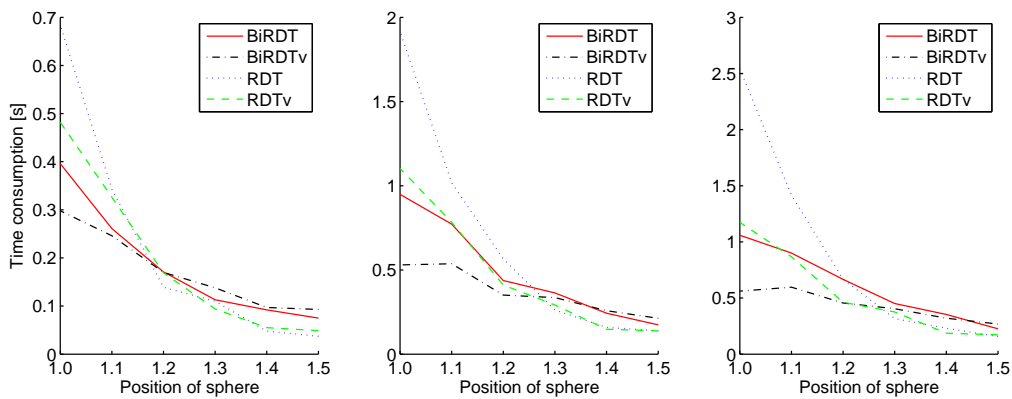


**Figure 3.9:** Evolution of the fastest path planning times for the scenario depicted in Fig. 3.8 and four different algorithms of PP with thresholds of the 50th (l.), the 90th (m.), and the 95th (r.) percentile; the bigger the position of sphere 5, the better the results.

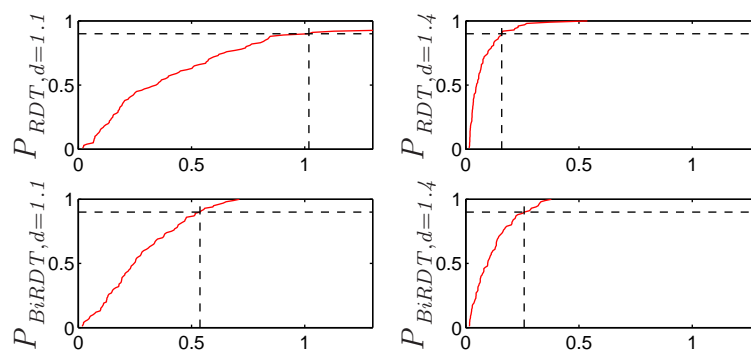


**Figure 3.10:** Detail of the benchmark shown in Fig. 3.9: While the BiRDT implementation shows better results than the RDT implementation for a low position of ( $d = 1.1$  m), it outperforms the RDT implementation at a higher position ( $d = 1.4$  m).

### 3.2.4.2 Solution: Parallelization of Different Algorithms (Generalized OR Paradigm)

As already explained in the introduction, two research directions have been proposed in the past to speed up complex path planning problems:

1. Parallelization of subtasks of path planning algorithm:  
Decreasing the time consumption of specific path planning algorithms
2. OR-parallelization of a specific path planning algorithm:  
Increasing likelihood of a fast result by executing several instances of one planner

We propose a promising third alternative:

3. OR-parallelization of different path planning algorithms:  
Increasing likelihood of a fast result by executing a number of instances of different planners and/or planner parameterizations

To denote this principle mathematically, we extend Eq. (3.2) [82, 43] to the Generalized OR Paradigm.

### 3.2.4.3 Generalized OR Paradigm: Definition and General Remarks

Let  $P_i(t)$  be the probability that a specific program  $i$  running on a single processor will find a solution within time  $t$ , and let  $P_{i,k}(t)$  be the corresponding probability of  $k$  instances of this specific program running in parallel on different processors will find a solution within time  $t$ . Furthermore, let the random variable  $T_1^j$  be the time it would take processor  $p_j$  to find a solution, if allowed to run to completion, where the  $T_1^j$ s are independent and identically distributed. Then, the probability  $1 - P_{i,k}(t)$  that the solution time for program  $i$  running on  $k$  processors will exceed  $t$  is just the probability that none of the  $k$  processors will find a solution within time  $t$ :

$$1 - P_{i,k}(t) = (1 - P_i(t))^k \quad (3.3)$$

Accordingly, the overall probability that none of the  $N$  different (differ with respect to the path planning algorithm and/or the parametrization of the algorithm) programs running on  $k_N$  dedicated processors will find a solution within time  $t$  is:

$$1 - P(t) = (1 - P_1(t))^{k_1} (1 - P_2(t))^{k_2} \dots (1 - P_N(t))^{k_N} \quad (3.4)$$

Thus, the overall probability that at least one of the  $N$  different programs running on  $k_N$  processors will find a solution within time  $t$  is:

$$P(t) = 1 - (1 - P_1(t))^{k_1} (1 - P_2(t))^{k_2} \dots (1 - P_N(t))^{k_N} \quad (3.5)$$

If at least one of the different programs has a probability  $P_i(t) > 0$  and is run in a massively parallel fashion ( $k_i \rightarrow \infty$ ),  $P(t) \rightarrow 1$ .

However, for each program there is a theoretical and practical minimum bound for the best-case execution time  $t_{BC,i}$  which depends on the algorithm, its parameterization, and the respective scenario. If there is no detailed previous knowledge about the scenario, it

can not be predicted a priori which program will exhibit the global minimum  $t_{BC}$  where  $P(t) = 0 \quad \forall t < t_{BC}$ . For achieving  $t_{BC}$ , all planners with all possible parameterizations (including infinitely small discretization steps of variables) would have to be executed with an infinite number of instances each in parallel.

In the far future, when computing resources virtually are not limited any more, this brute-force approach might indeed enable to determine the globally time-optimal solution of a path planning problem. However, in current hardware setups the computing resources are limited, such that a trade-off is necessary to exploit the potential advantage of the Generalized OR Paradigm.

In the following, the case of a limited number of programs executed in a OR parallel manner is considered. The effect of our approach can be shown by the evolution of the probabilities of some random processes and their combinations. Several sequences of random numbers were generated based on an exponential distribution function. They are characterized by an exponential coefficient (8, 10, 9, 11 in our case) and a static time offset (0.30s, 0.15s, 0.25s, 0.18s) to represent the characteristics of different path planner evaluations.

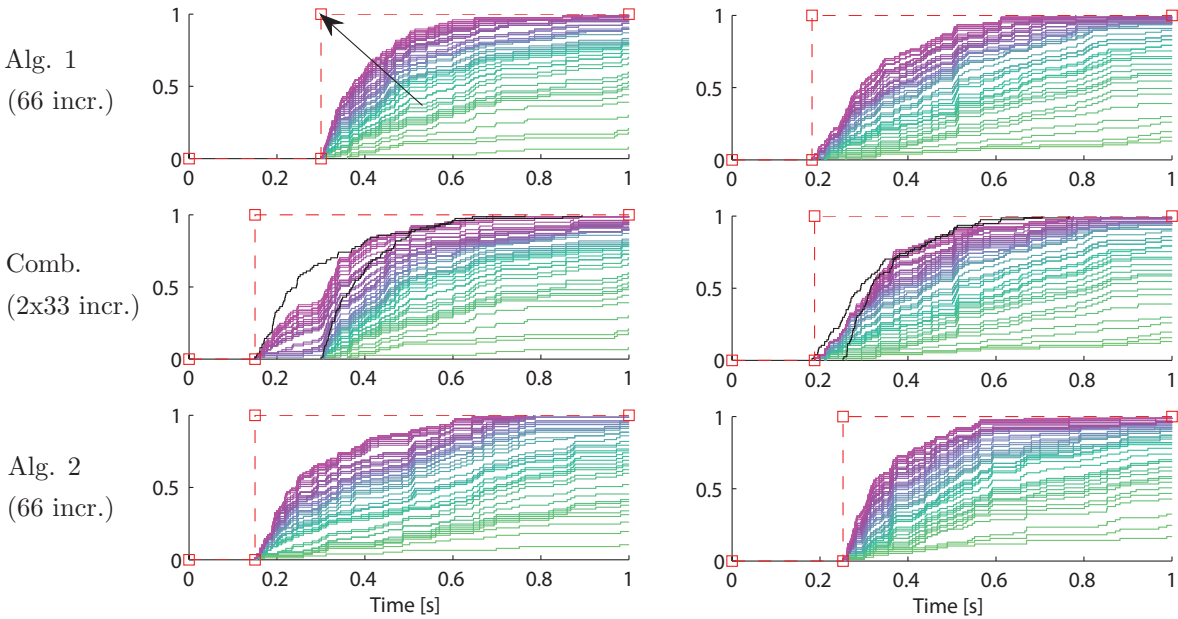


**Figure 3.11:** Evolution of the probability of finding a collision-free path. The arrow indicates that for an increasing number of programs, the probability approaches a step function.

For example, in Fig. 3.11 the probability of finding a collision-free path is depicted as a function of time and of number of programs. The arrow in the upper left axis indicates that for an increasing number of parallel path planning programs, the probability approaches a step function at time  $t = t_{offset} + t_{calc,min}$  which due to the probabilistical completeness of sampling-based path planning would be achieved for an infinite number of simultaneously starting programs. The upper and lower axes show four different occurrences of path planning probability functions for 1 to 66 programs running in parallel. In the middle

axis, the combinations of 33 of the upper and 33 of the lower algorithms are depicted. Note that in both cases a speedup with respect to the worse performing algorithm is achieved.

Based on Eq. (3.4), the general conclusion can be drawn that from an algorithmic point of view the performance of the overall sampling-based path planning will always increase if additional planners are started, because each planner contributes to the overall probability.

In the following, we point out four advantages and research directions arising from this.

### 3.2.4.4 Potential Advantage 1: Synergy of the Advantages of PRMs and RRTs

Often, path planning queries can be more quickly calculated for existing PRMs than for single-shot RRTs. However, building the PRM requires a significant amount of time, which limits their application. The best option might be to build one or more road maps while path planning queries are answered by other algorithms. Then, as long as the environment does not change significantly, the typically very efficient PRM queries can be performed. This way, the advantages of both PRMs and RRTs can be utilized. For the example given in Tab. 3.5, combinations of RRT-cla, RRT-vis, and PRM-vis could drastically reduce the worst-case maximum duration of path planning both during and after building a PRM.

In Fig. 3.12, the performance of the parallel execution of RRT-cla and RRT-vis is given for Scenario 3. As had been expected from the results of Tab. 3.5, the RRT-vis was better in the broad configuration space and the RRT-cla in the very narrow one. Due to this combination, the poor performance of the RRT-cla in the very narrow case is barely noticeable when compared to parallel executions of only RRT-vis. This underlines the increase of the reliability which is inherently achieved by the Generalized OR-parallelization.

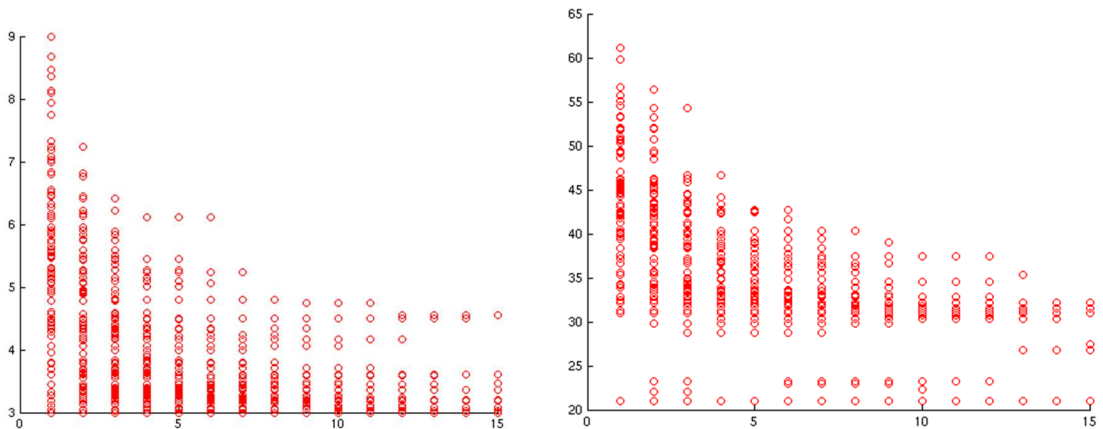


**Figure 3.12:** Decreasing the worst case computation time per run [ms] by increasing the number of RRT-based path planner pairs for Scenario 3 (“broad”, l. and “very narrow”, r.).

#### **3.2.4.5 Potential Advantage 2: Utilization of Different Parameterizations of Algorithms**

The choice of the parameters of an algorithm drastically influences its performance (see also subsection 3.2.2.5). One of the big problems with the parameterization is that due to the infinite combinations of robots and environments, most planners will perform badly for at least some “pathological” cases, for example where the C-space is extremely dense. However, the default parameter set of for instance a PRM planner might not be designed for solving this particular case, but to perform well in the majority of the planning tasks. Using our approach, well-proven default and purpose-built parameter sets can be used for arbitrary scenarios.

#### **3.2.4.6 Potential Advantage 3: Adaptive Parameterization of the Algorithms**

In addition to the utilization of different parameter sets for path planning algorithms, these parameters should be adapted online. In the previous sections, we pointed out that especially the performance of PRM planners relies on appropriate parameters such as the number of initial states or the desired density of the map. Based on PRM performance criteria such as query time and query success, these parameters can be adaptively balanced.

#### **3.2.4.7 Potential Advantage 4: Advanced Adaptive OR-Parallelization Scheme**

If there are enough processing resources that all relevant planning algorithms can be executed simultaneously, an advanced adaptive OR-parallelization can be realized: Based on the evolution of the path planning duration of the individual algorithms, the candidate(s) with the highest likelihood of fast path planning results is identified online and subsequently started more often than the other planners. Alternatively, the k-processor prediction method proposed in [44] can be utilized to gain an estimate of the path planning performance. Based on the definition of specific criteria, an optimization of the OR-parallelization can be performed. This optimization should take into account the quality of the estimation of the path planning durations; for example it has to ensure that sufficient “non-optimal” algorithms are running.

### **3.2.5 Conclusion**

Until recently, there had been no easy-to-use, powerful generic path planning software. Thus, the sampling-based path planning library SamPP was developed [66] and subsequently improved, enhanced, and evaluated. At first, we gave an overview of SamPP and its most fundamental aspects of it.

For the evaluation of SamPP, firstly it was successfully applied to a path planning scenario involving a robot with 10 DOF. This proved its ability to solve a high-dimensional path planning scenario. Secondly, it was applied to different car door kinematics with two DOF, where it shows a superior performance (typical maximum path planning duration  $\leq 20$  ms). For the case of 300 to 400 obstacles, nearly “worst-case” placed in the workspace of these car doors, we found typical mean values for the path planning time in the area of 50 ms for RRTs, 1500 ms for building a PRM, and 30 ms for PRM queries. Thirdly,

the influence of the parameterization of the path planning algorithms is discussed and recommendations for the parameter tuning are given. A comparison with the state of the art, open-source sampling-based path planning library OpenRAVE reveals that the performance of SamPP is indeed very high.

The evaluation results show that the performance of SamPP is indeed sufficient for the haptic real-time assistance of a human in various scenarios with two DOF even with single-threaded applications. This has been evaluated successfully by a user study which is described in subsection 4.1.5.

Furthermore, we enhanced the path planning performance for unknown or dynamical environments significantly by the OR-parallelization of different path planning queries. This Generalized OR Paradigm is a novel concept that to the best of our knowledge has not been proposed beforehand. In the future, it will enable path planning within the globally minimum time span by massively-parallel brute-force computation of all known path planning algorithms with finely discretized parameter sets.

To exploit the advantages of the Generalized OR Paradigm in the near future on current hardware, four promising research directions have been proposed: The combination of different algorithms (e.g. RRTs and PRMs), the concurrent use of different parameter sets of path planning algorithms, the online adaptation of these parameter sets to the respective environment, and the online adaptation of the types and numbers of parallel executed planning threads to the respective problem.

### 3.3 Collision Avoidance: Reducing the Risk of a Collision

Actuated car doors should be equipped with a collision avoidance system for several reasons:

1. During manual operation of the car door, the user can be prevented from inadvertently damaging the door. This is especially helpful if there are obstacles in the workspace of the door that the user did not see. Furthermore, it provides a high convenience in narrow parking lots, as the user does not have to worry too much about how wide the door can be opened.
2. It gives additional safety for the automatic car door operation. Though the commanded motion of the door given by the controller should be collision-free due to path planning, this is not necessarily the case:
  - a) Sensor noise or the limited capabilities of the implemented algorithms can lead to a path which indeed was never collision-free.
  - b) The collision-free path is so close to an obstacle that a potential position deviation arising from the non-linear door dynamics is sufficient to cause a collision.
  - c) There is no guarantee at all that the environment did not change since the determination of the “collision-free” path.

Collision avoidance with respect to obstacles as well as self-collisions has a long history in robotics. Common approaches include artificial potential fields [137], the collision Jacobian [131], certainty grids [176], and the virtual force field method [29]. However, it has been shown that these methods exhibit limitations, for instance the possibility of oscillations [144]. Furthermore, these algorithms are often not applicable to scenarios with a very high number of obstacles. This assumption is backed by our observation that no description of such a collision avoidance method has been proposed for problems involving a very high number of obstacles.

Current approaches focus on the tracking or prediction of obstacles, e.g. by Kalman filtering [272, 127, 167] or by the use of special-purpose vision systems. For instance, visual-servoing enables operation in the image plane, such that there is no need for handling 3D data (3DD) at all [177]. However, the method is not generic, requires specific hardware, and cannot be applied to car doors practically – their geometry would require a lot of vision systems. Another interesting approach formulates obstacle avoidance as a constrained optimization problem [30]. However, this cannot be solved easily in real-time for a very high number of obstacles by current standard computing hardware [169]. This is especially important for this work because collision avoidance is part of the haptic rendering loop.

As a work-around to this problem, multi-rate techniques have been proposed. Sometimes, this includes the generation of a “local model” with a very limited number of nodes to achieve a stiff real-time haptic interaction [128, 53]. For instance, [196] proposed using a virtual coupling to interconnect a fast “haptic thread” with a slow “contact thread”. This is also a typical example of how the haptic rendering of objects or a generic collision avoidance is achieved: A collision detection method calculates repulsive forces with respect to the given configuration.

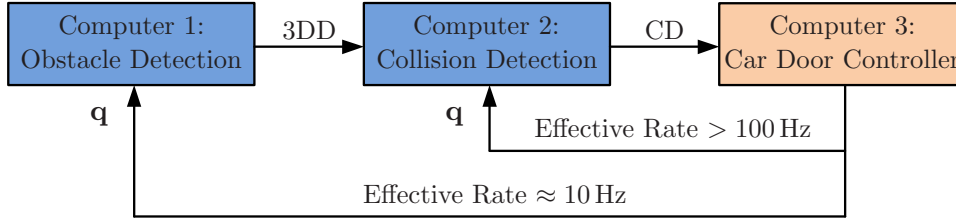


**Figure 3.13:** Implementation of a typical multi-rate architecture for an automotive obstacle avoidance system.

Collision detection is widely used in computer graphics and VR simulations. For a survey of collision detection see [157]. To achieve a high performance index for the collision avoidance system, collision detection has to be very efficient. Numerous comparisons have been made between collision detection algorithms as well as between their implementations (see [42, 279]). They all point out that the performance greatly depends on the respective scenario, e.g. the number, size, arrangement, and representation of the objects. Representative problems for the comparison of different implementations are given in [256].

Our specific benchmark scenarios were characterized by the following (see Appendix D.2):

- Relevant object: Moving car door body and kinematics
- Relevant obstacles: High, but limited number of 3D primitives ( $\leq 1000$  cubes)

Based on the 3DD provided by the obstacle detection system, a potential collision between the car door and other objects should be counteracted by the actuation of the car door. In our setup, an obstacle detection system is used which can operate both on simulated and real images (see Appendix D.1 and [241] for details). In Fig. 3.13, the overall architecture of the obstacle avoidance system for car doors is displayed. As the camera is attached to the car door, the car door state  $\mathbf{q}$  is required to calculate the 3DD, which is given in world coordinates  $\mathbf{x}$ . Based on the 3DD, collision detection is performed. The corresponding collision data CD is transmitted to the car door controller via UDP communication; see subsection 4.1.1 and Appendix E.

In the following, we examine different collision detection libraries for a realistic car door scenario. After that, we describe the implementation of a multi-threaded collision detection. Based on this, a variety of state-of-the-art collision avoidance methods can be utilized.

### 3.3.1 Performance Benchmark of Collision Detection Libraries

A variety of collision detection libraries (CDLs) have been developed in recent years. Most of them are implementations of the Separating Axes Theorem [104], the GJK algorithm [98], or the Lin-Canny algorithm [156]. Besides using different algorithms, they significantly differ in terms of the internal object representation: the bounding volumes (BV) and the bounding volume hierarchy (BVH).

An overview of relevant CDLs is given in Tab. 3.6 (left). All these CDLs can be used to check whether 3D objects intersect. Some of the CDLs can perform not only collision

detection (CD) between two or more objects, but can also compute the penetration depth (PD) and/or the minimal distance (MD) between them. The additional information that is provided by the PD and MD data are the location and the proximity between two objects. This information is very valuable for collision avoidance, because it enables the direct calculation of an appropriate assistance effect  $\mathbf{f}_{as}$ . Currently, the only libraries providing both PD and MD are BULLET [57] and SOLID [261].

To benchmark the CDLs, a realistic scenario had to be defined. The preconditions and assumptions for the overall collision avoidance were as follows:

- The position and orientation of the car door are known.
- The objects are static or moving slowly (maximum velocity: pedestrian speed).
- There is no object tracking. Only the low-level information (primitives) of the vision system is available.
- All current primitives (maximum number: 1000) computed by the vision system are provided to the respective CDL.

A quasi-static benchmark scenario accounting for these points has been defined, containing a bounding volume of the car door with 64 vertices, 10 oriented boxes that bound the left hand side of the car body, and 100 primitives representing two objects: a cylindrical one (like a lamppost) and an asymmetric one (like a bush).

Most CDLs do not support the use of spheres, so oriented cubes (Or. Cube) have been chosen for the bounding boxes of the feature points detected by the vision system; compare Appendix D.1. Every CDL has been benchmarked using the defined scenario by performing 10,000 consecutive runs. The position and orientation of both the door and the objects were randomized each time. A Linux system with an Intel Pentium M 1.76 GHz and 512 MB RAM served as a test bed. The minimum, mean, and maximum time of all runs was calculated and stored; see Tab. 3.6 (right).

The safety of the overall system is determined by the maximum time consumption that can occur, so in our case this is the most relevant factor. It turned out that SOLID outperformed all other libraries (both in maximum and mean time consumption). Besides the efficiency of the modified GJK algorithm relative to the defined scenario, a major reason for the fast execution of the single runs is due to the efficient way objects are handled by SOLID. One reason for the poor performance of other libraries results from their computationally expensive scene building. The only other library that also showed a good performance and is not restricted to CD is Bullet [57]. In the future, Bullet might become an interesting alternative to SOLID, because it is a rapidly advancing Open Source project, while SOLID is no longer enhanced.

It should be noted that the speed can further be increased by porting the algorithm to a FPGA design. For instance, [208] report a speed-up of factor 4 when compared to a state-of-the-art software intersection test.

#### 3.3.2 Multi-Threaded Collision Detection

For the collision detection, we chose to determine the minimum distance/penetration depth for each individual geometrical primitive using SOLID. Thus, the collision detection prob-

**Table 3.6:** Collision Detection Libraries (CDLs): Overview and Benchmark Results.

| Library Properties    |            | Benchmark: Maximum Time Consumption [ms] |         |         |         |
|-----------------------|------------|--|---------|---------|---------|
| Name, Version, Link   | Algorithm  | Obstacle                                 | CD only | CD & PD | CD & MD |
| Bullet, 2.61, [201]   | GJK (mod.) | Or. Cube                                 | x       | 32.03   | 32.03   |
| ColDet, 1.1, [188]    | Sep. Axis  | Pyramid                                  | 24.19   | x       | x       |
| ODE, 0.9, [229]       | Sep. Axis  | Or. Cube                                 | 24.32   | x       | x       |
| PQP, 1.3, [189]       | Sep. Axis  | Or. Cube                                 | 32.15   | x       | 33.61   |
| QuickCD, 1.0, [142]   | Sep. Axis  | Pyramid                                  | >100    | x       | x       |
| RAPID, 2.01, [190]    | Sep. Axis  | Or. Cube                                 | 35.47   | x       | x       |
| SOLID, 3.5.6, [260]   | GJK (mod.) | Or. Cube                                 | 19.48   | 24.65   | 21.64   |
| SWIFT++, 1.2, [191]   | LC (mod.)  | Or. Cube                                 | 56.31   | x       | 98.27   |
| V-Clip, 1.0, [174]    | LC (mod.)  | Or. Cube                                 | 82.15   | x       | 82.15   |
| V-COLLIDE, 1.1, [192] | Sep. Axis  | Or. Cube                                 | >100    | x       | x       |

lem is “embarrassingly parallel”. We intended to exploit this fact by a multi-threaded implementation whose algorithm is given in Alg. 1.

We initialize the program by setting up the UDP connections and building the scene as a 3D world in SOLID. For this, we use an approximate 3D VRML model of the car door and the predefined maximum number of primitives. After that, we copy this world for each of the  $n$  POSIX threads – a mere instantiation is not sufficient, because all threads would operate on the same 3D data.

In the main loop, the most current 3DD and  $\mathbf{q}$  is used to update each of the  $n$  3D worlds after all obstacles have been reset to the default location outside the workspace of the car door. After all of the threads finished the collision check for their portion of the obstacles, the worst of all collision states  $CS$  is picked as the collision data  $CD$  to be sent to the car door controller.

The effectiveness of our approach can be seen from the benchmark results given in Tab. 3.7: By increasing the number of collision threads, we achieved a significant decrease of the minimum, maximum, and average computation time. Using six parallel threads, a worst-case computation time  $< 5$  ms was achieved. In practice, this enables a real-time haptic collision avoidance support.

The benchmark was performed 100 times on a 32-core 64-bit computer with 128 GB RAM. The benchmark scenario was a car door with two DOF within a randomized number of obstacles within or near the workspace of the door. Their position as well as the configuration  $\mathbf{q}$  of the car door was randomized, too.

**Algorithm 1** Multi-Threaded Collision Detection.

---

**Require:**  $n > 0$ 

```
1: udpFromCamera.initialize(); udpFromCamera.run()
2: udpFromCarDoor.initialize(); udpFromCarDoor.run()
3: udpToCarDoor.initialize(); udpToCarDoor.run()
4:  $Q \leftarrow 0$  {car door configuration}
5:  $3DD \leftarrow 0$  {3D obstacle information}
6:  $CS \leftarrow 0$  {collision states}
7:  $CD \leftarrow 0$  {final collision data}

8: solid.world.initialize(Q, 3DD)

9: for  $i = 1$  to  $n$  do
10:   collision[n].initialize(solid.world)
11: end for

12: loop {use last received data  $q$  and  $x$  to calculate  $CS$ }
13:    $Q \leftarrow \textit{udpFromCarDoor.q}$ 
14:    $3DD \leftarrow \textit{udpFromCamera.3DD}$ 
15:    $\textit{num3DD} \leftarrow \textit{max}(\textit{size}(3DD))$ 
16:    $\textit{len3DD} \leftarrow (\textit{int})\textit{num3DD}/n$ 

17:   for  $i = 1$  to  $n$  do
18:     collision[n].q  $\leftarrow Q$ 
19:     collision[n].x  $\leftarrow \textit{default}$ 
20:     collision[n].x  $\leftarrow X(((i - 1)\textit{len3DD}) : \textit{min}(i(\textit{len3DD} - 1), \textit{num3DD}))$ 
21:     collision[n].solid.world.update()
22:     collision[n].run()
23:   end for

24:   while not all collision threads finished do
25:     sleep(10us)
26:   end while

27:    $CD \leftarrow \textit{worstCaseCollisionState}(CS)$ 
28:   udpToCarDoor.data  $\leftarrow CD$ 
29:   udpToCarDoor.send()
30: end loop
```

---

**Table 3.7:** Performance evaluation of the multi-threaded collision detection (measure:  $t$  [ms]).

| CD Threads | min  | max   | $\sigma$ | E     |
|------------|------|-------|----------|-------|
| 1          | 3.00 | 15.59 | 0.38     | 14.03 |
| 2          | 7.34 | 8.73  | 0.10     | 7.39  |
| 3          | 2.93 | 7.30  | 0.12     | 6.03  |
| 4          | 0.27 | 5.42  | 0.33     | 4.98  |
| 6          | 0.24 | 4.95  | 0.41     | 3.51  |

### 3.3.3 Collision Avoidance

#### 3.3.3.1 Basics and preconditions for the deceleration of car doors

The goal is collision avoidance which counteracts a contact situation between the car door and external obstacles. Similar to the notation of [131], this problem can be formulated in the state space notation as a switching to the maximum deceleration at the time-step  $t = t^0$ . If the switching event occurs right on the critical switching surface, the door will stop at time  $t_e$  right at the critical position  $\mathbf{q}_{crit}$ :

$$\begin{pmatrix} \dot{\mathbf{q}} \\ \mathbf{q} \end{pmatrix} = \begin{pmatrix} -\ddot{\mathbf{q}}_{max}t + \dot{\mathbf{q}}^0 \\ -\frac{\ddot{\mathbf{q}}_{max}}{2}t^2 + \dot{\mathbf{q}}^0t + \mathbf{q}^0 \end{pmatrix} \longrightarrow \begin{pmatrix} 0 \\ \mathbf{q}_{crit} \end{pmatrix} = \begin{pmatrix} -\ddot{\mathbf{q}}_{max}t_e + \dot{\mathbf{q}}^0 \\ -\frac{\ddot{\mathbf{q}}_{max}}{2}t_e^2 + \dot{\mathbf{q}}^0t_e + \mathbf{q}^0 \end{pmatrix} \quad (3.6)$$

If we assume that  $|\dot{\mathbf{q}}|$  is bounded by  $\dot{\mathbf{q}}_{max}$ , the worst-case deceleration duration is given by  $t_{e,wc} = \frac{\dot{\mathbf{q}}_{max}}{\ddot{\mathbf{q}}_{max}}$ . Thereby, the worst case angle where the full deceleration torque has to be applied is given by

$$\mathbf{q}_{e,wc} = -\frac{1}{2} \frac{\dot{\mathbf{q}}_{max}^2}{\ddot{\mathbf{q}}_{max}} + \frac{\dot{\mathbf{q}}_{max}\dot{\mathbf{q}}^0}{\ddot{\mathbf{q}}_{max}} + \mathbf{q}^0 \quad (3.7)$$

and the corresponding worst case motion between the application of the full deceleration torque and the actual stop of the door is

$$\Delta\mathbf{q}_{wc} = \mathbf{q}_{e,wc} - \mathbf{q}^0 = -\frac{1}{2} \frac{\dot{\mathbf{q}}_{max}^2}{\ddot{\mathbf{q}}_{max}} + \frac{\dot{\mathbf{q}}_{max}\dot{\mathbf{q}}^0}{\ddot{\mathbf{q}}_{max}} \Big|_{\dot{\mathbf{q}}^0=\dot{\mathbf{q}}_{max}} = \frac{1}{2} \frac{\dot{\mathbf{q}}_{max}^2}{\ddot{\mathbf{q}}_{max}}. \quad (3.8)$$

However, additionally the dynamics of the overall control loop have to be considered, especially the dead time  $t_{del}$  given by communication and computation of the collision avoidance loop. This is described in the following over-approximation:

$$\Delta\mathbf{q}_{wc,tot} = t_{del}\dot{\mathbf{q}}_{wc} \longrightarrow \Delta\mathbf{q}_{wc} = t_{del}\dot{\mathbf{q}}_{wc} + \frac{1}{2} \frac{\dot{\mathbf{q}}_{max}^2}{\ddot{\mathbf{q}}_{max}} \quad (3.9)$$

For a typical hardware setup of the prototype of an electro-mechanically actuated car door (see Fig. 3.14), the following components and time consumptions have to be considered (loop from sending current state to applying decelerating torque):

- ❶  $t_{Udp} \approx 2ms$  : Delay of UDP connection, possibly packet loss
- ❷  $t_{Cam} \approx 60ms$  : Duration of 3DD determination (based on sensor data)
- ❸  $t_{Udp} \approx 2ms$  : Delay of UDP connection, possibly packet loss
- ❹  $t_{Coll} \approx 5ms$  : Duration of collision detection and output calculation
- ❺  $t_{Udp} \approx 2ms$  : Delay of UDP connection, possibly packet loss
- ❻  $t_{Sim} \approx 1ms$  : Clock frequency of simulated controller
- ❼  $t_{Adc} \approx 0ms$  : A/D conversion time
- ❽  $t_{Pow} \approx 1ms$  : Bandwidth of inverter
- ❾  $t_{Act} \approx 3ms$  : Bandwidth of actuator

$$\longrightarrow \Delta t_{total} \approx 3 \cdot t_{UDP} + t_{Cam} + t_{Coll} + t_{Act} \approx 75ms \quad (3.10)$$

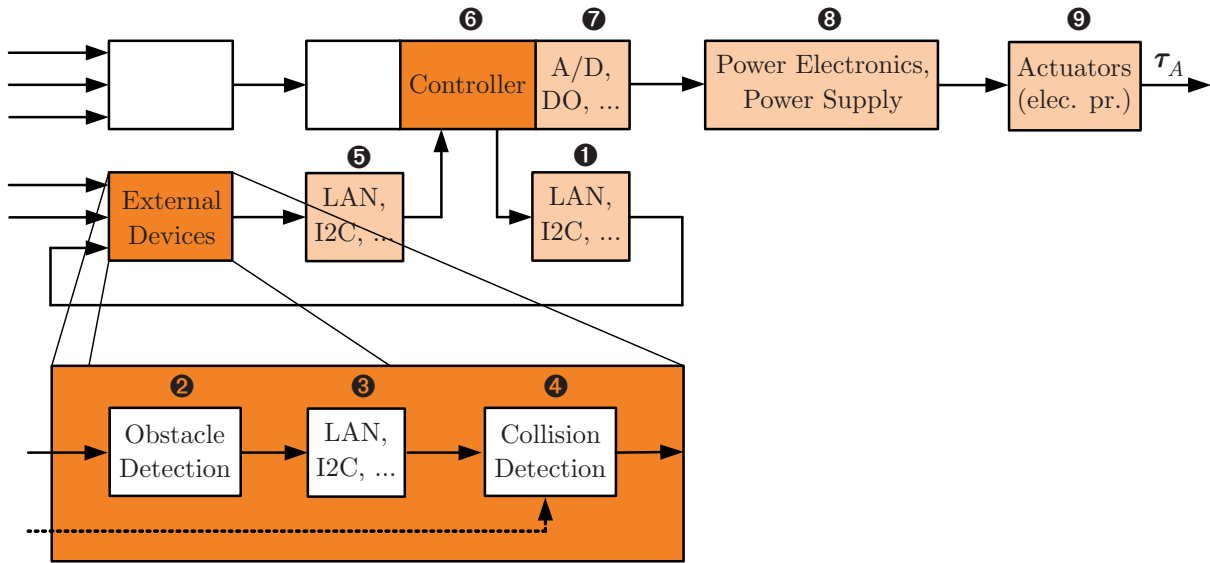


**Figure 3.14:** Relevant elements of the AAC-based collision avoidance implementation: The actuation effect  $\tau_A$  heavily depends on the structure and the time consumption of the individual elements of the overall system.

Obviously, with a time share of  $\approx 80\%$  the bottleneck of this loop is the obstacle detection system. This can be overcome by passing the system state  $\mathbf{q}$  directly from the door controller to the collision detection system. We assume the typical case that the obstacles are static or moving slowly. Then, the motion of the car door has much more impact on the collision situation so that we can pass the state of the car door directly to the collision detection. This results in a speed-up of factor 6:

$$\Delta t_{total} \approx 2 \cdot t_{UDP} + t_{Coll} + t_{Act} \approx 13ms \quad (3.11)$$

In our setup, advanced methods to deal with lag as for example proposed in [278] cannot be used, because in general there is no a-priori knowledge about the real or virtual environment.

### 3.3.3.2 Overview of Applicable Collision Avoidance Methods

The fast determination ( $< 5ms$ ) of the distance or the penetration of a car door and potential obstacles enables a variety of different methods for avoiding a collision. In the following, we give an overview of potential approaches and implementations.

Based on the multi-threaded collision detection described in subsection 3.3.2 and the preconditions given in subsection 3.3.3.1, high-performance collision avoidance can be implemented using one of the following methods:

1. Virtual repulsive force using Jacobian:

Based on the worst-case distance or the penetration vector of the collision check, a virtual force is applied on the model of the car door at the respective collision location. This can easily be implemented based on the Jacobian of the car door.

The virtual force has to be large enough to decelerate the approach such that no collision occurs.

2. Collision Jacobian, see [131]:

This collision-avoidance method supposes the use of homogeneous 3D shapes, which is not the case for car doors. However, it could either be modified accordingly, or the 3D shape of the car door could be over-approximated to form a homogeneous 3D shape.

3. Speed-dependent adaptation of the obstacle bounding box size:

The bounding boxes provided by the obstacle detection system (3DD) are increased by an additional safety margin  $r = f(\Delta\mathbf{q}_{wc}, \dot{\mathbf{q}})$ . Thus, a collision is indicated as soon as a critical configuration can possibly occur. This is an indirect and very conservative approach, as it operates on worst-case assumptions.

4. Direction-based adaptation of car door bounding box:

Similar to the adaptation of the obstacle bounding box size, the bounding box of the door can be adjusted by an additional safety margin. However, this can hardly be done in real-time for complex shapes. A remedy is the use of precomputed convex hulls of the moving door, which requires appropriate safety margins as well as a transformation according to the current door position and orientation.

5. Parallel collision detection for several car door bounding boxes:

Precomputed convex hulls of the door can also be used for another collision detection method: A finite number of car door bounding boxes with different safety margin can be checked for collision in parallel. The safety margins of the largest non-colliding bounding box can then be used to compute the upper limits for the motion of the door.

The above methods can be implemented with different characteristics, for instance:

1. Deceleration or full stop: The collision avoidance decelerates the door such that no collision occurs. A variation is the application of a full-stop in dangerous situations, such that for instance the human user necessarily notices the controller action.
2. Impact diminishing: If there is no chance to prevent the collision, at least the impact could be diminished by minimizing the collision velocity between obstacle and impact location at the car door.
3. Active avoidance: In combination with a kinodynamic motion planner, even an active avoidance could be implemented which in some situations even applies an accelerating torque to prevent a collision from happening.

A detailed investigation of these methods and approaches is beyond the scope of this thesis. Our own implementations are described in subsection 4.1.3, in subsection 4.2.6.2, and in subsection 5.2.3.4.

### 3.4 Summary

To achieve an intuitive, convenient, and safe operation of actuated car doors with arbitrary kinematics, three generic support methods have been investigated.

For mechanisms with more than one DOF, preferable paths or trajectories can for example be predefined, e.g. based on ergonomic investigations or on optimality criteria (minimum jerk, time, etc.). These motions can be utilized as Static Virtual Fixtures. Our advanced implementation combines these Static Virtual Fixtures with Dynamic Virtual Fixtures to achieve intuitive manual handling and to enable the operator to switch between predefined paths. This is supported by an online estimation of the intention of the user and a subsequent calculation and update of the Dynamic Virtual Fixture which guides the motion towards the predefined path with the highest likelihood.

Especially in the presence of obstacles, predefined paths must not be used without additional measures. One possibility is to compute collision-free paths online, which necessitates a near real-time path planner. This can be used as the foundation of Dynamic Virtual Fixtures during manual operation, or as controller input during automatic operation. We developed a suitable generic path planning library and showed that the performance is sufficient for a real-time haptic support. Furthermore, we proposed the Generalized OR Paradigm, which enables an advanced adaptation and optimization of multi-threaded path planning.

We described why collision avoidance is a prerequisite for both manual and automatic operation of a car door. With our multi-threaded approach, we achieved response times of  $\approx 13$  ms, enabling real-time haptic support and the use of bounding boxes which are tight approximations. Furthermore, several implementation approaches have been described.

One or more of these three methods can easily be integrated into AAC schemes, by applying their respective supportive effect  $\mathbf{f}_{as}$  in parallel to the human user input  $\mathbf{f}_u^*$  exerted on the virtual model (EOM) of the car door. Our applications of these methods with simulated car doors as well as with hardware prototypes are described in Chap. 4 and Chap. 5.

## 4 VRP of Actuated Car Doors: Control, Simulation, and Evaluation

Even the design of “conventional” rotational car doors with one DOF is a challenging task; compare Appendix A. For instance, while the mass of the car door body should be minimized to reduce overall power consumption, its rotational inertia resulting from the distribution of the mass is a design parameter for which no concrete guideline exists. The same holds for the choice of other elements and properties that affect the haptic interaction. In practice, engineers try to balance all factors based on best practices and personal experience. This procedure is not viable for car doors with more than one DOF, because there is no previous knowledge, and the overall dynamics resulting from the coupling of the single DOF can be very complicated. Additionally, the complexity increases when actuated car doors are to be developed, because the implementation of controllers offers a broad range of design alternatives. This necessitates appropriate tools for enabling an efficient and effective design of the car door and its controller.

Our approach is to utilize VRP with haptic feedback to develop, simulate, control, and evaluate new door concepts (compare Chap. 2). To achieve this efficiently and effectively, we had to develop a generic VRP test bed for car doors with arbitrary kinematics (Sec. 4.1) as well as a high-fidelity door simulator with one rotational DOF (Sec. 4.2). Using these tools, basic research is conducted for a variety of car doors to investigate which dynamics, controllers, and support methods (compare Chap. 3) are preferred by human users.

### 4.1 VRP of Actuated Car Doors with Several DOF

In this section, we describe a generic VRP test bed for the high-fidelity multi-modal simulation of actuated systems. We subsequently use this system to simulate different car doors with more than one DOF by Active Admittance Control (AAC, see Sec. 2.3), and to develop suitable controllers for them. On this foundation, a variety of user studies and evaluations were performed, enabling a rating of the doors in terms of, for example, usability and attractiveness without the need for any physical prototypes. To the best of our knowledge, this is the first time that actuated car doors with more than one DOF have been investigated. This assumption is supported by the fact that no patents or other publications prior to [242, 244] are known which deal with providing more than one DOF for manual car door operation.

#### 4.1.1 Generic VRP Test Bed

Our main concern is to develop actuated car doors which provide a superior haptic interaction for the users by utilizing haptic simulations. In Chap. 2, the history and the

basics of VRP with haptic feedback have been described. The haptic rendering of a virtual prototype depends on three criteria:

1. Accurate model of the virtual prototype (see subsection 2.2)
2. Appropriate interfaces, e.g. the haptic device
3. Advanced controller for rendering the model on the haptic device

This necessitates a high-fidelity haptic rendering device and a corresponding algorithm, because otherwise no qualified judgment of the simulated mechanism can be gained. Hardware issues are described in subsection 4.1.1.1; the controller for the haptic rendering is discussed in subsection 4.1.1.3. Furthermore, a networked system had to be set up which enables the simulation of all parts of the desired actuated system (compare Fig. 1.1). Thereby, computing-intensive applications such as obstacle detection, collision avoidance, and path planning are interconnected with the real-time haptic simulation. This enables the possibilities provided by Active Admittance Control (AAC) to be fully exploited.

### 4.1.1.1 Haptic Rendering: Hardware

An ideal haptic device for the rendering of arbitrary mechanisms displays the simulated mechanism as if it were a real mechanism such that the user cannot detect any difference between the two [7]. A variety of requirements have to be met to reach the so-called transparency [259]. For the realistic rendering of large mechanisms, in particular the following properties are crucial:

- Large Workspace ( $\gg 0.1 \text{ m}^3$ ) and sufficient number of actuated DOF
- High output capability ( $F \gg 25 \text{ N}$ ,  $\tau \gg 1 \text{ Nm}$ )
- High mechanical rigidity and control stiffness

There exist very few devices that exhibit these properties [166]. The ViSHaRD10 [259], which is used in this work and is displayed in Fig. 4.1, is one of them: It perfectly meets the requirements by providing a peak force of 170 N and a peak torque (pitch/yaw) of 13 Nm in a cylindrical, singularity-free six DOF workspace of  $\varnothing 1.7 \text{ m} \times 0.6 \text{ m}$ . In contrast, a standard industrial robot which could be a prospective interface in terms of stiffness and output capability fails in providing favorable dynamics and poses serious safety issues.

Active Admittance Control (AAC) aims at the kinesthetic haptic simulation. This corresponds to the motion and pose of the limbs of the human user. Besides this, users perceive tactile feedback when touching an object. Thus, to minimize confusion, the haptic interface should not only render the dynamics of a car door kinesthetically, but also should render the corresponding tactile feel of the surface. In fact, the end-effector would ideally *be* the interfacing part, such as a car door handle. Therefore, we had an inner and outer door handle manufactured out of a real car door to serve as end-effector of the ViSHARD10. These are depicted in Fig. 4.2.

### 4.1.1.2 System Architecture

The VRP system aims at realistically rendering a mechatronic system that will be integrated into the car communication architecture. Therefore, at a first glance it seems



**Figure 4.1:** VRP test bed for the high-fidelity haptic rendering of actuated car doors. The virtual scene is visualized by a projector. For an improved immersion, an HMD with a head tracking system to show the correct perspective can be used.



**Figure 4.2:** Inner (l.) and outer (r.) car door handles modified for use as end-effectors at the generic VRP test bed.

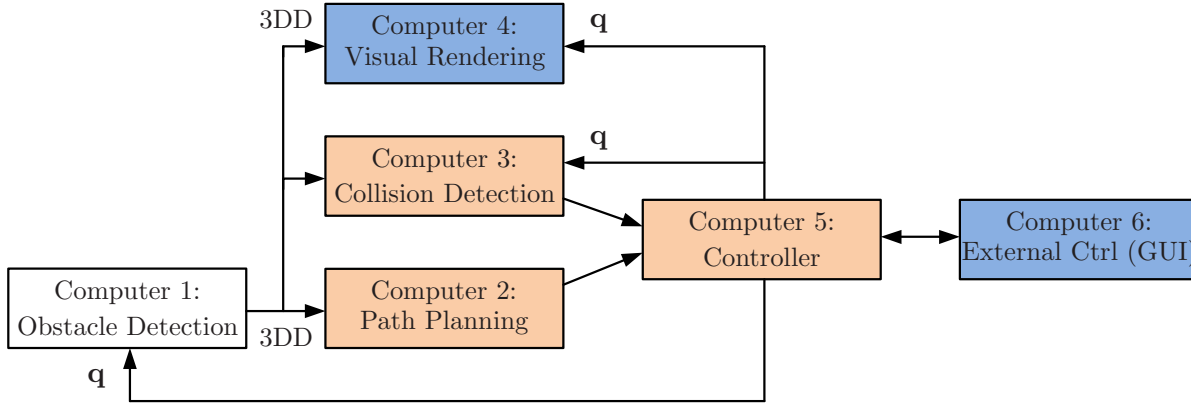


**Figure 4.3:** Architecture of the overall networked system for the VRP of actuated car doors where the computing-intensive tasks have been separated from the car door controller/simulator.

reasonable to make use of a fast communication medium that is already being used in cars such as FlexRay or MOST.

However, in contrast to an Ethernet-based communication they are rather complicated to use in our hardware setup. As we are only in a proof-of-concept stage, and as Ethernet is expected to find its way into the automotive mass production [210], using Ethernet with UDP or TCP seemed a sensible option. While TCP enables a safe communication without packet loss, UDP is considerably faster due to the lack of communication overhead. Thus, UDP has been the preferred choice in many real-time control applications, enabling a comparatively good QoS if many high-frequency connections have to be established.

The UDP-based architecture of the overall VRP test bed is shown in Fig. 4.3. We performed numerous tests to verify that a high QoS is achieved even if a high network load occurs. Even for demanding data exchange situations, we got very satisfying results (full details are provided in Appendix E). This means that we do not have to consider QoS issues in the following.

#### 4.1.1.3 Haptic Rendering: Feedback-Linearized Position Control

To achieve a high degree of transparency in the display of the simulated dynamics of the virtual prototype, the dynamics of the haptic device have to be masked toward the human user. There are several approaches for doing this; see for example [258] for an overview.

We implemented three joint-based controllers: a conventional PD controller, a computed torque (CT) controller, and a combined feedforward+PD (FFPD) controller. Implementation issues are described for the CT controller (see Appendix C.1) as well as for the FFPD controller (see Appendix C.2). The three controllers are compared with respect to three criteria: 1) Robustness with respect to the minimally renderable mass and inertia, 2) the motion tracking error, and 3) the subjective quality of the haptic rendering.

**Robustness:** One performance measure of admittance-type haptic devices is the minimally renderable mass and inertia [258]. We asked participants to iteratively try to cause

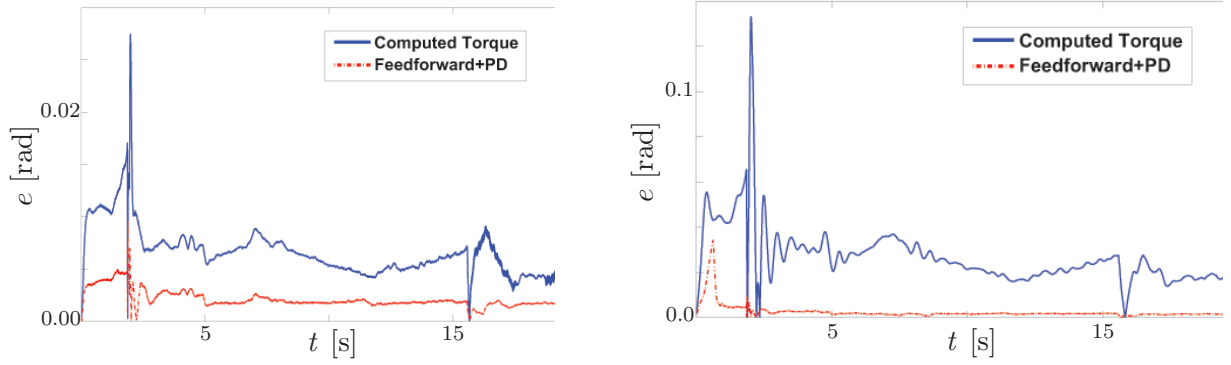


**Figure 4.4:** Motion tracking error in joint 4 of VISHARD10 for critical damping in all joints (l.) and heuristically tuned damping (r.) according to Tab. C.2 and Tab. C.1 [209].

instability of the haptic interaction while decreasing the simulated mass and inertia in a six DOF setting. The resulting minimum values are given in Tab. 4.1.

These values are a little bit higher than the findings of Ueberle, who reported a minimum mass of  $\text{diag}\{6, 7, 2\}$  and a minimum inertia of  $\text{diag}\{0.03, 0.02, 0.01\}$  for resolved acceleration control [257]. This difference is due to the fact that our end-effector exhibits a higher inertia when compared to the lightweight cylindrical one used in [257]. Inertias between the force sensing unit and the human user are known to affect the stability of haptic rendering; compare [200].

**Table 4.1:** Stability: Minimally renderable mass and inertia.

| Controller | Minimum mass [kg]          | Minimum inertia [kgm <sup>2</sup> ] |
|------------|----------------------------|-------------------------------------|
| PD         | $\text{diag}\{10, 12, 7\}$ | $\text{diag}\{0.05, 0.05, 0.03\}$   |
| CT         | $\text{diag}\{9, 10, 5\}$  | $\text{diag}\{0.08, 0.03, 0.01\}$   |
| FFPD       | $\text{diag}\{6, 7, 2\}$   | $\text{diag}\{0.03, 0.02, 0.01\}$   |

**Motion Tracking Error:** For a given user interaction force  $\mathbf{f}_u^*(t)$ , the joint error is determined. Generally, the FFPD implementation exhibited a smaller error than the PD and CT implementations. The reason lies in the fact that the PD-action of the CT controller is filtered by the estimated mass matrix. In Fig. 4.4, the joint 4 error is displayed.

**Subjective Quality of the Haptic Rendering:** We asked several subjects to subjectively compare the quality of the haptic rendering for the three control schemes for different interaction motions and forces. The only difference they noted was the lower stiffness in the wrist joints for the FFPD controller.

**Conclusion:** The FFPD controller provides a smaller tracking error and lower renderable masses/inertias than the CT controller. However, for critical damping it exhibits vibrations in the wrist joint and thus deteriorates haptic rendering if the stiffness is not

decreased. Therefore, our solution is a combination of both control approaches: We apply a CT controller to the four wrist joints and a FFPD controller to all other joints. The reference controller parameters are given in Tab. C.2 and Tab. C.1. However, for our special case of the simulation of actuated car doors with typical masses/inertias higher than 20 kg/10 kgm<sup>2</sup>, the perceived difference is almost negligible.

#### 4.1.2 Comparison of Five Different Car Door Kinematics

Within the framework of MechaTUM [92], a variety of car door concepts were developed at the department of Micro Technology and Medical Device Technology (MIMED) of the TU München. Some of them are depicted in Fig. 4.5.

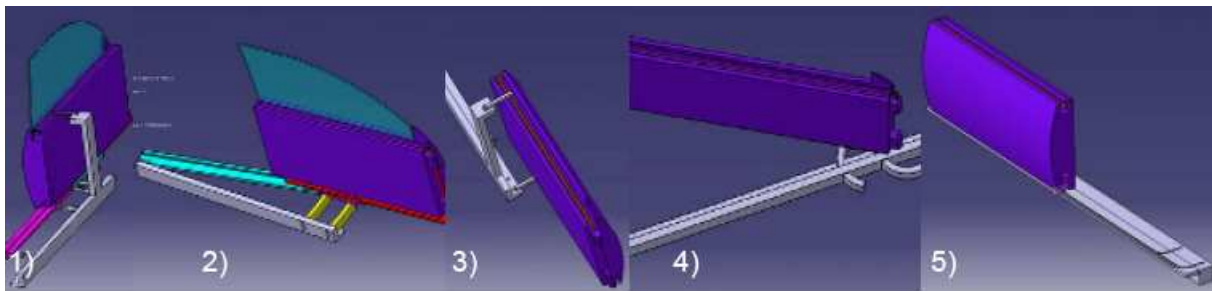


**Figure 4.5:** Different car door concepts investigated at the institute MIMED (TU München), including pivotable door sills (1,2), two-DOF doors (3,4), and a sliding door (5) [220].

Based on objective and subjective measures, a preselection had been performed. Two favorable concepts turned out to be a Two-Link Door (TLD) and a Swing-Sliding Door (SSD); compare the sketches given in Fig. B.1. For a heuristic evaluation of the appreciation of variations of these doors, five scenarios were set up at the VRP test bed:

- Scenario 1 (one DOF): Unactuated sliding door
- Scenario 2 (one DOF): TLD with the restriction  $q_2 = q_1$
- Scenario 3 (one DOF): TLD with the restriction  $q_2 = 5q_1$
- Scenario 4 (one DOF): SSD with the restriction  $q_2 = 0$  for  $q_1 < q_{1,max} = \pi/2$
- Scenario 5 (two DOF): SSD as given in Fig. B.1

The evaluation has been conducted together with Adel Olaf Sabbah from the Institute of Ergonomics of the TU München. We worked with 18 participants, most of whom were male scientists or students at the TU München. They had to rate each of the randomized scenarios on a CP10 scale, i.e. from 1 (“very bad”) to 10 points (“very good”). The results are given in Tab. 4.2.

Besides the absolute rating given by the participants, the relative order of the door concepts is given. This measure is calculated from the absolute ratings and corresponds to the preference of a door concept (neutral value: 3.00).

Obviously, scenario 2 is clearly preferred in this setup, and it is also absolutely rated very well. This result supported the decision to choose the TLD door concept as a demonstrator for the MechaTUM project. Its realization was based on our preparations given in Sec. 2.3 and subsection 4.1.5 and is described in Sec. 5.1.

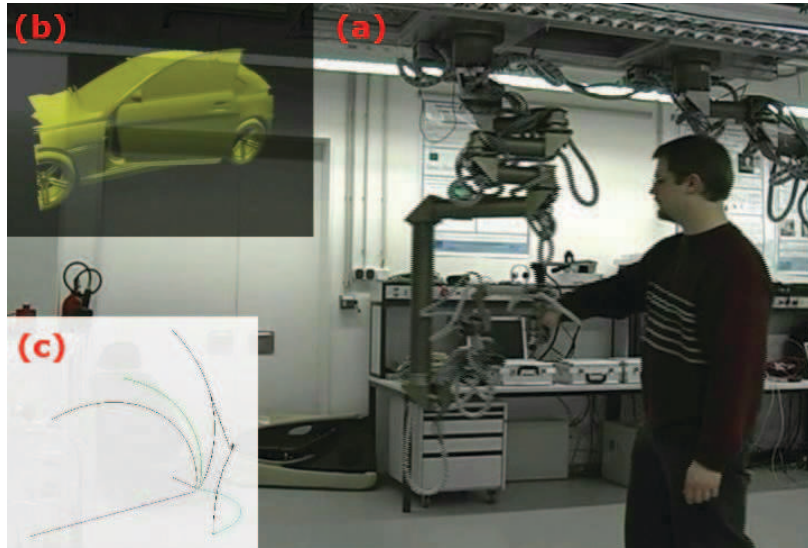


**Figure 4.6:** Simulation of a Free-Flying Car Door (FFD) used for the explorative user study: (a) shows a subject interacting with the haptic device VISHARD10, (b) the visual scene, and (c) the favorable paths used to haptically support the user [182].

### 4.1.3 Free-Flying Door (FFD): Preferred Guidance Depends on Person

The simulation of a “free-flying” car door (parameters: see Appendix B.1.1) with five corresponding favorable paths (conventional swinging door, sliding door, three variations of wing doors) was implemented for the haptic device VISHARD10 (see Fig. 4.6 (a)), and a corresponding, coarse 3D visualization was developed (see Fig. 4.6 (b)). The favorable paths are displayed in Fig. 4.6 (c). The inertial parameters of the door were chosen to equal a BMW 6 Series driver’s door; additional kinematical constraints and friction were not considered.

To assess the practicability and effectiveness of our approach, an explorative user study was conducted. It was not designed to get statistically significant results, but to give an initial impression of the acceptance of the car door simulation and its control. This should enable the identification of problems and further improvements. The study consisted of four parts (fixed order):

1. Introduction and familiarization of the participant
2. General rating of the simulated car door:
  - a) “How would you rate the usability of the car door in general?”
  - b) “How good does the operation of the swing door feel to you?”
  - c) “How good does the operation of the sliding door feel to you?”
  - d) “How easy is it for you to reach a desired path?”
  - e) “How easy is it for you to transit from one path to another?”
3. Rating of five parameter variations (V1-V5, randomized order):
  - a) “How would you rate the force threshold for leaving a path?”

- b) “How good is the guidance along a path?” (Static Virtual Fixture)
- c) “How good is the guidance between two paths?” (Dynamic Virtual Fixture)

4. Selection of preferred variation and remarks

The scale for all quantitative assessments was the same: ‘good‘ (1), ‘quite good‘ (2), ‘quite bad‘ (3) and ‘bad‘ (4). The personal characteristics of the participants and the quantitative results are given in Tab. 4.3. The small number, the similar age, and the similar scientific background of the participants does not allow a generalization of the results. However, very interesting tendencies could be recognized:

- The rating of the overall impression and the sliding door indicates that people like the idea and the feel of the proposed door.
- While the male participants rated the path arrival and departure as ‘quite good‘, the female participants rated it worse.
- There is a parameter variation (V2) whose force threshold was rated as ‘quite good‘ by both men and women.
- There is a parameter variation (V4) whose Static VF was rated well by both men and women.
- The Dynamic VF is rated very different: While the male participants strongly preferred the V1 setting, the female participants strongly preferred V5.
- Out of the six men, 50% preferred the V1 setting in general. All women preferred V5.
- All women stated that they preferred V5 because it required the minimum effort (small rendered stiffness).
- On average, the male participants preferred controller parameters which yielded a higher stiffness of the VF.
- Due to a strong correlation between gender and height, it is not clear which of these characteristics effects the preferences.

Although the experiments were confined to 10 subjects, there is a strong indication that an individual setting of the control parameters of an actuated car door can significantly increase user acceptance. Thus, we propose determining different sets of controller parameters optimized for respective user groups. In the field, based on these sets and a categorization of the user, the optimized parameter set can be chosen for the car door controller. This method and the intention recognition itself were two of the aspects filed for patent in [242].

**Table 4.2:** Absolute and relative rating of the five door simulations by 18 participants [220].

|          | Measure           | Scenario 1 | Scenario 2 | Scenario 3 | Scenario 4 | Scenario 5 |
|----------|-------------------|------------|------------|------------|------------|------------|
| Absolute | mean              | 5.72       | 7.83       | 6.72       | 6.11       | 6.94       |
|          | (1 to 10) st.dev. | 2.35       | 1.10       | 2.02       | 1.68       | 1.43       |
| Relative | mean              | 2.00       | 3.28       | 2.39       | 2.22       | 2.67       |
|          | (1 to 5) st.dev.  | 1.33       | 0.83       | 1.04       | 1.00       | 1.08       |

**Table 4.3:** Evaluation results for the experimental user study on the car door simulation based on Static and Dynamic Virtual Fixtures.

| Users                                     | Gender (Count)      |        | Men (6)   | Women (4)  | Total (10) |            |
|---|---------------------|--------|-----------|------------|------------|------------|
|   |                     | Age    |           | 27.7 (1.2) | 26.8 (2.4) | 27.3 (1.7) |
|   |                     | Height |           | 1.80 (7.9) | 1.74 (4.1) | 1.77 (7.0) |
| General                                   | Overall Impr.       |        | 1.5 (0.5) | 1.5 (0.6)  | 1.5 (0.5)  |            |
|   | Swing Door          |        | 1.8 (1.0) | 2.5 (0.6)  | 2.1 (0.9)  |            |
|   | Sliding Door        |        | 1.2 (0.4) | 1.5 (0.6)  | 1.3 (0.5)  |            |
|   | Path Arrival        |        | 2.0 (0.9) | 2.5 (0.6)  | 2.2 (0.8)  |            |
|   | Path Departure      |        | 2.0 (0.9) | 2.8 (1.3)  | 2.3 (1.1)  |            |
| V1-V5: Variation of Controller Parameters | Force Thres.        | V1     | 2.7 (1.2) | 2.5 (1.3)  | 2.6 (1.1)  |            |
|   |                     | V2     | 2.0 (0.9) | 2.0 (0.8)  | 2.0 (0.8)  |            |
|   |                     | V3     | 3.5 (0.8) | 3.3 (0.5)  | 3.4 (0.7)  |            |
|   |                     | V4     | 3.2 (1.2) | 4.0 (0.0)  | 3.5 (1.0)  |            |
|   |                     | V5     | 2.5 (1.2) | 1.5 (1.0)  | 2.1 (1.2)  |            |
|   | Static VF           | V1     | 1.8 (0.8) | 1.5 (1.0)  | 1.7 (0.8)  |            |
|   |                     | V2     | 1.5 (1.2) | 2.5 (1.0)  | 1.9 (1.2)  |            |
|   |                     | V3     | 2.2 (1.2) | 2.0 (1.4)  | 2.1 (1.2)  |            |
|   |                     | V4     | 1.7 (1.2) | 1.5 (0.6)  | 1.6 (1.0)  |            |
|   |                     | V5     | 1.8 (0.8) | 1.5 (0.6)  | 1.7 (0.7)  |            |
|   | Dynamic VF          | V1     | 1.3 (0.5) | 2.5 (0.6)  | 1.8 (0.8)  |            |
|   |                     | V2     | 2.2 (1.2) | 2.3 (1.0)  | 2.2 (1.0)  |            |
|   |                     | V3     | 2.3 (0.8) | 2.5 (0.6)  | 2.4 (0.7)  |            |
|   |                     | V4     | 2.0 (1.3) | 3.0 (1.4)  | 2.4 (1.3)  |            |
|   |                     | V5     | 2.2 (0.8) | 1.8 (1.0)  | 2.0 (0.8)  |            |
|   | Preferred Variation |        |           | V1 (0.5)   | V5 (0.0)   | V5 (0.5)   |

#### 4.1.4 Pivotal-Sliding Door (PSD): Dynamics Should be Adaptable

The PSD has already been introduced in subsection 2.3.3. Its kinematic configuration is depicted in Fig. B.1. A problem of this door concept is the coupling between the translational and the rotational DOF, which results in a poor usability of the mechanism. This can be overcome by compensating the real dynamics by a feedback-linearized position controller and implementing suitable virtual dynamics, i.e. defining the dynamics that are to be rendered by the actuation of the PSD.

Thus, an interesting question in the mechanical and the controller design of the PSD is how the real and/or haptically rendered dynamic parameters (mass/inertia, damping) should be chosen and whether this makes any significant difference for the human user interaction. We investigated this by a user study where the PSD had to be manually operated at the VRP test bed in three different modes; see also Fig. 4.7:

1. Pure swinging or sliding (brown, dotted)
2. Swinging or sliding in two-DOF mode (blue, solid)
3. Combined swing-sliding motion (red, dashed)

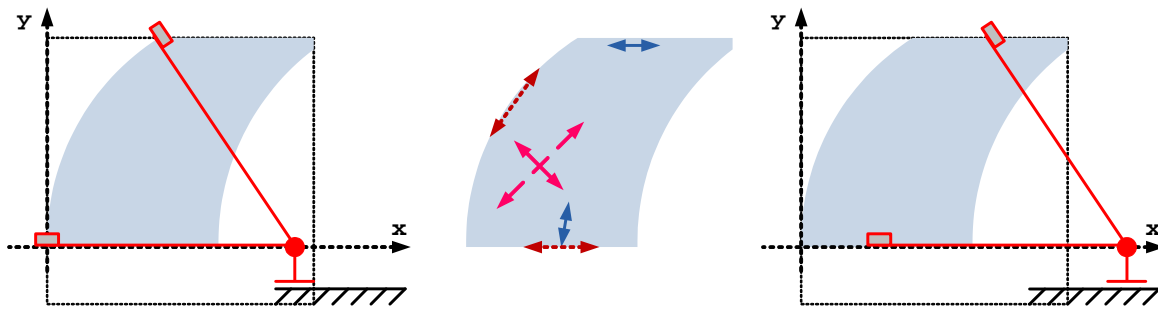


**Figure 4.7:** Haptic rendering of the PSD: The door handle can be moved in the combined work space of the PSD and the VISHARD10 (blue background). Possible configurations are depicted (l.) and (r.). In the middle, the three different modes for the manual operation are given.

##### 4.1.4.1 Part 1: Individual Parameter Selection for Pure Swinging and Sliding Motion

In a first step, the participants had to iteratively choose the mass and damping of each link in turn for a one-DOF motion. Thus, 50% of the participants started with a sliding motion and adjusted  $m_A$  and  $\mu_A$  before switching to the swinging motion and adjusting  $m_{DOOR}$  and  $\mu_{DOOR}$ . As default start parameter set, a dynamic subjectively chosen was used because it was expected to be nearer to the users' wishes than the reference set derived from the EOM of the mechanism. The reference sets and the corresponding mean values of the individually adjusted dynamics are given in Tab. 4.4 ("Part 1"); details can be found in Tab. F.1 and Tab. F.2. Obviously, the choice of the parameters depended heavily on the order of their adaptation: The participants starting with a swinging motion chose far lower masses and frictions than the ones starting with a sliding motion.

**Table 4.4:** Reference and preferred dynamics of the PSD. Details and standard deviations are given in Tab. F.1, Tab. F.2, and Tab. F.3.

|                                       | $m_A$ | $m_{DOOR}$ | $\Sigma m$ | $\mu_A$ | $\mu_{DOOR}$ |
|---------------------------------------|-------|------------|------------|---------|--------------|
| Reference 1 (mechanism)               | 4.00  | 34.80      | 38.80      | 0.04    | 0.04         |
| Reference 2 (subjective)              | 4.00  | 12.00      | 16.00      | 0.15    | 2.00         |
| Part 1: Sliding F. (mean of 7 users)  | 3.00  | 17.16      | 20.16      | 0.56    | 8.16         |
| Part 1: Swinging F. (mean of 7 users) | 1.83  | 12.30      | 14.13      | 0.14    | 5.00         |
| Part 1: Overall (mean of 14 users)    | 2.41  | 14.73      | 17.14      | 0.35    | 6.58         |
| Part 2: Overall (mean of 14 users)    | 1.13  | 20.26      | 21.39      | 1.34    | 9.01         |

#### 4.1.4.2 Part 2: Adjustment of the Parameter Selection for Motions with Two DOF

Based on this individual parameter setting derived by a one-DOF motion, the participants were to make a further adjustment by subjectively optimizing the interaction for two-DOF motions. The results are given in Tab. 4.4 (“Part 2”) and Tab. F.4. This can be interpreted as follows: The participants wanted to maximize the controllability of the car door at their interaction point. Thus, they reduced the mass and increased the damping of the sliding DOF significantly, such that they can operate both DOF with a similar effort.

#### 4.1.4.3 Part 3: Rating of the Adjusted Parameters in Relation to Two Reference Settings

Finally, the participants rated their individual parameter setting as well as the two predefined parameter sets for all three types of motion ( $Sl$  = one-DOF sliding,  $Sw$  = one-DOF swinging,  $Co$  = two-DOF motion). The scale ranged from 0 (extremely bad) to 10 (extremely good). The detailed results are given in Tab. F.5; the mean values can be seen from Tab. 4.5. Based on these rating, we calculated the best-case overall rating of the individually preferred parameters, which is denoted by  $\Sigma_{max} = \max(Sl) + \max(Sw) + \max(Co)$ . This value would be achieved if the parameter setting is selected situation-dependently for each user.

**Table 4.5:** PSD experiment part 3: Rating of all three parameter sets for three types of motion on a scale from 0 to 10. The overall rating of the individually preferred parameters is denoted by  $\Sigma_{max}$ . Details and standard deviations are given in Tab. F.5.

| Parameters      | Individual | Reference 1 | Reference 2 | $\Sigma_{max}$ |
|-----------------|------------|-------------|-------------|----------------|
| Rating: mean    | 7.55       | 5.36        | 6.02        | 23.80          |
| Rating: st.dev. | 1.38       | 1.92        | 1.60        | 2.28           |

It is clear that the individual parameter settings outperform the predefined reference settings significantly. Furthermore, the rating leads to an approval factor of  $\frac{23.8}{30} = 0.79$  with respect to the maximum rating sum of 30. This indicates that the users are really

content with the door dynamics if these are adapted with respect to the user and the mode of operation.

As already observed in subsection 4.1.3, there is no parameter setting which satisfies all users best. A clear indicator for this is the large standard deviation of the individualized dynamical parameters in Tab. F.1, Tab. F.2, and Tab. F.4.

Thus, an adaptation of the rendered dynamics with respect to the user and the motion of the door is highly recommendable for car doors with unusual kinematics such as the PSD. This has also been filed as a patent [242].

We found one correlation between the personal characteristics of the participants and their preferred dynamical parameters: Tall participants tended to choose higher masses/inertias, while shorter participants tended to choose lower ones. This could be utilized for a simple adaptation of the interaction behavior of an actuated car door: Based on a determination of the user height (car key or camera system) and parameter sets optimized for the 20th, the 50th and the 80th percentile of the typical user height, the appropriated parameter set can be interpolated.

### 4.1.5 Two-Link Door (TLD): Haptic User Support is Beneficial

In the following, the controllers for the automatic and manual operation of a TLD are described and evaluated. The implementation was done at the VRP introduced in subsection 4.1.1, and the overall structure of the system can be seen in Fig. 4.3.

We performed a thorough, large-scale user study to gain an insight into the preferred dynamics and controllers for the manual operation of the TLD. Specifically, we wanted to test our hypotheses, namely that the perceived dynamics of a car door do make a difference and that users appreciate haptic support functionalities.

#### 4.1.5.1 Controller for the Automatic Door Operation

**Triggering of Automatic Operation:** A finite state machine was developed for the high-level control of the car door. Its default super-state is manual operation; an automatic opening or closing operation has to be triggered by a remote signal. The automatic operation mode is left as soon as either the desired position has been reached or a manual interaction has been sensed.

**Path Planning:** After the triggering of the automatic operation, the current and the desired door configurations are sent to the path planning computer. Only after a collision-free path has been returned by it does the door controller calculate the corresponding trajectory and execute the motion control in real-time.

**Motion Controller:** For the computation of a suitable trajectory based on the collision-free path, at first a standard cubic trajectory planner has been utilized. However, it did not consider the limited actuation bandwidth and user-centered velocity and acceleration limits. Thus, we iteratively implemented and tuned the corresponding limits in the trajectory generation, until the resulting motions were deemed to be approved by novice users of the car door. Furthermore, we extended the trajectory generation such that current states

were used as constraints, which enabled an online motion execution without intermediary stop.

For the execution of the desired trajectory, both an independent joint PD controller and a resolved acceleration controller (based on the EOM of the TLD; see Appendix B.1.3) were implemented. Due to the compensation of external disturbances, the latter provided a far better interaction performance.

**Collision Avoidance:** The car door motion executed by the motion controller has been monitored by a reactive collision avoidance: The car door configuration was continuously sent to the simulated obstacle detection system (structure: see Fig. 4.3) and the collision detection computer. When the collision detection computer indicated a potential collision, the motion controller commanded a full stop. After the stop of the system, another request was sent to the path planning computer to determine a collision-free motion based on current data.

#### 4.1.5.2 Controller for the Manual Door Operation

**Virtual Walls:** To prevent damage to the car chassis,  $q_1$  has to be restricted. We chose

$$0 = q_{1,min} \leq q_1 \leq q_{1,max} = \pi/2 \quad (4.1)$$

which was expected to be suitable for the realization of this door concept. For an effective self-collision avoidance,  $q_2$  had to be limited, too. We chose the lower bound such that the door cannot exceed a parallel order with respect to the car chassis. An upper bound of  $q_{2,max} = 0$  seemed sensible to avoid door configurations with a very small entrance areas; see also [92]. Thus, we chose

$$-q_1 = q_{2,min} \leq q_2 \leq q_{2,max} = 0 \quad (4.2)$$

These constraints had been implemented as joint-space Virtual Walls (see Fig. 4.8).

In some situations, it might nonetheless be preferred by the user to deactivate these limits. Thus, intention recognition can be implemented to trigger the temporary deactivation of one or more of the Virtual Walls (VW). For instance, the restriction for  $q_2$  could be deactivated if the user exerts a large torque for a certain timespan. After the deactivation, a monitoring of the conditions Eq. (4.1) and Eq. (4.2) can be used for triggering the reactivation of the Virtual Walls.

**Adaptive Damping:** In addition to the Virtual Walls, a prior damping area has been implemented to provide a smooth manual operation; see also Fig. 4.8. The reason is that otherwise the closing motion is typically perceived as a hard impact on the “parallelism VW”. This impact is counteracted by speed- and direction-dependent adaptive damping, which was designed to provide a smooth interaction for both slow and high speeds.

**Coupling Compensation:** The VW implementation led to large accelerations of  $q_1$  when closing the door from a configuration near the kinematical singularity. This is due to the

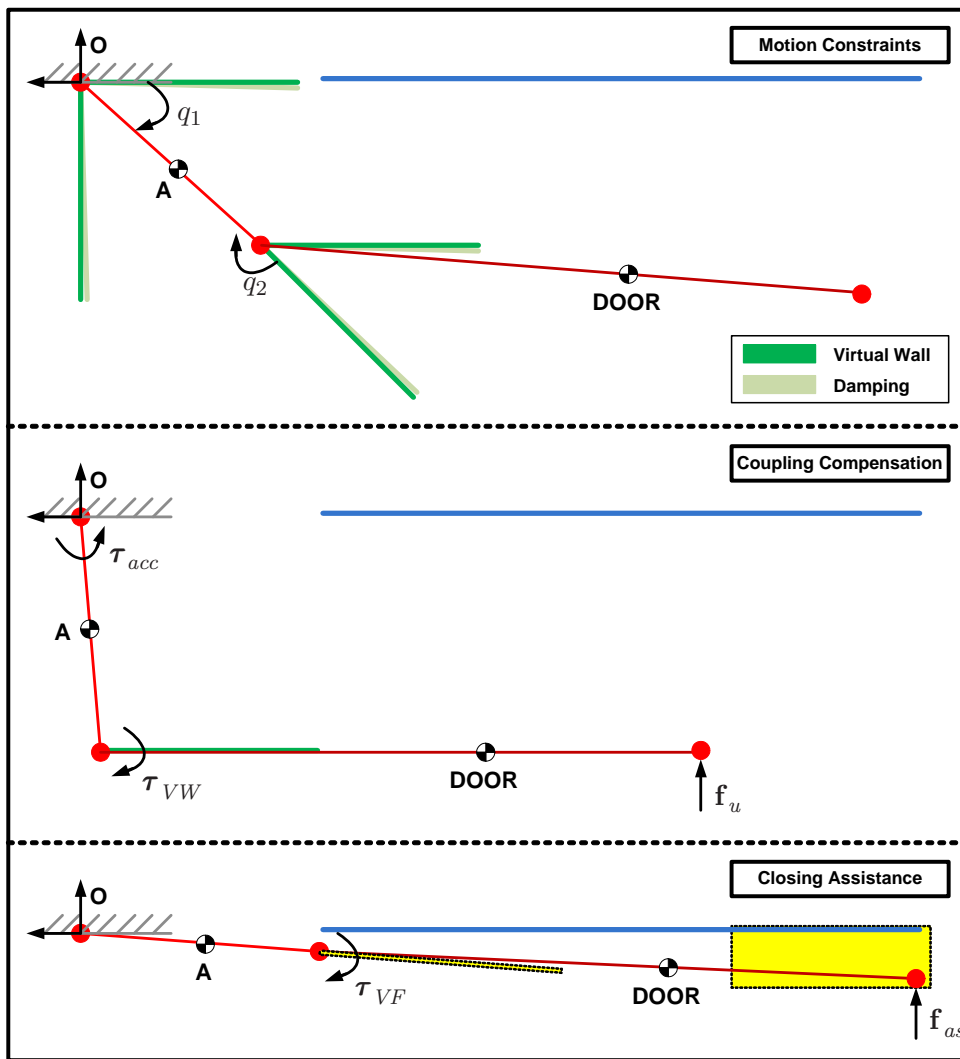


**Figure 4.8:** Three methods for the control and support of the manual interaction at the TLD: 1) The motion is constrained by Virtual Walls and Damping Areas; 2) a compensation controller damps coupling effects; 3) the closing of the door is supported by a Virtual Fixture in joint 1 and a supportive force  $f_{as}$  at the HIP.

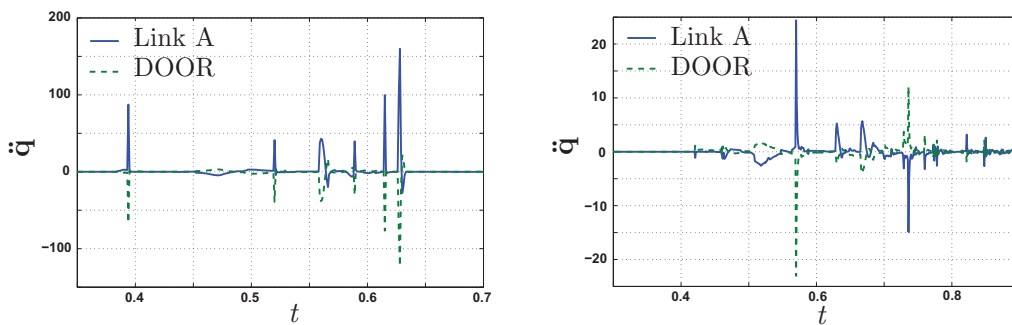


**Figure 4.9:** Effect of the coupling compensation when closing the door: The originally large acceleration (l.) is drastically reduced (r.) [212].

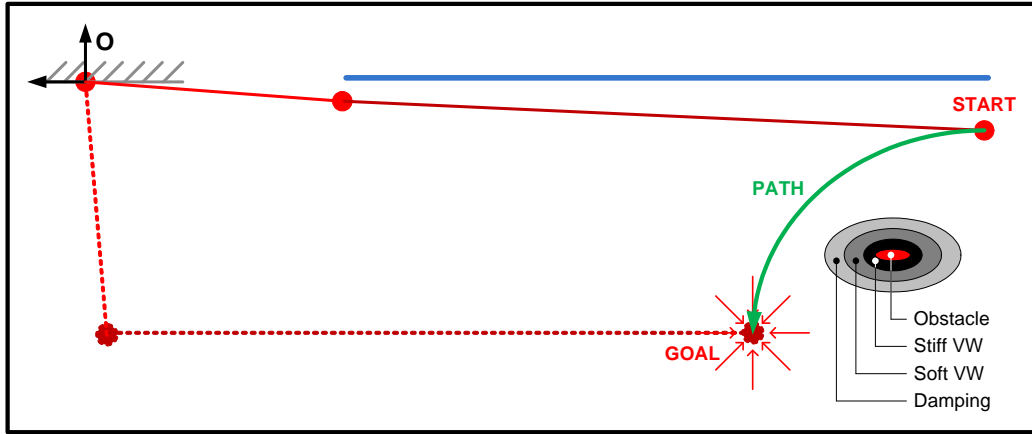


**Figure 4.10:** Real-time haptic interaction support by Static Virtual Fixtures (SVF) and Dynamic Virtual Fixtures (DVF) based on collision avoidance and path planning.

coupling of Link A and DOOR, and especially the disproportion of the mass/inertia of Link A with respect to the DOOR. We counteracted this effect by a coupling compensation, reducing  $\tau_{acc}$  and thereby  $\ddot{\mathbf{q}}$  significantly. This can be seen from the exemplary measurements given in Fig. 4.9.

**Closing Assistance:** The closing and locking of the door is supported by a small supportive force  $\mathbf{f}_{as}$  if the user moves the virtual door into a predefined proximity of the closing position. This is further improved by the application of a moderate Virtual Fixture ( $q_{2,r} = 0$ ) to joint 2; see Fig. 4.8.

**Path Guidance:** As depicted in Fig. 4.10, the user was supported by a small force to follow the collision-free path to the goal configuration. This has been implemented as Dynamic Virtual Fixture similar to subsection 3.1.2.2. At the desired goal configuration, an additional point fixture [160] is applied to assist the user in positioning the door.

**Collision Avoidance Support:** A multi-staged collision avoidance approach has been implemented for the real-time support of the haptic interaction. Three different-sized bounding boxes are used to distinguish between three levels of danger of a collision; see Fig. 4.10.

If the bounding box of the door enters the least critical overapproximation of an obstacle, a unidirectional damping is applied. Optionally, a perpendicular motion in this damping field is supported proactively by a simple intention estimation.

If the bounding box approaches the next clearance level, a repulsive spring force is additionally exerted. Finally, if the door gets very near to an obstacle, a stiff virtual wall is applied to prevent a collision. This multi-staged approach proved to be a good trade-off between usability and safety of the interaction in the presence of obstacles.



**Figure 4.11:** Screenshot of the scenario used for the evaluation of path planning and collision avoidance support during the TLD experiment.

#### 4.1.5.3 Setup and Participants of the Experiment

The proposed controllers should be investigated with respect to a slightly varied parameter setting of the TLD simulation: The link length had to be reduced from  $l_A = 0.45$  m to  $l_A = 0.24$  m in order to achieve a mechanically more robust construction and to meet close-to-production requirements (see Chap. 5.1.3 for more details). Besides these reference parameters, a “light” and a “heavy” car door parameter set were used to investigate the influence of these dynamics on the operator. The values are given in Tab. F.6.

In the Active Admittance, we introduced an output saturation of 30 Nm for each actuator to account for a realistic automotive hardware setup. This has a strong effect on the perception of the supportive functions: Even “stiff virtual walls” such as the ones used for the joint constraints can now be easily overcome by the operator, because the minimum renderable force is rather low:  $f_{min} = 30 \text{ Nm} / (l_A + l_{DOOR}) = 22.4 \text{ N}$ . However, a lot of other hardware properties were still idealized, such as the structural stiffness of the door, the dynamics of the power electronics and the like.

We defined two different 3D scenes, one with an obstacle for the investigation of path planning and collision avoidance (see Fig. 4.11), and one without. The selection of the 3D scenes as well as the current simulation parameters was performed by a graphical user interface (GUI) operated by one of the supervisors of the experiment. The GUI was designed such that each experimental condition could be activated quickly over just one selection field, minimizing the risk of a mix-up of parameters. This was very important due to the large number of randomized conditions.

20 people (12 men, 19 right-handed) participated in the experiment. All of them had previous experience in robotics experiments, so they were familiar with the evaluation on a VRP test bed. The personal characteristics of the participants are given in Tab. F.7.

There were two different types of rating tasks:

1. Absolute rating: The participants had to rate their impression of the manual car door operation on a scale from 0 (extremely bad) to 10 (extremely good).

2. Relative rating: The participants had to compare the manual operation of a car door with a reference simulation from -3 (much worse) via 0 (equal) to +3 (much better).

#### 4.1.5.4 Experiment: 33 Randomized Tasks, Rating Scales, and Relevant Results

In the following, the seven parts of the experiment and their 33 corresponding tasks and rating scales are briefly described. The parts and their corresponding tasks were randomized. Each task was combined with a rating request, thus we got 33 answers to our questions Q1–Q33 in the course of the experiment.

The answers are summarized in Tab. F.8 and Tab. F.9. In Tab. F.10, their correlation with the personal characteristics of the participants is given. Based on this data, the results of the experiment are derived. These are numbered and denoted in the form “RXX:”.

#### Part A: Rating of the Reference Parameter Set (Pure Mechanics) [0 to 10]

1. ... overall usability of the door
2. ... operability of the door
3. ... end positioning elements when fully opening/closing the door
4. ... characteristics of the closing motion

R01: Q1–Q4 got similar neutral ratings (e.g. Q1:5.85).

R02: Rating of the end positioning elements strongly depends on height and weight ( $\text{corr}(Q3,H)=0.69$ ).

#### Part B: Rating of the Reference/Light/Heavy Parametrized Mechanics for Rotation and Translation Separately [MIXED]

R03: The light door was rated best. It significantly outperformed the heavy door (Q7:+0.95 compared to Q9:-0.10).

R04: The older the participant, the lower the rating of the light door ( $\text{corr}(Q7,AGE)=-0.37$ ).

R05: The heavier the participant, the higher the rating of the heavy door ( $\text{corr}(Q9,W)=0.34$ ).

#### Part C: Rating of Controller Modules by Comparison to Pure Mechanics [-3 to 3]

11. ... overall usability of coupling compensation
12. ... closing with coupling compensation
13. ... overall usability of coupling compensation + closing assistance
14. ... closing with coupling compensation + closing assistance
15. ... overall usability of coupling compensation + adaptive damping
16. ... closing with coupling compensation + adaptive damping

R06: Coupling compensation proved to be very helpful (Q11:+0.9).

R07: Adding the adaptive damping did not bring a significant advantage (Q15:+0.9).

R08: Adding the closing assistance significantly lowered the approval (Q13:+0.35).

R09: The taller/heavier the participant, the higher the approval of the closing assistance ( $\text{corr}(Q11,H)=+0.34$ ) and the lower the approval of the adaptive damping ( $\text{corr}(Q15,H)=-0.28$ ).

#### **Part D: Rating of the Collision Avoidance (Controller Active, no Path Planning Support) [MIXED]**

For each of the three settings (1) no support; 2) damping and VW; 3) full support) three tasks had to be performed:

23. ... overall usability of the door
24. ... collision impact effect
25. ... moving the door around the obstacle

R10: An excellent rating is achieved by the full support (damping, VW, proactive movement support) ( $Q23:+0.65$  better than the very good rating  $Q17:7.25$ ).

R11: The heavier the participant, the lower the approval of the full support ( $\text{corr}(Q23,W)=-0.39$ ).

#### **Part E: Rating of the Collision Avoidance Scenario with all Supportive Functionalities Enabled [-3 to 3]**

26. ... with medium supportive path force (2.0 N)
27. ... with low supportive path force (1.2 N)
28. ... with high supportive path force (3.4 N)
29. ... with low supportive path force (1.2 N) and closing assistance

R12: The low path guidance is rated very well ( $Q27:+0.85$ ).

R13: The combination of low path guidance and closing assistance even exceeds this ( $Q29:+0.95$ ).

R14: The taller/heavier the participant, the worse the rating of  $Q29$  ( $\text{corr}(Q29,H)=-0.32$ ).

R15: The medium path guidance gets a good rating ( $Q26:+0.55$ ), but polarizes men and women ( $\text{corr}(Q26,Gender)=+0.36$ ).

#### **Part F: Rating of the Light/Medium/Heavy Parametrized Mechanics with all Supportive Functionalities Enabled [-3 to 3]**

R16: The light mechanism clearly outperforms the others and gets a very good absolute rating ( $Q30:7.25$ ).

#### **Part G: Rating of the Reference Parametrized Door with all Supportive Functionalities Enabled [-3 to 3]**

R17: The overall rating of the fully functional actuated car door is excellent ( $Q33:+1.30$ ).

R18: The taller/heavier the participant, the better the rating of  $Q33$  ( $\text{corr}(Q33,W)=+0.62$ ).

The distribution of the ratings of some important questions as well as a short explanation are given in Fig. 4.12.

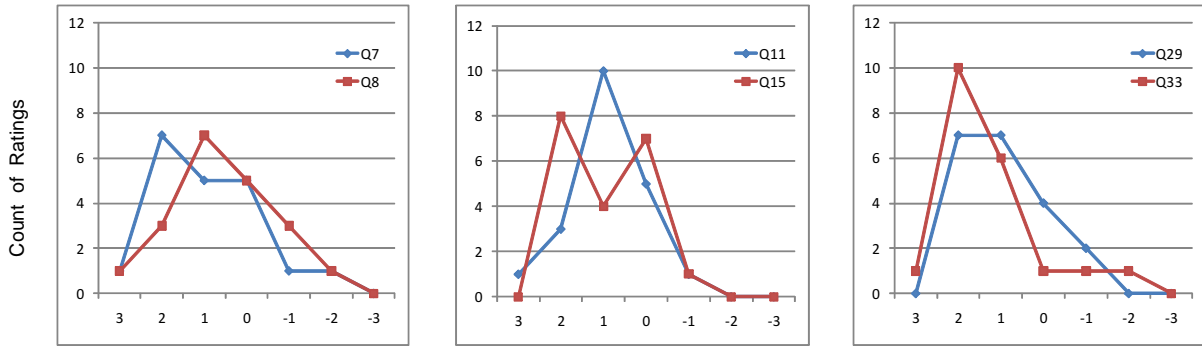


**Figure 4.12:** Count of the answers to some relative rating tasks: The “light” door is appreciated very much (l: Q7,Q8). The coupling compensation (m: Q11,Q15) is valued. The path guidance is appreciated very much (r: Q29), and 85% of the participants prefer the fully-functional support when compared to a purely mechanic door (r: Q33).

#### 4.1.5.5 Experiment: Statistical Analysis

Two-sample t-tests (19 DOF) revealed that the light door simulation F7/F8 is significantly preferred to the reference setting F5/F6 (F7/F5:  $t = 2.81$ ,  $p = 0.001$ ; F8/F6:  $t = 1.99$ ,  $p = 0.03$ ) and to the heavy door simulation F9/F10 (F7/F9:  $t = 2.81$ ,  $p = 0.006$ ; F8/F10:  $t = 3.9$ ,  $p < 0.001$ ).

The predominant approval of the real-time path guidance, which is based on the path planner described in Sec. 3.2, could also be verified: 70% of the participants preferred F29 to F1, while only 10% did not. Thus, the path planning support indeed brings a significant advantage to users when they handle a novel car door such as the TLD. Another finding is that a low path guidance force of 1.2 N was significantly preferred to a higher force of 3.4 N (two-sample t-test with 19 DOF for F27/F28:  $t = 5.96$ ,  $p < 0.001$ ).

An interesting question is whether the significant correlations of weight/height with several ratings are subject to the measure weight/height or to gender. Neither an ANOVA nor an ANOCVA showed significance for gender. Height and weight are heavily correlated. Thus, the measure “height” is seen as the independent variable significantly effecting the rating of many scenarios.

Finally, an ANOVA verified the statistical significance of the preference for the fully-functional support:  $F(1,18) = 11.2$ ,  $p_{Q33} = 0.0018$ .

#### 4.1.6 Summary

In this section, we proposed a VRP test bed with haptic feedback comprising automotive end-effectors and several networked computers to distribute computing tasks such as obstacle detection, collision avoidance, and path planning. We used the VRP test bed to evaluate five preliminary door concepts. The result was that a Two-Link Door (TLD) is the preferred concept. We investigated it in more detail together with two other door concepts, a Free-Flying Door (FFD) and a Pivotal-Sliding Door (PSD).

An evaluation of the FFD combined with the intention recognition described in Sec. 3.1

revealed that the ten participants liked the door simulation itself, whereas opinions on the haptic guidance based on intention recognition were polarized. It became evident that the preference for haptic support strongly depends on personal characteristics. For instance, all women preferred a “light” car door, while men did not. Thus, door dynamics do indeed matter.

During our investigation of the preferred dynamics of a PSD it became evident that these strongly depend on the movement of the door (swinging/sliding/combined) and on personal characteristics. The best ratings were achieved for the individually selected parameter sets. This is a clear indication that the car door dynamics should indeed be adaptable with respect to the current user as well as on the manual operation situation.

We developed a variety of controller modules for a TLD. A comprehensive evaluation with 20 participants revealed interesting facts:

1. The height/weight has a very strong influence on the preferred dynamics, but the gender does not.
2. Not all supportive functions are approved by participants: For instance, while the coupling compensation is liked very much, the closing assistance is not.
3. The collision avoidance support is appreciated very much.
4. The path planning support is rated very well for rather low guidance forces (1.2 N).
5. The lighter door simulations were preferred when compared to heavier doors, and get an excellent rating when combined with all assistive functions.

These are very important findings which enable the user-centered design of both unactuated and actuated car doors with more than one DOF. Based on the evaluation results, we strongly recommend determining the height of the user and to use it as input to an adaptable car door controller. The following general conclusion can be drawn:

Door dynamics do matter. An adaptive controller has to be used to provide a superior manual interaction. The adaptation should be based on situation and user, specifically his or her height.

Overall it can be stated that VRP is indeed very useful for both the development and the evaluation of car door concepts. We are the first and, up to now, the only ones to investigate the simulation, control, and evaluation of actuated car doors with more than one DOF. Most of our recommendations have also been filed as a patent [245].

## 4.2 VRP of Car Doors with One Rotational DOF

In Sec. 4.1, we proposed the VRP of car doors using a versatile haptic device, the ViSHARD10. This device (as well as other general-purpose haptic devices with more than one DOF) enables a quick display of different car door kinematics. However, being a general-purpose device, it is not task-optimized. For instance, each additional DOF with respect to the generalized coordinates of the simulated mechanism leads to an avoidable performance loss: The limited stiffness of the oversized linkage as well as the limited control stiffness of the additional joints. This may prevent a *very* realistic haptic simulation of car doors, limiting the informative value of the simulation results. Therefore, we intended to develop a dedicated, task-optimized haptic device for the high-fidelity rendering of car doors with one rotational DOF.

An ideal haptic device displays a virtual object such that the user cannot detect any difference between simulation and reality [7]. To ensure a high degree of this so-called transparency, a variety of requirements have to be met in the design of a haptic device [259]. One major issue is the workspace and the force output capability of the haptic device. Obviously, the simulation of a rotational car door requires a comparably large workspace ( $> 1\text{ m}^2$ ). Due to the rather hard mechanical constraints of real car doors, very stiff Virtual Walls (VW) need to be simulated (see also Chap. 3). Thus, both a large force output capability and a high mechanical stiffness are mandatory.

To achieve a high-fidelity haptic rendering of a car door, a lot of issues have to be taken into account; compare subsection 4.1.1. Some requirements can be achieved quite easily by using parts of a conventional car door handle and mounting them rigidly to an appropriate force sensor. In contrast, modeling the car door accurately, deriving the specific requirements for the design of the haptic device, and ultimately designing it properly is much harder. This is a difference compared to other investigations on high-fidelity rotational one DOF rendering, such as [11, 52, 81, 170].

In the following, we solve these problems and design a haptic device that indeed enables the high-fidelity rendering of a car door with one DOF. For this purpose, a detailed and accurate car door model is developed and validated. Based on this and on knowledge of the haptic user interaction, the requirements for the door simulator are derived. They are fulfilled by a very stiff mechanical construction and a high-fidelity rotational direct drive. We conduct an extensive user study with 17 participants to evaluate the quality of the haptic rendering. Furthermore, we evaluate the rendering of an inclined door, evaluate the preferred effort of manual interaction, and simulate and evaluate a semi-actuated car door.

### 4.2.1 Modeling and Specification Issues

For the design of a task-optimized haptic device, the main requirements have to be identified and fulfilled. This requires knowledge of the dynamics that have to be rendered as well as the human user interaction. Thus, we derive the performance specification for the haptic device based on a detailed model of the door and a characterization of the user interaction.

#### 4.2.1.1 User Interaction with a Car Door

We performed various tests and measurements to assess the haptic interaction between a car door and the human user. In our setup, it turned out that the maximum force exerted by the user,  $f_{U,max}$ , is predominantly below 90 N. Such large forces are exclusively applied to the outer rim or upper corner of the door when the user closes the door with a push. This means that even for long car doors<sup>1</sup>, the typical maximum torque exerted by the user is  $\tau_{U,max} = f_{U,max} \times r_{max} \leq 100$  Nm.

According to [32], kinesthetic interaction usually involves frequencies below 20 Hz. We assume that this holds for the interaction of a human with a car door<sup>2</sup>. Power spectra of force and position measurements of typical interaction scenarios at car doors back this assumption.

#### 4.2.1.2 Generic Model of rotational Car Doors

One way to model the car door is to consider all its haptically relevant properties and sub-elements as an impedance, resulting in the *internal* torque  $\tau_{door,i}$ :

$$\begin{aligned} \tau_{door,i} = & \tau_D(\dot{\varphi}, \varphi) + \tau_F(\dot{\varphi}, \varphi) + \tau_G(\varphi, \theta, \xi) + \tau_V(\dot{\varphi}, \varphi) + \\ & \tau_P(\dot{\varphi}, \varphi) + \tau_E(\dot{\varphi}, \varphi) + \tau_A(\dot{\varphi}, \varphi, \tau_{door,e}, t) + \tau_{r,i}(\dot{\varphi}, \varphi) \end{aligned} \quad (4.3)$$

where  $\varphi$  is the rotational DOF,  $\tau_D(\dot{\varphi}, \varphi)$  is the characteristic torque exerted by the door detent,  $\tau_F(\dot{\varphi}, \varphi)$  describes the friction in the door hinge,  $\tau_G(\varphi, \theta, \xi)$  is the influence of gravity (depending on the inclination  $(\theta, \xi)$  of the hinge relative to gravity),  $\tau_V(\dot{\varphi}, \varphi)$ ,  $\tau_P(\dot{\varphi}, \varphi)$ , and  $\tau_E(\dot{\varphi}, \varphi)$  are the contributions of the air ventilation, the rubber packing, and the mechanical end positioning elements of the door,  $\tau_A(\dot{\varphi}, \varphi, \tau_{door,e}, t)$  is the torque exerted by the (optional) actuator, and  $\tau_{r,i}(\dot{\varphi}, \varphi)$  are residual internal effects. The *external* torque is given by

$$\tau_{door,e} = \tau_U(t) + \tau_W(\dot{\varphi}, \varphi, t) + \tau_{r,e}(\dot{\varphi}, \varphi, t) \quad (4.4)$$

where  $\tau_U(t)$  describes the user interaction torque,  $\tau_W(\dot{\varphi}, \varphi, t)$  is the torque exerted by air resistance and wind, and  $\tau_{r,e}(\dot{\varphi}, \varphi, t)$  are residual external effects.  $\tau_{door} = \tau_{door,i} + \tau_{door,e}$  is the sum of all torques that act on the rotational DOF. Consequently, the overall dynamics of the car door is given by  $\tau_{door} = \ddot{\varphi}I_{\bar{z}\bar{z}}$ , where  $I_{\bar{z}\bar{z}}$  is the inertia of the door related to the rotational hinge. In the following, modeling errors and disturbances will be ignored ( $\tau_{r,i} = \tau_{r,e} = \tau_W = 0$ ,  $\tau_{door,e} = \tau_U(t)$ ).

Except the optional actuation torque  $\tau_A$ , the door model can be derived by measurements and analytical considerations (see [238] for details). In the following, we clarify why  $\tau_A$  does not have to be modeled exactly for the performance specification of the haptic device.

---

<sup>1</sup>Assumption about maximum perpendicular distance between hinge and interaction point at car door:  $r_{max} = 1.1$  m.

<sup>2</sup>Especially when rapidly closing the door, much higher frequencies occur due to an impact, but then the user lets the door loose such that there is no haptic interaction at the time of impact.

### 4.2.1.3 Characterization of the (Optional) Actuation

One key advantage of the haptic device was seen in the simulation of actuated car doors, because different actuation and controller concepts can rapidly be evaluated. An important question was whether the addition of an actuation model (see [244]) would affect the performance specification significantly.

In contrast to the other torque components,  $\tau_A$  highly depends on the implementation at hand, because the door designer has a relatively free choice of both actuator technology and functionality given. However, the actuator dynamics will be limited, and each realistic actuation concept would also increase the effective inertia  $I_{zz}$  and friction of the door. Consider this for two promising actuation concepts:

- DC motor with gearbox (compare [240, 164, 162]): Due to the gearbox, the overall inertia and friction of the system is increased significantly, which makes it easier to render the mechanical model. Additionally,  $\tau_A$  is expected to exhibit a rather low bandwidth and power output, because the automotive industry is very cost sensitive.
- Magneto-rheological dampers (compare [163, 269, 265]): The additional inertia is negligible. However, due to cost considerations, a permanent magnet will be used. This introduces a damping which cannot fully be compensated by the electromagnet [269, 15]. Furthermore, the bandwidth is typically below 50 Hz (compare [15]).

Thus, even for the worst-case scenario of reference steps commanded by the simulated controller,  $\tau_A$  will be rather limited in terms of power and bandwidth. For this reason, we omit it in the following considerations.

### 4.2.1.4 Gravity

In general, the door hinge is not aligned with the effective direction of gravity. It exhibits an inclination  $(\theta, \xi)$  that depends both on the construction of the door hinge and the tilt of the car body. This results in a gravitational torque  $\tau_G$ , which acts to minimize the potential energy. To model this torque, we calculate the shortest distance between the center of gravity (CG) and the rotational axis, which gives the lever  $l_{CG}$ . From this, we can derive the effective lever for gravity,  $l_{eff} = l_{CG} \cos(\frac{\pi}{2} - \varphi - \xi)$ , and then calculate the gravity torque:

$$\tau_G(\varphi, \theta, \xi) = mgl_{eff}(\varphi, \xi) \sin(\theta) \quad (4.5)$$

### 4.2.1.5 Friction

The door hinge exhibits several friction effects. Measurements revealed that the dry friction  $\tau_{F,D}$  is predominant, while the static friction  $\tau_{F,S}$  plays only a minor role. The friction can easily be modeled as a constant for every simulation step  $k$ :

If  $\dot{\varphi}_{k-1} = 0$  and  $|\sum \tau_k - \tau_F(\dot{\varphi}, \varphi)_k| > |\tau_{F,S}|$ , or if  $\dot{\varphi}_{k-1} \neq 0$  and  $|\sum \tau_k - \tau_F(\dot{\varphi}, \varphi)_k| > |\tau_{F,D}|$ , the door will move, thus  $\tau_{F,k} = \tau_{F,D}$  and  $\dot{\varphi}_k \neq 0$ . Otherwise, the door will not move, thus  $\dot{\varphi}_k = 0$  and  $\varphi_k = \varphi_{k-1}$ .

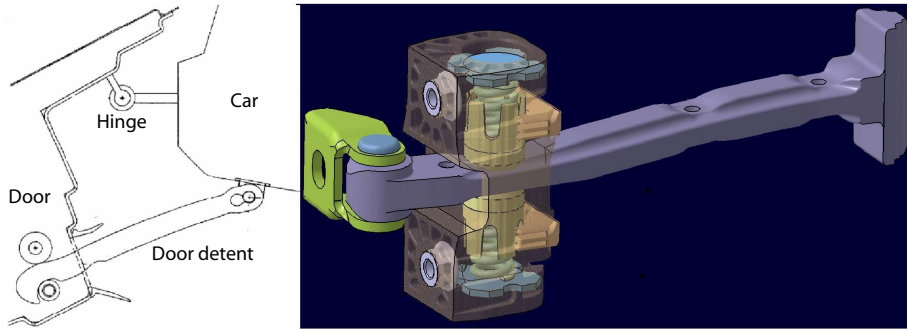


**Figure 4.13:** Location (l.) and mechanical scheme (r.) of the door detent of a BMW 3 Series car door (courtesy of BMW AG).

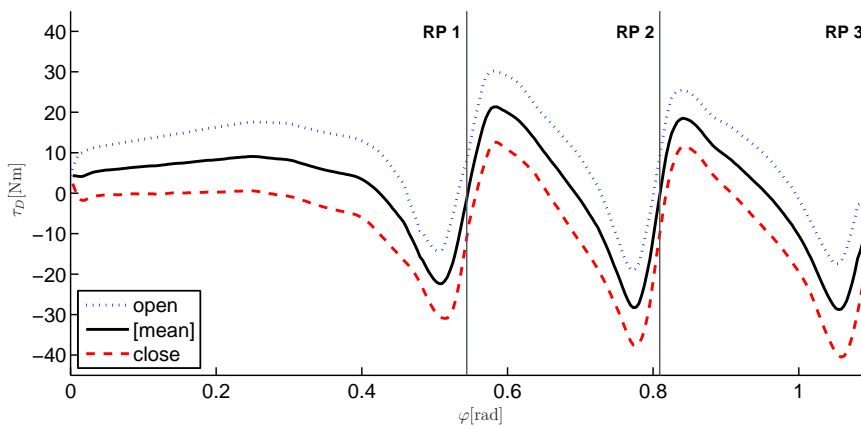


**Figure 4.14:** Measurement of the door detent torque  $\tau_D$  while opening and closing the door with constant velocity  $\dot{\varphi}$ . From the mean value (solid line) it can easily be seen that the detent provides three rest positions (RP) for placing the door.

#### 4.2.1.6 Door Detent

The door detent is located between the door and the front pillar of the car, as can be seen in Fig. 4.13. It is a mechanical component which is meant to bring an open car door into one of three rest positions, thereby holding the door even at moderate inclinations to provide a comfortable access to the car. This is achieved by means of a combination of a spring and a mechanical profile, resulting in a characteristic torque  $\tau_D$  which is depicted in Fig. 4.14.

Friction effects (mainly dry friction) account for different  $\tau_D$  when opening and closing, which can be seen by comparing them to the mean value (solid line). Accordingly, the door detent has been modeled as a separate look-up table for both movement directions.

#### 4.2.1.7 Air Ventilation

While the aerodynamic drag of the car door is negligible, the influence of the air ventilation of the car is not: Especially when the door is opened or closed with a high velocity ( $\dot{\varphi} > 0.5 \text{ rad/s}$ ) with the external door handle, the resisting torque  $\tau_V(\dot{\varphi}, \varphi)$  resulting from

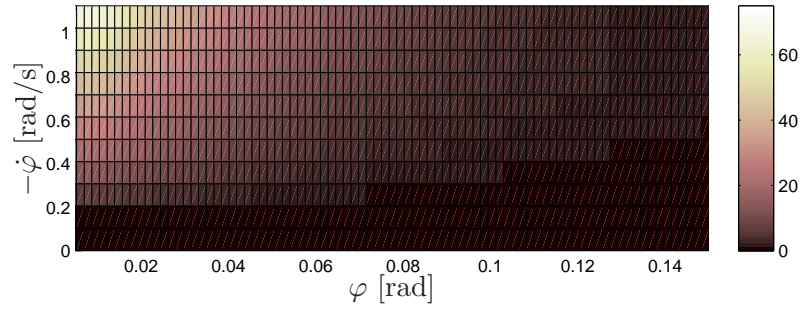


**Figure 4.15:** Calculated air ventilation torque  $\tau_V$  [Nm] based on measurements with different closing speeds  $\dot{\varphi}$ .

the decompression or compression of the air inside the car is significant.

For the sake of simplicity, in the following we assume that all car doors and all windows are fully closed, which gives the  $\tau_{V,max}(\dot{\varphi}, \varphi)$ . As soon as the car door presses against the rubber packing, the compressed air can only vanish through the ventilation slots of the car. Thereby, the design of air ventilation has a strong influence on the dynamics of the car door, especially for large velocities.

To quantify this effect, the pressure  $p(\dot{\varphi}, \varphi)$  within the car was measured while the door was closed with different velocities  $\dot{\varphi}$ . We assume that the pressure acts homogeneously on the inner surface area  $A$  of the car door, whose center exhibits a perpendicular distance  $r_A$  to the hinge axes. Accordingly, we model the effective torque caused by air compression/decompression as

$$\tau_V = p(\dot{\varphi}, \varphi)A \times r_A \quad (4.6)$$

This enabled an experimental identification: For different constant velocities  $\dot{x}$ , we measured  $p$  and  $\varphi$ . From these measurements, which are partly displayed in Fig. 4.15, we derived a look-up table for  $\tau_V$ .

#### 4.2.1.8 Rubber Packing

The car door protects the driver not only from collision impacts, but also from precipitation and noise. By effectively sealing the door, a rubber packing accounts for this. Towards the car door, the packing acts like a nonlinear spring with  $\tau_P$  depending heavily on position and mildly on velocity. Thus, the identification was done by measuring the static force at the external door handle for different  $\varphi$ .

#### 4.2.1.9 Maximum Opening Angle

There is a so-called “maximum” opening angle  $\varphi_{max}$  for the car door. Larger angles are counteracted by mechanical end positioning elements, which exhibit a spring-like behavior. The spring constant was determined by applying a constant torque on the car door and measuring the corresponding angle.

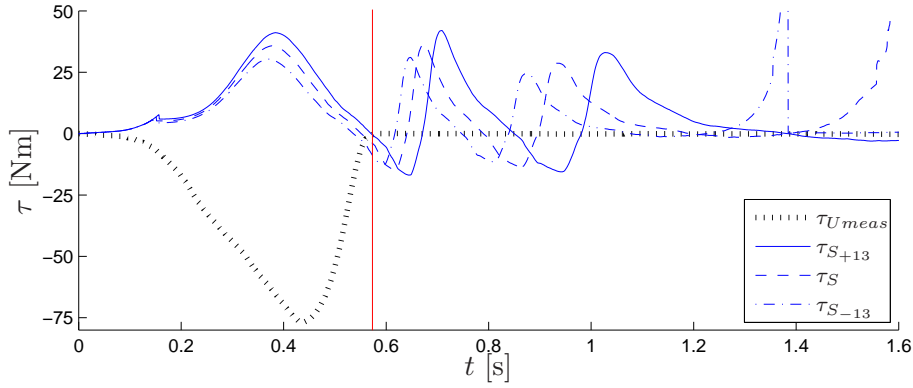


**Figure 4.16:** Measurement of typical user interaction torque  $\tau_U$  when closing the door with a fast motion and resulting internal door torque  $\tau_{door,i}$  (simulation) for a model scaling factor of 0.87 ( $\tau_{S-13}$ ), 1.00 ( $\tau_M$ ), and 1.13 ( $\tau_{S+13}$ ).

#### 4.2.1.10 Validation of the Door Model

For the validation of the updated model of the car door, we measured the interaction ( $\tau_{U_{meas}}, \varphi_{meas}$ ) with a car door that was rapidly closed by a human. Consecutively, we used  $\tau_{U_{meas}}$  as input for our door model, which was initialized with the start state of the real door ( $\dot{\varphi} = 0, \varphi = 1.087$  rad). In addition to the calculation of the motion for the standard simulation denoted by  $S$ , we varied the internal torque contribution  $\tau_{door,i}$  by  $\pm 13\%$ .  $\tau_U$  and the three different simulated torques are displayed in Fig. 4.16. The resulting simulated motions and their deviation from the measurement  $\varphi_{meas}$  are given in Fig. 4.17. The end of the user interaction is displayed by the red vertical line.

Obviously, while the variations of  $\pm 13\%$  show a strong deviation,  $\varphi_S$  and  $\varphi_{meas}$  are very close for a significant time. Only at the end of the closing there is a slight difference. The force measurement is not responsible for this deviation, as it occurred more than 0.2 s after the force signal settled at zero. So there might be a minor error in the model of the door. However, compared to the manufacturing tolerances of car doors (e.g. Coulomb friction in the door hinges:  $\tau_{F,C} = 4 \text{ Nm} \pm 2 \text{ Nm}$ ), this error is insignificant. Thus, we have a reliable dynamical model for the performance specification and the simulation of the car door.

#### 4.2.1.11 Selection of Admittance Control

The model of the car door can be haptically rendered by an impedance or an admittance control scheme. Admittance control would require the calculation of the reference acceleration  $\ddot{\varphi}_{ref}$  of the car door based on the simulated state ( $\dot{\varphi}_{ref}, \varphi_{ref}$ ) and the measurement of the user interaction  $\tau_U$  as

$$\ddot{\varphi}_{ref} = (\tau_{door,i}(\dot{\varphi}, \varphi, \tau_U, t, \theta, \xi) + \tau_U) / I_{zz} \quad (4.7)$$

Impedance control would require the calculation of the reference user interaction torque  $\tau_{ref}$  based on the measurement of the state ( $\dot{\varphi}, \varphi$ ) and the acceleration  $\ddot{\varphi}$ .

Admittance control is usually the preferred option when an inertia  $I_{zz,sim}$  has to be rendered which deviates significantly from the inertia of the device  $I_{zz,dev}$  [258]. Car doors

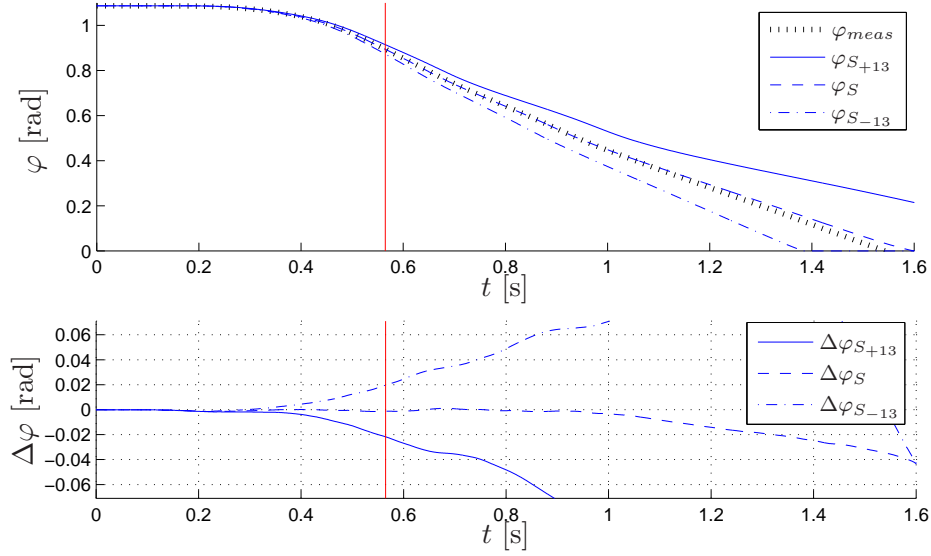


**Figure 4.17:** Resulting motion for a  $\tau_{U_{meas}}$ : Measurement (thick dashed line) and simulation for a model scaling factor of 0.87 ( $\varphi_{S-13}$ ), 1.00 ( $\varphi_M$ ), and 1.13 ( $\varphi_{S+13}$ ).  $\Delta\varphi$  denotes the difference between measurement and simulation.

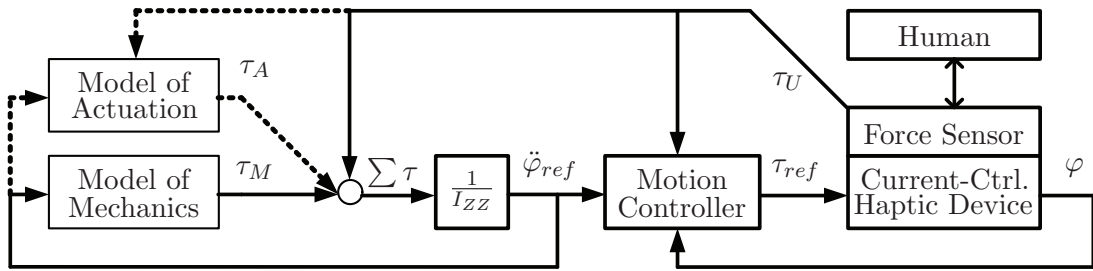


**Figure 4.18:** Modified active admittance control scheme for the haptic rendering of rotational car doors. The inclusion of the actuation is indicated by the dashed lines.

exhibit a much higher inertia than a typical haptic device, so we chose admittance control. A further benefit is that due to its underlying motion control loop it counteracts unmodeled dynamics of the haptic device.

In accordance with Sec. 2.3 and specifically Fig. 2.6, we used an active admittance control scheme for modeling and haptically rendering the car door. Due to the partitioning of the overall torque at this car door given in Eq. (4.3), we can sum-up all effective torques in  $\tau_{EOM} = \tau_U + \tau_{door,i}$  acting on the inertia of the car door,  $I_{zz}$ . Thus, we end up with the implementation depicted in Fig. 4.18 where the user torque  $\tau_U$  acts in parallel with the contributions of the actuation  $\tau_A$  and the mechanical elements  $\tau_M = \tau_{door,i} - \tau_A$  on the inertia  $I_{zz}$  of the simulated door, providing the reference motion  $\ddot{\varphi}_{ref}$ . Note that the motion controller should include feedback-linearization (e.g. compensation of  $\tau_U$ ) as well as feedforward-control (e.g. resolved acceleration control) in order to provide a good performance [258]; compare also subsection 4.1.1.3.

## 4.2.2 Performance Specification of the Haptic Device

The main requirements for the haptic device and its drive lay in the areas of current-control bandwidth, mechanical properties, torque output, and motion measurement.

### 4.2.2.1 Current-Control Bandwidth

A realistic simulation in the admittance display mode requires a step in the reference acceleration to be propagated to the current-controller of the haptic device. A typical PD position controller would not be suitable for this, because the step would be significantly shaped by a rather slow motion control loop (typical:  $\omega_0 \leq 50$  Hz). Rather, a feedforward control has to be used. We propose the advanced control scheme shown in Fig. 4.18. Based on (4.7), the reference acceleration  $\ddot{\varphi}_{ref}$  is calculated. It is tracked by a PD position controller with acceleration feedforward. Additionally, a feedback compensation linearizes the current-controlled plant. Thus, a stiff position control can be realized (see also [257]).

Which conditions have to be satisfied in order that the effective acceleration  $\ddot{\varphi}$  caused by  $\Delta\tau_{ref}$  is almost the same for reality and simulation (Fig. 4.18)? Obviously, the closed current-control loop of the haptic device should not be slower than that of the actuated door. However, if the actuated car door exhibits much more damping (due to friction) than the drive of the haptic device, this condition can be relaxed. We chose a lower limit of 500 Hz for the current-control bandwidth.

### 4.2.2.2 Maximum Speed

According to measurements, the maximum speed of the tip of the car door is  $\approx 4$  m/s in world coordinates. It occurs when the user applies a force at the very end of the door, thus when  $r > 0.8$  m. This means that the maximum rotational speed  $\dot{\varphi}_{max}$  that has to be displayed by the haptic device is  $\dot{\varphi}_{max} < 5$  rad/s  $< 1$  RPS.

### 4.2.2.3 Maximum Torque Output

The peak torque output capability of the drive, denoted by  $\tau_{max}$ , has to be at least 100 Nm to compensate  $\tau_U$  if necessary. However, such a high torque has to be displayed for a very short time only ( $t_{\tau_{max}} < 0.1$  s), so the rated torque may be considerably smaller. Note that  $\tau_{max}$  should not be exceedingly high, because it diminishes safety. Thus, a trade-off has to be found. For our case, we considered an upper bound of 150 Nm as appropriate.

### 4.2.2.4 Necessity to Use a Direct Drive

For many applications, including haptic rendering, relatively high torques and low velocities are desired when compared to the properties of standard electric motors. Thus, gearboxes between motor and load (often with transmission rates  $\gg 1$ ) are usually used to adapt these properties accordingly. Unfortunately, they introduce additional dynamics to the system. Depending on the respective gear concept, the most significant effects may be backlash, elasticity, and/or friction. Each of these effects can be detrimental for realistic haptic rendering.

In many practical haptic scenarios, only minor forces/torques ( $\leq 10\text{ N}/\leq 1\text{ Nm}$ ) have to be displayed to the user. This means that the influence of the physical elasticity of the gear may not be perceptible to the user, which allows the use of “zero-backlash” gears like the well-known Harmonic Drive. However, in our scenario  $100\text{ Nm} \leq \tau_{max} \leq 150\text{ Nm}$  is required. If we used a rather elastic gearbox, this torque would cause a significant contortion between end-effector and drive, immediately destroying the haptic illusion. If we used a gearbox which exhibits backlash, this backlash would become noticeable due to the long rod. Therefore, the use of a gearbox would inhibit high-fidelity haptic rendering, so the best way was to pass on a transmission and couple the load directly to the motor, which then is called Direct Drive (DD). Previous research has shown that DDs are suitable for achieving a high-fidelity control of a robot; compare for instance [79, 80]. While different types of motors can be used as a DD, the most common one is the brushless permanent magnet synchronous motor (PMSM, *brushless DC*). Such PMSM-DDs usually provide a very good dynamic response due to a small electrical time constant and the “missing” mechanical transmission components, as well as high torque at stall.

#### 4.2.2.5 Configuration

PMSM-DDs are available in two configurations: “frameless” and “standalone”. If the motor is to be an integral part of the device (which is often the case for machine tools), the motor should be delivered “frameless”, i.e. without housing and bearing. This means that the machine designer is responsible for the integration, which includes aspects such as providing sufficient heat dissipation, selecting an appropriate feedback device, and achieving a stiff construction with low friction. In contrast, “standalone” motors are complete servo motors which can be directly mounted on the load. These sometimes come with very stable bearings which resist more than the load we require. This is a key advantage, because then there is no need for mounting an external bearing, which would be prone to introduce backlash and unknown friction to the drive. Therefore, it is desirable to use a “standalone” DD with a sufficiently stable bearing.

#### 4.2.2.6 Mechanical Rigidity

A high-fidelity rendering of a car door requires a very stiff display of all non-simulated DOF. As every DOF of a robot introduces additional elasticities, amongst other detrimental effects, this motivates the building of a robot with only one rotational DOF. This requires that the DOF exhibits the same orientation as the hinge of the simulated car door. Furthermore, it should be possible to use various interaction points and adequate end-effectors, for instance the outer or the inner door handle. This can be achieved by mounting a stiff rod with a length  $r_{rod} = 1.1\text{ m}$  on a rotational drive, enabling the rendering of even very long doors. Various end-effectors can then be attached to the rod to simulate different interaction points.

The rod and the drive should withstand at least moderate unwanted forces exerted by the user orthogonally to the DOF. Even for a moderate force of  $f_U = 20\text{ N}$  acting at the very end of the rod causes an axial load of  $f_L = (m_{rod} + m_{ee})g + f_U < 100\text{ N}$  and a moment load of  $\tau_L = 220\text{ Nm}$ .

**Table 4.6:** Overview of Some Rotational Direct Drives for High-Fidelity Haptic Rendering.

|                 | Units            | Min.       | Danaher M.<br>DH101A<br>S600 | NSK<br>YSB5120<br>M-ESB-YSB | Parker<br>190ST2M<br>C3S150V4 | Parker<br>DR5300A<br>DR5000A | YASKAWA<br>SGMCS-80M<br>SGDH-15AE |
|-----------------|------------------|------------|------------------------------|-----------------------------|-------------------------------|------------------------------|-----------------------------------|
| Max. Torque     | Nm               | $\geq 100$ | 120                          | 120                         | 119                           | 300                          | 240                               |
| Max. Rot. Speed | RPS              | $\geq 1$   | 5.0                          | 3                           | 8.3                           | 5.0                          | 5.0                               |
| Position Res.   | bit              | $> 15$     | 20                           | $\approx 20$                | 16                            | $\approx 19$                 | 20                                |
| Abs. Pos. Acc.  | arc sec          | -          | $\pm 27$                     | $\pm 150$                   | $\pm 600$                     | $\pm 45$                     | $\pm 15$                          |
| Repeatability   | arc sec          | -          | $\pm 1.2$                    | $\pm 1.6$                   |                               | $\pm 5.0$                    | $\pm 1.3$                         |
| Max. Axial Load | N                | $\geq 500$ | 52000                        | 19600                       | 25000                         | 3991                         | 9000                              |
| Max. Mom. Load  | Nm               | $\geq 100$ | 437                          | 400                         |                               | 20                           | 180                               |
| Inertia         | kgm <sup>2</sup> | $\leq 1$   | 0.069                        |                             | 0.010                         | 0.340                        | 0.063                             |

#### 4.2.2.7 Position Measurement

According to [129], humans have a spatial resolution of up to  $5\ \mu\text{m}$ . Given a maximum lever length of 1.1 m, an ideal haptic device would therefore require at least a positioning accuracy and repeatability of  $< 1$  arcsec and thus a position resolution of  $\gg 20$  bit. For our case, a lower rotational resolution of about 16 bit should be sufficient, because the handling of a car door does not involve precise positioning. However, a higher resolution enables a higher angular stiffness of the motion-controlled direct drives, so resolutions of up to 20 bit are recommended [122].

### 4.2.3 Design of the Haptic Device

#### 4.2.3.1 Selection of a Suitable Direct Drive

It was a surprisingly difficult task to find a DD that fulfilled all requirements. Many otherwise interesting PMSM-DDs (e.g. ALXION 145 STK or Intellidrive SRT-67) were not available in a standalone configuration (without bearing). Furthermore, most of the motors come with either far too low or far too high torques, so  $\tau_{max}$  was also a major constraint. Other issues were the position resolution and the maximum moment load.

Finally, we identified some suitable PMSM-DDs, which may also be of interest for other haptic applications: the DH101A of Danaher Motion, the YSB5120 of NSK, and the 190ST2M of Parker. As can be seen in Tab. 4.6, these motors fulfill our requirements. When we learned that the 190ST2M exhibits a superb low friction and a very low torque ripple, we chose it despite the fact that the other two alternatives might have provided a similar behavior.

#### 4.2.3.2 Motion and Force Sensors

To improve the quality of the position resolution, we mounted an additional 16-bit incremental encoder to the 190ST2M, which is originally equipped with a resolver. In combination with quadrature-encoder technology, this enabled a resolution of 18 bit.

A precise measurement of the interaction force up to 100 N is mandatory to achieve a high-fidelity haptic rendering. We chose the 85040 from burster, which was mounted between the end of the rod and the door handle.



**Figure 4.19:** Setup of the high-fidelity haptic car door simulator with visual feedback (l.) and the corresponding user-friendly GUI for interactively changing simulation parameters.

#### 4.2.3.3 Safety Measures

The haptic device had to be designed to ensure a safe operation because it is not only to be used by professionals, but also by participants of user studies. Therefore, a variety of safety measures have been implemented:

- **Emergency sensors:** Mechanical switches ensure that the device does not hit the mechanical bounds. Additionally, an automatic vigilance device and an emergency stop switch enable manual emergency braking.
- **Software:** The driver unit as well as the real-time control model monitor a variety of signals. If one of them triggers an emergency, the power stage of the driver unit is disabled and emergency braking is performed.
- **Braking:** In the event of emergency, the movement of the drive has to be stopped very quickly. We chose the INTORQ 14.115 in combination with an additional high-speed switchgear. This gives a breaking time of  $t_{stop} \approx 45$  ms.
- **Mechanical bounds:** As the angle is confined to  $\Delta\phi \leq \frac{\pi}{2}$ , a mechanical construction is used to set a hard motion limit.

#### 4.2.3.4 Mechanical Construction

The very stiff mechanical construction featuring the safety construction and the end-effector with the force sensor is displayed in Fig. 4.19 (l.). In its background, a large

visual display enables a high-quality graphical rendering of the virtual door. The right picture shows the graphical user interface (GUI) that we designed in order to enable an easy, interactive modification of simulation parameters for the people working with the simulator.

#### 4.2.4 Evaluation of the Transparency of the Haptic Rendering

The realization and evaluation of highly transparent haptic rendering has a long tradition; compare for example the psychophysical research regarding the perception of spatial and temporal torque variation for the manual interaction at rotational knobs [250] or on thresholds for the detection of dynamic changes in a rotary switches [273].

To evaluate the quality of our haptic simulation we conducted a user-experiment comparing the dynamics of the simulated door to those from a real door. We raised the following research questions (Q) in this context:

1. Can participants detect the difference between the real door and the simulation?
2. Is there a negative trend in subjective perception with decreasing quality of the haptic simulation?
3. Do the users note small variations in the haptic simulation ( $\pm 13\%$ )?

##### 4.2.4.1 Evaluation of the Door Simulator by a User Study

We wanted to achieve a direct comparison of the haptic simulation with the corresponding real car door (BMW 3 Series). For our investigations, besides the door model described in this thesis (denoted as  $S$ ) we also used four variations of it. The variations were achieved by scaling the internal door torque:

$$\tau_{door,i_{S(k-1)}} = k\tau_{door,i}, \text{ where } k = \{0.61, 0.74, 0.87, 1.13\} \quad (4.8)$$

These variations are denoted as  $S_{-13}$ ,  $S_{-26}$ , and  $S_{-39}$  (negative scalings) and  $S_{+13}$  (positive scaling) in the following. The three negative scalings were introduced to investigate the trend in subjective ratings with decreasing quality of the simulation model. The positive scaling was used to investigate the small change of  $S_{-13}$  also in the opposite direction  $S_{+13}$ . In this way we gain information on the symmetry of the effects of parameter changes. We were interested if participants can already detect the lower quality of the simulation model in this interval (the torque variation can be seen in Fig. 4.17). Because we wanted to avoid unnecessary workload, we did not introduce the positive variations 26% and 39%. Additionally to the five comparisons between the real door and the simulations mentioned above, the participants compared the real door with itself (denoted as  $R$ ) to have a reference of the perceptual capacities of the users.

Each participant had to judge all six comparisons (repeated measurement design) twice, resulting in 12 trials. In this way we gained insights into intrapersonal reliability (difference between two judgments of the same condition) and increased the overall reliability of the data set. We asked participants to describe the perceived difference of each of the six condition-pairs on a four-point scale:



**Figure 4.20:** Experimental setup: Real door (l.) and haptic device (r.) with equally adjusted feet positioning elements for the blindfolded participants.

1. I feel no difference at all.
2. I feel rather no difference.
3. I feel rather a difference.
4. I feel a difference.

The two middle levels were included to enable a non-binary decision, because we assumed that this further increases the reliability. Additionally, the participants expressed a more detailed description of the perceived level of identity of two conditions by rating it on a 10-point scale (10  $\equiv$  absolutely identical, 0  $\equiv$  absolutely not identical).

The experimental setup with the haptic device right to the real door can be seen in Fig. 4.20. To eliminate confounding auditory or visual information, participants were blind-folded throughout the whole experiment and wore headphones playing pink noise during the actual door/simulation-testing. Because the two setups could not be moved around, we guided the participants along confusing trajectories between the experimental trials. In this way, the spatial information about which door was the real one was removed. The real door was equipped with the same door handle as the haptic device to avoid a difference in the geometrical information. This was additionally ensured by the fact that participants wore thick rubber gloves to impair the tactile perception.

Furthermore, we randomized the order of the presented comparisons, so any information learned through the experiment would influence the trials in the same way when results are averaged. To ensure that the leverage and the resulting dynamic configurations do not disturb the perception of the door dynamics, we standardized the feet positions of the participants in each trial (polystyrene elements in front of the setups, see Fig. 4.20).

One remaining challenge to control unwanted influences on the actual kinesthetic perception of the door dynamics was a small vibration found in all simulator conditions. This

**Table 4.7:** Percentages of answers on the four-point scale of perceived difference between the six conditions and the real door.

| condition                | $R$  | $S_{+13}$ | $S$  | $S_{-13}$ | $S_{-26}$ | $S_{-39}$ |
|--------------------------|------|-----------|------|-----------|-----------|-----------|
| No difference (%)        | 91.7 | 8.3       | 0.0  | 0.0       | 8.3       | 0.0       |
| Rather no difference (%) | 8.3  | 0.0       | 33.3 | 41.7      | 0.0       | 0.0       |
| Rather a difference (%)  | 0.0  | 25.0      | 33.3 | 25.0      | 8.3       | 0.0       |
| Difference (%)           | 0.0  | 66.7      | 33.3 | 33.3      | 83.3      | 100.0     |

could be decreased in future implementations by reducing the current ripple caused by the PWM stage [186, 23] or by applying an advanced Direct Torque Control scheme [96, 198]. We counteracted the vibration in two ways: a) participants were explicitly instructed that vibrations had to be ignored and b) we used a small shaker to cause a similar vibration at the real door. A comparison of the power spectrum of the two test stands revealed differences in the vibration frequencies and amplitudes. However, in a pretest with three participants only one reported a perception of the vibration differences.

Seventeen participants (8 females; age:  $26 \pm 5.8$ ) took part in the experiment. First, they were instructed about the task. Then, they were blindfolded and led to the experimental setup where we introduced all six conditions to them. Thus, the participants knew the amount of differences beforehand and had a reference for their judgments. The participants were trained by guidance to move the door in a standardized fashion (in terms of velocity and angle range): They had to make two slow and two fast movements across two distinctive rest positions of the door detent (approximately corresponds to  $0.25 \text{ rad} \leq \varphi \leq 0.95 \text{ rad}$ ). This pattern was kept constant when participants performed the movement alone in the actual experiment. Then, the experimenter only guided the participants' preferred hand to the door handles.

#### 4.2.4.2 Results

One male participant had to be excluded from the analysis because he did not give task-relevant answers (his values in both scales were more than three standard deviations away from the mean value). For the remaining 12 participants Tab. 4.7 reports the percentages of answers on the four-point scale for felt differences between the six conditions with the real door (based on all data points, i.e. 24 values).

It can be seen that participants did not always recognize the real door compared to itself which reflects a general inaccuracy in the judgments. However, it is obvious that the haptic simulation model ( $S$ ) was not comparable with the real door in subjective perception. If the quality of the simulation model was reduced, the difference to the real door was more clearly perceived. An exception is the  $S_{-13}$  condition which was rated even better than  $S$ .

A similar pattern can be found when illustrating the subjective rating on the 10-point scale (see Fig. 4.21). This analysis is based on the *mean* values per person and condition. This transformation is necessary to allow for inference statistic analysis which demands independence of data points [91], which cannot be guaranteed with repeated measures for the same condition. We conducted a one-factorial repeated measurement ANOVA (analysis of variance) to test for an influence on the door-comparisons presented on the subjective

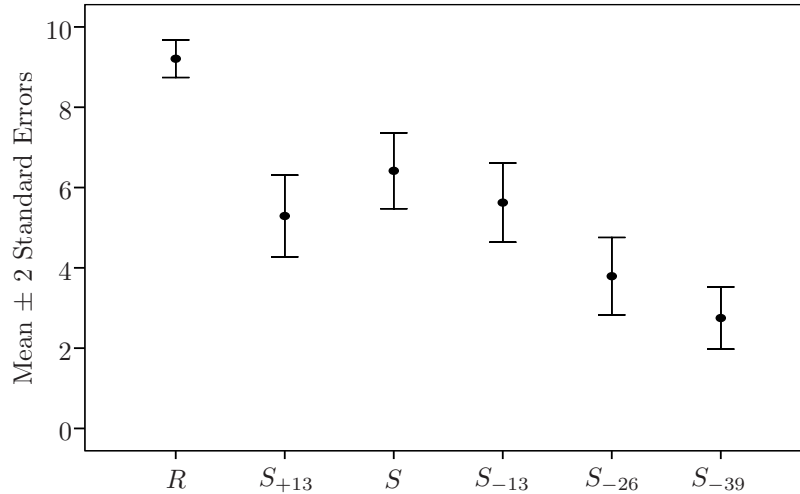


**Figure 4.21:** Mean values per participant on the 10-point scale: The real condition is correctly perceived as identical with itself, whereas with decreased quality of the haptic simulation the two conditions are judged less identical.

**Table 4.8:** Bonferroni adjusted post-hoc tests for the differences between experimental conditions and the real door (significant differences on a 5% level are marked with \*).

| Condition               | <i>R</i> | <i>S</i> <sub>+13</sub> | <i>S</i> | <i>S</i> <sub>-13</sub> | <i>S</i> <sub>-26</sub> | <i>S</i> <sub>-39</sub> |
|-------------------------|----------|-------------------------|----------|-------------------------|-------------------------|-------------------------|
| <i>R</i>                | -        | 0.000*                  | 0.000*   | 0.000*                  | 0.000*                  | 0.000*                  |
| <i>S</i> <sub>+13</sub> | 0.000*   | -                       | 0.610    | 31.000                  | 0.174                   | 0.040*                  |
| <i>S</i>                | 0.000*   | 0.610                   | -        | 1.000                   | 0.002*                  | 0.001*                  |
| <i>S</i> <sub>-13</sub> | 0.000*   | 1.000                   | 1.000    | -                       | 0.044*                  | 0.002*                  |
| <i>S</i> <sub>-26</sub> | 0.000*   | 0.174                   | 0.002*   | 0.044*                  | -                       | 1.000                   |
| <i>S</i> <sub>-39</sub> | 0.000*   | 0.040*                  | 0.001*   | 0.002*                  | 1.000                   | -                       |

judgment on the 10-point scale. A significantly big effect of this factor was found:  $F(5, 55) = 39.06$ ;  $p < 0.001$ ; partial  $\eta^2 = 0.780$ . Therefore, we report the Bonferroni-adjusted pairwise comparisons of the six different conditions in Tab. 4.8. As expected from the previous analysis, the real door is rated significantly more frequently identical to itself than any other condition. The *S*<sub>-39</sub> condition and *S*<sub>-26</sub> condition were judged significantly less identical with the real door than any other condition. However, there were no significant differences found between the comparison with *S* and the  $\pm 13\%$  deviation. Participants did not note differences within this interval. This may explain, why the *S*<sub>-13</sub> condition is rated better than *S* in the first analysis.

#### 4.2.4.3 Discussion

In relation to our research questions we can summarize the results as follows: Participants can clearly detect the difference between the haptic simulation model and the real door in 33.3% of the cases and were unsure in 66.6% of the cases (two middle levels of four-point scale; compare Tab. 4.7). However, they never misjudged the simulation for the real door

(Q1). To gain deeper insights into the subjective perception of the differences we introduced a 10-point scale judging how identical two presented conditions (one of them always the real door) were. Descriptive results show a clear trend of subjective judgment worsening with decreasing quality (in terms of lower scaling parameter  $k$ ) of the haptic simulation. Hence, participants could actually perceive these differences in simulations (Q2). However, the inference statistic analysis revealed that the differences within 13% deviation around the simulation model are not significant, meaning that descriptive differences cannot be generated on a larger population (Q3).

We have to assume that the difference can be felt somewhere between -13% and -26% deviation from  $S$ . To estimate the exact value here can be the subject of more elaborated evaluations of the haptic simulation. One possible explanation for the perceived difference between the real door and the haptic simulation model can be seen in the different vibrations of the two test stands, which may have provided information to the participants regarding which one they were judging.

For the quality of the haptic simulation the current results hint that there is room for improvement. This is in accordance with a recent investigation on the perception of a haptically rendered knob, where one conclusion was that the rendering of detents should technically be improved [249]. At this state of development, fine differences in parameters (within a 13% interval) should not be tested with the haptic simulation, whereas bigger deviations can be investigated.

## 4.2.5 Additional Evaluations and Results

Besides the investigation of the transparency of haptic rendering for conventional doors, the experiment partly described in Sec. 4.2.4.1 aimed at some additional research questions:

- Does the transparency perception change if the door and the simulator are inclined?
- Does an increase of the energy consumption of the manual door operation significantly affect the usability?
- Is a negative-damping support provided by an actuation appreciated by users?

These topics formed the latter part of the experiment described. The results are briefly described in the following.

### 4.2.5.1 Transparency of the Rendering of Inclined Doors

To investigate the transparency of the rendering of inclined doors, the whole setup was modified to correspond to an inclination of  $3.5^\circ$  and  $5.0^\circ$ . This was achieved by lifting the frame at which the real car door was attached to, which necessitated an adjustment of the height of the ground level the participants walked on as well as the height of the simulator. The inclination setup can be seen in Fig. 4.22.

In the reference simulations, the corresponding inclination was defined. Additionally, we defined one lower and one higher inclination to enable a comparison.

The inclination part of the experiment was conducted the same way as described in subsection 4.2.4.1. The corresponding results are depicted in Fig. 4.23. Obviously, for both inclinations the real condition was no longer discriminated clearly from the best



**Figure 4.22:** Experimental hardware setup for the investigation of the transparency of the haptic rendering of an inclined car door.

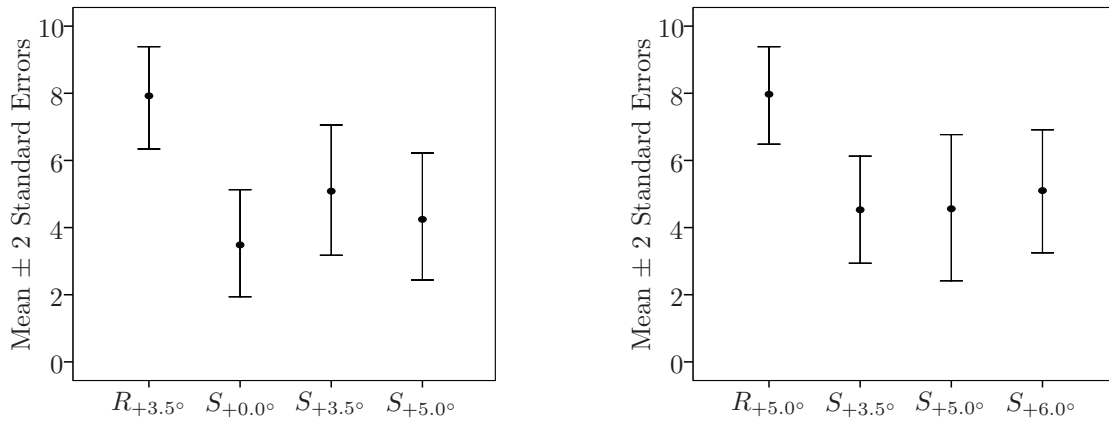


**Figure 4.23:** Mean values on the 10-point scale for the inclined setup: The real condition is not discriminated clearly from simulations. This can be seen from the interference of the intervals for  $R_{+3.5^\circ}$  and  $S_{+3.5^\circ}$  (l.) and for  $R_{+5.0^\circ}$  and  $S_{+5.0^\circ}/S_{+6.0^\circ}$  (r.).

simulations when compared to Fig. 4.21, because the intervals for  $R_{+3.5^\circ}$  and  $S_{+3.5^\circ}$  as well as  $R_{+5.0^\circ}$  and  $S_{+5.0^\circ}/S_{+6.0^\circ}$  interfere. This is mainly due to the fact that the gravity effect on the manual operation is a load for the operator and makes it harder for him or her to feel small differences.

#### 4.2.5.2 Preferred Effort: Variation of Friction and Door Detent

After the inclination part of the experiment, we asked the participants to compare variations of the door simulation to the reference simulation  $S$ . Our intention was to get a coarse impression of the preferred effort of the manual operation of a car door. The hypothesis was that a heuristic finding in the automotive industry is true: Small and medium efforts are well accepted by users, but large efforts are not.

For this purpose, we set up six simulations. In three simulations ( $S_{xC,1,0D}$ ), we varied the

| Rating  | $S_{0C,1.0D}$ | $S_{5C,1.0D}$ | $S_{8C,1.0D}$ | $S_{0C,1.2D}$ | $S_{5C,1.2D}$ | $S_{8C,1.2D}$ |
|---------|---------------|---------------|---------------|---------------|---------------|---------------|
| Much w. | 0             | 3             | 1             | 2             | 8             | 5             |
| Worse   | 1             | 4             | 6             | 5             | 6             | 8             |
| Neutral | 7             | 2             | 5             | 5             | 2             | 3             |
| Better  | 7             | 6             | 4             | 5             | 1             | 1             |
| Much b. | 2             | 2             | 1             | 0             | 0             | 0             |

**Figure 4.24:** Evaluation of the preferred effort: Count of the ratings for the opening motion.

| Rating  | $S_{0C,1.0D}$ | $S_{5C,1.0D}$ | $S_{8C,1.0D}$ | $S_{0C,1.2D}$ | $S_{5C,1.2D}$ | $S_{8C,1.2D}$ |
|---------|---------------|---------------|---------------|---------------|---------------|---------------|
| Much w. | 1             | 1             | 4             | 6             | 7             | 6             |
| Worse   | 3             | 3             | 8             | 9             | 8             | 11            |
| Neutral | 6             | 5             | 3             | 1             | 1             | 0             |
| Better  | 6             | 7             | 2             | 1             | 1             | 0             |
| Much b. | 1             | 1             | 0             | 0             | 0             | 0             |

**Figure 4.25:** Evaluation of the preferred effort: Count of the ratings for the closing motion.

Coulomb friction to equal 0/5/8 Nm. In three more simulations ( $S_{xC,1.2D}$ ), we additionally increased the door detent torque by 20%. The rating scale ranged from 2 (“much better”) to -2 (“much worse”). The evaluation results are given in Fig. 4.24 (opening motion) and Fig. 4.25 (closing motion) by the count of the corresponding ratings.

There is a significant tendency in the results for both the opening and the closing effort: The larger the Coulomb friction and the larger the door detent torque, the lower the appreciation by the participants. Accordingly, the door simulation providing the minimum effort,  $S_{0C,1.0D}$ , was rated best.

Another interesting finding is that the acceptance of a high effort depends on the mode of operation: Obviously, it is more disturbing for closing motions. This is due to the fact that people tend to close doors with a push, while the opening motion is typically slower.

This fact should be exploited in the controller design of actuated car doors: Instead of searching for an overall trade-off for the rendered dynamics, the dynamics should be adapted for each mode of operation individually. Based on the result displayed in Fig. 4.25, a high potential for increasing the level of comfort of the user is especially seen in supporting the closing process.

#### 4.2.6 Simulation and Evaluation of a Semi-Actuated Car Door

In [163], an actuated car door comprising an electro-rheological damper has been proposed. This damper is a semi-active actuator as it only can be used to decelerate the door. Thus, on the one hand its capability to render specific door dynamics is very limited, because it cannot increase the kinetic energy of the door. On the other hand, the intrinsic passivity of this adaptive damper makes it interesting for the automotive industry due to safety concerns.

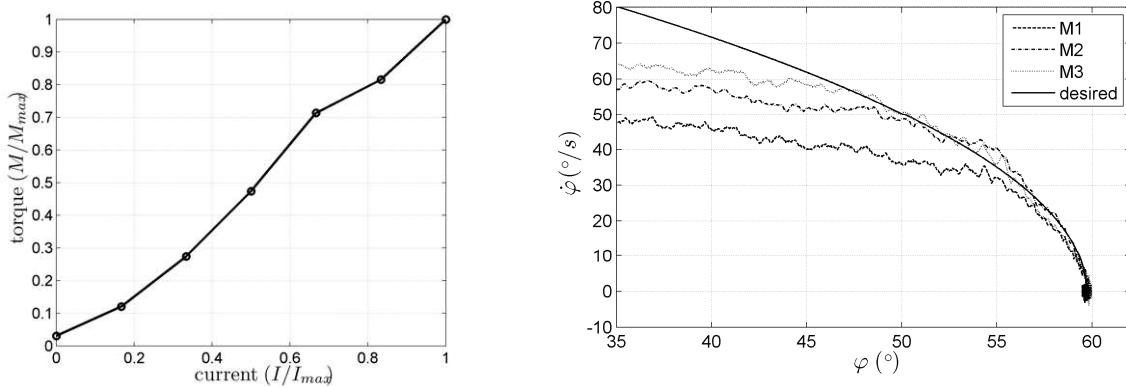


**Figure 4.26:** Actuated door proposed in [163]: Characteristics of the electro-rheological actuator (l.) and measured deceleration trajectories (r.).

#### 4.2.6.1 Hardware Model

Besides the characteristic diagram given in Fig. 4.26 (l.), a model of the damper was provided in [163]: Due to the large inductance of the electric circuit, the actuation was approximated by a low-pass with time constant of  $T = 0.01$  s and an adjustable gain.

Our intention was to investigate the haptics of a BMW 3 Series door combined with such an adaptive damper. Thus, we applied the model of the adaptive damper to the door model described in subsection 4.2.1.2.

#### 4.2.6.2 Deceleration, Collision Avoidance, and Variable Door Detent

In [163], a deceleration algorithm, a simple collision avoidance, and a variable door detent were introduced. Corresponding measured deceleration trajectories can be seen in Fig. 4.26 (r.). However, the whole control structure is aimed at the automatic control, not at a manual operation of the car door. Accordingly, no test of the manual operation of an actively damped car door has been performed in [163] or, to the best of our knowledge, in any other publication. In the following, we describe our experience with collision avoidance and door detent implementations for the haptic simulation of the car door.

Our implementation of the collision avoidance presented in [163] worked well for standard scenarios; compare Fig. 4.27. However, if a user moves the door very quickly, the counteracting torque is not sufficient to stop the door before an obstacle. To improve this, we propose a variation of the collision avoidance, where the decelerating torque of the adaptive damper is applied in a PWM manner (see Fig. 4.28). This effectively conveyed to users that they should not further accelerate the door, effectively preventing collisions. The disadvantage of this method is that less kinetic energy is dissipated. However, as long as the user operates the door manually, his or her impact on the motion of the door is much more important.

Thus, a promising approach is to combine both methods: As long as the user operates the door, the PWM method should be applied, and in all other cases the more energy-dissipating conventional method should be applied. This worked well at the car door simulator, where the interaction force was used as a measure to distinguish between manual

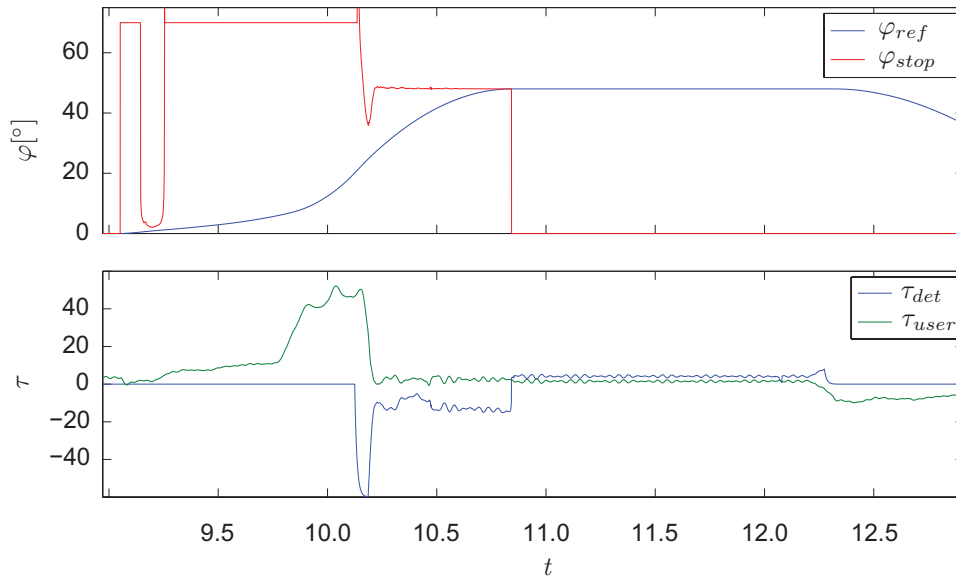


**Figure 4.27:** Collision avoidance method 1 (example:  $\varphi_{stop} = 48^\circ$ ): The braking torque is limited to  $\tau_{det,max} = 60$  Nm and is applied only for  $\varphi_{ref} > 30^\circ$ .

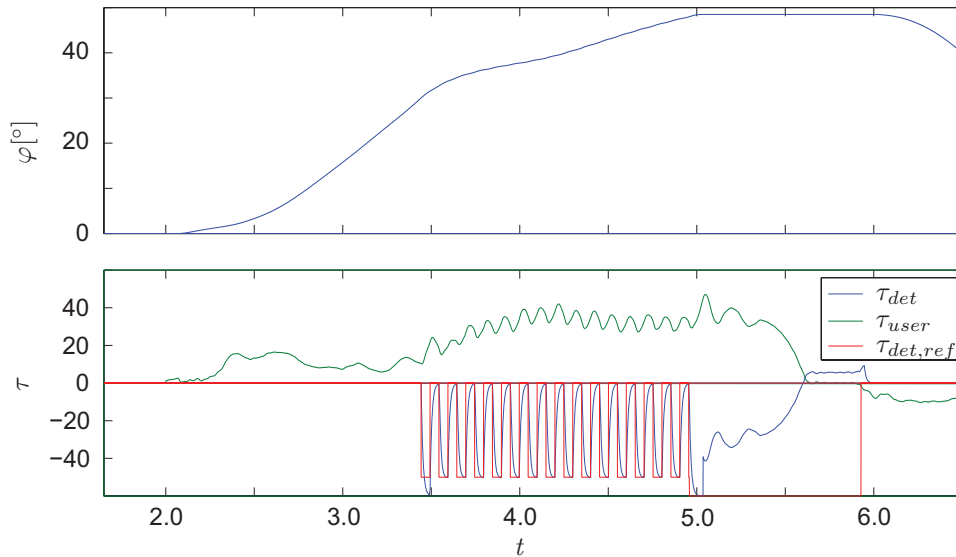


**Figure 4.28:** Collision avoidance method 2 (example:  $\varphi_{stop} = 48^\circ$ ): The braking torque is limited to  $\tau_{det,max} = 60$  Nm and is applied in a PWM manner with  $T = 0.1$  s only for  $\varphi_{ref} > 30^\circ$ .

| Rating  | $S_{DD,1.0,o}$ | $S_{DD,0.8,o}$ | $S_{DD,1.2,o}$ | $S_{DD,1.0,c}$ | $S_{DD,0.8,c}$ | $S_{DD,1.2,c}$ |
|---------|----------------|----------------|----------------|----------------|----------------|----------------|
| Much w. | 4              | 1              | 2              | 1              | 0              | 0              |
| Worse   | 6              | 6              | 5              | 3              | 6              | 5              |
| Neutral | 1              | 1              | 2              | 2              | 5              | 3              |
| Better  | 3              | 4              | 3              | 7              | 3              | 4              |
| Much b. | 3              | 5              | 5              | 4              | 3              | 5              |

**Figure 4.29:** Results of the evaluation of the simulated variable door detent.

and automatic operation.

The variable car door detent proposed in [163] is similar to the one proposed by us in [240]: If the door detent is activated, a virtual fixture counteracts a motion of the door until a predefined force or velocity threshold is exceeded; see also Fig. 5.21. We implemented this for the adaptive damper simulation.

#### 4.2.6.3 Evaluation of the Variable Door Detent

In the comprehensive evaluation as described in subsection 4.2.4 and subsection 4.2.5, the last part was to rate a car door simulation without a mechanical door detent, but with the active variable door detent. Due to the absence of the mechanical door detent, the only dissipating element was the Coulomb friction of the door hinge. Thus, the door could easily be moved after the variable door detent was unlocked.

The evaluation of the door detent was undertaken according to the evaluation of the preferred effort (subsection 4.2.5.2). The participants compared three variations of the variable door detent against the reference simulation  $S$ : the reference implementation  $S_{DD,1.0}$  and two versions with a lower  $S_{DD,0.8}$  and a higher  $S_{DD,1.2}$  force threshold for the deactivation of the variable door detent. The results can be seen in Fig. 4.29.

Obviously, the best rating was achieved by the highest force threshold ( $S_{DD,1.2}$ ) for both the opening and closing motion. However, even this setting polarized the participants, with five disapproving the manual interaction during closing and seven the one during opening the door. We think that the predominant reason for the disapproval was the unexpected low friction, as this led to a larger-than-expected acceleration of the door. Some participants stated that they were concerned about this behavior.

It should be noted that there was a positive learning effect: Between the first and the last opening motion, the average rating improved by 0.31 points; the average rating of the closing motion even improved by 0.46 points. This is a clear indication that some users began to like the manual door operation after they had got used to it. Many user comments made during and after the experiment support this observation.

#### 4.2.7 Summary

We derived the basics for the performance specification of the haptic car door simulator with one rotational DOF based on the analysis of a typical worst-case user interaction and a detailed model of a car door. It was pointed out that the promising inclusion of

actuation effects into the haptic rendering of car doors does not impose serious additional restrictions. Furthermore, a very detailed model for a BMW 3 Series driver's car door was derived and implemented. The accuracy of the overall model was shown by comparing the simulated motion with measurements. In the performance specification we concluded that a one-DOF setup consisting of a direct drive with a high mechanical stiffness, a maximum torque output of  $100 \text{ Nm} \leq \tau_{max} \leq 150 \text{ Nm}$ , and a high control bandwidth have to be used.

We compiled appropriate direct drives, selected one and created a backlash-free, very stiff haptic device to which various end-effectors can be attached. Accurate force and position sensors enable a high-fidelity rendering. Various measures ensure a safe operation of the device. To ensure an efficient and safe use of the car door simulator at BMW Group, a 15-page manual has been developed. It explains some basics, presents the architecture of the hardware and software, and provides a step-by-step guidance for operating the door simulator.

To evaluate the quality of the door simulation, an extensive user study with 17 participants was conducted. We found that the participants can distinguish between simulation and reality. However, the standard model of the car door is rated rather similar to reality, and linear deviations from the standard model were rated linearly decreasing. An important result is that the haptic simulation can reliably be used to evaluate different door concepts if the difference between them is at least in the area of 13% to 26%, or 5 Nm to 10 Nm, respectively. However, if the door was inclined, the participants could no longer clearly discriminate between reality and simulation.

When we investigated the preferred efforts for the manual operation of the door, we found that the larger the Coulomb friction and the larger the door detent torque, the lower the appreciation by the participants. This was more evident for closing motions, because people tend to close doors with a push, while the opening motion is typically slower. This fact should be exploited in the controller design of actuated car doors: Instead of searching for an overall trade-off for the rendered dynamics, the dynamics should be adapted for each mode of operation individually.

Finally, we simulated a car door actuated by an electro-rheological damper. A user study showed that an active variable door detent rendered by this door polarized the participants. Further improvements, especially the inclusion of a suitable friction, could raise the approval of this assistance function.

## 5 Control and Evaluation of Two Physical Prototypes of Actuated Car Doors

Actuated car doors with more than one degree of freedom (DOF) have been filed as a patent [242], investigated, and evaluated by us for the first time. We utilized Virtual Reality Prototyping (VRP, described in Chap. 2) to develop and haptically simulate a variety of actuated car doors (Sec. 4.1), for instance a Two-Link Car Door (TLD). The implemented, generic functionalities include intention recognition (Sec. 3.1), path planning (Sec. 3.2), collision avoidance (Sec. 3.3), and an adaptation of rendered dynamics. Several user studies showed benefits and a significant user approval of the proposed concepts.

To put these results into practice and to verify them, together with the institutes RCS and MiMed (TU München) we developed the prototype of an actuated TLD within the research project MechaTUM. Our research questions were whether and to what extent the VRP implementations could be transferred to the prototype, and if the haptic support of the door operation is appreciated as much as could be expected from the VRP evaluation results (see subsection 4.1.5). The control and very positive evaluation of the TLD prototype are described in Sec. 5.1.

However, a series development of this TLD for the automotive mass market would raise several difficulties, for instance in the domain of mechanical engineering (stiffness, weight, and wear issues). In fact, a major reason for the predominance of conventional car doors is that this is a mature technology which enables a cheap, reliable, and relatively light weight construction. This motivated the design of a close-to-series actuated car door.

A prototype of an actuated car door with one rotational DOF was developed by BMW Forschung und Technik GmbH. We developed and investigated force measurement concepts (patent pending [245]) for such a conventional car door structure. Furthermore, we implemented a variety of controllers for the manual operation of this door. Together with the successful user study, these issues are described in Sec. 5.2.

### 5.1 Two-Link Door Prototype with Two Actuated DOF

The TLD prototype and the overall structure of the controlled system are described in subsection 5.1.1. An identification reveals the existence of three elasticities, one of which is highly nonlinear. For the five generalized coordinates, no full state controller can be achieved. Therefore, in subsection 5.1.2 a combination of position and damping controllers is implemented which enables a sufficient automatic door operation. In subsection 5.1.3, the transfer of the overall structure and the implemented methods used for the VRP simulation described in Sec. 4.1 is discussed. An interesting result is that the control solution developed on the VRP test bed is indeed applicable to the real-world prototype without major modifications. Both manual and automatic operation of the prototype are

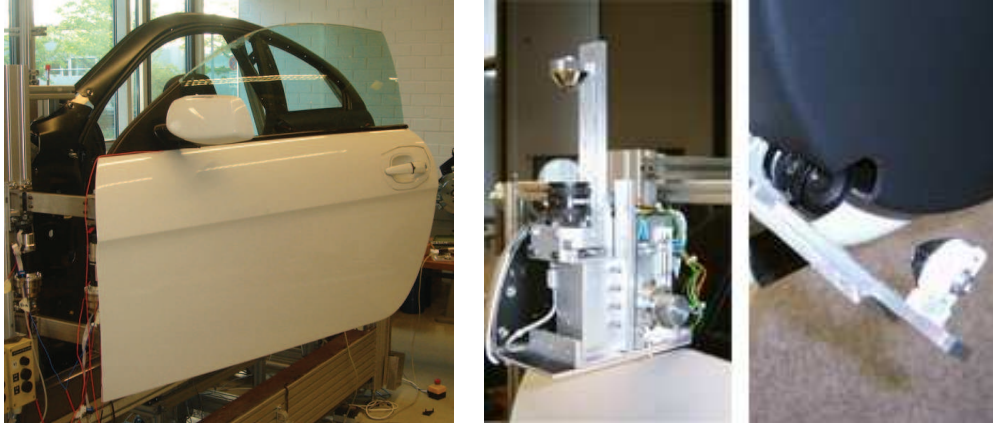


**Figure 5.1:** Setup of the prototype of the TLD, featuring two omni-directional cameras (m: mounted on top of the door mirror, r: mounted at the car door edge) provided by RCS (TU München) for enabling collision avoidance and clamping protection.

evaluated with very positive results in two user studies with a total of 51 participants (see subsection 5.1.4.2).

### 5.1.1 System Description

The mechanical design and realization of the TLD prototype was performed at the institute MiMed (TU München). It was decided to use a conventional car door body and a corresponding car chassis frame. To achieve a stable and at the same time compact construction, the link length between joint 1 and joint 2 was chosen to be only 0.24 m. This is significantly less than the 0.45 m of the VRP simulation, resulting in a reduced workspace.

To enable a backlash-free haptic interaction, drives consisting of a DC motor (maxon RE40) and a Harmonic Drive transmission (CSG-14-100-2UH) were chosen. While these are (almost) backlash-free, due to their “FlexSpine” they come with a limited stiffness. In addition to this elasticity, the shafts connecting transmissions and structure were expected to exhibit another non-negligible elasticity.

#### 5.1.1.1 Elasticity

We performed the following experiment to identify the joint stiffness: The joint configuration was fixed to  $\mathbf{q} = (\frac{\pi}{4}, 0)^T$  by the brakes of the DC motors. The corresponding work space coordinates of joint 1, joint 2, and the outer door handle (haptic interaction point, HIP) were measured by using a high-accuracy 3D meter, the FaroArm™ Quantum (accuracy:  $\pm 1.6e^{-5}$  m). Afterwards, a constant external force was exerted at the HIP. The work space coordinates of joint 1, joint 2, and the HIP were measured again.

The results enabled the determination of the overall joint stiffness:  $k_{jnt} = 1305 \text{ Nm/rad}$ . Furthermore, they revealed that there is another significant elasticity in the system: The structure of the car door body, and in particular its connection with drive 2. The overall car door body stiffness measured in the experiment resulted in  $k_{door} = 2763 \text{ Nm/rad}$ .

Unfortunately, more thorough investigations revealed that this car door body stiffness

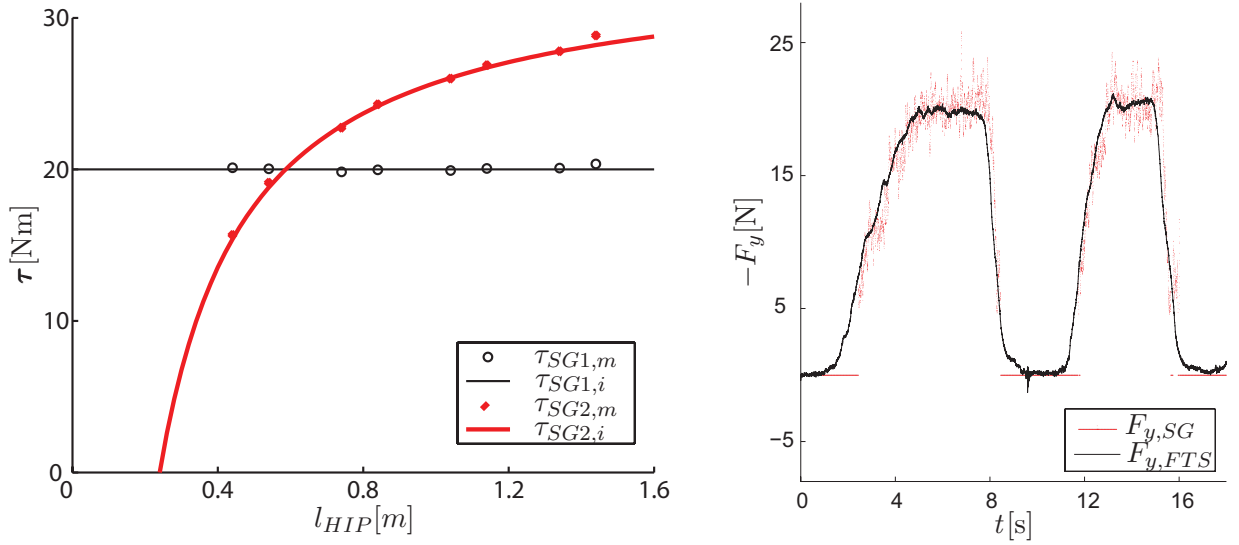


**Figure 5.2:** Validation of force and joint torque measurement of strain gauges (SG) and force-torque-sensor (FTS):  $\tau_{SG1,i} = 20$  Nm was applied by motor 1 while the brake of drive 2 was engaged and the HIP was varied. The resulting  $\tau_{SG2,m}$  closely matches the predicted value  $\tau_{SG2,i}$  (l.). However, the strain-gauge based reconstruction of a user interaction force  $F_y$  exhibits significant noise and a limited bandwidth (r.).

$k_{door}$  is highly nonlinear, and that it could not be sufficiently approximated by a spring model. The reason was found in the mechanical structure of the mounting of joint 2, which snapped to one direction when an effective torque of  $\tau_{snap} \approx 20$  Nm was applied to joint 2.

### 5.1.1.2 Measurement of the Joint Torques

The advanced control of flexible mechanisms requires the measurement of joint states (compare [231, 232]). In our hardware setup, we did not have the possibility to measure the joint displacement caused by elasticity directly. However, we were able to apply strain gauges to the drive shafts. The location of the strain gauges on the shaft was identical for both drives, but did not represent the center of the shaft distortion. After compensating for this eccentricity, a linear measurement of the joint torques and the elastic joint distortion was achieved. This can be seen in Fig. 5.2 (l.), where the measurements exhibit a very close relation with the predicted theoretical values for a given measurement setup.

### 5.1.1.3 Measurement of the User Interaction Force

For a direct transfer and comparison of the results of the research conducted by Virtual Reality Prototyping (see Sec. 4.1), it was expected to be necessary to develop a comparable measurement of the user interaction force  $\mathbf{f}_u$ . At the VRP test bed, a six-DOF force-torque-sensor (FTS) had been utilized. As the development of the TLD prototype was seen as a proof-of-concept rather than a close-to-series product development, hardware cost was no constraint. Thus, a similar FTS was integrated into the car door body such that a modified external door handle could be mounted on it. This can be seen in Fig. 5.3.

After compensating for gravity and the offset from the COS, a high-quality measurement



**Figure 5.3:** CAD drawings showing how the FTS was integrated into the car door body.

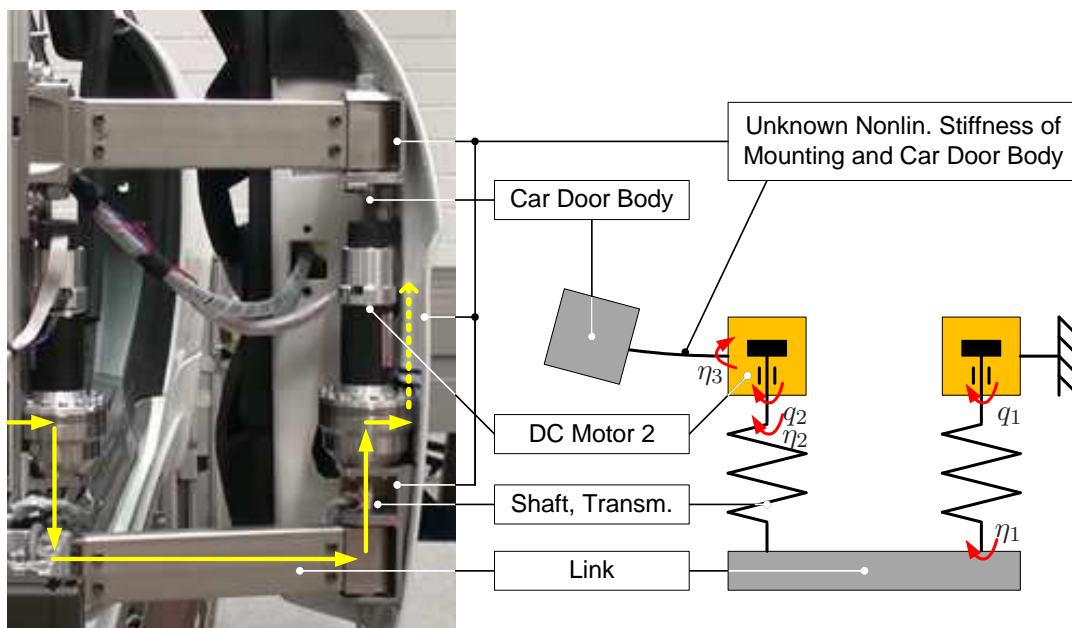


**Figure 5.4:** Transmission of force within the TLD prototype (l.) and its approximation as mass-spring-damper model with five generalized coordinates (r.).

of force and torque was achieved ( $e < 2\%$ ). While applying a user force at the external door handle, the FTS measurement was compared to a strain-gauge based reconstruction of the force. As can be seen in Fig. 5.2 (r.), the FTS is indeed necessary to achieve a high-quality force determination.

#### 5.1.1.4 Dynamical Model and Control Issues

The elasticities of the TLD mechanism displayed in Fig. 5.4 (l.) have been identified in subsection 5.1.1.1. Obviously, in addition to the two DOF given by the drives, three generalized displacement variables describe the configuration of the flexible mechanism. This leads to the approximate mass-spring-damper scheme of the TLD given by Fig. 5.4 (r.) and the corresponding state vector  $\mathbf{x} = (\dot{q}_1, q_1, \dot{\eta}_1, \eta_1, \dot{\eta}_2, \eta_2, \dot{q}_2, q_2, \dot{\eta}_3, \eta_3)^T$ .

The system matrix  $\mathbf{A}$  and the input matrix  $\mathbf{B}$  of the prototype have been calculated by

an approximate dynamics model in Autolev, which is described in Appendix B.3.2. The (normalized) output matrix  $\mathbf{C}$  is determined by the availability of (raw and filtered) sensor signals for all states but door position and velocity:

$$\mathbf{A} = \begin{pmatrix} -d/I_{dr1} & 0 & 0 & k_{jnt}/I_{dr1} & 0 & 0 & 0 & 0 & 0 & 0 \\ 1 & 0 & 0 & 0 & 0 & 0 & 0 & 0 & 0 & 0 \\ d/I_{dr1} & 0 & 0 & -k_{jnt}c_3 & 0 & k_{jnt}/I_{link} & -dc_1 & 0 & 0 & 0 \\ 0 & 0 & 1 & 0 & 0 & 0 & 0 & 0 & 0 & 0 \\ 0 & 0 & 0 & k_{jnt}/I_{link} & 0 & -k_{jnt}c_4 & -dc_2 & 0 & 0 & 0 \\ 0 & 0 & 0 & 0 & 1 & 0 & 0 & 0 & 0 & 0 \\ 0 & 0 & 0 & 0 & 0 & k_{jnt}/I_{dr2} & -dc_5 & 0 & 0 & k_{door}/I_{mnt} \\ 0 & 0 & 0 & 0 & 0 & 0 & 1 & 0 & 0 & 0 \\ 0 & 0 & 0 & 0 & 0 & 0 & d/I_{mnt} & 0 & 0 & -k_{door}c_6 \\ 0 & 0 & 0 & 0 & 0 & 0 & 0 & 0 & 1 & 0 \end{pmatrix} \quad (5.1)$$

$$\mathbf{B} = \begin{pmatrix} 1/I_{dr1} & 0 \\ 0 & 0 \\ -1/I_{dr1} & c_1 \\ 0 & 0 \\ 0 & c_2 \\ 0 & 0 \\ 0 & c_5 \\ 0 & 0 \\ 0 & -1/I_{mnt} \\ 0 & 0 \end{pmatrix}, \quad \mathbf{C} = \begin{pmatrix} 1 & 0 & 0 & 0 & 0 & 0 & 0 & 0 & 0 & 0 \\ 0 & 1 & 0 & 0 & 0 & 0 & 0 & 0 & 0 & 0 \\ 0 & 0 & 1 & 0 & 0 & 0 & 0 & 0 & 0 & 0 \\ 0 & 0 & 0 & 1 & 0 & 0 & 0 & 0 & 0 & 0 \\ 0 & 0 & 0 & 0 & 1 & 0 & 0 & 0 & 0 & 0 \\ 0 & 0 & 0 & 0 & 0 & 1 & 0 & 0 & 0 & 0 \\ 0 & 0 & 0 & 0 & 0 & 0 & 1 & 0 & 0 & 0 \\ 0 & 0 & 0 & 0 & 0 & 0 & 0 & 1 & 0 & 0 \\ 0 & 0 & 0 & 0 & 0 & 0 & 0 & 0 & 0 & 0 \\ 0 & 0 & 0 & 0 & 0 & 0 & 0 & 0 & 0 & 0 \end{pmatrix} \quad (5.2)$$

where  $d$  is the damping and friction of the drives,  $k_{jnt}$  and  $k_{door}$  are the stiffness of the joints and door,  $I_{dr1}$  and  $I_{dr2}$  the inertia of the drives,  $I_{link}$ ,  $I_{mnt}$ , and  $I_{door}$ , the inertia of link, the door mounting, and the door, and  $c_x$  are constants:

$$\begin{aligned} c_0 &= (I_{link} + I_{dr2} + I_{mnt}) \\ c_1 &= (I_{dr2}I_{door} + I_{mnt}(I_{dr2} + I_{mnt} + I_{door}) - (I_{dr2} + I_{mnt})(I_{mnt} + I_{door}))/c_0 \\ c_2 &= ((I_{dr2} + I_{mnt})(I_{mnt} + I_{door}) - I_{dr2}I_{door} - I_{mnt}(I_{link} + I_{dr2} + I_{mnt} + I_{door}))/c_0 \\ c_3 &= (I_{dr1} + I_{link})/(I_{dr1}I_{link}) \\ c_4 &= (I_{link} + I_{dr2})/(I_{link}I_{dr2}) \\ c_5 &= (I_{dr2} + I_{mnt})/(I_{dr2}I_{mnt}) \\ c_6 &= (I_{mnt} + I_{door})/(I_{mnt}I_{door}) \end{aligned}$$

The numerical values and a short system analysis are given in Appendix B.4. The analysis revealed that the system is not fully controllable and observable in practice:

- The controllability matrix is ill-conditioned (rank=8), because the dynamics of the overall system is predominantly determined by the inertia of the door body. Its

acceleration requires high torques, which significantly affect the other system states due to the elasticities and the low inertia of the linkages.

- Due to the absence of a sensor for the motion of the door, the output matrix and the observability matrix do not have full rank (rank=8).

Thus, a full state control can not be achieved. Furthermore, there were a number of additional problems affecting the controller design:

1. Due to limited resources, no detailed parameter identification could be performed. This holds especially for  $k_{door}$ , the highly nonlinear spring characteristics of the car door body (see subsection 5.1.1.1).
2. The linkage displayed in Fig. 5.4 did not exhibit an ideal warp resistance. Thus, load changes resulted in a distortion of the relative position of the upper and lower link.
3. The maximum torque of the drives was limited to  $< 30Nm$ , which is rather small with respect to the inertia of the door.

### 5.1.2 Closed-Loop Position Control

To achieve an automatic operation of the car door prototype (overview of the system and signals: see Fig. G.1), a closed-loop position control was mandatory. The general problem of the position control of an elastic mechanism has been an active field of research for decades. A comprehensive overview is given in [197].

In [9, 10], a thorough investigation of the state space control of robots with elastic joints has been conducted. For instance, it has been shown that a measurement of the elastic joint distortion is indeed a suitable signal for this purpose. However, the proposed control methods were based on several assumptions that were not given in our case: The configuration differs significantly with respect to the unactuated mass given by the link between drive 1 and drive 2 (see Fig. 5.4), and the system is neither fully controllable in practice nor fully observable.

As a detailed study of the high-performance position control of the TLD was beyond the scope of this thesis, we implemented a simple controller for the reduced state vector  $\mathbf{x}_{red} = (\dot{q}_1, q_1, \eta_1, \eta_1, \dot{q}_2, q_2, \dot{q}_2, q_2)^T$ . A stiff position control of the drives and a medium damping of the elastic deformation of the joints was achieved. The excitation of the elastic modes was effectively suppressed by notch filters for the corresponding resonance frequencies.

As the bandwidth of the overall position control was rather low ( $< 1.5 \text{ rad/s}$ ), it was unsuitable for the position-based admittance control of the manual interaction at the car door. However, it was sufficient for the automatic operation of the door.

### 5.1.3 Transfer and Modification of the Controller Developed by VRP

In subsection 4.1.5, a simulation with controllers for the automatic and manual operation of the TLD has been developed and evaluated on a VRP test bed. An important goal of VRP is to be suitable for the development of solutions which can directly be transferred to real-world problems. Thus, an interesting question was whether this could be achieved in

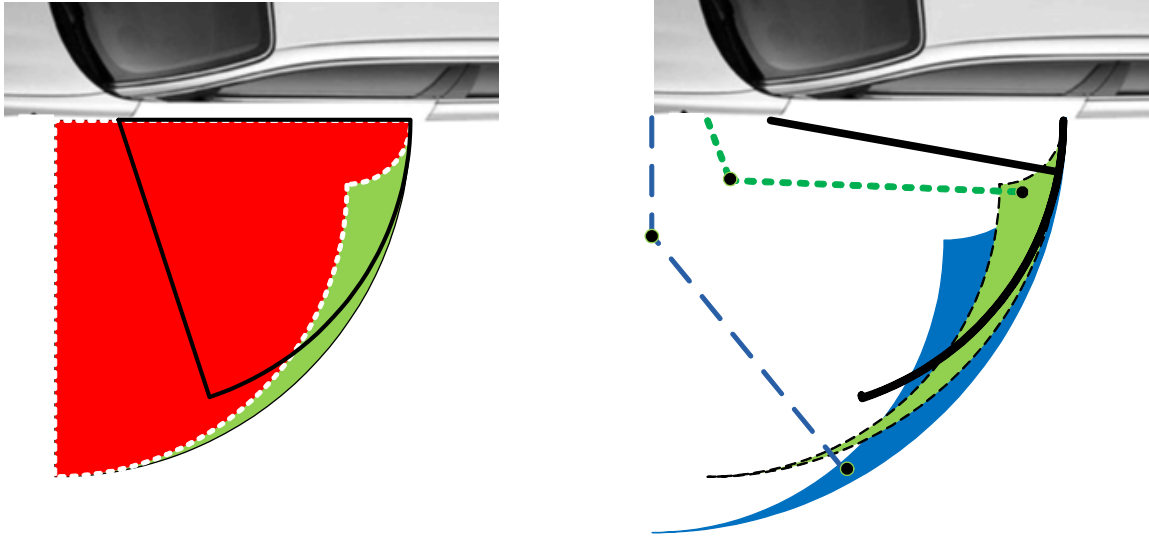


**Figure 5.5:** Cartesian workspace of the TLD prototype ( $l_L = 0.24$  m) with respect to the outer handle of the driver’s door: The upper and lower bounds are displayed together with the swept volume on the left side, the resulting workspace for the outer door handle on the right side (dashed green area). The thick solid lines indicate the characteristics of a conventional door, the largest area on the right side (blue) the characteristics of the original TLD VRP simulation ( $l_L = 0.45$  m).

our case, especially since there were major differences between the TLD VRP simulation and the real-world prototype (see also subsection 5.1.1):

- The length of the link between car door body and the car was 0.24 m instead of 0.45 m. This results in a significant reduction of the Cartesian workspace; see Fig. 5.5.
- The prototype possessed significant elasticities, one of which was heavily nonlinear. This resulted in a higher compliance of the door than the VRP simulation exhibited during the manual interaction with the stopped TLD.
- The inertias, masses, and frictions were different. For instance, due to demounted elements like electric window lift and door lock, the car door body of the prototype possessed a smaller mass and inertia than the simulation ( $15 \text{ kg} + 3 \text{ kg} < 26 \text{ kg}$ ,  $10.5 \text{ kgm}^2 < 14.38 \text{ kgm}^2$ ).

However, it turned out that the methods and controllers developed by VRP technology in subsection 4.1.5 could be easily transferred to and integrated into the TLD prototype:

1. The structure of the overall networked system depicted in Fig. 4.3 could be preserved. We just exchanged the simulation of the obstacle detection based on a virtual scene with a real obstacle detection system which comprised two omni-directional cameras provided by the institute RCS (TU München). The first camera was mounted on top of the driver’s door mirror, monitoring the outer workspace of the door, and the second camera was attached to the inner side of the door to detect clamping situations (Fig. 5.1).

2. The model of the door was naturally substituted by its physical instance. This means that the inputs of the Active Admittance (AA) were replaced by available sensor signals, and the reference actuation torque  $\tau_{A,r}$  was directly commanded to the drives of the prototype (see Fig. G.1).
3. Based on the additional signals and requirements, the simple state machine that had been used in subsection 4.1.5 to determine the control mode of the door had to be enhanced:
  - a) To enable an intuitive interaction of the human user with the door, the controller should switch to a manual control mode whenever a manual interaction is detected by the force sensing. Vice versa, automatic opening and closing should be instantaneously triggerable by a remote control.
  - b) To achieve a sufficient quality of the clamping detection by the inner door vision system, a one-DOF motion of the door was required. Thus, a linear static virtual fixture (SVF) for ( $q_1 = [0\dots0.2 \text{ rad}]$ ,  $q_2 = 0$ ) has been defined for manual operation.

A simplified version of the state machine is shown in Fig. G.2.

4. Analogously to the SVF for manual operation, the workspace of the path planner was reduced. The only other change that had to be made was the adjustment of the kinematics model (link length).
5. The collision avoidance did not have to be changed.
6. The controller for the manual operation (subsection 4.1.5.2) could be directly transferred. Due to the different properties of the simulation and the prototype, this had not been expected. However, the haptic support was subjectively perceived rather similarly between the VRP test bed and the prototype. This may be due to the fact that not only the prototype, but also the haptic device ViSHARD10 exhibits structural and joint elasticity, damping the display of supportive forces.

In summary, only minor modifications of the control framework and implemented methods were necessary, which clearly shows the practicality and effectiveness of our VRP approach (see also Fig. 1.1).

The operation of the TLD is displayed in several figures. In Fig. 5.6, the automatic operation and support of the ingress triggered by a remote control is shown. A special feature of the MechaTUM setup was an actuated seat which additionally helped to decrease the level of discomfort during egress and ingress (see also Fig. G.3). Another feature that has not been discussed is clamping protection, which is shown in Fig. G.4 and Fig. G.5.

Fig. 5.7 shows the automatic operation based on path planning for a very demanding scenario which exhibited small corridors in the workspace of the door. Finally, Fig. G.6 gives an impression of the dynamic obstacle detection system developed by the institute RCS.

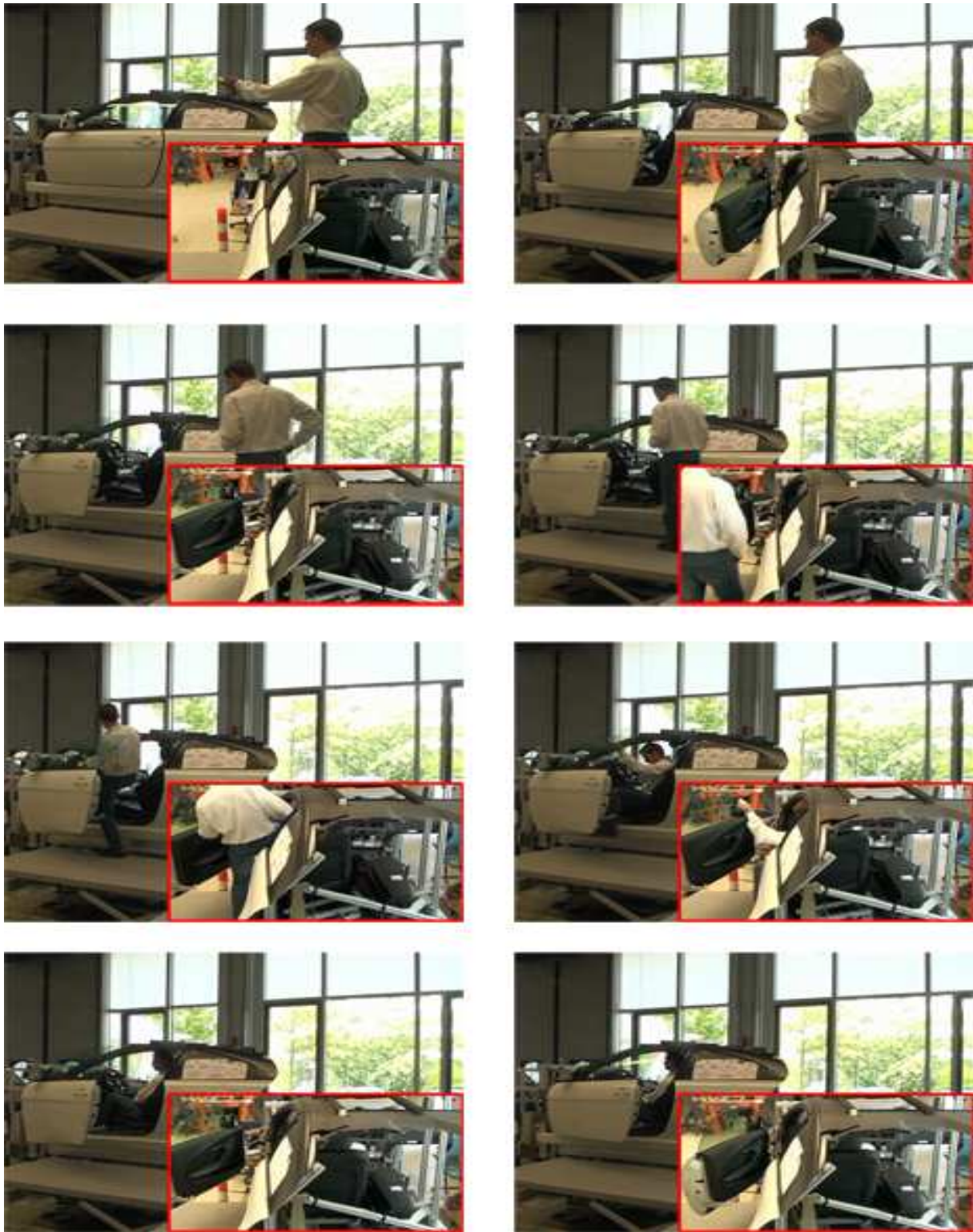


**Figure 5.6:** Automatic operation of the overall MechaTUM prototype: After the door has opened wide enough, the actuated seat emerges to the individually optimized ingress position. As soon as a load is recognized by the seat, it returns to its interior position, and the door can be automatically closed.

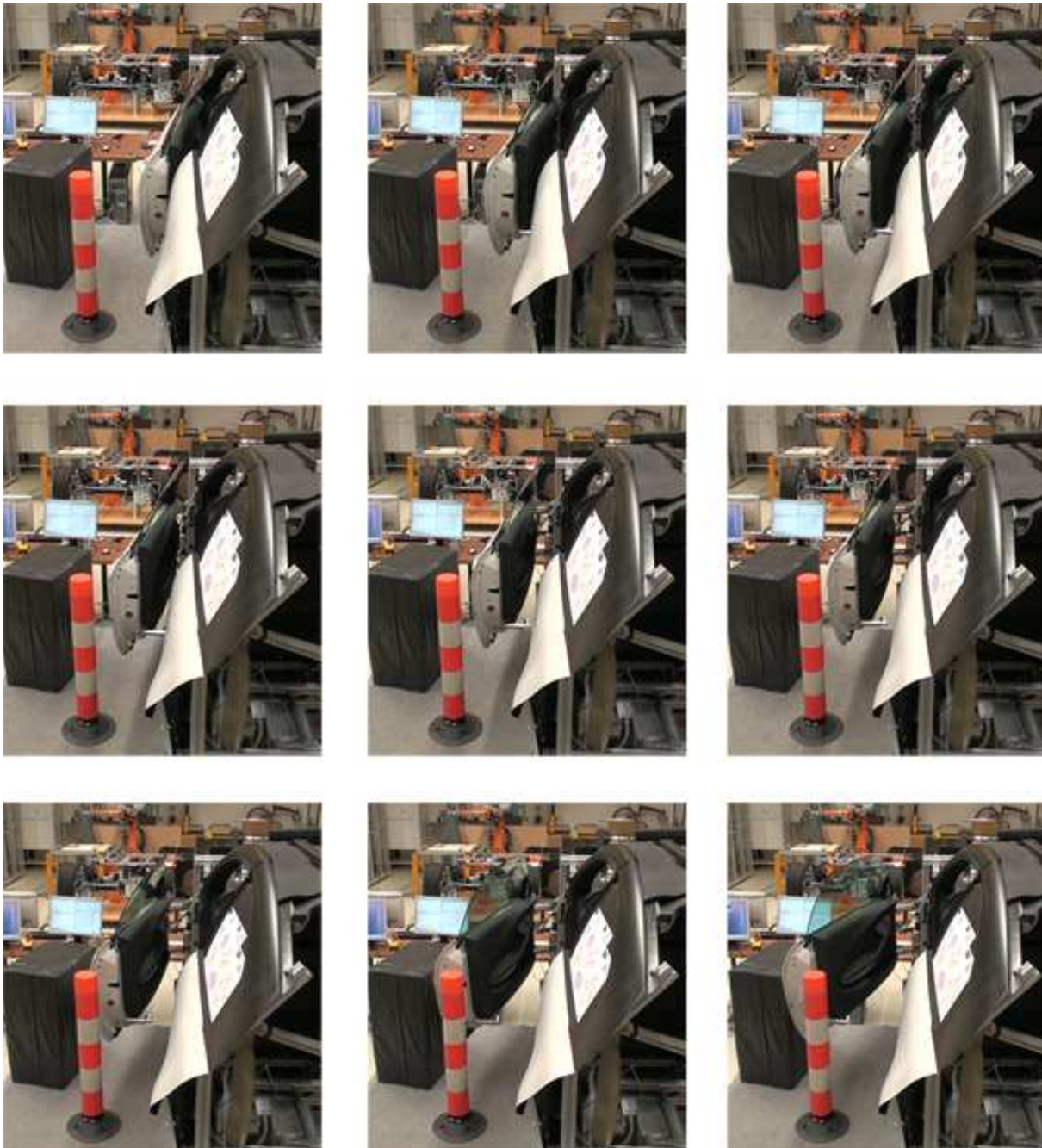


**Figure 5.7:** Example of the path planning based automatic operation of the door: If there are obstacles in the workspace of the door, the results of a path planner are input to the controller to automatically open the door if a collision-free path exists. This works even in very complex scenarios, such as the one depicted here.

### 5.1.4 Experimental Evaluation

In close collaboration with Olaf Adel Sabbah of the institute LfE (TU München), we prepared and designed two user studies for the evaluation of the prototype.

The first user study was conducted by the LfE and aimed at the evaluation of the overall MechaTUM prototype shown in Fig. 5.1 and Fig. 5.6, i.e. the actuated door, the actuated seat, and the combination of both. Eleven users participated in the experiment, all of whom had a professional background in ergonomics. Thus, this was far from being a representative study, but was thought to provide a deep insight into the overall level of comfort of the system. The details related to the TLD prototype are discussed in subsection 5.1.5 and compared to the second user study.

The second user study was intended to serve as a representative evaluation of the attractiveness of the actuated car door to potential customers. It is described in detail in the following.

#### 5.1.4.1 Design of the User Study

**Research Questions and Hypotheses:** First of all, we wanted to find out whether the proposed TLD prototype is appreciated by potential customers. Furthermore, user feedback should help to identify potential for future improvements to the system. Finally, we wanted to validate our research hypotheses: 1) The support functionality significantly improves the comfort of use. 2) People appreciate the supported manual as well as the automatic operation of the door, and the door is desirable to them.

**Methods:** For evaluating the attractiveness (arousal of desire) of interactive products, a special questionnaire was developed by Hassenzahl et al.: The AttrakDiff™ [115, 114]. It consists of semantic pairs of polarizing adjectives, enabling the rating of the pragmatic (practicability) and hedonic (joy of use) quality of a product as well as its attractiveness. Thus, this was seen as the ideal tool for gathering insights into the perception of the novel actuated car door and its approval by the participants.

Furthermore, we wanted to gain a quantitative measure for the level of discomfort of using the door. For this, the well-known NASA task load index (NASA-TLX) [113, 112] was chosen. It helps to determine the “load” of a task, distinguishing the six categories “mental”, “physical”, and “temporal” demand, “performance”, “effort”, and “frustration”.

**Scenarios for Door Operation:** The most demanding ingress/egress situation was seen in the configuration given in Fig. 5.8 (1.): An obstacle is placed such that the car door has to be moved around it. This situation was expected to give the best contrast between different modes of operation. The investigation of the following modes was deemed to be essential: Unsupported manual door operation (deactivated motors), manual door operation with haptic support, and automatic door operation.

**Evaluation Sheet:** Due to the use of the AttrakDiff and NASA TLX methods, the questionnaires for the three scenarios/tasks were in part predefined. Data related to the participants (gender, age, etc.) and their attitude towards and experience of the use of cars

(driver's licence, identification, etc.) should be gathered to enable a detailed analysis of the evaluation results. The final questionnaire can be seen in Appendix F.3.

### 5.1.4.2 Experiment

The large-scale experiment was conducted at an open day of TU München, which was attended by an audience sufficiently representative of potential customers of cars.

Overall, 40 people participated in the experiment, most of them in small groups of two to five. 70% of the participants were male, the average age was 32 years ( $\pm 15$  years), and the average body height 1.77 m ( $\pm 0.09$  m). 50% of the participants possessed a driver's licence for more than 5 years, and more than 50% drove more than 10,000 km per year themselves. 60% stated that they had a high or very high identification with their car, and accordingly only 37.5% stated that cars are just a means of transportation for them.

The duration of the experiment was approximately 20–25 minutes. Its progression is described below:

1. The car door prototype was briefly introduced to the participants. It was explained that the goal of the study was the rating of different modes of operation of the door.
2. The participants received the evaluation sheet (see Appendix F.3) and a pencil. They were asked to fill out the personal characteristics section (page 1).
3. Task 1 (*MECH*): The unsupported manual operation of the door was demonstrated by opening the door by moving it around the obstacle. The participants were asked to do this themselves and evaluate it afterwards by the two corresponding tables in the evaluation sheet.
4. Task 2 (*SUPP*): Analogously to task 1, the supported manual operation of the door was demonstrated and evaluated.
5. Task 3 (*AUTO*): Analogously to task 1, the automatic operation of the door triggered by the remote controller was demonstrated and evaluated.
6. After the three tasks, the participants were asked to make general remarks on the door and the experiment (page 8).

The order of the tasks was intentionally not randomized: The participants started with the mode of operation that was closest to what they were used to, namely task *MECH*, the manual operation of a purely mechanical door. A start with the task *SUPP* or *AUTO* would have required a trial phase before the tasks, which was not possible during the limited time of evaluation.

### 5.1.4.3 Results, Analysis, and Discussion Related to NASA TLX

The results related to NASA TLX are given in Tab. 5.1. It can be clearly seen that the load of the unsupported operation of the door (task *MECH*) was rated as medium to high: In all six categories, values above the median of the rating scale were given, and the overall load was rated with 36.9 out of 60 maximum points.

In contrast, the load of the other two tasks (*SUPP* and *AUTO*) was rated with only 24.9 and 23.0 out of 60 maximum points. This is due to a drastically reduced effort, which

was caused by a lower physical demand and a more quickly and better operation of the door.

By performing two-sample t-tests (39 DOF), the significance of this improvement is shown both for the supported manual operation ( $p < 0.001$ ) and the automatic operation ( $p < 0.001$ ). Thus, hypothesis 1 is accepted: The support functionality indeed significantly improves the level of comfort of use.

**Table 5.1:** Results of the NASA TLX questionnaire for the three tasks (scale: 0.5 (very low load) to 10 (very high load)).

| Task        |         | Perf. | Temp. | Frust. | Mental | Effort | Phys. | OVERALL |
|-------------|---------|-------|-------|--------|--------|--------|-------|---------|
| <i>MECH</i> | mean    | 5.30  | 6.68  | 6.26   | 5.54   | 6.69   | 6.46  | 36.9    |
|             | st.dev. | 2.63  | 2.54  | 2.86   | 2.69   | 2.26   | 2.48  | 15.3    |
| <i>SUPP</i> | mean    | 7.70  | 3.76  | 3.30   | 4.03   | 3.14   | 2.95  | 24.9    |
|             | st.dev. | 2.12  | 1.99  | 2.08   | 2.33   | 1.98   | 1.46  | 11.6    |
| <i>AUTO</i> | mean    | 7.79  | 6.59  | 3.96   | 1.96   | 1.48   | 1.26  | 23.0    |
|             | st.dev. | 2.45  | 3.21  | 2.85   | 2.12   | 1.39   | 1.05  | 12.1    |

Interestingly, the criterion “performance” (in German: “Aufgabenerfüllung”) was rated badly, preventing an even better overall rating. In our opinion, this was due to uncertainty among the participants of whether they did operate the door *correctly* rather than whether they did it *successfully*. In fact, all of them did open the door successfully and could get into the car. Thus, we are convinced that the rating of this category has been influenced by an insufficient description of the aspect that should be rated.

Another anomaly had been expected: The negative rating of the temporal demand of the automatic door operation. As was described in subsection 5.1.2, the automatic motion of the door was rather slow due to the limited position-control bandwidth.

Interestingly and in accordance to our findings described in subsection 4.1.5.5, no significant influence of gender has been detected. Instead, the body height appears to be a predominant factor: A correlation analysis reveals the tendencies that the taller the participant,

- the worse the rating of all load categories during task *MECH*
- the worse the performance rating during task *SUPP*
- the less frustration during task *SUPP*

As already stated in Sec. 4.1, this motivates the adaptation of the car door controller to the body height of the respective human operator.

#### 5.1.4.4 Results Related to AttrakDiff

The evaluation results gained by the AttrakDiff questionnaire are displayed in detail in Fig. F.1, where for all three tasks the mean of the 28 adjective pairs is given. Based on this, the AttrakDiff measures have been calculated. They are given in Tab. 5.2 and are discussed in the following:

**Table 5.2:** Results of the AttrakDiff questionnaire for the three tasks (scale: -3 (very low) to 3 (very high)).

| Task        |         | PQ    | HQ-I | HQ-S | ATT   |
|-------------|---------|-------|------|------|-------|
| <i>MECH</i> | mean    | -0.76 | 0.28 | 1.35 | -0.10 |
|             | st.dev. | 1.75  | 1.68 | 1.36 | 1.80  |
| <i>SUPP</i> | mean    | 0.70  | 1.28 | 1.58 | 1.28  |
|             | st.dev. | 1.50  | 1.18 | 1.06 | 1.32  |
| <i>AUTO</i> | mean    | 0.69  | 1.32 | 1.49 | 1.32  |
|             | st.dev. | 1.62  | 1.36 | 1.39 | 1.48  |

1. PQ: On average, the pragmatic quality was rated negatively for task *MECH* (no haptic support) and positively for task *SUPP* and task *AUTO*. This had been expected, and it is in accordance with the negative rating of task *MECH* of the NASA TLX; compare subsection 5.1.4.3. The standard deviation is rather high for all three tasks.
2. HQ-I: The hedonic quality with respect to identity was rated high for task *SUPP* and task *AUTO*. This indicates that the participants see the actuated car door as a positive status symbol rather than as something they would be embarrassed to be associated with.
3. HQ-S: Interestingly, the hedonic quality with respect to stimulation (and all of its seven adjective pairs) were very similar for all three tasks. Thus, the actuation did not influence the perceived stimulation.
4. ATT: The attractiveness was rated neutral for task *MECH*, but very positive for task *SUPP* and task *AUTO*. This indicates that the actuation is indeed a desirable feature of the TLD.

Thus, while there are no big differences in the hedonic quality of the three modes of operation, the pragmatic quality and the attractiveness of the TLD is significantly higher if the actuators are used.

For a more detailed analysis of the rating of technical and ergonomical aspects, we identified the corresponding most relevant adjective pairs in Fig. F.1. Not surprisingly, most of them were of the group PQ rather than of HQ-I, HQ-S, or ATT. They are discussed in the following, where task *MECH*  $\rightarrow$  task *SUPP* clarifies the improvement of the mean rating of task *SUPP* with respect to *MECH*:

- Simple/complicated (“einfach”) (PQ):  $-1.18 \rightarrow 0.98$
- Practical/impractical (“praktisch”) (PQ):  $0.20 \rightarrow 1.73$
- Straightforward/cumbersome (“direkt”) (PQ):  $-1.18 \rightarrow 0.88$
- Predictable/unpredictable (“vorhersagbar”) (PQ):  $-0.30 \rightarrow 0.85$
- Manageable/unruly (“handhabbar”) (PQ):  $-1.05 \rightarrow 0.98$
- Pleasant/unpleasant (“angenehm”) (ATT):  $-1.00 \rightarrow 1.60$

These ratings clearly show the benefit of the haptic user assistance.

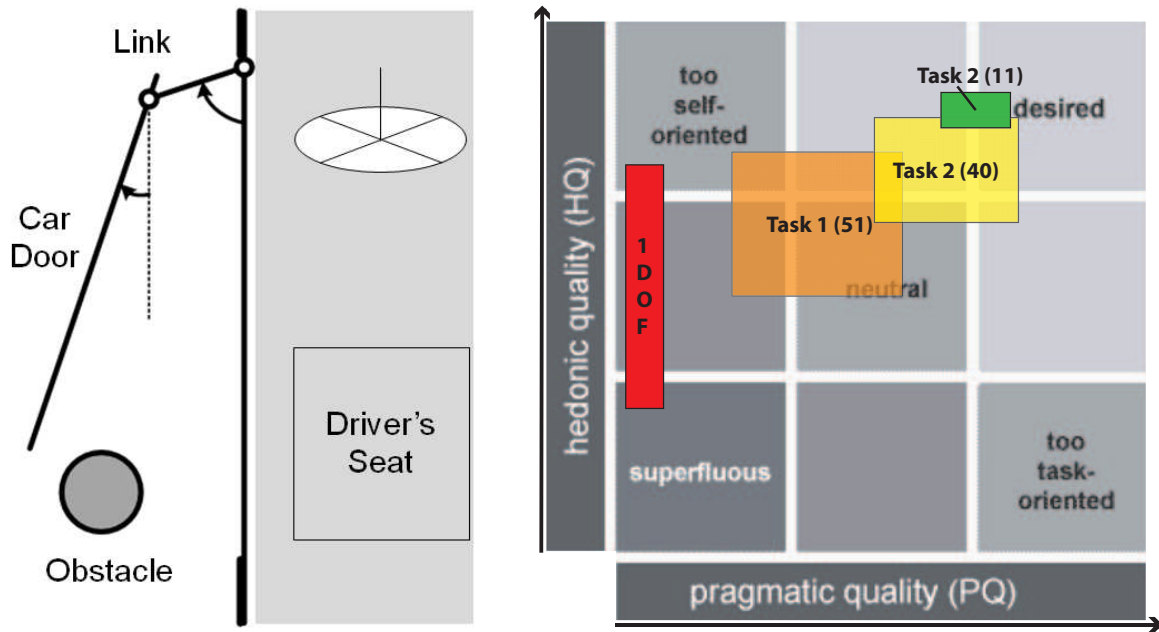


**Figure 5.8:** Scenario for the evaluation of the TLD prototype (l.) and corresponding AttrakDiff results for the manual door operation (r.).

A correlation analysis indicated that there was one personal factor that dominated the rating of these six aspects: The more the participants saw automobiles just as a means of transportation (“pragmatic users”), the higher their rating for both task *MECH* and task *SUPP*. ANOVAs revealed that this tendency is statistically significant for task *SUPP*, but not for task *MECH*. For instance, the task *SUPP* ratings of “simple” ( $F(1,40) = 3.96, p < 0.001$ ) and of “pleasant” ( $F(1,40) = 3.96, p < 0.001$ ) were significant while the corresponding task *MECH* ratings were not.

Indeed, the “pragmatic users” rated the six aforementioned aspects on average slightly better than the other users ( $-0.71$  and  $1.32$  compared to  $-0.95$  and  $1.03$  for task *MECH*/task *SUPP*). However, the relative improvement from task *MECH* to task *SUPP* was the same for both groups ( $1.98$  compared to  $2.03$ ). This means that the actuation support of the TLD prototype improved the usability significantly and equally for both groups.

### 5.1.5 Summary

Despite the fact that the VRP simulation model was quite different from the physical prototype, most of the methods and controllers of the virtual prototype could easily be transferred to the physical prototype. This clearly indicates the effectiveness of the VRP approach for actuated mechanisms.

To summarize and compare the results gained by our user study and the one conducted with ergonomics experts by LfE, the results for the manual door operation are consolidated in one diagram which is depicted in Fig. 5.8 (r.). The centers of the boxes represent the mean values of the hedonic and pragmatic quality, while the size of the boxes is determined by the standard deviation.

If we locked the second DOF, the door could not be opened wide enough to access the car. Thus, the usability would have been rated very badly (indicated by box “1DOF”).

With both DOF free, but unactuated, the users could manually move the door around the obstacle (task *MECH*). They generally rated the usability poorly, because it is not easy to move the door in such a situation (compare subsection 5.1.4.4). There was virtually no difference between the rating of the first group (11 experts in ergonomics) and our second group (40 participants). This leads to one common box for task *MECH* based on the results of 51 users.

However, when we activated the control of the door (task *SUPP*), the door was rated much better: Both groups rated the pragmatic quality more positive. While the second group did rate the hedonic quality already positively, the first group rated it even better and much more homogeneously: The standard deviations were very small, revealing a *common sense* of the ergonomics experts that the door provides both a high hedonic and a high pragmatic quality.

It is remarkable that even for such a “worst-case” parking situation a good usability has been achieved with the haptic support provided by the controller of the actuated car door. An analysis of the adjective pairs related to technical and ergonomical aspects provided further evidence that the actuation support of the TLD prototype is indeed necessary to achieve a convenient and intuitive manual interaction.

## 5.2 Close-to-Series Door Prototype with One Actuated DOF

Conventional car doors with one rotational DOF exhibit a considerable discomfort to the user in some situations, for example while parking in a small lot or on a steep incline. Due to the usual constant rest positions given by door detent, the user may have to fix the door manually during egress to prevent damage to the door and adjacent cars. For moderate inclinations, this specific problem has recently been overcome by employing a (purely mechanical) variable door detent [234]. Using an actuator instead of such a mechanical door detent, the level of comfort and the safety of operation of the door can be increased; compare the functionalities described in Chap. 4.

In the past, a lot of different actuated car doors with one (rotational or sliding) DOF have been filed as patents and published. However, most concepts focused on the automatic operation of such doors: Supervisory systems were used to block the movement of the car door in the event of a possible collision [271, 87], and some automatic systems provide a procedure for unlocking the door [17] or for opening and closing the door [111, 143]. For instance, in [163] a vehicle door system comprising a magneto-rheological actuator is proposed. It allows the adjustment of the damping, thereby enabling several functionalities like a variable door detent, deceleration, and a limitation of the door opening. While this actuator has the benefit of being inherently safe, unfortunately it is only semi-active and cannot be used for creating an accelerating torque. This prevents both versatile haptic feedback and automatic opening/closing of the door.

Only a few considered haptic interaction explicitly. In [107], a door is described that is moved by an actuator, dependent on several sensor signals like inclination of the car, the force between actuator and door, and information about obstacles in the workspace of the door. A different approach to modify the dynamics of the door are impedance or admittance control schemes, where motion sensors are used to measure the acceleration of the car door (see also [218]). Several control systems are described that use one or more force sensors in the inner and/or the outer door handle [253, 93, 139]. They claim to achieve a force-controlled motion of the car door such that the haptic interaction feels somehow convenient to the user. As the force sensors are not collocated with the actuator, this assumes that the user must operate the door at one or more predefined interaction points (e.g. the outer door handle). This is a disadvantage for everyday situations where many people touch the door at various locations (e.g. at its upper corner).

While these approaches contain valuable ideas, neither a detailed description of the actual implementation nor an evaluation of the haptic interaction with these systems has been given before our publications [239, 240]. Furthermore, they did not comprise a combination of automatic and manual handling of the door with effective collision prevention. Thus, it is not clear whether these systems would provide a benefit for the user and if they would be appreciated.

We discuss the development, control, and evaluation of a conventional car door enhanced by actuation, focusing on the haptic interaction between the human and the car door. A vision-based system for the determination of the haptic interaction point (HIP) is proposed to measure the interaction force. By means of low-cost, state-of-the-art actuators, sensors,

and control technology, a conventional car door is redesigned to enhance safety and comfort to the user. Besides an automatic control, four different impedance control concepts were implemented and evaluated on an experimental vehicle using rapid prototyping hardware. The evaluation results show that a superior manual handling of the car door is achieved that is intuitive and convenient.

### 5.2.1 Measurement of the User Interaction Force

#### 5.2.1.1 Basics of the Measurement of Interaction Forces at a Car Door

A force determination is highly desirable for the control of the manual interaction of an actuated car door. It can either be the main input to the controller or be used in parallel with motion information. For admittance control implementations it is mandatory, and even impedance control implementations benefit significantly from it [258].

During our course of research, we observed that there are three main intentional areas of interaction at a car door: At the inner door handle, at the outer door handle, and at the outer rim (full-framed doors) or just below the door window (frameless doors)<sup>1</sup>. In each area, the points of the effective haptic interaction greatly depend on the specific situation (obstacles, narrow parking lot, inclination, etc.) and the user (height, weight, force output, habits, etc.). Furthermore, they are stochastically distributed both inter- and intra-personally. This makes the precise force measurement at car doors a compelling task. To assist the user in all phases of door operation, a force determination is desired for all three areas.

The interaction between user and car door leads to a specific pressure distribution, which leads to strain and deformation and may result in a change of the overall motion of the door. The physical effects pressure, deformation, and acceleration can often be measured by an immense number of available sensors [95, 126]. This enables an indirect determination of the interaction force.

Broadly speaking, sensors for the determination of an interaction force can be categorized into deformation-based and acceleration-based; compare [268]. We intended to investigate the use of promising sensors of both categories. For a selection of appropriate sensor types, popular sensor classes have been evaluated based on four criteria:

1. How good is the achievable measurement quality under realistic conditions (temperature, humidity, vibration, etc.)?
2. Is the thermal and mechanical robustness sufficient for the requirements of the automotive industry?
3. How much effort will it cost to establish the sensors in large-scale production?
4. What are the expected costs for large-scale production ( $\geq 100,000/\text{year}$ )?

After discussions with experts in the automotive industry, we rated the sensors subjectively. The results are given in Tab. 5.3 (++: very positive, 0: neutral, --: very negative, x: no information).

---

<sup>1</sup>The fourth major area is at the inner door side, where many people use their elbow to push the door open before egress. However, this is not guided intentional motion, so we do not consider force measurements for this area further.

**Table 5.3:** Overview of potentially applicable force sensors and their rating with respect to four important aspects.

|             | Sensor type      | Measurement | Robustness | Integration | Overall costs |
|-------------|------------------|-------------|------------|-------------|---------------|
| Deformation | Resistive        | +           | ++         | -           | -             |
|             | Capacitive/ind.  | +           | +          | --          | +             |
|             | Magneto-elastic  | x           | -          | -           | x             |
|             | Piezo-electrical | +           | +          | ++          | -             |
| Acc.        | Acc. (relative)  | ++          | -          | --          | --            |
|             | Acc. (absolute)  | +           | ++         | ++          | -             |
|             | Angle/velocity   | +           | +          | +           | +             |

### 5.2.1.2 Determination of the HIP (Patent Pending)

For all motion-based force measurement schemes, knowledge about the haptic interaction point (HIP) is essential. If it is known whether the user is inside or outside the car, a rough assumption of the HIP could be utilized: If the user is outside the car, he or she will most likely interact with the car door somewhere between the external door handle and the rim of the door. This can be approximated as

$$l_{o,u,est} = \frac{1}{2}(l_{o,u,max} + l_{o,u,min}) \approx 1.2 \text{ m} \quad \text{with} \quad e_i = \frac{l_{o,u,max} - l_{o,u,est}}{l_{o,u,est}} \approx 0.1 \quad (5.3)$$

where  $l_{o,u,est}$ ,  $l_{o,u,max}$  and  $l_{o,u,min}$  are the estimated, maximum, and minimum distance of the HIP from the axis of rotation and  $e_i$  is the estimation error. This error in the motion-based force determination would be acceptable for most haptic control schemes. However, if this scheme is applied to the inner side of the door, the error is much larger:

$$l_{i,u,est} = \frac{1}{2}(l_{i,u,max} + l_{i,u,min}) \approx 0.7 \text{ m} \quad \text{with} \quad e_i = \frac{l_{i,u,max} - l_{i,u,est}}{l_{i,u,est}} \approx 0.4 \quad (5.4)$$

This is not acceptable if a high-quality haptic interaction is to be achieved. Thus, at least the inner side would require additional sensors for the determination of the HIP at all relevant locations of the inner side of the car door. This would come with significant hardware and integration costs.

However, there is a way to achieve this without additional hardware and thus with negligible cost: The use of cameras which are anyway part of the car. As can be seen from current research [106, 264, 84, 219, 155, 228] as well as from industrial activities [255], there is a significant trend to use cameras for the monitoring of both outer and inner side of vehicles.

For instance, the hardware of the system described in [219] would be well-suited for monitoring the interaction at the outer side of the car door body, especially in the area of the external door handle. This can be achieved by integrating a camera into the outer mirror. The principle which has been filed as a patent by us in [245] is displayed in Fig. 5.9.

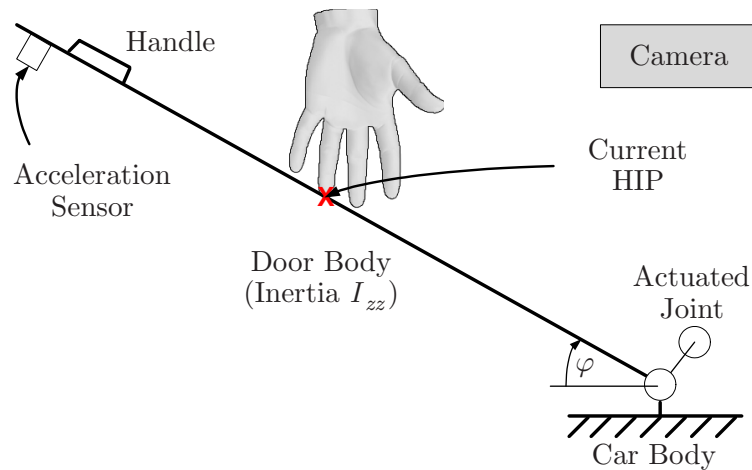


**Figure 5.9:** Camera-based system for the determination of the user interaction force at a car door filed as a patent in [245].

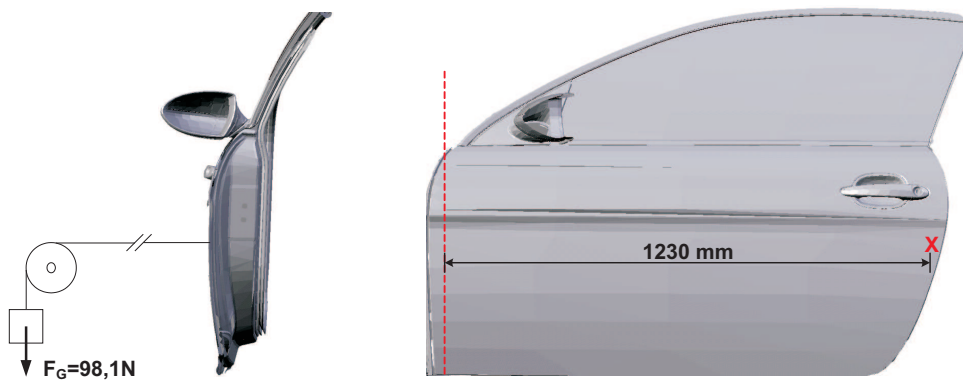


**Figure 5.10:** Test bed for validating acceleration measurements at a car door.

### 5.2.1.3 Acceleration-Based Measurement of the Interaction Force

A very detailed model of the dynamics of a car door was derived in subsection 4.2.1.2. If the acceleration and the haptic interaction point (HIP) are known (see subsection 5.2.1.2), the interaction force  $f_u$  can easily be determined by these equations<sup>2</sup>.

An actuated car door needs position feedback to be effectively controlled. By differentiating and filtering this signal, the acceleration can be determined. However, due to the limited resolution and noise, the filtered acceleration signal is expected to exhibit an unacceptable phase lag.

Thus, a dedicated acceleration sensor has to be used. Combined with position feedback, an extended Kalman filter can be implemented to provide high-quality motion feedback. We tested this for a low-cost acceleration sensor (BG 2166.10.31 [181]) on a test bed with position feedback, which is depicted in Fig. 5.10. In our experiments, the sensor (bandwidth: 20 Hz) combined with a Butterworth filter of 3rd grade provided a very good acceleration signal.

<sup>2</sup>Inclination parts are already part of many cars, so the gravity effect can be calculated from available sensor data without the need for additional sensors

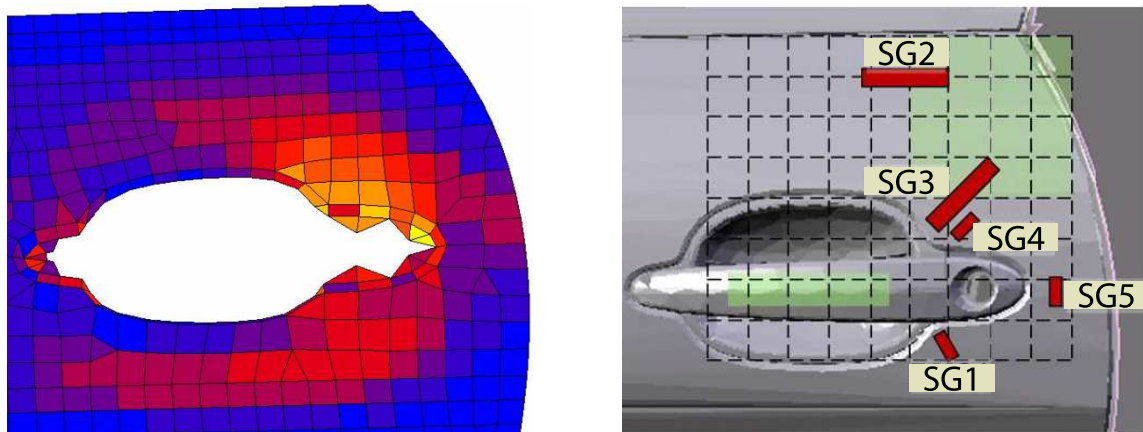


**Figure 5.11:** Typical mechanical stress when the door is pulled at the external door handle (l.) and placement of the five strain gauges (r.) used for the measurements given in Fig. 5.12.

#### 5.2.1.4 Local Effects-Based Measurement of the Interaction Force

In Tab. 5.3, several sensors for the force determination based on local deformations or pressure have been compiled. Two sensor classes are investigated in the following: strain gauges and piezo-resistive foil sensors.

**Strain Gauges:** These can be used to gather the local deformation of a substrate. An FEM-analysis depicted in Fig. 5.11 (l.) revealed the location of the maximum stress for a load acting on the external door handle, and another one the stress for a push at a location on the upper right of the car door. Based on this information, five promising locations for the placement of strain gauges have been identified – see the red cuboids in Fig. 5.11 (r.). Accordingly, strain gauges have been applied to a test bed. For the measurement, a carrier frequency setup (225 Hz) was utilized. By a precise spring scale, we applied a force of 40 N on an area of 50 mm<sup>2</sup> for all nodes of the raster which can be seen in Fig. 5.11 (r.).

The corresponding output of all five strain gauges is given in Fig. 5.12. As expected, SG3 and SG4 provided the highest outputs and thus the best SNR. However, there is a strong nonlinear dependence from the HIP. Thus, the HIP has to be known. The most promising way to achieve this is the vision-based determination described in subsection 5.2.1.2. Another option would be the usage of a lot of strain gauges, which would enable reasoning on the HIP. However, this is most likely too expensive for realistic setups. Further experiments revealed that the signal of SG4 is similar to the acceleration for closing motions, but not for opening motions where the movable mechanism of the external door handle results in a nonlinear stress evolution. Thus, the accuracy is rather limited.

**Piezo-Resistive Foil Sensors:** On the inner side of car doors, the typical HIPs (inner door handle, elbow-area) are usually coated with leather, textile, or plastics. Thus, flexible foil sensors are predestined for the measurement of user interaction. Twenty piezo-resistive foil sensor pads were applied to the inner door handle. A study with 19 participants revealed that two pads would be sufficient to determine the principal load at the door handle.

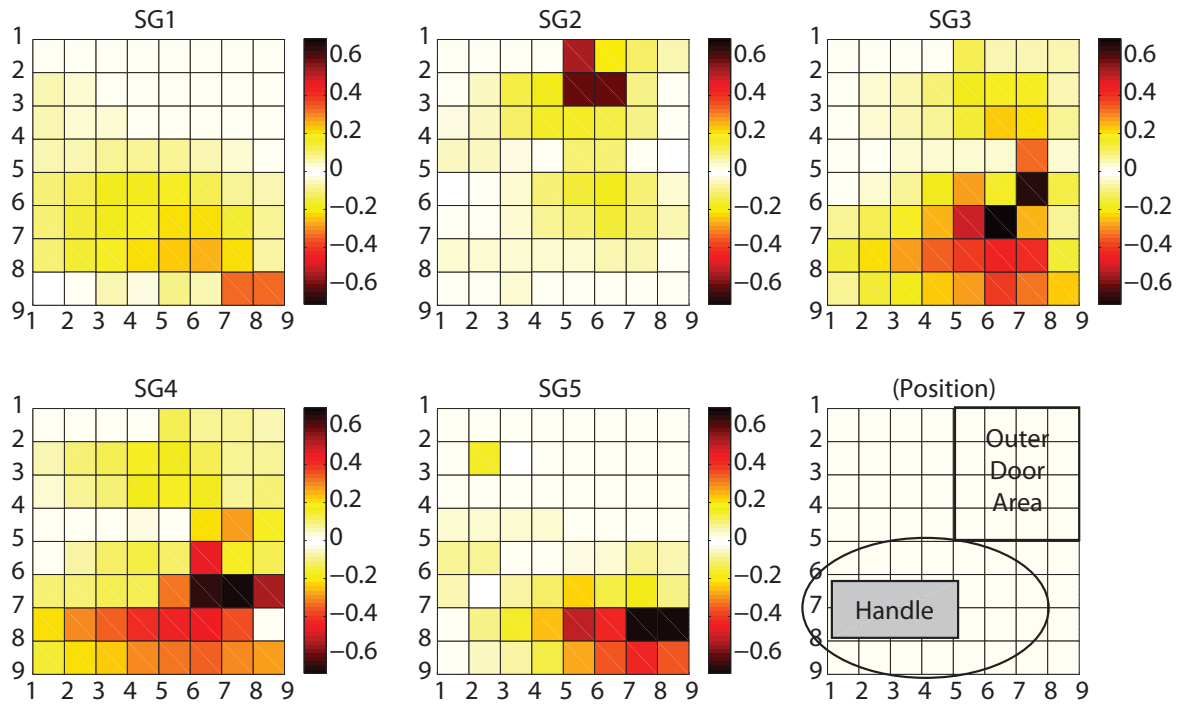


**Figure 5.12:** Output of the five strain gauges for a load of 40 N applied to all nodes of the raster given in Fig. 5.11.

However, the accuracy was limited ( $\pm 40\%$ ), and there are unsolved problems such as the reaction to a heavy load resulting from a firm grip of the handle. Thus, this concept is not very promising.

### 5.2.1.5 Conclusion

Based on the findings described in this subsection, we conclude that the most promising sensor concept for the determination of the interaction force at a one-DOF car door is given by a combination of motion sensors with a camera-based determination of the HIP. Both from a technical and an economical point of view, an actuated car door should be equipped with a position and acceleration sensor to achieve an effective determination of position, velocity, and acceleration, which in turn can be used to determine the interaction force which is necessary for some haptic control schemes.

## 5.2.2 System Description

In the following, the hardware setup of an actuated car door developed and built by BMW Forschung und Technik GmbH is described. Models are derived for the mechanism and its actuation.

### 5.2.2.1 Hardware Setup

The complete experimental setup of the actuated car door can be seen in Fig. 5.13. A close-to-production linear actuator is integrated in the hollow space of the door, forming

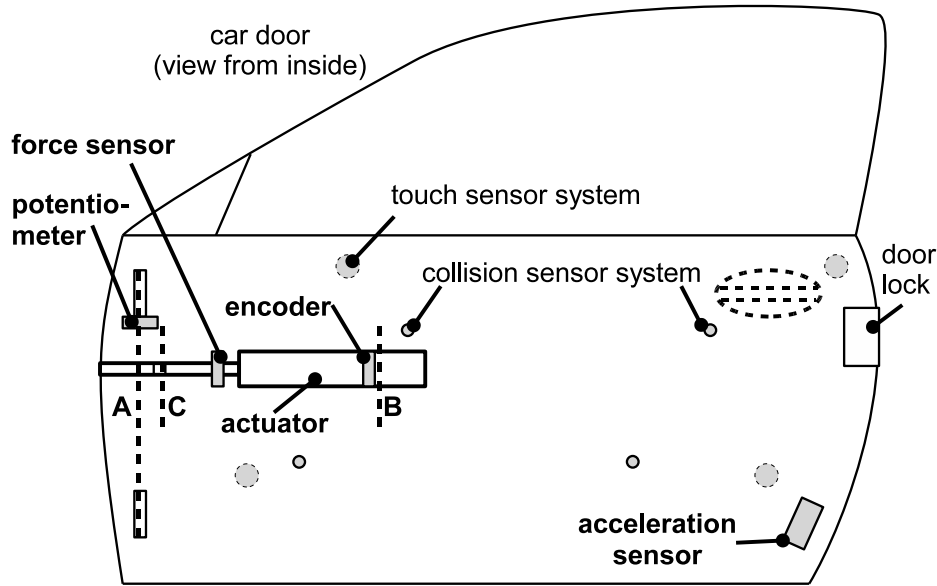


**Figure 5.13:** Hardware scheme of the car door, showing the actuator, the sensors, and the axes  $A$ ,  $B$ , and  $C$  (side view of this passenger's car door).

the kinematic configuration which is displayed in Fig. 5.14. The actuator is attached to a stiff location ( $B$ ) near the middle of the door, so that a high stiffness is achieved and that the actuation force does not distort the door structure. Additionally, mounting of the actuator is realized between the rigid front column of the car and a separate door flange designed for high stiffness and low bearing backlash.

As no vision system was integrated in the door, the measurement of interaction force could not be done based on acceleration measurement alone. Thus, for the high-bandwidth determination of the interaction force, which is required by some control schemes, a one-DOF force sensor was used. It was placed in series with the driving rod of the actuator.

With respect to a potential future mass production of the actuated car door, relatively inexpensive sensors were used:

- Analog (high-precision potentiometer at door hinge) and digital<sup>3</sup> (incremental encoder at the motor shaft, 480 counts/rev) position sensors (resolution of each:  $\Delta\varphi \approx 0.06^\circ$ )
- Translational acceleration sensor (one DOF, near external door handle, resolution  $\Delta\ddot{x} < 0.001 \text{ g}$ )

Furthermore, several peripheral sensors are included in the test rig. The inclination of the car is measured by a two-axes acceleration sensor which is oriented in the horizontal plane. A new mechatronic door lock supports automatic opening and closing of the door. Proprietary systems for obstacle detection in the workspace of the door and detection of door touch by user, both based on ultrasonic transducers, are included in the test rig for demonstration purposes. Though the sensors and the overall collision detection system are not discussed in this thesis, we suppose that it provides the maximum, collision-free

<sup>3</sup>Due to its collocation with the actuator, we used the digital sensor to achieve a high-bandwidth motion control.

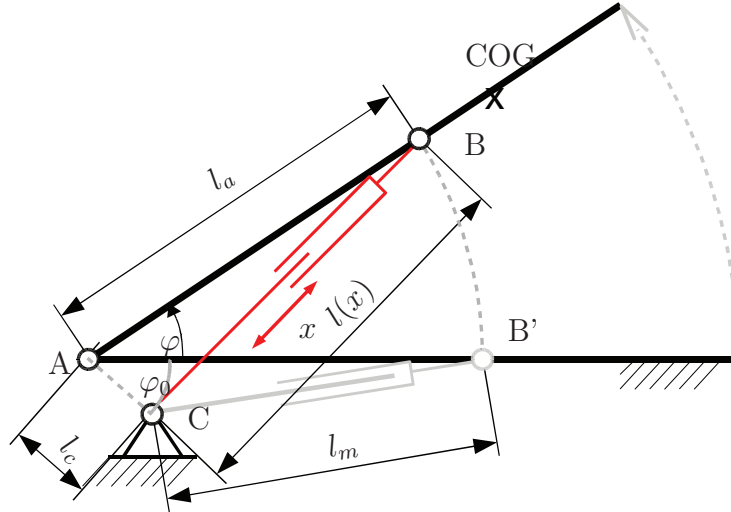


**Figure 5.14:** Kinematics of the actuated front passenger door with prismatic actuator (top view).

opening angle  $\varphi_{obs}$  of the car door (assumption: no fast-moving obstacles). The control system is developed using MATLAB/Simulink and executed in real-time on a dSPACE AutoBox equipped with appropriate interface cards.

### 5.2.2.2 Mechanical Modeling

Due to the high stiffness of the door and the rigid structure of the actuation, the door system is assumed to be ideally stiff. This leads to a simple kinematic model with three rotational joints A (door hinge), B (actuator, at door), and C (actuator, at front column), which is displayed in Fig. 5.14.

For the control design, the mapping between joint space and workspace (forward/inverse kinematics) has to be known. The angle of the door  $\varphi$  is defined as the workspace coordinate, while  $x$  denotes the coordinate of the actuator (closed door:  $x_0 = 0$ ). With the geometrical parameters  $l_a$ ,  $l_c$ , and  $l_m$ , the forward kinematics are given by

$$\varphi = f(x) = \arccos\left(\frac{l_a^2 + l_c^2 - (l_m + x)^2}{2l_al_c}\right) - \varphi_0 \quad (5.5)$$

and the inverse kinematics are given by

$$x = f^{-1}(\varphi) = \sqrt{l_a^2 + l_c^2 - 2l_al_c \cos(\varphi + \varphi_0)} - l_m \quad (5.6)$$

where  $\varphi_0 = f(l_a, l_c, l_m) = \text{const}$ . Due to deliberate mechanical design,  $\varphi$  and  $x$  are rather linearly linked for  $0 \leq \varphi \leq 1.28$  rad (and  $0 \leq x \leq 0.09$  m, respectively), which can also be seen from the Taylor series expansion of Eq. (5.6). This, in turn, provides an almost linear mapping from the actuator force  $F_a$  to the workspace torque  $\tau_a$ , which is important for avoiding excessive actuator requirements. The mapping is described by the Jacobian

$$J(s)^T = J(s) = \frac{F_a}{\tau_a} = \frac{d\varphi}{dx}. \quad (5.7)$$

Although this is not an intuitive notation, it reflects the fact that the joint space is given by  $x$ , while  $\varphi$  describes the workspace.

The dynamic behavior of the actuated car door can be described by its equations of motion:

$$M(\varphi)\ddot{\varphi} + N(\varphi, \dot{\varphi}) + G(\varphi, \gamma_r, \gamma_p) + \tau_f(\varphi, \dot{\varphi}) = \tau_a - \tau_{ext}, \quad (5.8)$$

where  $M$  is the inertia of the moving parts,  $N$  the Coriolis and centrifugal forces,  $G$  the gravitational forces.  $\tau_{ext}$  is an external torque (induced for example by the user) which acts besides the actuation torque  $\tau_a$ . It should be noted that  $G$  is determined by the inclination of both the car and the door hinge. The overall inclination of the door is given by  $\gamma_r$  (roll) and  $\gamma_p$  (pitch).

The torque resulting from friction is given by

$$\tau_f(\varphi, \dot{\varphi}) = \tau_{f1} + J^{-1}F_{f2}, \quad (5.9)$$

where  $\tau_{f1}$  is the friction of the door hinge and  $F_{f2}$  is the friction of the actuator. The modeling and compensation of friction is a well explored field; see [18, 71]. In our hardware setup, measurements revealed that  $\tau_{f1}$  can accurately be modeled by a pure Coulomb friction term in our hardware setup. Furthermore, it turned out that it is sufficient to take the nonlinear friction of the actuator  $F_{f2}$  only implicitly into account, which is described in subsection 5.2.2.3. Thus, more advanced methods for the handling of friction (as for instance described in [116]) were not necessary.

### 5.2.2.3 Modeling of the Actuation

The actuator consists of a brushed DC motor and a transmission, which is a combination of a planetary drive and a spindle (overall transmission ratio  $r$ ).

Using standard, low-cost equipment, a high-bandwidth current control scheme can be implemented. For this reason, we set an explicit modeling of the electrical part aside and assume both an ideal current control ( $I = I_r$ ) and a constant ratio  $c_m$  of motor current  $I$  and motor torque  $\tau_m$ , which gives  $\tau_m = c_m I$ .

To derive the transfer function of the actuator, we performed an experimental identification: The motor was controlled to a constant speed  $n_m$ . While measuring  $n_m$  and  $I$ , we applied different constant forces  $F_a$  on the linear rod. The identification revealed that  $I$  can be modeled as a combination of two terms, one proportional to  $F_a$  and the other nonlinearly depending on the velocity  $\dot{x}$ :

$$I = f(F_a, \dot{x}) = \frac{1}{c_m \eta(\tau_m, n_m) r} F_a + I_0(\dot{x}), \quad (5.10)$$

where  $\eta(\tau_m, n_m)$  denotes the degree of efficiency of the transmission and  $I_0(\dot{x})$  is the armature current without external actuator load ( $F_a = 0$ ). It should be noted that  $\eta(\tau_m, n_m)$  is relatively low, and that it heavily depends on the direction of power flow, i.e. whether the motor accelerates or decelerates the door.  $I_0(\dot{x})$  is proportional to the friction of the actuator  $F_{f2}$ , which contains both a Coulomb and a viscous component, as can be seen

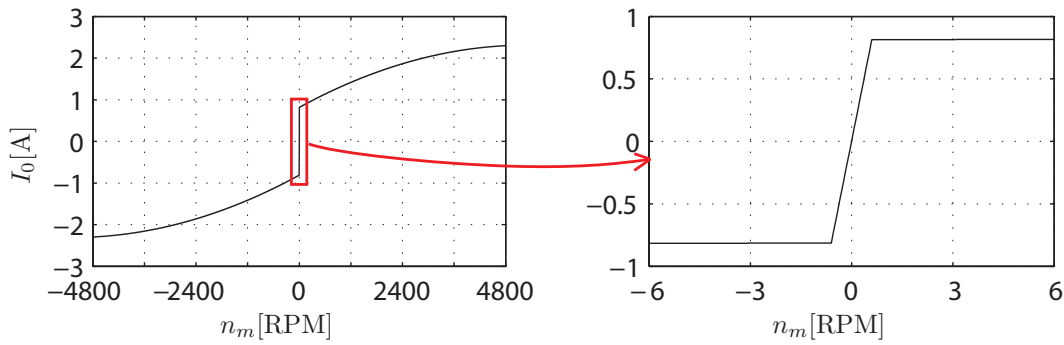


**Figure 5.15:** Speed-dependent friction component  $I_0$  of motor current  $I$  (l: full-scale view, r: zoom that clarifies Coulomb friction influence).

in Fig. 5.15. Based on this identification, we built a look-up table that is displayed in Fig. 5.16. Depending on the desired force  $F_a$  and the motor speed  $n_m$ , the corresponding motor current  $I$  is chosen by linear interpolation. To avoid discontinuities, a finite slope was chosen for the transition from small negative to small positive values of  $n_m$ .

## 5.2.3 Automatic Door Operation

### 5.2.3.1 Discrete State Control

To enable various modes of manual and automatic operation of the car door, a discrete state controller coordinating the complete system was developed. It consists of discrete system states with dedicated regulating actions, e.g. choice of the valid control structure, setting the brake, or triggering the automatic door lock. The state transitions represent the inputs from user control elements (e.g. various buttons for the door operation) and the collision and touch sensor system. An overview of the implemented modes of operation is given in Tab. 5.4, while Fig. 5.17 shows the implemented state machine, which consists of the modes of operation (lower case) and the user-induced transitions (upper case).

To make the state flow of the door more clear, a possible sequence of operation could look like this: The door is initially in mode Ready (rdy) at standstill waiting for inputs. Now the user pushes a control element to trigger the signal AO and the door will enter the mode Auto Open (ao). During the opening motion, the user again pushes a control element or simply touches the door, triggering the signal TOUCH. The door will immediately perform a Regular Stop (rs) and return to the mode Ready when Regular Stop indicates FINISH. If the user is still in touch with the door and thus TOUCH is on, the Hand Mode (hd) will be entered right afterwards, enabling further manual operation of the door.

### 5.2.3.2 Trajectory Planning

In order to get a smooth, well-defined motion of the door, a trajectory planner is used. It calculates the reference signals  $(\varphi_r, \dot{\varphi}_r, \ddot{\varphi}_r)$  for the position control of the door, which is a transition of the door from an actual state  $(\varphi_0, \dot{\varphi}_0)$  to an end state  $(\varphi_e, \dot{\varphi}_e)$  with a transition duration  $\Delta t$ .  $\Delta t$  is found with respect to the maximum acceleration of the

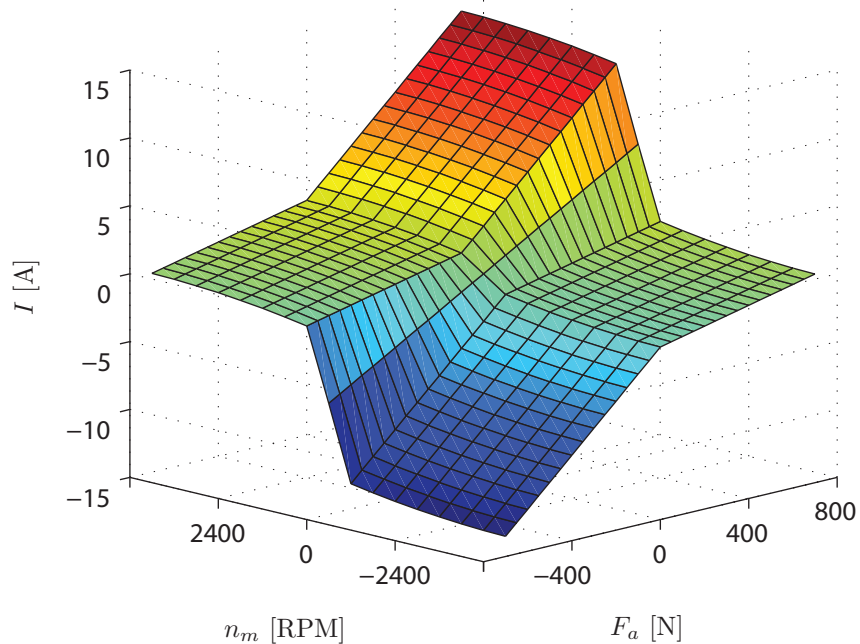


**Figure 5.16:** Look-up table for the calculation of the motor torque  $\tau_m = c_m I$  based on the motor speed  $n_m$  and the desired actuator force  $F_a$ .

**Table 5.4:** Modes of operation of the door and related user signals (lower case indicates STATE, upper case indicates transition).

| Mode name (state)     | Description (triggering signal condition) |
|-----------------------|---|
| Ready (rdy)           | idle (FINISH received from previous mode) |
| Auto Open (ao)        | open completely (AO is triggered)         |
| Auto Close (ac)       | close completely (AC is triggered)        |
| Auto Push Open (apo)  | open slowly (APO is pushed)               |
| Auto Push Close (apc) | close slowly (APC is pushed)              |
| Push Stop (ps)        | stop (APO/APC has been released)          |
| Regular Stop (rs)     | stop regularly (new triggering signal)    |
| Emergency Stop (es)   | stop short (EMERGENCY is triggered)       |
| Hand Mode (hd)        | manual, power-assisted operation (TOUCH)  |

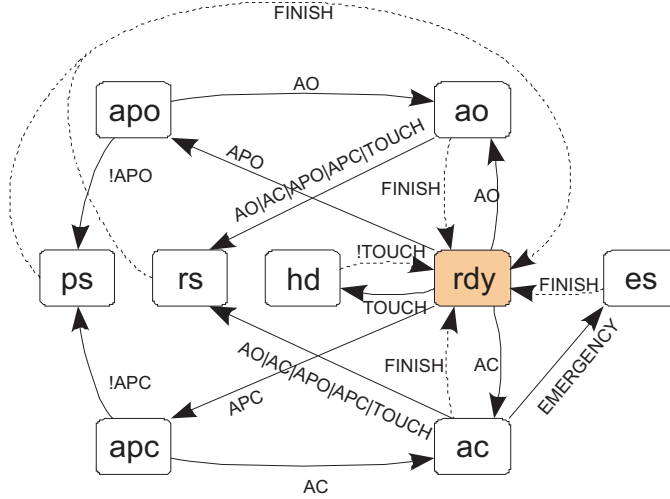


**Figure 5.17:** State machine controlling the (manual or automatic) mode of operation of the door.

actuator. Another important input is the maximum allowed opening angle  $\varphi_{obs}$ , which is determined by the collision sensor system. If no obstacles are present in the workspace of the door, obviously  $\varphi_{obs} = \varphi_{max}$  holds.

Depending on the active discrete state, different polynomials and boundary conditions are used for path interpolation, such as quadratic or cubic polynomials. The reference trajectory is then fed to the motion controlled door, as can be seen in Fig. 5.18.

### 5.2.3.3 Motion control

As already mentioned, a high-bandwidth current controller was used. Based on the look-up table displayed in Fig. 5.16, a well-defined actuation torque  $\tau_a$  can be generated. This, in turn, allows the realization of a motion-control loop.

As shown in Fig. 5.18, the motion control is realized by a PD controller with acceleration feedforward [258]. This gives the desired acceleration

$$\ddot{\varphi}_c = \ddot{\varphi}_r + K_p(\varphi_r - \varphi) + K_d(\dot{\varphi}_r - \dot{\varphi}), \quad (5.11)$$

where  $K_p$  and  $K_d$  are the PD control gains. The kinetic model of the door (Eq. (5.8)) is used for feedback linearization:

$$\tau_{a,c} = M(\varphi)\ddot{\varphi}_c + N(\varphi, \dot{\varphi}) + G(\varphi) + \tau_f(\varphi, \dot{\varphi}). \quad (5.12)$$

Thus,  $N$ ,  $G$ , and  $\tau_f$  are compensated and  $\ddot{\varphi}_c \approx \ddot{\varphi}$  [258]. To avoid oscillations, which could confuse the user, and at the same time to have a fast system response, critical damping is chosen by setting  $K_d = 2\sqrt{K_p}$ , where  $K_p$  is experimentally chosen. For a Lyapunov proof of stability, see [223, 233].

We tried to increase the quality of  $(\varphi, \dot{\varphi})$  by employing the acceleration sensor mentioned in subsection 5.2.2.1. The output of this sensor depends on the inclination of the car door and is therefore nonlinearly coupled with the signal of the position sensors. Therefore,

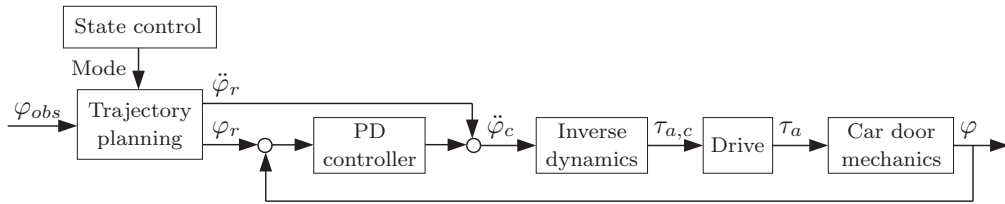


**Figure 5.18:** Motion control with state control and trajectory planning.

an Extended Kalman Filter (EKF) has been developed according to [267] to estimate the state of the system. To implement it, both the process and the measurement noise were quantified: The variance of the acceleration signal was  $5.63 \cdot 10^{-5} \text{ m}^2/\text{s}^4$ , and the variance of the position signal given by the potentiometer was  $3.06 \cdot 10^{-8} \text{ rad}^2$ .

The validation of the EKF at the experimental door under motion control revealed a quite smooth velocity signal, but also a significant phase lag between the estimated and the measured position. This can be explained by the limited stiffness of the door and the backlash of the actuation, which were idealized in the model.

The phase lag caused low-frequent oscillations of the door. Thus, only the encoder was used for state feedback to keep the elasticity of the mechanical structure out of the loop.

#### 5.2.3.4 Safety Aspects

During the door operation, the safety of the user and others involved in the workspace of the door has to be ensured. This applies to the automatic door operation in particular, since motions of the door are not directly induced by physical interaction. Furthermore, they might have been unintentionally caused by the user or might happen unexpectedly to others.

The discrete state controller comprises an emergency state implementing a simple bang-bang controller which can be triggered during the automatic closing of the door. Additionally, the error signal of the motion control is monitored. It reflects the unmodeled disturbances, including the user interaction. If the error exceeds a predefined threshold during automatic mode, the actuator is disabled. Furthermore, this signal could be used to switch from ready to the hand mode.

### 5.2.4 Manual Door Operation: Prearrangements

Based on the models of the mechanics and the actuation, a controller for the manual operation of the car door can be implemented. Before doing so, we explain why we focused on impedance control schemes. In addition, we present two common components of them.

#### 5.2.4.1 Selection of Impedance Control

With the use of kinesthetic feedback technology, we want to achieve a superior haptic interaction of the car door: Defined dynamic properties should be displayed with high quality. This includes defining the relation between the force  $F$  and motion  $\dot{x}$  of a rigid

body, which can be done either by an impedance  $Z = \frac{F}{\dot{x}}$  or an admittance  $Y = \frac{\dot{x}}{F}$ . Accordingly, such “virtual dynamics” are usually rendered by an impedance or an admittance controlled haptic device, see also Chap. 2.

Impedance control does not require an explicit measurement of the interaction torque  $\tau_{ext}$ . This is a great benefit, because the reliable measurement of the interaction force with a car door is complex and expensive if no camera is utilized; see subsection 5.2.1 and [243].

For haptic rendering, all following control concepts in this chapter contain consistently the same virtual door impedance and thus are denoted as impedance control. To achieve a high-bandwidth impedance control, the dynamics of the car door are partially compensated, see subsection 5.2.4.2. The desired impedance is formed by superposition of the individual functional contributions explained in subsection 5.2.4.3.

#### 5.2.4.2 Model Feedforward

Due to the lack of direct measurement of the user interaction force, the dynamic properties of the door cannot be shaped within a closed control loop when using impedance control. Therefore, based on Eq. (5.8) we do a feedforward compensation of the dynamics of the door:

$$\tau_{fwd} = \tilde{M}(\varphi)\ddot{\varphi} + \tilde{N}(\varphi, \dot{\varphi}) + \tilde{G}(\varphi) + \tilde{\tau}_{f2}(\varphi, \dot{\varphi}). \quad (5.13)$$

While it was possible to fully compensate  $N(\varphi, \dot{\varphi})$  and  $G(\varphi, \dot{\varphi})$ ,  $M(\varphi)$  could only be compensated in part ( $\approx 40\%$ ) due to stability problems. It should be noted that this compensation requires an explicit measurement of  $\ddot{\varphi}$ . Furthermore, the friction of the door hinge  $\tau_{f1}$  is not compensated to maintain stability, whereas  $F_{f2}$  is implicitly compensated by using the look-up table in Fig. 5.16.

Due to the compensation of  $G(\varphi, \dot{\varphi})$ , the inclination of the car does not affect the perceived dynamics of the car door. This is assumed to provide a convenient handling of the door even if the car is inclined, because the user will not have to counteract gravity himself. Furthermore, it enables the use of even a large angle of inclination of the door hinge without affecting the level of comfort of the user. Thereby, one important constraint in the design of a car door is not relevant for actuated car doors.

#### 5.2.4.3 Synthesis of the Virtual Door Impedance

Using an appropriate impedance in the control scheme, many different functionalities can be realized (compare also Chap. 3 and Chap. 4):

- Prevention of a position drift due to disturbances
- Reliable positioning at low velocities ( $\dot{\varphi} \approx 0$ )
- Smooth overcoming of the stick friction
- Active motion support, especially in the case of a freely swinging door operation (e.g. full opening)
- Collision avoidance

This motivated the implementation of various effects like a variable door stop (by controlling online-calculated references similar to [163] and subsection 4.2.6.2), a variable

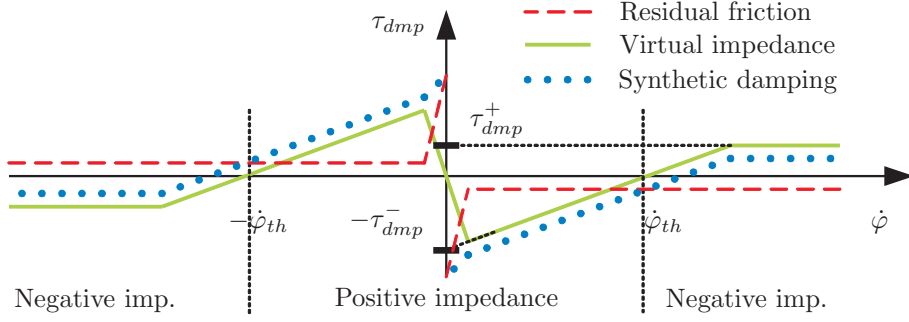


**Figure 5.19:** Synthetic damping (dotted), given by the residual friction (dashed) and the added virtual impedance (solid).

damping, a stepless door notch (subsection 4.2.6.2), and an active closing support. The overall virtual door impedance that we defined is given by

$$\tau_{imp}(\varphi, \dot{\varphi}, \varphi_{obs}) = \tau_{stp}(\varphi, \dot{\varphi}, \varphi_{obs}) + \tau_{dmp}(\dot{\varphi}) + \tau_{nch}(\varphi, \dot{\varphi}) + \tau_{lck}(\varphi, \dot{\varphi}) \quad (5.14)$$

which obviously is a superposition of four different impedances. In the following, these impedance modules, which provide an active user assistance, are described.

**Synthetic Damping** Variable damping is a key element in providing situation-dependent support. At standstill, increased damping can help the user to overcome the breakaway torque (static friction) in a smooth manner. Furthermore, it could support the positioning of the door at low velocities. At higher velocities, when the user is thought to intend a full opening or closing of the door, negative damping can support this motion.

To set up such variable damping, a continuous virtual damping has to be defined that takes into account the residual friction of the door, i.e. the part of the physical friction that has not been compensated by the motion control (see Fig. 5.19, dashed line). We propose a virtual impedance with the damping characteristics

$$\tau_{dmp}(\dot{\varphi}) = \text{sign}(\dot{\varphi}) \cdot \min \left[ \frac{|\dot{\varphi}| - \dot{\varphi}_{th}}{\dot{\varphi}_{th}} \tau_{dmp}^-, \tau_{dmp}^+ \right], \quad (5.15)$$

where  $\tau_{dmp}^-$  and  $\tau_{dmp}^+$  are positive torque constants and  $\dot{\varphi}_{th}$  is the threshold velocity.  $\tau_{dmp}^+$  is an upper limit for the support of fast movements of the door, and  $\tau_{dmp}^-$  is a measure for the synthesized static friction which the human has to overcome to move the door. To avoid chattering-like effects for noisy measurements of  $\dot{\varphi} \approx 0$ , we implemented this damping with a finite slope. This gave the virtual damping shown in Fig. 5.19 (solid line), which adds up with the residual friction (dashed line) to the overall synthetic damping (dotted line).

The synthetic damping appropriately supports the user by impeding or supporting the motion of the door. In particular, moderate and fast motions are supported by a small negative damping (similar to conventional friction compensation). This is a simple form of intention recognition.

Note that the velocity threshold  $\dot{\varphi}_{th}$  has to be tuned carefully and that the transitions between the intervals of impedance should be continuous to achieve a smooth haptic

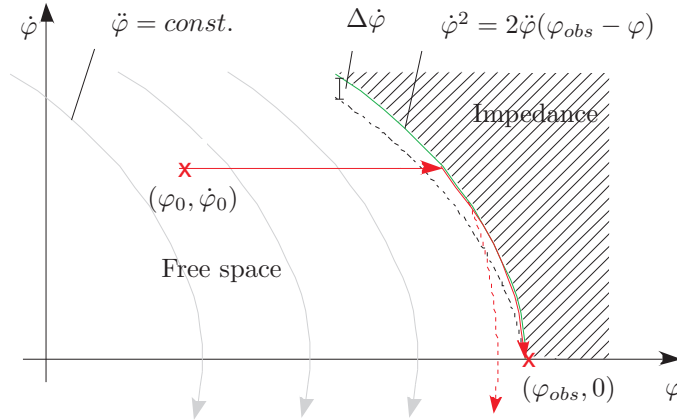


**Figure 5.20:** Variable door stop in the state space.

feedback for the user.

**Variable Door Stop** To provide a safe and smooth deceleration of the door based on the maximum opening angle  $\varphi_{obs}$  determined by the collision detection system, a variable door stop similar to [163] was developed. It monitors the door in state space. With a given constant deceleration of the door  $\ddot{\varphi}$ , the trajectory

$$\dot{\varphi}^2 = 2\ddot{\varphi}(\varphi_{obs} - \varphi) \quad (5.16)$$

just leading into the desired end state  $(\varphi_{obs}, 0)$  separates the state space into two areas rendered as free space and impedance. In Fig. 5.20 a possible trajectory of the door state is shown. Starting from an initial state  $(\varphi_0, \dot{\varphi}_0)$ , the door is in free space movement. If  $\varphi_{obs}$  is likely to be violated and thus the door state intersects the deceleration trajectory (Eq. (5.16)), the active impedance control law

$$\tau_{stp}(\varphi, \dot{\varphi}, \varphi_{obs}) = K_p(\varphi_r - \varphi) + K_d(\dot{\varphi}_r - \dot{\varphi}) \quad (5.17)$$

is applied, where  $K_p$  and  $K_d$  are the active PD control gains. With  $(\varphi_r, \dot{\varphi}_r)$  being the reference state determined by Eq. (5.16), the door state is controlled to decelerate by the impedance given in Eq. (5.17).

After that, a stiff virtual wall (PD controller) counteracts a violation of  $\varphi_{obs}$  for a certain time period. Finally, a pure D controller renders a viscous damping, which enables the user to move the (damped) door even into the potential unsafe area. This might be necessary in the case of an erroneous collision detection.

It is noticeable that a user might interact during the deceleration process. If the user intends to slow down or even reverse the door by himself, the velocity error signal exceeds some limit  $\Delta\dot{\varphi}$  and the impedance can be retracted (see Fig. 5.20, dashed trajectory branch).

**Stepless Door Notch** Furthermore, to prevent a drift of the door at standstill (due to wind, sensor noise, etc.), the physical static friction is enhanced by a stepless door notch

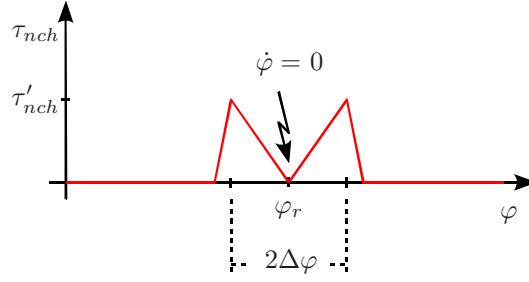


**Figure 5.21:** Characteristics of the door notch for  $\dot{\varphi} \rightarrow 0$ .

functionality. It is given by the active impedance

$$\tau_{nch}(\varphi, \dot{\varphi}) = K_p(\varphi_r - \varphi) - K_d\dot{\varphi} \quad (5.18)$$

which is hooked up in the actual position  $\varphi_r$  of the door on engage, i.e. at  $\dot{\varphi}_r = \dot{\varphi} = 0$  (see Fig. 5.21).  $K_p$  and  $K_d$  are control gains subject to the state of the door. The door notch can smoothly be released by modifying  $K_p$  and  $K_d$  according to a displacement  $|\Delta\varphi|$ .

**Locking Support** If the user tries to close the car door with insufficient velocity (or kinetic energy), the door lock cannot engage. If the velocity is inappropriately high, a noise and mechanical wear will occur. For this reason, we propose an active impedance that ensures a well-defined door velocity for a reliable lock operation just before the mechatronic door lock catches the door:

$$\tau_{lck}(\varphi, \dot{\varphi}) = K_d(\dot{\varphi}_r - \dot{\varphi}). \quad (5.19)$$

This is a pure velocity feedback control with gain  $K_d$ , and the velocity reference  $\dot{\varphi}_r$  is chosen to meet the door lock requirements. Engagement of the controller is done depending on the state of the door.

## 5.2.5 Manual Door Operation: Control Schemes

The main goal was to achieve a haptic interaction with the car door that is appreciated by the user. We wanted to realize this by the virtual door impedance defined in subsection 5.2.4.3. As motivated in subsection 5.2.4.1, impedance control was the best choice for this.

We found four promising, well-established impedance control concepts and implemented them such that they were heuristically stable for all relevant user interactions. In a subjective manner, their performance was evaluated experimentally, and the according hardware effort was analyzed.

### 5.2.5.1 Impedance Control without Force Feedback

A simple implementation of impedance control is to employ open-loop control of the actuator force:

$$F_{a,r} = J(\tau_{imp} + \tau_{fwd}), \quad (5.20)$$

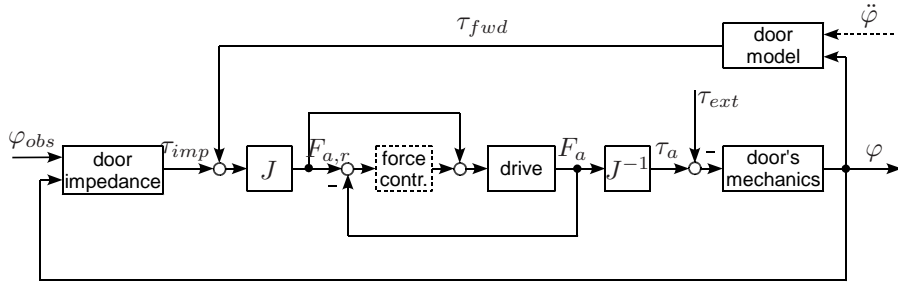


**Figure 5.22:** Impedance control of the car door; dotted block indicates actuator force feedback.

where  $\tau_{imp}$  and  $\tau_{fwd}$  are the torques resulting from the virtual impedance and the door model, respectively. Only force feedforward is active here, so the dotted block in Fig. 5.22 representing the force controller is set to zero. Thus, exact modeling of the drive especially regarding friction is essential [41], and a compensation of the inertia of the door is not possible. However, we achieved quite comfortable haptic feedback with this control concept. An interesting benefit is given by the hardware configuration: The open-loop force control only requires the measurements of state  $(\varphi, \dot{\varphi})$  and inclination  $(\gamma_r, \gamma_p)$ .

### 5.2.5.2 Impedance Control with Force Feedback

A measurement of the actuator force  $F_a$  allows the extension of the previous approach by explicit force control; see Fig. 5.22. Using a PD force-feedforward controller according to

$$F_{a,c} = K_p(F_{a,r} - F_a) + K_d \frac{d}{dt}(F_{a,r} - F_a) + F_{a,r}, \quad (5.21)$$

where  $K_p$ ,  $K_d$  are controller gains. Thereby, the closed-loop bandwidth of the force loop is improved by the phase lead of the differentiator [79] and a high-bandwidth force tracking performance can be achieved. This control scheme provided a subjectively very good haptic interaction with the door. Compared to other approaches, major advantages of this feedback of actuator force are:

- Improvement of steady state accuracy of rendered forces in the presence of model uncertainties
- Good starting characteristics of the actuator due to effective reduction of static friction

### 5.2.5.3 Position-Based Impedance Control with Force Feedback

A PD-type motion controller with acceleration feedforward and feedback linearization [258] is used for the control of the actuator state  $(x, \dot{x})$ , and a force  $F_{a,c} = m_{\Theta} \ddot{x}_c$  is commanded with  $m_{\Theta}$  being the inertia of the actuator. As can be seen in Fig. 5.23, this loop is driven by a model of the actuator, which gives the force control law

$$F_{a,r} - F_a = m'_{\Theta} \ddot{x}_r + d'_{\Theta} \dot{x}_r. \quad (5.22)$$

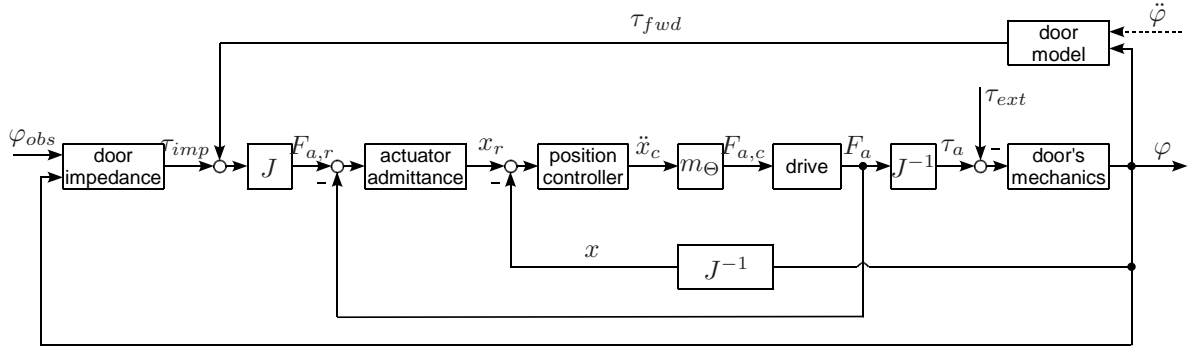


**Figure 5.23:** Position-based impedance control with force feedback.

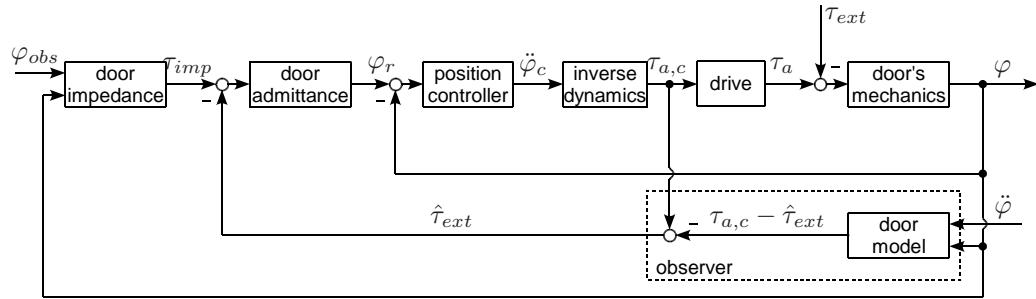


**Figure 5.24:** Position-based impedance control with force observer.

It thereby requires the measurement of the actuator force  $F_a$ .  $m'_\Theta$  and  $d'_\Theta$  are the parameters of this admittance, which can be chosen by the system designer. They directly affect the overall dynamic perceived by the user. Reasonable values for mass and damping were found to be  $0.5m_\Theta \leq m'_\Theta \leq 1.5m_\Theta$  and  $d'_\Theta = 500 \text{ Ns/m}$ . Due to the constant, rather low damping, the overall damping characteristics are close to the virtual door impedance described in subsection 5.2.4.3.

The benefits of this scheme are:

- Improved rejection of unmodeled friction effects of the actuator by use of a high gain motion control
- Possibility to render an increased inertia of the door without a measurement of  $\ddot{\varphi}$

Unfortunately, due to the inherent gear backlash of the drive, this control concept yielded a rather limited performance.

#### 5.2.5.4 Position-Based Impedance Control with Force Observer

A combination of the virtual impedance defined in subsection 5.2.4.3 and an admittance model of the door is proposed. This defines the overall system dynamics, as can be seen in Fig. 5.24.

Again, a motion controller similar to [258] has been used, leaving out only the acceleration feedforward. Similar to Eq. (5.22) an admittance

$$\tau_{imp} - \tau_{ext} = \Theta'_D \ddot{\varphi}_r + d'_D \dot{\varphi}_r \quad (5.23)$$

is set up now, where  $\Theta'_D$  and  $d'_D$  are the desired inertia and damping of the actuated car door, respectively. Reasonable values are given by  $0.5\Theta_D \leq \Theta'_D \leq 1.5\Theta_D$  and a rather low damping  $d'_D = 2 \text{ Nms/rad}$ .

The external interaction force  $\tau_{ext}$  needed to drive the admittance (Eq. (5.23)) can be estimated by an observer [194, 78]. Therefore, a model of the inverse dynamics of the door is used (see (Eq. (5.8))).

For the correct estimation of interaction force ( $\hat{\tau}_{ext} = \tau_{ext}$ ) we assume that  $\tau_{a,c} = \tau_a$  holds, so no explicit measurement of the actuator force is conducted. This relation given by the drive model has been validated for the control scheme in subsection 5.2.5.1 by means of the force sensor. However, the observer requires the measurement of the acceleration  $\ddot{\varphi}$ . Advantages of this observer-based approach are:

- Possibility to model the global inertia and damping of the door with respect to the workspace coordinate  $\varphi$
- Effective suppression of nonlinearities (e.g. friction of door and actuator)

However, the performance was rather limited. The reason for this is that the actuation and the measurement of acceleration were not collocated, as also mentioned in [79]. The finite structural stiffness of the mechanical elements in between accounts for higher-order dynamics, which have been neglected in the observer model.

### 5.2.5.5 Summary

The best (subjectively measured) performance of all four implementations was achieved by the impedance control with force feedback (subsection 5.2.5.2). A low gain loop explicitly closed on the actuator force improves force tracking performance, which directly affects the quality of haptic rendering. By measuring the actuator force at the output, the (time-varying) friction of a (low cost) actuator can be compensated effectively. The control scheme requires the measurement of position, acceleration, and actuator force, and thus is rather costly when compared to the three alternative control concepts. Nonetheless, as it yielded the subjectively best haptic sensation, we chose it as the reference setting for the evaluation described in subsection 5.2.6.

From a performance point of view, the most promising alternative would be the use of impedance control without force feedback. Thus, the force sensor could be omitted, significantly lowering the cost of the overall system.

Stability problems arising from high-gain control loops can be avoided using these two schemes. However, the rendering of high impedances such as the door stop requires accordingly high controller gains. The control gains for the state feedback are limited in practice due to several nonlinearities:

- Backlash of the transmission
- Finite stiffness of the mechanical structure
- Current limit of the actuator

This results in a rather low bandwidth of the position tracking, which is the main reason for the poor performance of the position-based control schemes. Technically, it would

have been no problem to use a better transmission and a more powerful actuator. This surely would result in a much better performance of the position-based control schemes, possibly making them an interesting alternative. However, as a good performance could be achieved with the impedance control of our low-cost hardware setup, we believe that a good trade-off between performance and costs has indeed been found.

## 5.2.6 Manual Door Operation: Evaluation

We experimentally evaluated the manual door operation through a user study with 16 participants. The results indicate that the haptic interaction with this actuated car door is indeed appreciated by the users.

### 5.2.6.1 Design of the User Study

**Selection of the Evaluation Parameters** The most relevant parameters for the haptic interaction with the actuated car door were expected to be rendered mass, damping, deceleration, and the parameters of the variable door stop (conventional door:  $M \approx 26$  kg,  $F_{f1} \approx 3$  Nm). The graduations described in Tab. 5.5 were thought to allow a quantitative assessment of the influence of these parameters on the haptic perception of the door. They contain a combination which provided a very good haptic interaction during the development of the control concept: ‘natural’ mass (m2), ‘low’ damping (d2), stepless door notch ‘active’, ‘high’ deceleration, ‘high’ stop damping and ‘short’ release time. This combination was used as reference setting in the user study.

**Table 5.5:** Evaluation parameters for the user study. The reference settings are given in **bold**.

| Parameters  | Graduations    |                        |                     |
|---|----------------|------------------------|---------------------|
| rel. mass $\frac{M'}{M}$                                  | ‘low’, m1: 0.6 | <b>‘nat.’, m2: 1.0</b> | ‘high’, m3: 1.4     |
| damp. $\frac{\tau_{dmp}^+}{\dot{\varphi}_{th}}$ [Nms/rad] | ‘none’, d1: 0  | <b>‘low’, d2: 5</b>    | ‘high’, d3: 8       |
| door notch $\tau_{nch}$                                   | ‘inactive’     |                        | <b>‘active’</b>     |
| decel. $\ddot{\varphi}_{max}$ [rad/s <sup>2</sup> ]       | ‘low’: 1.00    |                        | <b>‘high’: 1.75</b> |
| damping $K_d$   | ‘low’: 75      |                        | <b>‘high’: 150</b>  |
| release time $t_r$ [s]                                    | ‘long’: 1.5    |                        | <b>‘short’: 0.5</b> |

**Design of an Evaluation Sheet** Based on Tab. 5.5, an evaluation sheet was designed.

The first part consisted of four questions which should give the general impression of the users: general usability (Q1), manual operation of the door (Q2), equivalence of desired and actual motion (Q3), and the behavior at door stop (Q4). Possible answers were good (3), rather good (2), rather bad (1), and bad (0).

The second part was designed to allow a full-factorial analysis of the influence of mass and damping on the haptic interaction with the door. This is done by allowing the participant to judge on each setting, e.g. m1d3, in comparison to the reference setting m2d2. Possible answers were as follows: much better (2), better (1), no difference (0), worse (-1), and much worse (-2).

**Table 5.6:** Evaluation results for the actuated car door based on a user study with 16 participants.

|    | mean  | st.dev. |  |      | mean  | st.dev. |
|----|-------|---------|--|------|-------|---------|
| Q1 | 2.56  | 0.61    |  | m1d1 | -1.06 | 1.03    |
| Q2 | 2.44  | 0.70    |  | m1d2 | -0.31 | 1.21    |
| Q3 | 2.63  | 0.60    |  | m1d3 | -0.19 | 1.13    |
| Q4 | 2.38  | 0.78    |  | m2d1 | -0.31 | 0.68    |
| Q5 | -0.31 | 1.04    |  | m2d2 | -     | -       |
| Q6 | -0.88 | 1.11    |  | m2d3 | 0.06  | 1.03    |
| Q7 | -1.00 | 1.06    |  | m3d1 | -0.56 | 1.06    |
| Q8 | 0.13  | 1.17    |  | m3d2 | -0.38 | 0.99    |
| Q9 | 2.50  | 0.71    |  | m3d3 | -0.25 | 1.25    |

The third part consisted of four questions, each going along with one variation of  $\tau_{nch}$ ,  $\ddot{\varphi}$ ,  $t_r$ , and  $K_d$ : Preferable without stepless door notch (Q5), with lower deceleration (Q6), with longer time for deactivating door stop (Q7), and with low damping (Q8)? These questions could be answered on a scale of five steps, analogous to the second part.

The evaluation finished with Q9, which equals Q1.

### 5.2.6.2 Experiment and Results

We had 16 participants (15 male). Their mean age was 42.4 years ( $\sigma = 11.06$ ), and only one participant was not right-handed. All participants were employees of BMW. The group therefore certainly was not statistically matched to the general population of car door users. Indeed, we expected to get much more critical ratings on the performance of the actuated door, because many of these automotive experts are focused on achieving the best customer acceptance for the individual car parts they design. This group therefore promised to give valuable insights into how the actuated car door performs and whether it would be accepted by potential customers.

The participants conducted the experiment in the order given by the evaluation sheet. We intentionally did not randomize the order of the questions in the first part, because Q1 and Q2 should be answered right before the user could significantly adapt to the novel door. This gives a valid estimate of the *first impression* of the door, which is considered to be an important criterion for customer acceptance in the automotive industry. In the second part, we randomized the order of the mass-damping-settings to prevent a bias of the evaluation by learning effects. After this part, every participant had operated the door for more than 15 minutes. Therefore, we assumed that each user had got used to the door by then, such that no significant adaption would take place in part 3. Accordingly, Q5–Q8 were not randomized.

While the participants moved the door with the respective controller parameter setting, an investigator asked them the questions, operated the control elements, and filled out the the evaluation sheet. This might have slightly biased the evaluation of Q1–Q4 and Q9. However, we believe that this is not relevant because of the professional participants. The results of the evaluation are displayed in Tab. 5.6.

### 5.2.6.3 Analysis and Discussion of the User Study

As can be seen from the mean values of Q1–Q4, people liked the actuated car door and its features. Only a few participants rated aspects to be “rather bad”, and no-one rated any aspect to be “bad”. This suggests that the proposed concept would be accepted by customers.

The comparison of different mass and damping settings revealed that m2d2 and m2d3 were liked most. To analyze the results in detail, at first a two-factorial ANOVA (Analysis of Variance) was used. The 3x3 design that has been chosen allows the analysis of the influence of mass and damping (independent variables) on the rating of the manual operation of the car door (dependent variables).  $p = 0.05$  was used as threshold of significance. Under consideration of the sphericity, the mass showed to be not significant ( $F(1.314, 15) = 1.019$ ,  $p > 0.05$ ,  $\eta^2 = 0.64$ ). The damping proved to be significant ( $F(2, 15) = 6.818$ ,  $p < 0.05$ ). The interaction of both factors was not significant ( $F(4, 60) = 0.815$ ,  $p > 0.05$ ).

A pairwise comparison of all graduations of the damping according to the Bonferroni correction showed only for one pair a significant difference: ‘no damping’ and ‘high damping’ ( $t(15) = 0.521$ ,  $p < 0.05$ ). Thus, regardless of the mass, high damping positively influences the haptic interaction with the car door in our setup.

Opinions on the stepless door notch were divided, see the results for Q5 in Tab. 5.6: Half the participants liked this functionality, while the other half reported that it disturbed the operation of the door. This corresponds to the evaluation result of the variable door detent described in Chap. 4.2.6.3. Thus, the simulation result provided a reliable prediction of the rating of such an effect at a real door.

The mean values of Q6 and Q7 revealed that the deceleration should indeed be high and that the time for releasing the door right after a stop should be short, just as in the reference parametrization. However, according to Q8, there is no clear tendency on the variation of the damping  $K_d$ .

A statistical evaluation revealed that two factors of the variable door stop were significant when comparing the reference setting with the alternative setting: the deceleration ( $t(15) = 8.05$ ,  $p < 0.05$ ) and the release time ( $t(15) = 3.651$ ,  $p < 0.05$ ).

Interestingly, there were no significant differences in the general estimation of the actuated car door at the beginning and the end of the experiment: Q1 and Q9 lead to similar, very good results. Of the 16 participants, a majority – 10 people – rated the door with the best value of the given graduations, and a further 4 rated it with the second best. This approval of 87.5% of the participants suggests that the actuated car door is not only liked right from the start by the users, but also after people get used to it.

### 5.2.7 Summary

We investigated a variety of sensor concepts for the determination of the interaction force at one-DOF rotational car doors. Based on our findings, the most promising concept is given by a combination of motion sensors with a camera-based determination of the HIP. The latter has been filed as a patent in [245]. Both from a technical and an economical point of view, an actuated car door should be equipped with a position and acceleration sensor to achieve an effective determination of position, velocity, and acceleration, which

in turn can be used to determine the interaction force which is necessary for some haptic control schemes.

We showed a way to design an actuated car door such that potential customers like it both at first contact and after getting used to it. Furthermore, due to its clever mechanical concept, it can be built into conventional car doors without great modifications. The main components of the door are a linear drive, a current-controlled amplifier, and sensors for position, acceleration, and actuator force.

While this setup enables an advanced automatic door operation, our main focus here was the control and evaluation of the manual door operation. We implemented and tested four different impedance control schemes. The impedance control with force feedback was the best choice for this door for several reasons. We used this control scheme to render specified impedances, i.e. haptic effects that are meant to support the user while he or she operates the door. One such effect was a variable door detent that allows the placing of the door at a desired location where it is fixed by a position controller.

A major advantage is the possibility to vary the dynamic properties of the door (mass, damping, and “synthetic” haptic effects). Indeed, an evaluation with 16 participants revealed that some of the controller parameters had a statistically significant influence on the feeling of the users. For example, higher damping was clearly preferred to a low damping.

The most important result of the evaluation was that a majority of 87.5% of the participants liked the car door, with 62.5% giving the highest grading. This approval was found both at the first contact of the participants with the novel door, and after they got used to it. From this we reason that the customer acceptance of our actuated car door would be relatively high and hence it would be promising to market such doors.

It should be noted that these positive results were successfully validated in a follow-up study conducted by Michael Gräf at BMW Forschung und Technik GmbH which is described in [240]. The goal was to find out which elements of the overall system contributed to this approval, and to what extent. This information would be helpful in evaluating the trade-off between hardware effort and user satisfaction. 19 different configurations were presented, including a full- and semi-active control mode of the actuator and a collision avoidance scenario. The configurations should be rated on a scale from 1 (very bad) to 6 (very good). Eighteen men and 9 women with an average age of 38.7 years ( $\sigma = 11$ ) participated in the experiment. The analysis of the user study revealed that the fully-actuated car door provides the best handling. After the evaluation, 89% of the participants told that they generally appreciated the actuated door, and 89% the collision avoidance.

## 6 Conclusion and Future Work

This thesis described many aspects of the simulation, haptic control, and evaluation of actuated mechanisms using the example of car doors with one or more degrees of freedom (DOF). We were the first to propose concepts and controllers for actuated car doors with more than one DOF and filed a corresponding generic patent [242]. Furthermore, a promising force determination method has also been filed as a patent [245], and advanced methods and controllers have been developed for several virtual and physical car door prototypes. Our extensive evaluations revealed a predominant approval of and desire for car doors with one and two actuated DOF. Based on our results, the automotive industry can confidently start to develop actuated car doors for the mass market.

### 6.1 Concluding Remarks

#### **Virtual Reality Prototyping by Active Admittance Control**

Virtual Reality Prototyping (VRP) with haptic feedback offers great benefits in the development process of actuated systems. By introducing the Active Admittance (AA), we proposed a generic, straightforward admittance control scheme for the haptic rendering of actuated mechanisms. It extends the conventional admittance control by modeling the actuation and the movable parts of the mechanism separately. The actuation includes models of all significant elements of the actuation loop, particularly the sensors, the controller, the actuators, and the transmission. The modeling of these components is supported by a comprehensive overview of the haptically relevant properties of mechatronic systems. Based on the AA, the actuation effect and the resulting simulated motion is calculated and can be displayed by a haptic device. The controller design and stability issues of Active Admittance Control (AAC) have been discussed. Due to the analogy of human and controller effecting the same object, functionality aspects and methodologies can be derived from shared and supervisory control. Stability considerations are based on the abundant research on the control of haptic interfaces. However, no common approach is suited or desired for the generic control design of actuated systems. Rather, the control design has to carefully consider the specific goals and restrictions of the mechatronic system in order to choose the appropriate control structure. Therefore, a guideline is proposed to help in the identification of the least conservative control structure. AAC has successfully been demonstrated by modeling and haptically rendering a novel actuated car door with two DOF.

#### **Generic Methods for the Haptic Support of Human-System-Interaction**

AAC is also very well suited for the integration of assistive functions in the controller of the simulated system. In Chap. 3, to achieve an intuitive, convenient, and safe operation of actuated car doors with arbitrary kinematics, three generic support methods have been

developed. For mechanisms with more than one DOF, preferable paths or trajectories can be predefined offline, e.g. based on ergonomic investigations or on optimality criterion. These motions can be utilized as Static Virtual Fixtures. Our advanced implementation combines these Static Virtual Fixtures with Dynamic Virtual Fixtures to achieve an intuitive manual handling and to enable the operator to switch between predefined paths. This is supported by an online estimation of the intention of the user and a subsequent calculation and update of the Dynamic Virtual Fixture which guides the motion towards the predefined path with the highest likelihood. Especially in the presence of obstacles, predefined paths must not be used without additional measures. One possibility is to compute collision-free paths online, which necessitates a near real-time path planner. This can be used as the foundation of Dynamic Virtual Fixtures during manual operation, or as controller input during automatic operation. We developed a suitable generic path planner and showed that the performance is sufficient for a real-time haptic support. Furthermore, we proposed the Generalized OR Paradigm, which enables an advanced adaptation and optimization of multi-threaded path planning. It has been described why collision avoidance is a prerequisite for both manual and automatic operation of a car door. Through our multi-threaded approach, we achieved response times of  $\approx 13$  ms, enabling a real-time haptic support and the use of bounding boxes which are tight approximations. Furthermore, several implementation approaches have been described. The proposed support methods can easily be integrated into AAC schemes by applying their respective supportive effect in parallel to the human user input exerted on the virtual model (EOM) of the car door. Our applications of these methods to simulated car doors as well as to hardware prototypes have been described in Chap. 4 and Chap. 5.

### **VRP of Actuated Car Doors in General**

Up to now, there have been no concrete guidelines for the design of the dynamics of an actuated car door. In practice, the engineers try to balance all factors based on best practices and personal experience. This is not viable for car doors with more than one DOF, because there is no previous knowledge, and the overall dynamics resulting from the coupling of the single DOF can be very complicated. The complexity increases even further when actuated car doors are to be developed – the design of a controller that provides a desired haptic interaction characteristic necessitates appropriate tools. Our approach is to utilize VRP with haptic feedback to develop, simulate, control, and evaluate new door concepts.

### **VRP of Actuated Car Doors with Several DOF**

In Sec. 4.1, we proposed a VRP test bed with haptic feedback comprising automotive end-effectors and several networked computers to distribute computing tasks such as obstacle detection, collision avoidance, and path planning. We used the VRP test bed to evaluate five preliminary door concepts. The result was that a Two-Link Door (TLD) is the preferred concept. We investigated it in more detail together with two other door concepts, a Free-Flying Door (FFD) and a Pivotal-Sliding Door (PSD). An evaluation of the FFD combined with the intention recognition described in Sec. 3.1 revealed that the ten participants liked the door simulation itself, whereas the haptic guidance based on intention

recognition resulted in polarized opinions. It became evident that the preference for haptic support strongly depends on personal characteristics. For instance, all the women preferred a “light” car door, while the men did not. This indicates that door dynamics indeed do matter. During our investigation of the preferred dynamics of a PSD it became evident that these dynamics strongly depend on the movement of the door (swinging/sliding/combined) and on personal characteristics. The best ratings were achieved for the individually selected parameter sets. This is a clear indication that the car door dynamics should be adaptable with respect to the current user as well as to the manual operation situation. We developed a variety of controller modules for a TLD. A comprehensive evaluation with 20 participants revealed that: 1) The height/weight of the user has a very strong influence on the preferred dynamics, but the gender has not. 2) Most, but not all of the supportive functions are approved by participants. 3) The haptic support given by collision avoidance and path planning is appreciated very much. 4) Light doors were preferred and received an excellent rating when combined with all assistive functions. These are very important findings which enable the user-centered design of both unactuated and actuated car doors with more than one DOF. Based on the evaluation results, we strongly recommend determining the height of the user and to use this information as input to an adaptable car door controller. We draw the conclusion that door dynamics do matter and that an adaptive controller has to be used to provide a superior manual interaction. The adaptation should be based on situation and user, specifically his or her height. Overall it can be stated that VRP is indeed very useful for both the development and the evaluation of car door concepts.

### **VRP of Car Doors with One Rotational DOF**

Car doors with one rotational DOF are dominating the market today, and they will be important also in the future. For the design of a high-fidelity haptic device for the simulation of car doors with one rotational DOF, in Sec. 4.2 the basics for the performance specification based on the analysis of a typical worst-case user interaction and a detailed model of a car door have been derived. It was pointed out that the promising inclusion of actuation effects in the haptic rendering of car doors does not impose significant additional restrictions. Furthermore, a very detailed model for a BMW 3 Series driver’s car door has been derived and implemented. The accuracy of the overall model was shown by comparing the simulated motion with measurements. In the performance specification we concluded that a one-DOF hardware setup consisting of a direct drive with a high mechanical stiffness, torque output, and a high control bandwidth have to be provided. We created a backlash-free, very stiff haptic device to which various end-effectors can be attached. Accurate force and position sensors enable a high-fidelity rendering. Various measures ensure safe operation of the device. An extensive user study with 17 participants was conducted. We found that the participants can distinguish between simulation and reality. However, the standard model of the car door is rated rather similarly to reality, and linear deviations from the standard model were rated linearly decreasing. An important result is that the haptic simulation can reliably be used to evaluate different door concepts if the difference between them is at least in the area of 13% to 26%, or 5 Nm to 10 Nm, respectively. When we investigated the preferred efforts for the manual operation of the door, we found that

the larger the Coulomb friction and the larger the door detent torque, the lower is the appreciation by the participants. This was more evident for closing motions, because people tend to close doors with a push, while the opening motion is typically slower. This fact should be exploited in the controller design of actuated car doors: Instead of searching for an overall trade-off for the rendered dynamics, the dynamics should be adapted for each mode of operation individually.

### **Control and Evaluation of an Actuated TLD Prototype**

To put these results from simulation into practice, together with MiMed (TU München) we developed the prototype of an actuated Two-Link Car Door (TLD) in the framework of MechaTUM. The prototype’s hardware setup, control of manual and automatic operation, and successful evaluation are described in Sec. 5.1. It utilizes a variety of assistive functions described in this thesis: A state machine providing a joint seat/door action, path planning, collision avoidance, and clamping protection during manual and automatic operation. Results of the large-scale AttrakDiff evaluation of the manual operation of the TLD prototype were presented: Even in a complicated usage scenario, a good usability was achieved with the haptic support provided by the controller of the actuated car door – the level of discomfort was significantly decreased. The rating of ergonomics experts leads to the conclusion that such a door is indeed “desired”, exhibiting both a high hedonic and pragmatic quality. This is an excellent result for such a worst-case parking situation.

### **Control and Evaluation of an Actuated Conventional Car Door Prototype**

Furthermore, in Sec. 5.2 we developed and investigated force measurement concepts for rotational car doors with one DOF which have in part been filed as a patent in [245], and we investigated the advanced control of a close-to-mass-production actuated car door provided by BMW Forschung und Technik GmbH. By utilizing a linear, non-backdrivable actuator and various sensors, both automatic and manual door operations are enabled. A discrete state controller ensures a safe operation of the door, including automatic opening and closing. The realization of a supportive, high-quality haptic interaction with the car door for the manual operation is the principal part of our work. Due to the impracticality of a direct measurement of the user interaction force at a car door, we chose impedance control to render the desired dynamics. The impedance was designed to provide a convenient, intuitive, and safe manual handling of the door. We implemented and tested four different impedance control schemes, of which impedance control with actuator force feedback performed best. Two experimental evaluations with 16 and 27 participants revealed a predominant approval of the actuated car door.

## **6.2 Future Work**

The investigation of the VRP-based simulation, control, and evaluation of actuated mechanisms with more than one DOF was in many aspects virgin soil. While we tried to get the big picture, not all relevant aspects could be investigated by in-depth studies. Possible extensions of this work and promising research directions are pointed out in the following:

- Active Admittance Control (AAC): A thorough investigation of AAC should be conducted with respect to the robust stability of the overall haptic simulation. In the end, specific design guidelines should be derived to guarantee a robustly stable design of the controllers of haptically simulated mechatronic systems.
- Virtual Reality Prototyping (VRP): The ideal of a truly transparent rendering requires hardware and software that overcomes the current limitations. Potential is especially seen in the hardware-driven increase of motion control bandwidth. For instance, the one-DOF car door simulator could further be enhanced by replacing the current direct drive by an even more dynamical one.
- Path planning: As pointed out in this thesis, the proposed Generalized OR-Parallelization could be utilized by several approaches to achieve a real-time path planning even in complex and changing environments:
  - Combination of different algorithms (e.g. RRTs and PRMs) to achieve a synergy of their individual advantages
  - Concurrent use of different parameter sets of path planning algorithms
  - Online adaptation of these parameter sets to the respective environment
  - Online adaptation of the types and numbers of parallel executed planning threads to the respective environment

Ultimately, when computing resources are virtually not limited any more, the parallel execution of a large number of all known path planning algorithms with all possible parameterizations will enable the determination of a collision-free trajectory within a timespan near the global minimum.

- Psychology of the haptic interaction at car doors: More detailed psychological studies should be conducted to determine the preferred dynamics and assistive functions of actuated mechanisms. Specifically, guidelines for user studies should be provided that enable a valid determination of the preferred dynamics of a mechanism even if it possesses complex kinematics.
- Safety: The most critical issue for making actuated car doors a success in the automotive industry is seen in the area of safety. It will require a lot of effort to set up appropriate guidelines for the design and operation of novel doors, and finally to implement this functionality during the serial development of cars.

However, we are confident that these challenges will be met. In the future, VRP with haptic feedback will be established in industrial design, and actuated car doors providing a superior manual interaction will find their way into automotive mass production.



# A State of the Art of Unactuated Car Doors

Even in the design of conventional car doors, there are a variety of typical challenges:

- Reducing weight of the door is mandatory to lower the overall power consumption of the car.
- However, the inertia  $I_{zz}$  of the car door should usually not be reduced significantly. From an ergonomical point of view, the velocity of the car door should not have to be very high to achieve a complete closing of the door after a push by the user:  $\dot{\mathbf{q}} \leq \dot{\mathbf{q}}_{erg,crit}$ . This means that there is a lower bound for the inertia in terms of the kinetic energy  $E_{kin,crit}$  which is necessary for a full closing of the door:  $I_{zz} \geq \frac{2E_{kin,crit}}{\dot{\mathbf{q}}_{erg,crit}^2}$ .
- No experiments are known which indicate whether users prefer the usual, a higher, or a lower inertia of the door.

In the automotive mass market, up to now the following one-DOF car doors prevail:

1. Front-/Roof-Hinged Swing Doors
  - a) Rotational axis at the A-pillar of the car chassis (>98% market share in 2009)
  - b) Rotational axis at the roof (e.g. Mercedes-Benz SLS AMG)
2. Rearwards-Opening Sliding Doors

Due to safety concerns, most other types of car doors have disappeared. Regulations issued by the Economic Commission for Europe, specifically the ECE R11.03, defined and limited the design possibilities [73, 222]. Based on these, rear-hinged rear doors have been re-introduced by the Rolls Royce Phantom in 2003 and the Opel Meriva in 2010. The various measures for providing safety of the overall door system are described in [222]. This gives an impression of how tedious even the development of close-to-conventional car doors is, which is the main reason for the slow development of alternative door concepts.

Lately, a two-DOF kinematic has been proposed to enable a sliding door movement without the necessity for exterior rails [19]. However, it also aimed at one-DOF movements.

## B Technical Details Related to the AAC of Car Doors

### B.1 EOM of Several Simulated Car Doors

Generally, the dynamics of a rigid mechanism can be expressed by the canonical equation

$$\mathbf{H}(\mathbf{q})\ddot{\mathbf{q}} + \mathbf{C}(\mathbf{q}, \dot{\mathbf{q}})\dot{\mathbf{q}} + \boldsymbol{\tau}_G(\mathbf{q}) + \boldsymbol{\tau}_F(\mathbf{q}, \dot{\mathbf{q}}) = \boldsymbol{\tau}_A + \mathbf{J}^T \mathbf{f} \quad (\text{B.1})$$

where  $\mathbf{H}(\mathbf{q})$  represents the joint space inertia,  $\mathbf{C}(\mathbf{q}, \dot{\mathbf{q}})\dot{\mathbf{q}}$  the joint space Coriolis and centrifugal terms,  $\boldsymbol{\tau}_G(\mathbf{q})$  and  $\boldsymbol{\tau}_F(\mathbf{q}, \dot{\mathbf{q}})$  the gravity and friction effect,  $\boldsymbol{\tau}_A$  the actuation and  $\mathbf{J}^T \mathbf{f}$  the external forces and torques acting on the mechanism.

During our course of research, we simulated a variety of different car door kinematics with more than one DOF. Some kinematics are depicted in Fig. B.1, and they will be shortly described with their respective EOM in the following. In the sketches of the kinematics, some relevant parameters as well as the minimal coordinates are indicated to give a better understanding of the model. Without loss of generality, all DOF are assumed to be orthogonal with respect to gravity, such that no gravity wrench is acting on the mechanisms.

#### B.1.1 Car Door Body and Free-Flying Door (FFD)

Throughout the thesis, the same model of the car door body has been used for all more-than-one-DOF simulations: The driver's door of a BMW 6 Coupe. Its VRML model is depicted in Fig. D.6, and the most relevant geometrical (with respect to the car COS) and dynamic parameters are given in the following.

**Table B.1:** Geometrical parameters: Location of COG and hinge

|  | x      | y       | z      |
|--|--------|---------|--------|
| COG (window closed)                    | 1.3384 | -0.7919 | 0.4261 |
| COG (window opened)                    | 1.2634 | -0.7613 | 0.3590 |
| Middle of upper door hinge             | 0.6959 | -0.8495 | 0.4574 |
| Middle of lower door hinge             | 0.6931 | -0.8578 | 0.1375 |
| Door hinge used for coarse simulations | 0.6940 | -0.8530 |        |

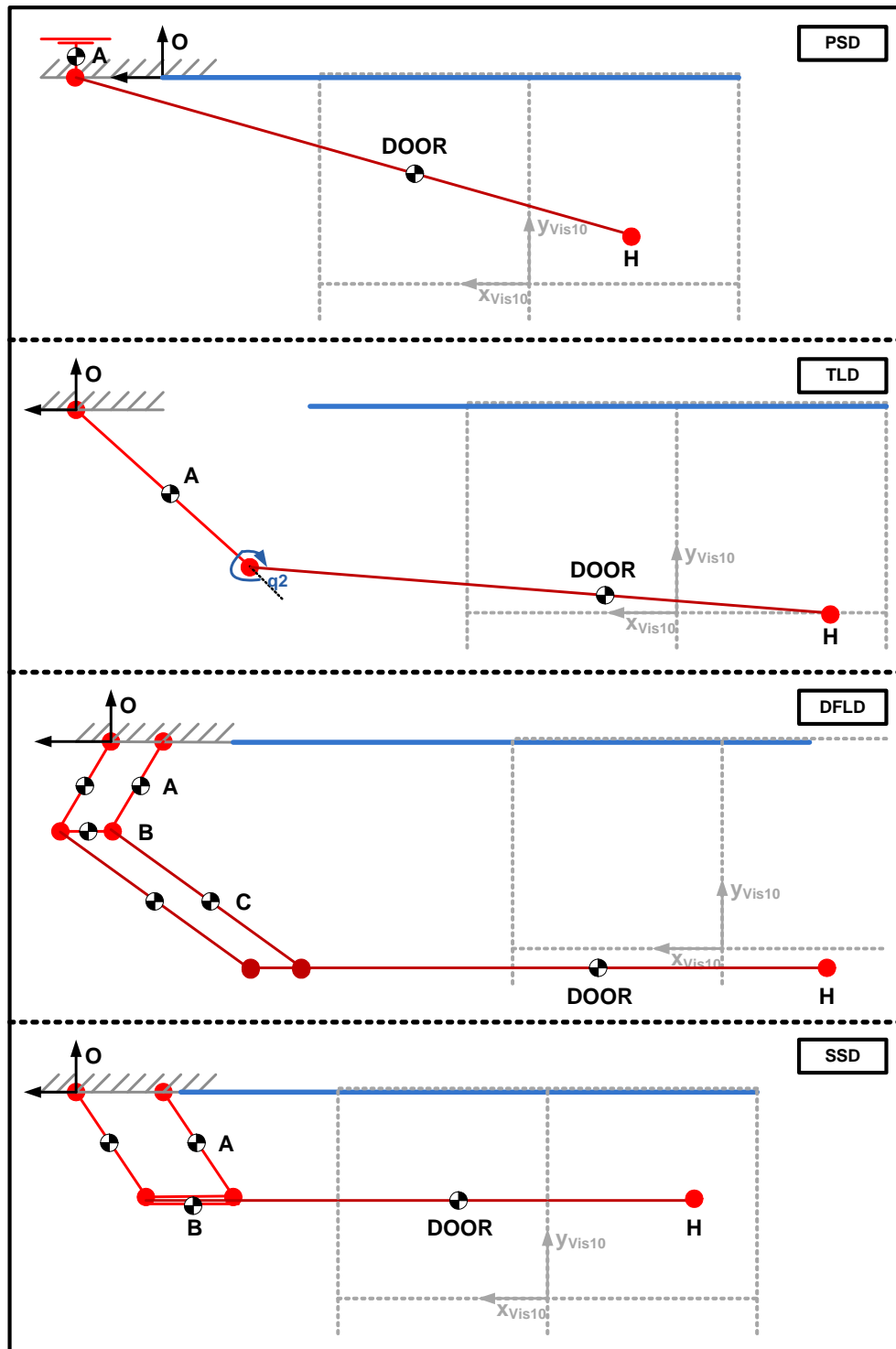


**Figure B.1:** Overview of the two-DOF car doors simulated at the VRP test bed: 1) Pivotable-Sliding Door (PSD), 2) Two-Link Door (TLD), 3) Double-Four-Link Door (DFLD), 4) Swing-Sliding Door (SSD). The door body DOOR is the same as the one described in Appendix B.1.1. The fully closed position of the door is indicated by the solid blue line. The renderable workspace for the haptic interaction point H in x-y-coordinates is given by the  $V_{ISHARD10}$  is depicted in dashed line.

**Table B.2:** Geometrical parameters: Levers

|                              |              |      |
|------------------------------|--------------|------|
| Lever from COG to door hinge | $l_{COG}[m]$ | 0.65 |
| Lever from HIP to door hinge | $l_{HIP}[m]$ | 1.10 |

**Table B.3:** Dynamic parameters

|                                    |                        |                |
|------------------------------------|------------------------|----------------|
| Mass                               | $m[\text{kg}]$         | 26.0           |
| Inertia with respect to door hinge | $I_{zz}[\text{kgm}^2]$ | 14.38          |
| Coulomb friction of the door hinge | $\mu[\text{Ns/rad}]$   | $1.5 \pm 50\%$ |

$$\mathbf{I}_{Hinge} = \begin{pmatrix} 3.71 & 1.09 & 5.42 \\ 1.09 & 17.70 & 0.64 \\ 5.42 & 0.64 & 14.38 \end{pmatrix} \quad (\text{B.2})$$

$$\mathbf{I}_{COG} = \begin{pmatrix} 1.35 & 0.09 & 0.45 \\ 0.09 & 4.59 & 0.21 \\ 0.46 & 0.21 & 3.46 \end{pmatrix} \quad (\text{B.3})$$

### B.1.2 Pivotal Sliding Door (PSD)

The parameters of the Pivotal Sliding Door (PSD) simulated in subsection 2.3.3 and subsection 4.1.4 is given in Tab. B.4.

**Table B.4:** Parameters of the simulated PSD

| $m_1 [kg]$ | $m_2 [kg]$ | $I_{ZZ} [\frac{kg}{m^2}]$ | $l_{IP} [m]$ | $l_2 [m]$ | $\mu_1 [\frac{Ns}{m}]$ | $\mu_2 [\frac{Ns}{rad}]$ | $T_1 [ms]$ | $T_2 [ms]$ |
|------------|------------|---------------------------|--------------|-----------|------------------------|--------------------------|------------|------------|
| 6.0        | 24         | 3.2                       | 1.2          | 0.58      | 1.5                    | 2.5                      | 4.0        | 5.0        |

### B.1.3 Two-Link Door (TLD)

The proposed Two-Link Door (TLD) consisting of one rotation link and the car door body is shown in Fig. B.1. One side of the rotation link A is set on the car body through a hinge axis. The other side will be combined with the car door through a hinge axis. When the user opens and closes the door, both links will be rotated round its hinge axis.

| link        | $m$ [kg] | $l$ [m] | $I_{zz}$ [kgm <sup>2</sup> ] | $\mu$ [Ns/rad] |
|-------------|----------|---------|------------------------------|----------------|
| <i>A</i>    | 0.715    | 0.45    | 0.00368                      | 2              |
| <i>Door</i> | 26.0     | 1.10    | 14.38                        | 1.5            |

**Table B.5:** Parameters of the TLD used for the VRP.

Using the Autolev TLD model given in Appendix B.3.1, the EOM have been derived:

$$\begin{aligned}
 & \begin{pmatrix} M_{TLD11} & 0 \\ 0 & M_{TLD22} \end{pmatrix} \begin{pmatrix} \ddot{q}_1 \\ \ddot{q}_2 \end{pmatrix} + \begin{pmatrix} C_{TLD11} & C_{TLD12} \\ C_{TLD21} & C_{TLD22} \end{pmatrix} \begin{pmatrix} \dot{q}_1 \\ \dot{q}_2 \end{pmatrix} \\
 & = \begin{pmatrix} T_{TLD11} & T_{TLD12} & T_{TLD13} & T_{TLD14} & T_{TLD15} \\ T_{TLD21} & T_{TLD22} & T_{TLD23} & T_{TLD24} & T_{TLD25} \end{pmatrix} \begin{pmatrix} f_{I_X} \\ f_{I_Y} \\ \tau_{IP} \\ \tau_A \\ \tau_T \end{pmatrix} \quad (B.4)
 \end{aligned}$$

where  $M_{TLD_{xx}} = f(q_1, q_2)$ ,  $T_{TLD_{xx}} = f(q_1, q_2)$  and  $C_{TLD_{xx}} = f(\dot{q}_1, \dot{q}_2, q_1, q_2)$ .

With the help of the acceleration, the equation of movement of the end-effector will be determined through the Jacobian.

$$\begin{cases} \dot{X}_{Vis10} = l_A \dot{q}_1 \sin(q_1) + l_{DOOR}(\dot{q}_1 + \dot{q}_2) \sin(q_1 + q_2) \\ \dot{Y}_{Vis10} = -l_A \dot{q}_1 \cos(q_1) - l_{DOOR}(\dot{q}_1 + \dot{q}_2) \cos(q_1 + q_2) \\ \dot{\vartheta}_{Vis10} = \dot{q}_1 + \dot{q}_2 \end{cases} \quad (B.5)$$

## B.2 Typical Opening Paths of Some Car Doors

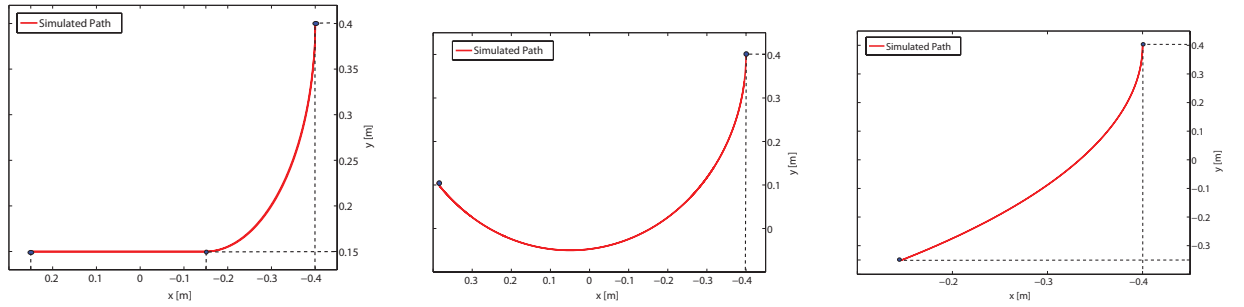


**Figure B.2:** Typical opening path for the PSD (l.) and the TLD (transmission ratio: 1 (m.) and 5 (r.)) [85].

## B.3 Autolev Code

### B.3.1 Autolev Code of the TLD VRP Simulation

```

%-----
%   File:  tld_simulation.al
% Problem:  VRP simulation of the idealized TLD
% Author:  Michael Strolz, strolz@tum.de
%-----
%   Declarations
NEWTONIAN  N
FRAMES    E
BODIES    A, T
POINTS    AT, IP
%-----
%   Variables
VARIABLES  q{2}'
VARIABLES  U{2}'
VARIABLES  TAU_ACT_A
VARIABLES  TAU_ACT_T
VARIABLES  F_I_X, F_I_Y
VARIABLES  TAU_I_Z
%-----
%   Constants, Mass, Inertia
CONSTANTS  MU_H_AE, MU_H_AT % Static Friction
CONSTANTS  MU_R_AE, MU_R_AT % Dynamic Friction
CONSTANTS  L_A
CONSTANTS  L_AtoT
CONSTANTS  L_TtoIP
MASS       A=M_A, T=M_T
INERTIA A, 0, 0, I_A_zz
INERTIA T, 0, 0, I_T_zz
%-----
%   Geometry relating unit vectors, Position vectors
SIMPROT(N, E, 3, 0)
SIMPROT(N, A, 3, q1)
SIMPROT(A, T, 3, q2)
P_Eo_AT> = -L_A*A1>           % Position vector from Eo to AT
P_AT_To> = -L_AtoT*T1>       % Position vector from AT to To
P_Eo_Ao> = 0.5*P_Eo_AT>      % Position vector from Eo to Ao
P_AT_IP> = P_AT_To> - L_TtoIP*T1> % Position vector from AT to IP
q1' = U1;
q2' = U2;
%-----
%   Angular velocities
W_E_N> = 0>
W_A_N> = U1*A3>
W_T_A> = U2*T3>
%-----
%   Velocities
V_Eo_N> = 0>
v2pts(N, A, Eo, Ao)

```

```
v2pts(N, A, Eo, AT)
v2pts(N, T, AT, To)
v2pts(N, T, AT, IP)
%-----
%           Forces and Torques
FORCE_IP> += (F_I_X*N1> + F_I_Y*N2>)
Torque(E/A, - MU_R_AE*W_A_E> + TAU_ACT_A*A3>)
Torque(A/T, - MU_R_AT*W_T_A> + TAU_ACT_T*T3> + TAU_I_Z*T3>)
%-----
%           Equations of motion
ZERO = FR() + FRSTAR()
KE()
KANE()
%-----
%           Reformed result
solve( ZERO, U1', U2')
%-----
%           Save output
Save tld_simulation.all
%-----
%           End of file
```

### B.3.2 Autolev Code of the TLD Prototype

```

%-----
%      File:  tld_prototype.al
% Problem:  Dynamics of the elastic TLD prototype
% Author:   Michael Strolz, strolz@tum.de
%-----
%      Newtonian, bodies, points
Newtonian      N
Points         0
Bodies        B1, B2, B3, B4, B5
Points        S1, S2, S3, S4, S5
Points        S1cog, S2cog, S3cog, S4cog, S5cog
%-----
%      Declarations and parameters (partly estimated)
MotionVariables'  Q1'', Q2'', Q3'', Q4'', Q5''
Constants        L_B1 = 0.0
Constants        L_B2 = 0.24
Constants        L_B3 = 0.0
Constants        L_B4 = 0.0
Constants        L_B5 = 1.10
Constants        L_B1cog = 0.0
Constants        L_B2cog = 0.12
Constants        L_B3cog = 0.0
Constants        L_B4cog = 0.0
Constants        L_B5cog = 0.65
Constants        M_B1 = 0.5
Constants        M_B2 = 2.2
Constants        M_B3 = 0.5
Constants        M_B4 = 3.0
Constants        M_B5 = 15.0
Constants        IZZ_B1 = 0.0015
Constants        IZZ_B2 = 0.0002
Constants        IZZ_B3 = 0.0015
Constants        IZZ_B4 = 0.5
Constants        IZZ_B5 = 10.0
Constants        STIFFNESS_Q2 = 1305
Constants        STIFFNESS_Q3 = 1305
Constants        STIFFNESS_Q5 = 2763
Constants        DAMPING_Q1 = 1.5
Constants        DAMPING_Q4 = 1.5
Variables        TORQUE_ACT_Q1
Variables        TORQUE_ACT_Q4
%-----
%      Mass, inertia
Mass            B1 = M_B1
Mass            B2 = M_B2
Mass            B3 = M_B3
Mass            B4 = M_B4
Mass            B5 = M_B5
Inertia        B1, 0,0, IZZ_B1,0,0,0
Inertia        B2, 0,0, IZZ_B2,0,0,0
Inertia        B3, 0,0, IZZ_B3,0,0,0
Inertia        B4, 0,0, IZZ_B4,0,0,0

```

```

Inertia          B5, 0,0,IZZ_B5,0,0,0
%-----
%      Geometry relating unit vectors
Simprot( N,  B1, 3, Q1 )
Simprot( B1, B2, 3, Q2 )
Simprot( B2, B3, 3, Q3 )
Simprot( B3, B4, 3, Q4 )
Simprot( B4, B5, 3, Q5 )
%-----
%      Position vectors from origin(n-1) to origin(n)/COG(n)
P_0_S1> = L_B1 * B11>
P_S1_S2> = L_B2 * B21>
P_S2_S3> = L_B3 * B31>
P_S3_S4> = L_B4 * B41>
P_S4_S5> = L_B5 * B51>
P_0_S1cog> = L_B1cog * B11>
P_S1_S2cog> = L_B2cog * B21>
P_S2_S3cog> = L_B3cog * B31>
P_S3_S4cog> = L_B4cog * B41>
P_S4_S5cog> = L_B5cog * B51>
%-----
%      Angular velocities
W_B1_N> = Q1'*B13>
W_B2_B1> = Q2'*B23>
W_B3_B2> = Q3'*B33>
W_B4_B3> = Q4'*B43>
W_B5_B4> = Q5'*B53>
%-----
%      Angular velocities referring to Newtonian frame
W_B2_N> = W_B1_N> + W_B2_B1>
W_B3_N> = W_B2_N> + W_B3_B2>
W_B4_N> = W_B3_N> + W_B4_B3>
W_B5_N> = W_B4_N> + W_B5_B4>
%-----
%      Angular accelerations referring to Newtonian frame
A_B10_N> = DT(W_B1_N>, N)
A_B20_N> = DT(W_B2_N>, N)
A_B30_N> = DT(W_B3_N>, N)
A_B40_N> = DT(W_B4_N>, N)
A_B50_N> = DT(W_B5_N>, N)
%-----
%      Linear velocities
V_0_N> = 0>
v2pts(N,B1,0,S1)
v2pts(N,B1,0,S1cog)
v2pts(N,B2,S1,S2)
v2pts(N,B2,S1,S2cog)
v2pts(N,B3,S2,S3)
v2pts(N,B3,S2,S3cog)
v2pts(N,B4,S3,S4)
v2pts(N,B4,S3,S4cog)
v2pts(N,B5,S4,S5)
v2pts(N,B5,S4,S5cog)

```

```
V_B10_N> = V_S1cog_N>
V_B20_N> = V_S2cog_N>
V_B30_N> = V_S3cog_N>
V_B40_N> = V_S4cog_N>
V_B50_N> = V_S5cog_N>
%-----
%           Linear accelerations
A_0_N> = 0>
a2pts(N,B1,0,S1)
a2pts(N,B1,0,S1cog)
a2pts(N,B2,S1,S2)
a2pts(N,B2,S1,S2cog)
a2pts(N,B3,S2,S3)
a2pts(N,B3,S2,S3cog)
a2pts(N,B4,S3,S4)
a2pts(N,B4,S3,S4cog)
a2pts(N,B5,S4,S5)
a2pts(N,B5,S4,S5cog)
%-----
%           Torques
Torque( N/B1, -DAMPING_Q1*Q1'*B13> + TORQUE_ACT_Q1*B13>)
Torque(B1/B2, -STIFFNESS_Q2*Q2*B23>)
Torque(B2/B3, -STIFFNESS_Q3*Q3*B33>)
Torque(B3/B4, -DAMPING_Q4*Q4'*B43> + TORQUE_ACT_Q4*B43>)
Torque(B4/B5, -STIFFNESS_Q5*Q5*B53>)
%-----
%           Equations of motion
Zero = Fr() + FrStar()
KE()
Kane( )
%-----
%           Reformed result
solve( ZERO, Q1'', Q2'', Q3'', Q4'', Q5'')
%-----
%           Save output
Save tld_prototype.all
%-----
%           End of file
```

## B.4 System Analysis of the TLD Prototype

In this section, fundamental properties of the TLD prototype are described.

System Matrix:

$$\mathbf{A} = 10^6 \begin{pmatrix} -0.0010 & 0 & 0 & 0.8700 & 0 & 0 & 0 & 0 & 0 & 0 \\ 0.0000 & 0 & 0 & 0 & 0 & 0 & 0 & 0 & 0 & 0 \\ 0.0010 & 0 & 0 & -7.3950 & 0 & 6.5250 & 0 & 0 & 0 & 0 \\ 0 & 0 & 0.0000 & 0 & 0 & 0 & 0 & 0 & 0 & 0 \\ 0 & 0 & 0 & 6.5250 & 0 & -7.3950 & 0.0000 & 0 & 0 & 0 \\ 0 & 0 & 0 & 0 & 0.0000 & 0 & 0 & 0 & 0 & 0 \\ 0 & 0 & 0 & 0 & 0 & 0.8700 & -0.0010 & 0 & 0 & 0.0055 \\ 0 & 0 & 0 & 0 & 0 & 0 & 0.0000 & 0 & 0 & 0 \\ 0 & 0 & 0 & 0 & 0 & 0 & 0.0000 & 0 & 0 & -0.0058 \\ 0 & 0 & 0 & 0 & 0 & 0 & 0 & 0 & 0.0000 & 0 \end{pmatrix} \quad (\text{B.6})$$

Eigenvalues of  $\mathbf{A}$  and their condition:

$$eig(\mathbf{A}) = 10^3 \begin{pmatrix} 0 \\ 0 \\ -0.0146 + 3.7270i \\ -0.0146 - 3.7270i \\ -0.1733 + 0.7903i \\ -0.1733 - 0.7903i \\ -0.6243 \\ -0.0000 + 0.0761i \\ -0.0000 - 0.0761i \\ -1.0030 \end{pmatrix}, \quad condeig(\mathbf{A}) = 10^3 \begin{pmatrix} 0.0010 \\ 0.0010 \\ 1.8709 \\ 1.8709 \\ 0.7017 \\ 0.7017 \\ 0.6295 \\ 0.0381 \\ 0.0381 \\ 0.1058 \end{pmatrix} \quad (\text{B.7})$$

Input matrix:

$$\mathbf{B} = \begin{pmatrix} 666.6667 & 0 \\ 0 & 0 \\ -666.6667 & 0 \\ 0 & 0 \\ 0 & -0.0002 \\ 0 & 0 \\ 0 & 668.6667 \\ 0 & 0 \\ 0 & -2.0000 \\ 0 & 0 \end{pmatrix} \quad (\text{B.8})$$

# C Feedback-Linearized Position Controller for VISHARD10

## C.1 Computed Torque (CT) Control

One of the first and best-known model based control concepts for robot manipulators is Computed Torque (CT) control depicted in Fig. C.1. The closed-loop dynamics resulting from the control law

$$\tau = \tilde{M}(\mathbf{q})(\ddot{\mathbf{q}}_d + K_p \mathbf{e} + K_d \dot{\mathbf{e}}) + \tilde{C}(\mathbf{q}, \dot{\mathbf{q}})\dot{\mathbf{q}} + \tilde{\mathbf{g}}(\mathbf{q}) \quad (\text{C.1})$$

and

$$K_p = \text{diag} \{w_1^2, \dots, w_n^2\} \quad (\text{C.2})$$

$$K_d = \text{diag} \{2\xi_1 w_1, \dots, 2\xi_n w_n\} \quad (\text{C.3})$$

where  $w_i$  and  $\xi_i$  are the bandwidth and the damping for joint  $q_i$  [259, 223] are described by linear differential equations [134].

Typically, the highest possible bandwidth  $w_{i,max}$  and a critical damping  $\xi_i = 1, i = 1, \dots, n$  are chosen [226].  $w_{i,max}$  depends on the resonant modes given by the elasticity of the joints and links of the robot [199]. This is usually done empirically by an iterative process: The bandwidth is increased, while  $\xi_i$  is adapted to the corresponding critical damping.

At the VISHARD10, the critical damping parameters that were found for the individual joints resulted in an overall inconvenient high-frequency vibrations of the SCARA joints 1-4. This can be seen in Fig. C.2.

The practical case of critical damping is achieved with  $\xi_{1,2,3,4} = 0.4$ . Tab. C.1 shows all empirically determined controller parameters.

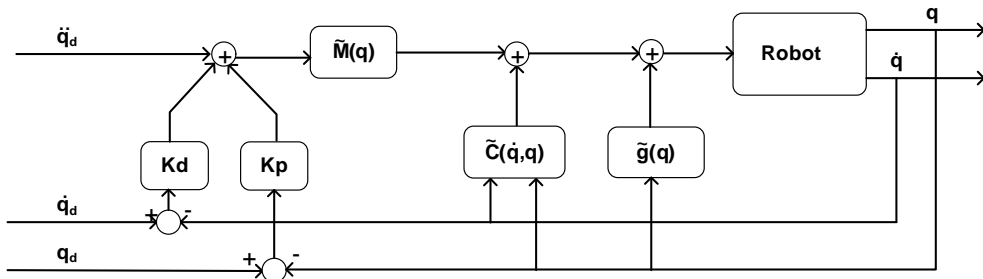


**Figure C.1:** Computed Torque (CT) control scheme [209].

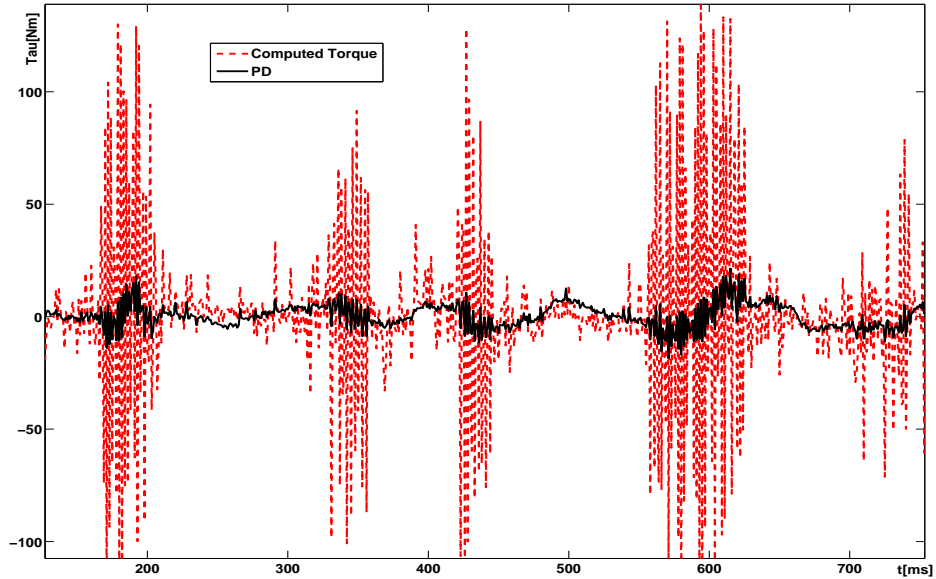


**Figure C.2:** SCARA torque  $\tau_{q3}$  for the “critical” damping, compared to the torque resulting from a PD controller [209].

| joint | $K_{p,i}$ | $\xi$ |
|-------|-----------|-------|
| 1     | 400       | 0.4   |
| 2     | 400       | 0.4   |
| 3     | 400       | 0.4   |
| 4     | 500       | 0.4   |
| 5     | 500       | 1     |
| 6     | 900       | 1     |
| 7     | 900       | 1     |
| 8     | 4000      | 1     |
| 9     | 2000      | 1     |
| 10    | 2000      | 1     |

**Table C.1:** CT controller: Empirically determined controller parameters.

## C.2 Feedforward+PD (FFPD) Control

The Feedforward+PD (FFPD) control scheme is given by the control law

$$\tau = \tilde{M}(\mathbf{q}_d)\ddot{\mathbf{q}}_d + \tilde{C}(\mathbf{q}_d, \dot{\mathbf{q}}_d)\dot{\mathbf{q}}_d + \tilde{\mathbf{g}}(\mathbf{q}_d) + K_p\mathbf{e} + K_d\dot{\mathbf{e}} \quad (\text{C.4})$$

where  $\mathbf{e} = \mathbf{q}_d - \mathbf{q}$  and  $K_p, K_d \in \mathfrak{R}^{n \times n}$  are symmetric, positive definite matrices.

Obviously, due to the model-based approach Fig. C.3 exhibits a very similar structure to Fig. C.1. However, it leads to very different theoretical and practical issues; compare the Lyapunov-based stability proof [134, 217]. Stability is achieved only if the positive definite matrices  $K_p$  and  $K_d$  exceed a critical lower limit. They can be derived by a model of the robot manipulator and the maximum values of velocity and acceleration. The latter information is not given for a haptic interface, so we chose the same practical approach for determining the controller parameters as described in Appendix C.1.

While the critical damping of the CT approach exhibited problems in the SCARA joints, in the FFPD approach oscillations occurred in the wrist joints. They vanished for  $\xi_{8,9,10} = 0.1$ . Of course, this comes with a significant overshoot, which per se is not desirable in haptic rendering. However, when rendering rather large masses/inertias, this was not perceived by several users. Tab. C.2 shows the final empirically determined controller parameters.

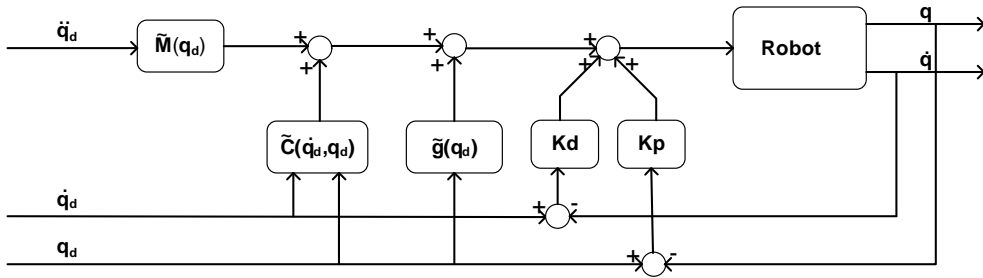


Figure C.3: Feedforward+PD (FFPD) Control Scheme [209].

| joint | $K_{p,i}$ | $\xi$ |
|-------|-----------|-------|
| 1     | 700       | 1     |
| 2     | 600       | 1     |
| 3     | 700       | 1     |
| 4     | 1000      | 1     |
| 5     | 500       | 1     |
| 6     | 900       | 1     |
| 7     | 900       | 1     |
| 8     | 2000      | 0.1   |
| 9     | 2000      | 0.1   |
| 10    | 1000      | 0.1   |

Table C.2: FFPD controller: Empirically determined controller parameters.

# D Technical Details Related to Collision Avoidance and Path Planning

## D.1 Obstacle Detection System provided by RCS (TU München)

A description of the obstacle detection developed by Christian Scharfenberger at the institute RCS (TU München) is given in [241]. In the following, the most important assumptions, features, and interfaces are presented.

The vision system processes images to identify (up to several hundred) feature points in the region of interest. Based on these, a 3D model of the workspace of the car door is generated. It consists of primitive bounding boxes (e.g. spheres) with the center of each locating a feature point. The dimension of each primitive varies with the predicted position of the point. If the position cannot be determined exactly in case of noise or other disturbances, then the volume of the primitive is increased. Thus, due to the uncertainties of the vision system, the 3DD varies both in the number and the size of the primitives bounding the objects in the workspace of the door. Fig. D.1 illustrates the process of model generation using simulated images.

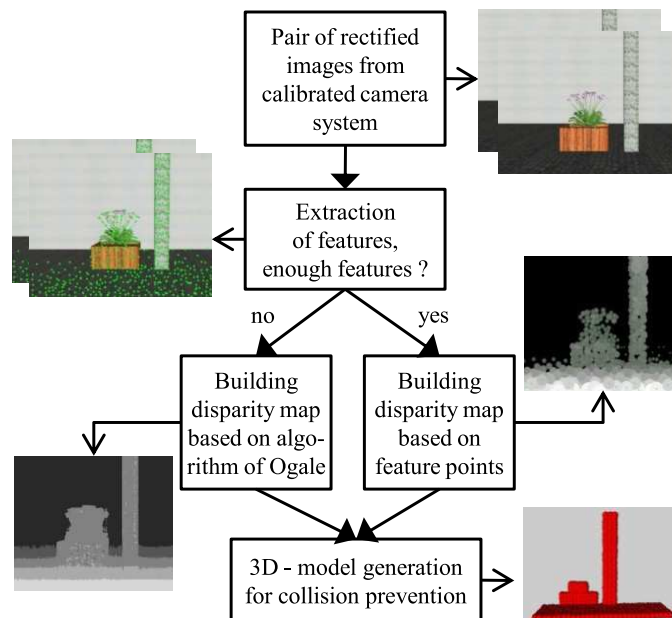


**Figure D.1:** Generating a disparity map with a pair of rectified images from a calibrated camera system. Based on this map, a 3D model of the workspace for collision avoidance is provided, consisting of primitives (e.g. spheres) [241].

## **D.2 Benchmark Scenarios for Obstacle Detection and Collision Avoidance**

In collaboration with RCS (TU München) and BMW Group, six benchmark scenarios have been defined for the obstacle detection and the collision avoidance. These are named and in part displayed in the following.

### **D.2.1 Scenarios for the Camera Mounted on the Door Mirror**

#### **D.2.1.1 Scenario 1: Wall**

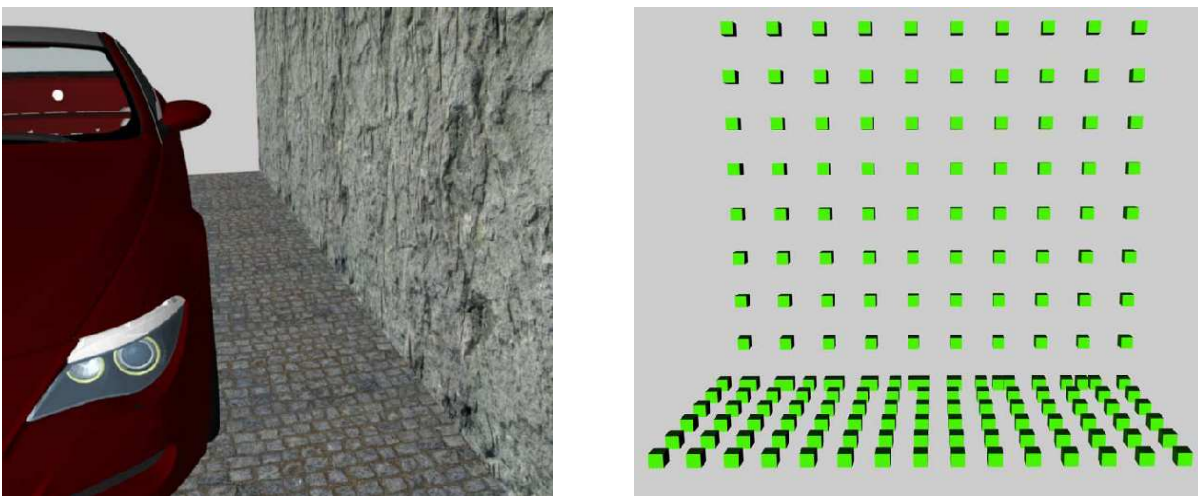


**Figure D.2:** Scenario 1: Wall in parallel to the driver's door.

#### **D.2.1.2 Scenario 2: Pillar**

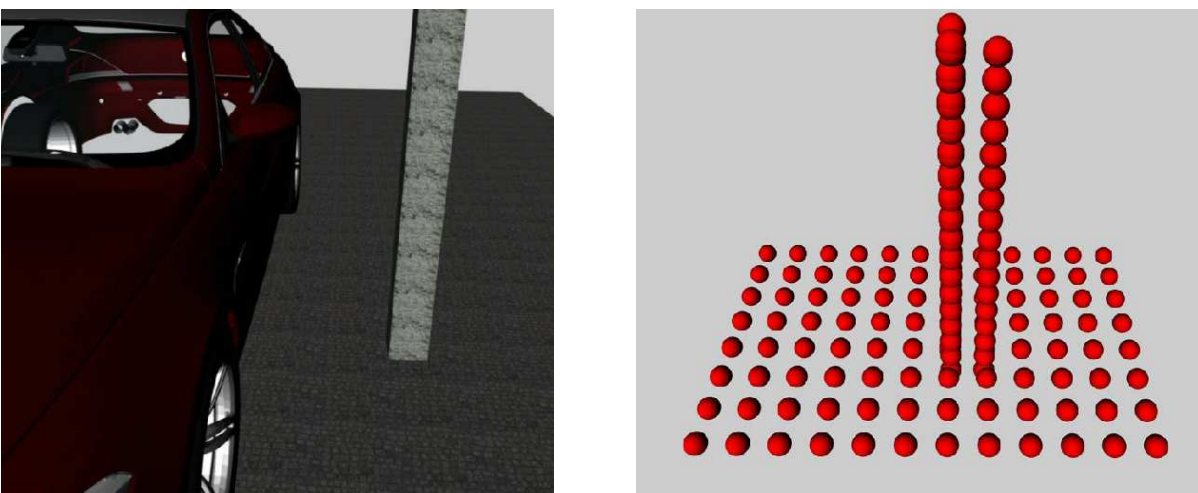


**Figure D.3:** Scenario 1: Pillar or lamppost in the workspace of the driver's door.

### D.2.1.3 Scenario 3: Bunch

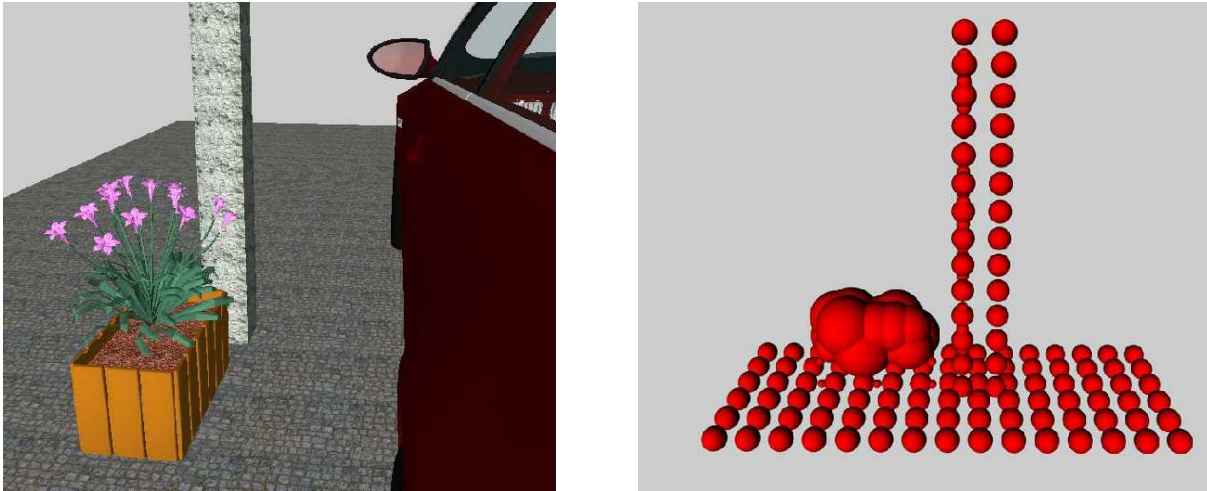


**Figure D.4:** Scenario 3: Obstacle with a complex shape, e.g. a bunch of flowers.

### D.2.1.4 Scenario 4: Parking Lot



**Figure D.5:** Scenario 4: Parking lot, i.e. another car in parallel to the driver's door.

## D.2.2 Scenarios for the Camera Mounted on the Inner Edge of the Door

In addition to the four scenarios previously described, two scenarios have been included to verify the clamping protection of actuated car doors:

- Scenario 5: Clamping of hand of user outside of car
- Scenario 6: Clamping of foot of user inside of car

### **D.3 VRML Models of the Exemplary Car Door Body**

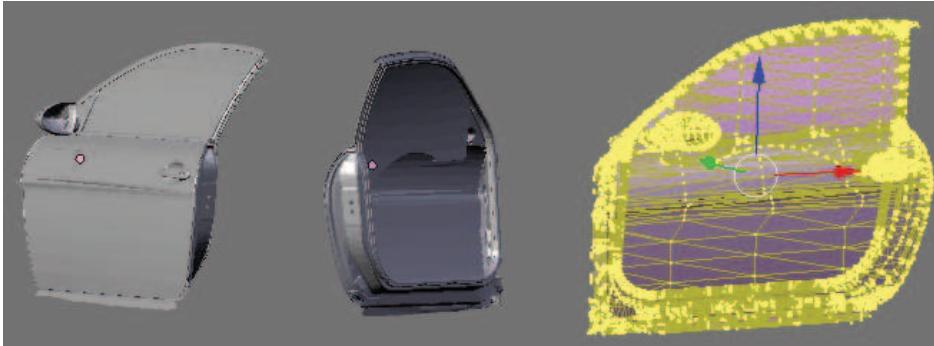


**Figure D.6:** Original VRML model of a car door featuring 97148 vertices [119].

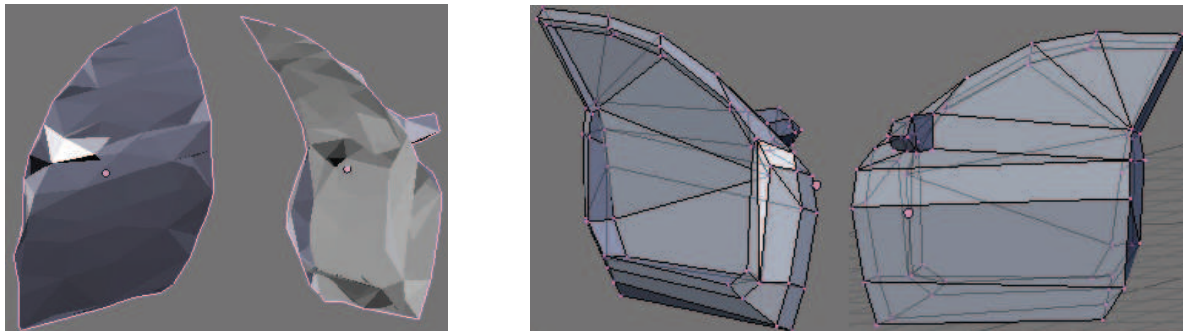


**Figure D.7:** Reduced VRML models of Fig. D.6, featuring 93 (l.) and 64 (r.) vertices [119].

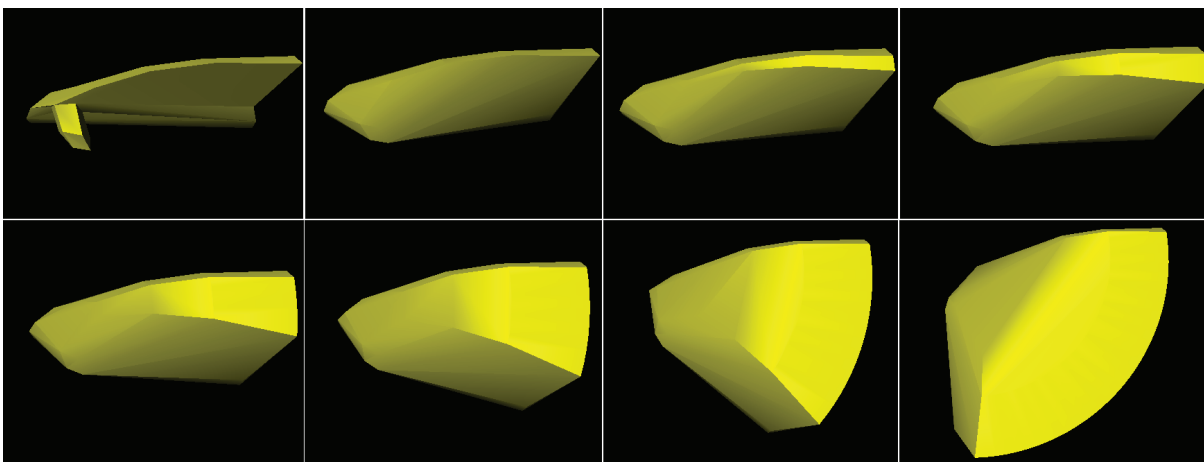


**Figure D.8:** Convex swept volume VRML models for different one-DOF opening motions [119].

## D.4 SamPP: Representation of Kinematics

In robotics, it is often convenient to divide the configuration space in the configuration of the (usually) movable robot base on the one hand and the configuration of the joints of the manipulator on the other hand. The base configuration can generically be described by a transformation with respect to a world coordinate frame (maximum number of DOF: 6). This equals a sequence of three translational and three rotational joints, all of which are independent of each other. Thus, the base configuration can be expressed by a subset of the generic joint parameters.

Our generic definition of joint parameters is briefly described in the following:

- ID: Unique number of robot part (foundation of the overall kinematic tree)
- PARENT: ID of the predecessor robot part in the kinematic tree
- REFJOINT: [only if joint is of type dependent:] ID of reference joint
- TYPE: description of the DOF of the robot part
  - RIGID: the robot part represents no DOF
  - TRANS: translational DOF
  - TRANS\_CSTR: constrained translational DOF
  - TRANS\_DPT: no DOF, translational motion depends on REFJOINT
  - ROT: unconstrained rotational DOF
  - ROT\_CSTR: constrained rotational DOF
  - ROT\_DPT: no DOF, rotational motion depends on REFJOINT
- MIN: [only if joint is of type \_CSTR:] minimum value of DOF
- MAX: [only if joint is of type \_CSTR:] maximum value of DOF
- DH\_A: DH parameter (translation along x-axis)
- DH\_D: DH parameter (translation along z-axis)
- DH\_ALPHA: DH parameter (rotation around x-axis)
- DH\_THETA: DH parameter (rotation around z-axis)
- WEIGHT: weighting factor for this DOF

Accordingly, the base parameters are the subset without ID labels, joint type \_DPT, and the Denavit-Hartenberg (DH) parameters.

# E Notes on the QoS of the Communication Infrastructure

In the following, the choice of UDP as the communication protocol for the networked VRP system is discussed, and its QoS is heuristically evaluated in terms of packet loss.

## E.1 Selection of Ethernet and the UDP Protocol

The communication between the different computers is based on Ethernet. In haptic rendering architectures, instead of the TCP protocol, UDP is used to achieve the utmost performance. This comes with the risk of a non-restorable packet loss. However, in practical implementations the safety of the overall system is much more endangered by the packet loss prevention mechanism of TCP, which can cause a major time delay, than by the loss of one or two packets in a row. It has only be taken care that important signals are sent more than one time. Preferably, important signals are sent a constant rate no matter whether a update of the corresponding variables occurred or not. This has been implemented using separate, constant-rate communication threads for each network connection.

Given the proposed communication architecture and a 100 MBit-Ethernet, there should be no overload and thus no significant loss of data: If we assume a communication overhead of approx. 50 Byte and a maximum data amount of 20 double values, the maximum UDP packet size is below 250 Byte. If 10 communication threads are running with a frequency of 1 kHz, this makes a maximum communication load of

$$\frac{250 \text{ Byte} \cdot 1 \text{ kHz}}{100 \text{ MBit/s}} = 0.02 \quad (\text{E.1})$$

This is rather light load which is not supposed to degrade QoS. However, we decided to verify this assumption empirically.

## E.2 Heuristic Evaluation of the UDP-Based Communication

To quantify the real QoS in our network, we performed a heuristic evaluation based on several combinations of UDP connections, frequency and disturbance load in the network. This tests are described in the following chapters.

### E.2.1 Evaluation in the Absence of Disturbances

For a first coarse examination, we implemented 10 UDP-connections both in C++ and in Simulink using a communication library. The results are shown in Tab. E.1 and Tab. E.2, where  $f$  is the chosen UDP frequency,  $N_c$  is the number of network connections,  $N_s$  and  $N_l$  are the number of sent and lost UDP packets, and  $N_l/N_s$  is the lost packet ratio. As can be seen, the lost packet ratio was very small in this evaluation.

| $N_c \times f$ | $N_s$   | $N_l$ | $N_l / N_s$ (%) |
|----------------|---------|-------|-----------------|
| 10 x 5kHz      | 3385504 | 134   | 0.0040          |
|                | 3363037 | 122   | 0.0040          |
|                | 3185023 | 799   | 0.0250          |
| 10 x 1kHz      | 3468267 | 30    | 0.0009          |
|                | 3296312 | 60    | 0.0020          |
|                | 3305564 | 21    | 0.0006          |

**Table E.1:** Data loss for a native C++ application ( $\Delta t = 10$  min).

| $N_c \times f$ | $N_s$   | $N_l$ | $N_l / N_s$ (%) |
|----------------|---------|-------|-----------------|
| 7 x 1kHz       | 2096833 | 1793  | 0.086           |
|                | 2095208 | 1669  | 0.080           |
|                | 2096263 | 1916  | 0.091           |
| 10 x 1kHz      | 2997039 | 3295  | 0.10            |
|                | 2996041 | 3456  | 0.12            |
|                | 2996087 | 3528  | 0.11            |

**Table E.2:** Data loss for a Simulink application ( $\Delta t = 5$  min).

### E.2.2 Evaluation in the Presence of Disturbances

The following scenarios were defined for the evaluation of the influence of network or computer load:

1. No additional network or computer load
2. Booting another disk-less Linux computer in the same subnet after 1/5/6/8 minutes
3. Copying large data on one of the computers

The error rate that we found was typically between  $N_l/N_s = 0.1\%$  and  $N_l/N_s = 0.5\%$ .

A critical factor of a networked system is the maximum time consumption for receiving an updated value. This means that it is usually much more critical to miss 10 data packets in a row than to miss 1000 data packets individually. Therefore, we analyzed the lost packets with respect to their consecutiveness. We found that typically 90% to 95% of all errors that occur are individual ones. The probability of five or more consecutive errors is below 0.002%. This can be seen in Fig. E.1 and Fig. E.2.

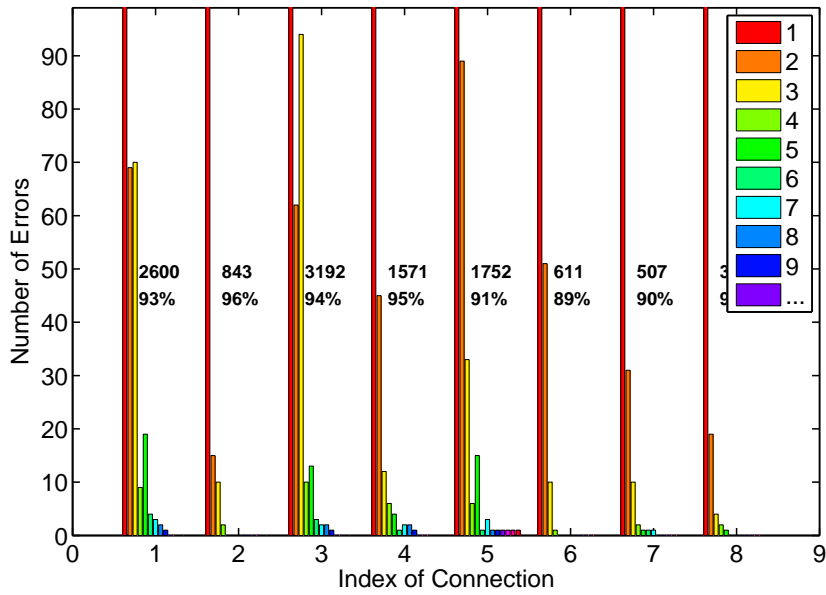


**Figure E.1:** Number of consecutive errors for each connection: The upper number gives the total number of lost packets ( $N_l$ ), while the lower percentage gives the share of the non-consecutive errors in relation to all lost packets (typically 90% to 95%).

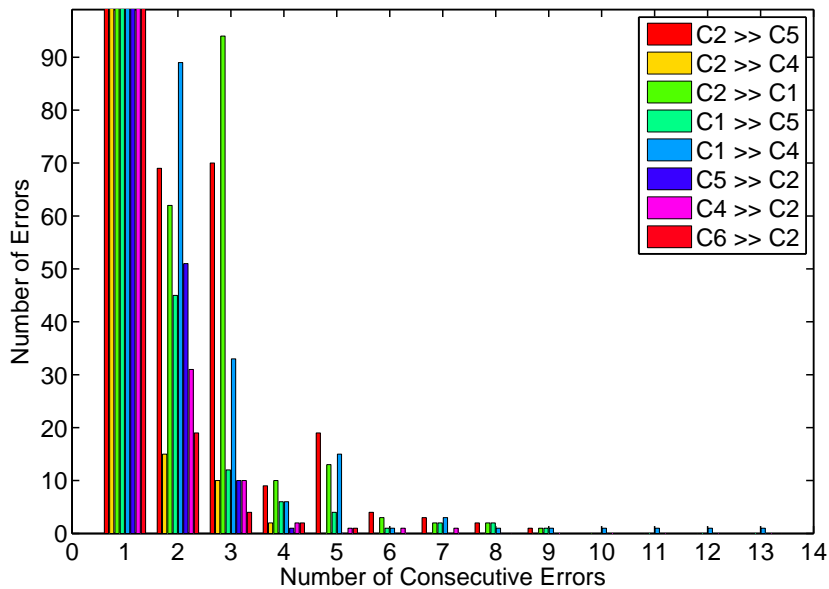


**Figure E.2:** Sorted data of Fig. E.1: Obviously, in comparison to  $N_s \approx 3000000$  it is a rare event that more than five consecutive errors occur (below 0.002%).

## F Detailed Evaluation Results

### F.1 Evaluation of the VRP Simulation of the PSD

In this section, details related to the results described in subsection 4.1.4 are given.

**Table F.1:** PSD Experiment part 1: Individually selected parameters of the seven participants that did the sliding motion first and the swinging motion thereafter.

|              | $m_A$ | $m_{DOOR}$ | $\Sigma m$ | $\mu_A$ | $\mu_{DOOR}$ |
|--------------|-------|------------|------------|---------|--------------|
| Sliding F. 1 | 0.40  | 4.60       | 5.00       | 0.00    | 2.50         |
| Sliding F. 2 | 0.40  | 23.00      | 23.40      | 0.10    | 5.00         |
| Sliding F. 3 | 2.00  | 11.50      | 13.50      | 0.40    | 5.00         |
| Sliding F. 4 | 12.00 | 22.50      | 34.50      | 0.75    | 6.00         |
| Sliding F. 5 | 1.20  | 22.50      | 23.70      | 1.05    | 4.60         |
| Sliding F. 6 | 4.00  | 18.00      | 22.00      | 0.15    | 22.00        |
| Sliding F. 7 | 1.00  | 18.00      | 19.00      | 1.50    | 12.00        |
| mean         | 3.00  | 17.16      | 20.16      | 0.56    | 8.16         |
| st.dev.      | 4.16  | 6.86       | 9.20       | 0.56    | 6.78         |

**Table F.2:** PSD Experiment part 1: Individually selected parameters of the seven participants that did the swinging motion first and the sliding motion thereafter.

|               | $m_A$ | $m_{DOOR}$ | $\Sigma m$ | $\mu_A$ | $\mu_{DOOR}$ |
|---------------|-------|------------|------------|---------|--------------|
| Swinging F. 1 | 0.40  | 4.60       | 5.00       | 0.04    | 5.00         |
| Swinging F. 2 | 2.00  | 11.50      | 13.50      | 0.12    | 10.00        |
| Swinging F. 3 | 0.40  | 11.50      | 11.90      | 0.00    | 0.00         |
| Swinging F. 4 | 1.00  | 13.50      | 14.50      | 0.30    | 8.00         |
| Swinging F. 5 | 4.00  | 18.00      | 22.00      | 0.45    | 2.00         |
| Swinging F. 6 | 1.00  | 13.50      | 14.50      | 0.00    | 2.00         |
| Swinging F. 7 | 4.00  | 13.50      | 17.50      | 0.08    | 8.00         |
| mean          | 1.83  | 12.30      | 14.13      | 0.14    | 5.00         |
| st.dev.       | 1.58  | 4.03       | 5.20       | 0.17    | 3.79         |

**Table F.3:** PSD Experiment part 1: Overall average and standard deviation of the 14 participants that did the swinging and sliding motion consecutively.

|         | $m_A$ | $m_{DOOR}$ | $\Sigma m$ | $\mu_A$ | $\mu_{DOOR}$ |
|---------|-------|------------|------------|---------|--------------|
| mean    | 2.41  | 14.73      | 17.14      | 0.35    | 6.58         |
| st.dev. | 3.08  | 5.96       | 7.83       | 0.45    | 5.52         |

**Table F.4:** PSD Experiment part 2: Final parameter setting adapted by the participants during two-DOF motions based on their previous individual setting described in Tab. F.1 and Tab. F.2.

|           | $m_A$ | $m_{DOOR}$ | $\Sigma m$ | $\mu_A$ | $\mu_{DOOR}$ |
|-----------|-------|------------|------------|---------|--------------|
| Person 1  | 0.80  | 2.30       | 3.10       | 0.06    | 1.00         |
| Person 2  | 0.40  | 4.60       | 5.00       | 0.40    | 5.00         |
| Person 3  | 0.80  | 9.20       | 10.00      | 0.02    | 1.50         |
| Person 4  | 0.80  | 23.00      | 23.80      | 0.12    | 10.00        |
| Person 5  | 0.80  | 11.50      | 12.30      | 0.80    | 5.00         |
| Person 6  | 0.80  | 23.00      | 23.80      | 0.10    | 15.00        |
| Person 7  | 1.20  | 48.00      | 49.20      | 0.15    | 20.00        |
| Person 8  | 1.00  | 12.00      | 13.00      | 1.20    | 12.00        |
| Person 9  | 1.00  | 36.00      | 37.00      | 0.03    | 6.00         |
| Person 10 | 1.20  | 48.00      | 49.20      | 0.60    | 4.60         |
| Person 11 | 1.00  | 18.00      | 19.00      | 0.15    | 4.00         |
| Person 12 | 1.00  | 12.00      | 13.00      | 13.50   | 22.00        |
| Person 13 | 1.00  | 18.00      | 19.00      | 1.50    | 12.00        |
| Person 14 | 4.00  | 18.00      | 22.00      | 0.15    | 8.00         |
| mean      | 1.13  | 20.26      | 21.39      | 1.34    | 9.01         |
| st.dev.   | 0.85  | 14.47      | 14.60      | 3.53    | 6.51         |

**Table F.5:** PSD Experiment part 3: Rating of all three parameter sets for three types of motion (Sl = one-DOF sliding, Sw = one-DOF swinging, Co = two-DOF motion) on a scale from 0 (extremely bad) to 10 (extremely good). The overall rating of the individually preferred parameters is denoted by  $\Sigma_{max} = \max(Sl) + \max(Sw) + \max(Co)$ .

| Parameters | Individual |      |      | Reference 1 |      |      | Reference 2 |      |      | $\Sigma_{max}$ |
|------------|------------|------|------|-------------|------|------|-------------|------|------|----------------|
|            | Sl         | Sw   | Co   | Sl          | Sw   | Co   | Sl          | Sw   | Co   |                |
| Person 1   | 9          | 9    | 8    | 5           | 6    | 5    | 5           | 6    | 5    | 26             |
| Person 2   | 9          | 9    | 10   | 4           | 6    | 3    | 1           | 6    | 4    | 28             |
| Person 3   | 9          | 6    | 8    | 7           | 5    | 7    | 8           | 6    | 8    | 23             |
| Person 4   | 6          | 8    | 7    | 5           | 8    | 7    | 7           | 9    | 4    | 23             |
| Person 5   | 8          | 7    | 8    | 4           | 6    | 5    | 4           | 5    | 5    | 23             |
| Person 6   | 5          | 7    | 6    | 4           | 7    | 5    | 7           | 7    | 7    | 21             |
| Person 7   | 7          | 9    | 8    | 2           | 3    | 2    | 7           | 6    | 7    | 24             |
| Person 8   | 8          | 8    | 8    | 8           | 6    | 7    | 4           | 6    | 5    | 24             |
| Person 9   | 3          | 8    | 5    | 3           | 9    | 6    | 8           | 7    | 8    | 25             |
| Person 10  | 6          | 7    | 7    | 4           | 3    | 4    | 7           | 8    | 8    | 23             |
| Person 11  | 7          | 8    | 9    | 8           | 6    | 8    | 3           | 6    | 4    | 25             |
| Person 12  | 9          | 9    | 9    | 7           | 2    | 1    | 7           | 6    | 5    | 27             |
| Person 13  | 7          | 8    | 8    | 7           | 6    | 5    | 5           | 7    | 6    | 23             |
| Person 14  | 6          | 7    | 7    | 7           | 6    | 6    | 6           | 7    | 6    | 21             |
| mean       | 7.07       | 7.86 | 7.71 | 5.36        | 5.64 | 5.07 | 5.64        | 6.57 | 5.86 | 23.80          |
| st.dev.    | 1.77       | 0.95 | 1.27 | 1.95        | 1.91 | 2.02 | 2.06        | 1.02 | 1.51 | 2.28           |
| mean       | 7.55       |      |      | 5.36        |      |      | 6.02        |      |      |                |
| st.dev.    | 1.38       |      |      | 1.92        |      |      | 1.60        |      |      |                |

## F.2 Evaluation of the VRP Simulation of the TLD

In this section, details related to the results described in subsection 4.1.5 are given.

**Table F.6:** Three parameter sets for the simulated dynamics of the TLD experiment (compare the original parameter set, Tab. B.3).

| Par. Set  | Link        | $m[kg]$ | $l[m]$ | $I_{zz}[kgm^2]$ | $\mu[\frac{Ns}{rad}]$ |
|-----------|-------------|---------|--------|-----------------|-----------------------|
| Light     | <i>A</i>    | 0.90    | 0.24   | 0.0217          | 0.18                  |
| Door      | <i>Door</i> | 18.2    | 1.10   | 7.19            | 0.21                  |
| Reference | <i>A</i>    | 1.28    | 0.24   | 0.0217          | 0.2                   |
| Door      | <i>Door</i> | 26.0    | 1.10   | 14.38           | 0.3                   |
| Heavy     | <i>A</i>    | 3.58    | 0.24   | 0.0217          | 0.8                   |
| Door      | <i>Door</i> | 37.1    | 1.10   | 17.20           | 0.9                   |

**Table F.7:** Personal characteristics of the participants of the TLD experiment conducted at the VRP test bed, where “Hand=r?” indicates if the right hand has been used to manually operate the car door simulation.

| Person  | Height | Weight | Hand=r? | Age  | Gender=m? |
|---------|--------|--------|---------|------|-----------|
| 1       | 1.80   | 70     | 0       | 26   | 1         |
| 2       | 1.85   | 95     | 1       | 22   | 1         |
| 3       | 1.85   | 70     | 1       | 23   | 1         |
| 4       | 1.65   | 60     | 1       | 22   | 0         |
| 5       | 1.80   | 70     | 0       | 25   | 1         |
| 6       | 1.79   | 66     | 1       | 28   | 1         |
| 7       | 1.83   | 78     | 1       | 25   | 1         |
| 8       | 1.80   | 90     | 0       | 26   | 1         |
| 9       | 1.72   | 60     | 0       | 31   | 1         |
| 10      | 1.70   | 70     | 0       | 24   | 1         |
| 11      | 1.69   | 61     | 1       | 27   | 0         |
| 12      | 1.60   | 50     | 1       | 27   | 0         |
| 13      | 1.84   | 72     | 0       | 31   | 1         |
| 14      | 1.57   | 41     | 1       | 27   | 0         |
| 15      | 1.75   | 70     | 0       | 27   | 0         |
| 16      | 1.70   | 70     | 0       | 26   | 0         |
| 17      | 1.71   | 65     | 1       | 27   | 0         |
| 18      | 1.80   | 68     | 1       | 24   | 0         |
| 19      | 1.81   | 100    | 0       | 25   | 1         |
| 20      | 1.76   | 80     | 0       | 26   | 1         |
| mean    | 1.75   | 70.3   | 0.5     | 26.0 | 0.6       |
| st.dev. | 0.08   | 13.88  | 0.51    | 2.42 | 0.50      |

Table F.8: Raw data of the TLD experiment conducted at the VRP test bed (part 1 of 2).

| Area     | Mech. Ref. Door |      |      |      | Movement of Pure Mechanics |      |                 |      |       |       | Controller Modules |      |      |      |      |      |
|----------|-----------------|------|------|------|----------------------------|------|-----------------|------|-------|-------|--------------------|------|------|------|------|------|
| Scale/R. | [0-10]          |      |      |      | [0-10]                     |      | [-3-3], R:F5/F6 |      |       |       | [-3-3], R:F1       |      |      |      |      |      |
| Question | F1              | F2   | F3   | F4   | F5                         | F6   | F7              | F8   | F9    | F10   | F11                | F12  | F13  | F14  | F15  | F16  |
| 1        | 6               | 6    | 4    | 8    | 5                          | 8    | 2               | 2    | 2     | -2    | 1                  | 1    | 0    | -1   | 2    | 2    |
| 2        | 6               | 7    | 6    | 5    | 7                          | 8    | 0               | 1    | 2     | -1    | 1                  | 2    | 2    | 0    | 1    | 2    |
| 3        | 8               | 7    | 6    | 6    | 7                          | 8    | 1               | 1    | 1     | -2    | 1                  | 3    | 1    | 0    | 0    | 3    |
| 4        | 6               | 7    | 3    | 4    | 8                          | 5    | 2               | 1    | -1    | -1    | 1                  | 1    | 0    | 1    | 2    | 3    |
| 5        | 8               | 9    | 8    | 7    | 7                          | 4    | 2               | 2    | -1    | -2    | 2                  | 2    | 0    | 0    | 0    | 0    |
| 6        | 7               | 5    | 4    | 6    | 7                          | 4    | 0               | 1    | -2    | -3    | 0                  | -2   | -2   | -1   | 0    | 2    |
| 7        | 4               | 4    | 5    | 3    | 5                          | 3    | 3               | 3    | 2     | 1     | 2                  | 2    | -1   | 1    | 0    | -1   |
| 8        | 4               | 3    | 4    | 5    | 4                          | 6    | 0               | 0    | 2     | -1    | 0                  | -1   | 1    | 1    | 0    | -3   |
| 9        | 4               | 2    | 6    | 3    | 7                          | 4    | 1               | -1   | -1    | 1     | 1                  | 2    | 1    | 1    | 2    | -1   |
| 10       | 5               | 5    | 5    | 3    | 4                          | 2    | 2               | 1    | -2    | -2    | 2                  | 1    | 2    | -1   | 2    | 2    |
| 11       | 7               | 9    | 6    | 7    | 6                          | 5    | 1               | 0    | 0     | -1    | -1                 | 0    | 0    | 0    | -1   | 1    |
| 12       | 7               | 7    | 5    | 8    | 5                          | 4    | 1               | 1    | 0     | -2    | 0                  | 0    | -2   | -1   | 0    | -3   |
| 13       | 7               | 4    | 7    | 8    | 8                          | 4    | -1              | -1   | -2    | -2    | 1                  | 1    | 1    | 1    | 0    | 1    |
| 14       | 5               | 6    | 3    | 4    | 6                          | 5    | 0               | 0    | -1    | -1    | 0                  | 0    | 1    | -1   | 2    | 2    |
| 15       | 5               | 8    | 5    | 10   | 7                          | 5    | 2               | -1   | 1     | 1     | 3                  | 3    | 1    | 0    | 1    | 2    |
| 16       | 5               | 7    | 3    | 5    | 6                          | 4    | 2               | 0    | 3     | 1     | 1                  | 1    | 0    | 0    | 1    | 1    |
| 17       | 8               | 4    | 6    | 8    | 10                         | 10   | -2              | -2   | -3    | -3    | 0                  | 2    | 0    | 1    | 2    | 2    |
| 18       | 5               | 6    | 7    | 2    | 7                          | 6    | 2               | 2    | -2    | -3    | 1                  | 1    | 1    | 1    | 2    | 2    |
| 19       | 5               | 6    | 5    | 4    | 8                          | 7    | 0               | 1    | -1    | -1    | 1                  | 1    | 1    | 1    | 1    | 1    |
| 20       | 5               | 7    | 6    | 3    | 4                          | 4    | 1               | 0    | 1     | 0     | 1                  | 1    | 0    | 0    | 2    | 2    |
| mean     | 5.85            | 5.95 | 5.20 | 5.45 | 6.40                       | 5.30 | 0.95            | 0.55 | -0.10 | -1.15 | 0.90               | 1.05 | 0.35 | 0.15 | 0.95 | 1.00 |
| st.dev.  | 1.35            | 1.88 | 1.40 | 2.24 | 1.57                       | 2.00 | 1.23            | 1.23 | 1.74  | 1.35  | 0.91               | 1.23 | 1.09 | 0.81 | 1.00 | 1.75 |

Table F.9: Raw data of the TLD experiment conducted at the VRP test bed (part 2 of 2).

| Area     | Collision Avoidance |      |      |                       |      |       |      |      |      | Path Planning |      |       |      | All Modules |      |      | FULL |
|----------|---------------------|------|------|-----------------------|------|-------|------|------|------|---------------|------|-------|------|-------------|------|------|------|
|          | [0-10]              |      |      | [-3-3], R:F17/F18/F19 |      |       |      |      |      | [-3-3], R:F19 |      |       |      | [0-10]      |      |      | R:1  |
| Question | F17                 | F18  | F19  | F20                   | F21  | F22   | F23  | F24  | F25  | F26           | F27  | F28   | F29  | F30         | F31  | F32  | F33  |
| 1        | 8                   | 7    | 8    | 0                     | 0    | -1    | 2    | -1   | 1    | 2             | 3    | -2    | 2    | 8           | 6    | 4    | 2    |
| 2        | 8                   | 8    | 8    | 0                     | 2    | -2    | 0    | 1    | 1    | 1             | 2    | 1     | -1   | 8           | 7    | 9    | 2    |
| 3        | 8                   | 6    | 8    | 1                     | -2   | 1     | 1    | -1   | 2    | -1            | 2    | -2    | 0    | 9           | 7    | 7    | 3    |
| 4        | 7                   | 8    | 9    | 1                     | 2    | -1    | 0    | 3    | -1   | 1             | 2    | -1    | 2    | 8           | 9    | 7    | 2    |
| 5        | 7                   | 6    | 9    | 2                     | -1   | -1    | 1    | 1    | 1    | 2             | -2   | -3    | 2    | 9           | 10   | 6    | 1    |
| 6        | 9                   | 5    | 6    | 0                     | 1    | -2    | 1    | 2    | 1    | 2             | 2    | 0     | 2    | 7           | 8    | 4    | 1    |
| 7        | 6                   | 5    | 3    | 1                     | 1    | 1     | 1    | 1    | 2    | 0             | 2    | -1    | -1   | 5           | 6    | 6    | 2    |
| 8        | 5                   | 7    | 3    | -1                    | -1   | -1    | -1   | -1   | -1   | 0             | 2    | 2     | 1    | 7           | 5    | 6    | 2    |
| 9        | 8                   | 3    | 6    | 0                     | -1   | 0     | 0    | -1   | 1    | 1             | 1    | -3    | 1    | 7           | 8    | 6    | 2    |
| 10       | 5                   | 7    | 5    | 2                     | 0    | -1    | 2    | 0    | 2    | 1             | 1    | -1    | 2    | 4           | 7    | 0    | 1    |
| 11       | 8                   | 6    | 8    | 1                     | 0    | 1     | 2    | -2   | 2    | 0             | 1    | -2    | 1    | 8           | 8    | 7    | 1    |
| 12       | 6                   | 1    | 6    | 0                     | 0    | -1    | 1    | 0    | -1   | -1            | 0    | -2    | 0    | 6           | 5    | 3    | -1   |
| 13       | 8                   | 5    | 3    | 0                     | 2    | 0     | 0    | 2    | 1    | 1             | 0    | -1    | 0    | 6           | 6    | 5    | 0    |
| 14       | 6                   | 7    | 6    | 0                     | -2   | -1    | 1    | 2    | 2    | 1             | 0    | -1    | 1    | 6           | 5    | 3    | -2   |
| 15       | 8                   | 3    | 10   | 3                     | -2   | 1     | 1    | -1   | 3    | 1             | -2   | -1    | 0    | 8           | 3    | 6    | 1    |
| 16       | 8                   | 3    | 7    | -1                    | 2    | -2    | 1    | 2    | 0    | -1            | 0    | -2    | 2    | 8           | 6    | 10   | 2    |
| 17       | 7                   | 8    | 2    | 1                     | 0    | -2    | 1    | 0    | 1    | 1             | 3    | 1     | 2    | 8           | 9    | 8    | 2    |
| 18       | 8                   | 5    | 6    | 2                     | 0    | 1     | -1   | 0    | -1   | -2            | 1    | -3    | 1    | 8           | 9    | 4    | 1    |
| 19       | 8                   | 7    | 7    | 0                     | 1    | -1    | 0    | 0    | 1    | -1            | 0    | -2    | 1    | 7           | 7    | 7    | 2    |
| 20       | 7                   | 8    | 8    | -1                    | 2    | -1    | 0    | 2    | -2   | 3             | -1   | -1    | 1    | 8           | 4    | 7    | 2    |
| mean     | 7.25                | 5.75 | 6.40 | 0.55                  | 0.20 | -0.60 | 0.65 | 0.45 | 0.75 | 0.55          | 0.85 | -1.20 | 0.95 | 7.25        | 6.75 | 5.75 | 1.30 |
| st.dev.  | 1.12                | 2.00 | 2.26 | 1.10                  | 1.40 | 1.10  | 0.88 | 1.39 | 1.33 | 1.28          | 1.46 | 1.36  | 1.00 | 1.29        | 1.83 | 2.29 | 1.17 |

**Table F.10:** Correlation of the personal and the raw data of the TLD experiment conducted at the VRP test bed.

|        | Height | Weight | Age   | Gender |
|--------|--------|--------|-------|--------|
| Height | 1.00   |        |       |        |
| Weight | 0.76   | 1.00   |       |        |
| Age    | -0.14  | -0.32  | 1.00  |        |
| Gender | 0.69   | 0.58   | 0.03  | 1.00   |
| F1     | 0.05   | -0.24  | -0.03 | -0.09  |
| F2     | -0.14  | -0.10  | -0.44 | -0.36  |
| F3     | 0.47   | 0.19   | 0.11  | 0.27   |
| F4     | 0.00   | -0.16  | 0.31  | -0.21  |
| F5     | 0.10   | -0.04  | 0.09  | -0.25  |
| F6     | 0.26   | 0.25   | -0.26 | -0.08  |
| F7     | -0.01  | -0.08  | -0.37 | -0.03  |
| F8     | 0.29   | 0.17   | -0.57 | 0.29   |
| F9     | 0.22   | 0.34   | -0.26 | 0.13   |
| F10    | -0.08  | 0.13   | 0.13  | -0.02  |
| F11    | 0.34   | 0.27   | -0.22 | 0.25   |
| F12    | 0.28   | 0.15   | -0.23 | 0.03   |
| F13    | 0.22   | 0.34   | -0.21 | 0.17   |
| F14    | 0.36   | 0.40   | 0.03  | 0.03   |
| F15    | -0.28  | -0.13  | -0.13 | -0.15  |
| F16    | 0.09   | -0.05  | -0.35 | -0.12  |
| F26    | 0.01   | -0.04  | 0.21  | 0.36   |
| F27    | 0.16   | 0.07   | -0.21 | 0.13   |
| F28    | 0.11   | 0.33   | -0.10 | 0.11   |
| F29    | -0.32  | -0.25  | 0.04  | -0.15  |
| F30    | 0.24   | 0.11   | -0.23 | -0.16  |
| F31    | 0.10   | -0.08  | -0.21 | 0.00   |
| F32    | 0.27   | 0.40   | -0.15 | -0.09  |
| F33    | 0.59   | 0.62   | -0.37 | 0.39   |

## **F.3 Evaluation of the TLD Prototype**

In this section, details related to the questionnaire and the results described in Sec. 5.1 are given.

In the questionnaire, the pages 4/5 and 6/7 were equal to the pages 2/3 except for the heading, which was “Modus 2: Manuelle Türbedienung mit Servo-Unterstützung” and “Modus 3: Voll-Automatische Türbewegung über Fernbedienung”, respectively.

Fig. F.1 shows the detailed results gathered by the AttrakDiff questionnaire.

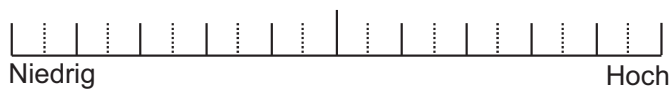




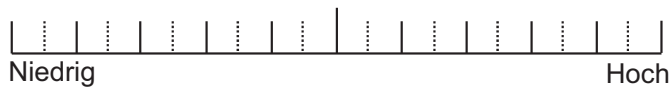
## Modus 1: Manuelle Türbedienung ohne Servo-Unterstützung

### Beurteilung A: Beanspruchung durch die Türbedienung

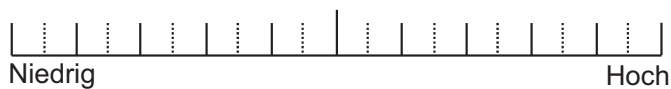
Geistige Anforderung



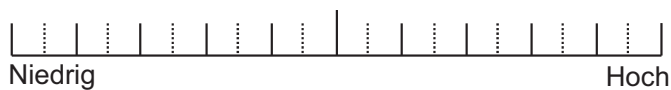
Körperliche Anforderung



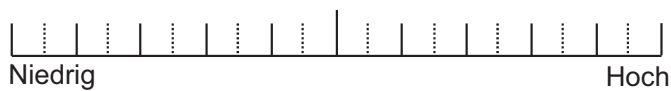
Zeitliche Anforderung



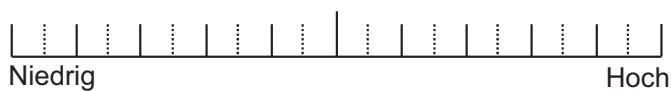
Aufgabenerfüllung



Anstrengung



Frustration



### Beurteilung B: Subjektive Bewertung der Türbedienung

Nachfolgend finden Sie Wortpaare, mit deren Hilfe Sie eine Beurteilung der Fahrzeugtür vornehmen können. Sie stellen jeweils extreme Gegensätze dar, zwischen denen eine Abstufung möglich ist.

Denken Sie nicht lange über die Wortpaare nach, sondern geben Sie bitte die Einschätzung ab, die Ihnen spontan in den Sinn kommt.



| Bitte geben Sie für die Türbedienung jeweils Ihre persönliche Einschätzung ab. |           |                        |
|--|-----------|------------------------|
| menschlich   | — — — — — | technisch              |
| isolierend   | — — — — — | verbindend             |
| angenehm   | — — — — — | unangenehm             |
| originell  | — — — — — | konventionell          |
| einfach  | — — — — — | kompliziert            |
| fachmännisch   | — — — — — | laienhaft              |
| hässlich   | — — — — — | schön                  |
| sympathisch  | — — — — — | unsympathisch          |
| umständlich  | — — — — — | direkt                 |
| stilvoll   | — — — — — | stilllos               |
| voraussagbar   | — — — — — | unberechenbar          |
| minderwertig   | — — — — — | wertvoll               |
| ausgrenzend  | — — — — — | einbeziehend           |
| nicht vorzeigbar   | — — — — — | vorzeigbar             |
| zurückweisend  | — — — — — | einladend              |
| phantasielos   | — — — — — | kreativ                |
| gut  | — — — — — | schlecht               |
| verwirrend   | — — — — — | übersichtlich          |
| abstoßend  | — — — — — | anziehend              |
| mutig  | — — — — — | vorsichtig             |
| innovativ  | — — — — — | konservativ            |
| lahm   | — — — — — | fesselnd               |
| harmlos  | — — — — — | herausfordernd         |
| motivierend  | — — — — — | entmutigend            |
| praktisch  | — — — — — | unpraktisch            |
| neuartig   | — — — — — | herkömmlich            |
| widerspenstig  | — — — — — | handhabbar             |
| bringt mich den<br>Leuten näher  | — — — — — | trennt mich von Leuten |



## Anmerkung und Verbesserungsvorschläge

Zur Tür

---

---

---

---

Zum Sitz

---

---

---

---

Zum Gesamtsystem

---

---

---

---

Zum Fragebogen

---

---

---

---

**Vielen Dank für Ihre Unterstützung!**

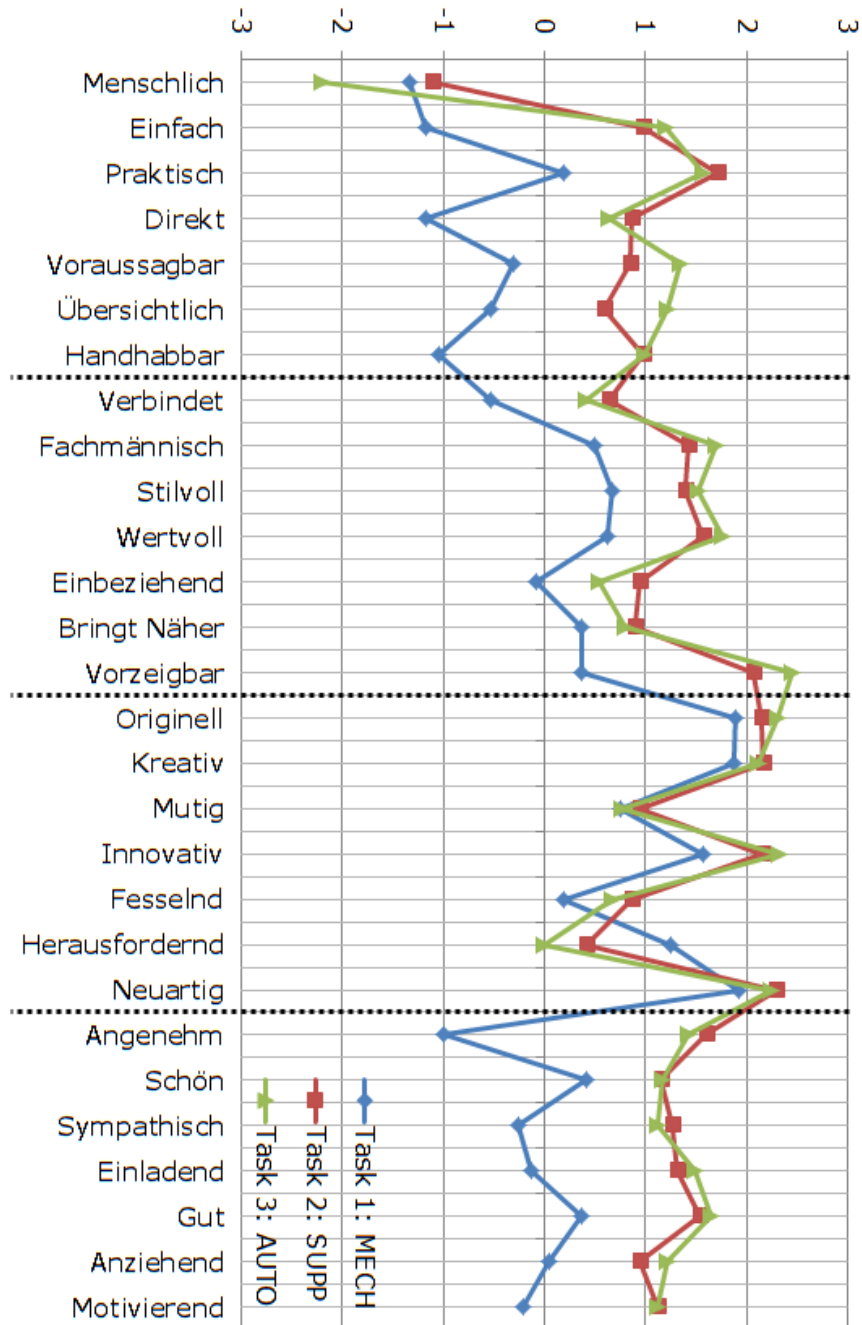


**Figure F.1:** Detailed results of the study described in subsection 5.1.4 gathered by the AttrakDiff questionnaire. From left to right seven adjectives represent each the pragmatic quality (PQ), the hedonic qualities for identity and stimulation (HQ-I, HQ-S), and the attractiveness (ATT).

# G Technical Details Related to the TLD Prototype

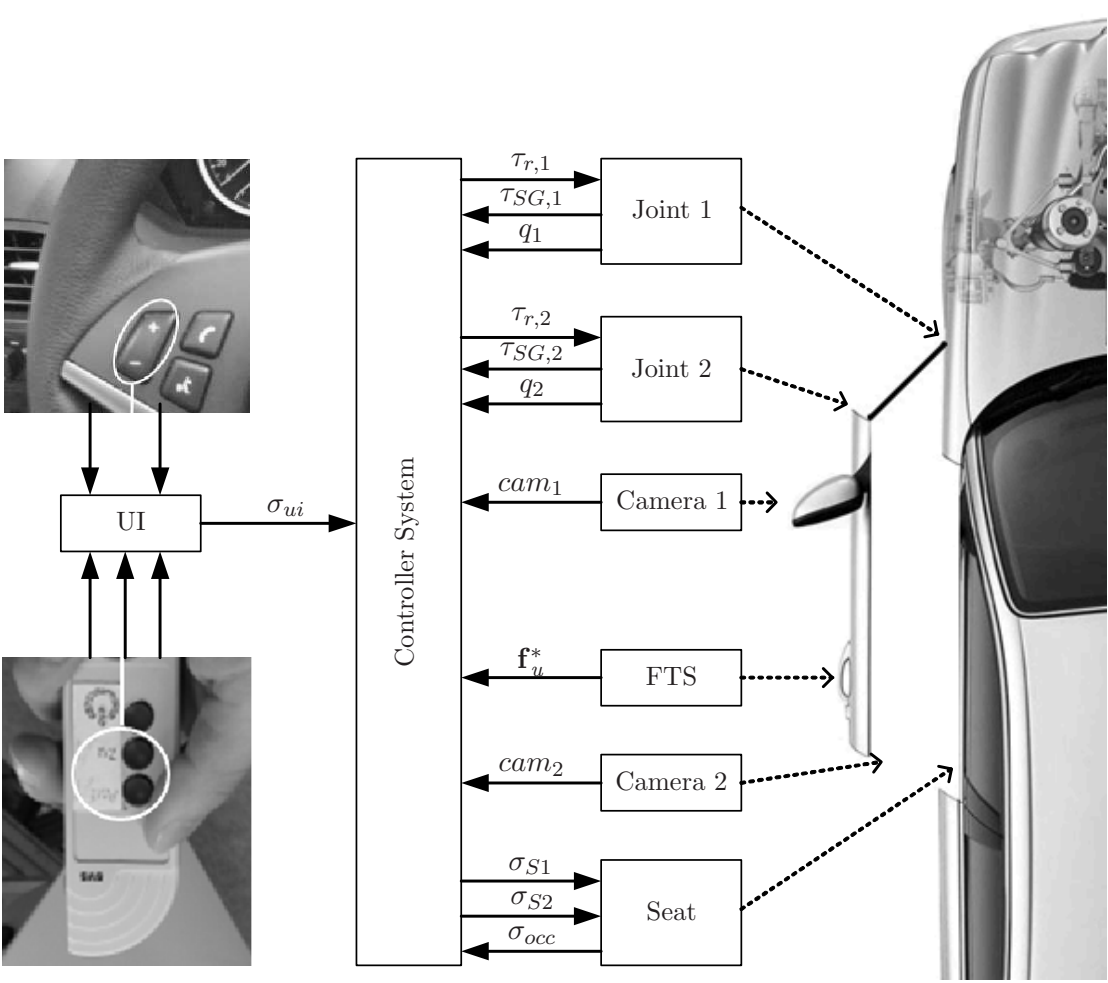


**Figure G.1:** Overview of the signals of the complete TLD prototype hardware setup.

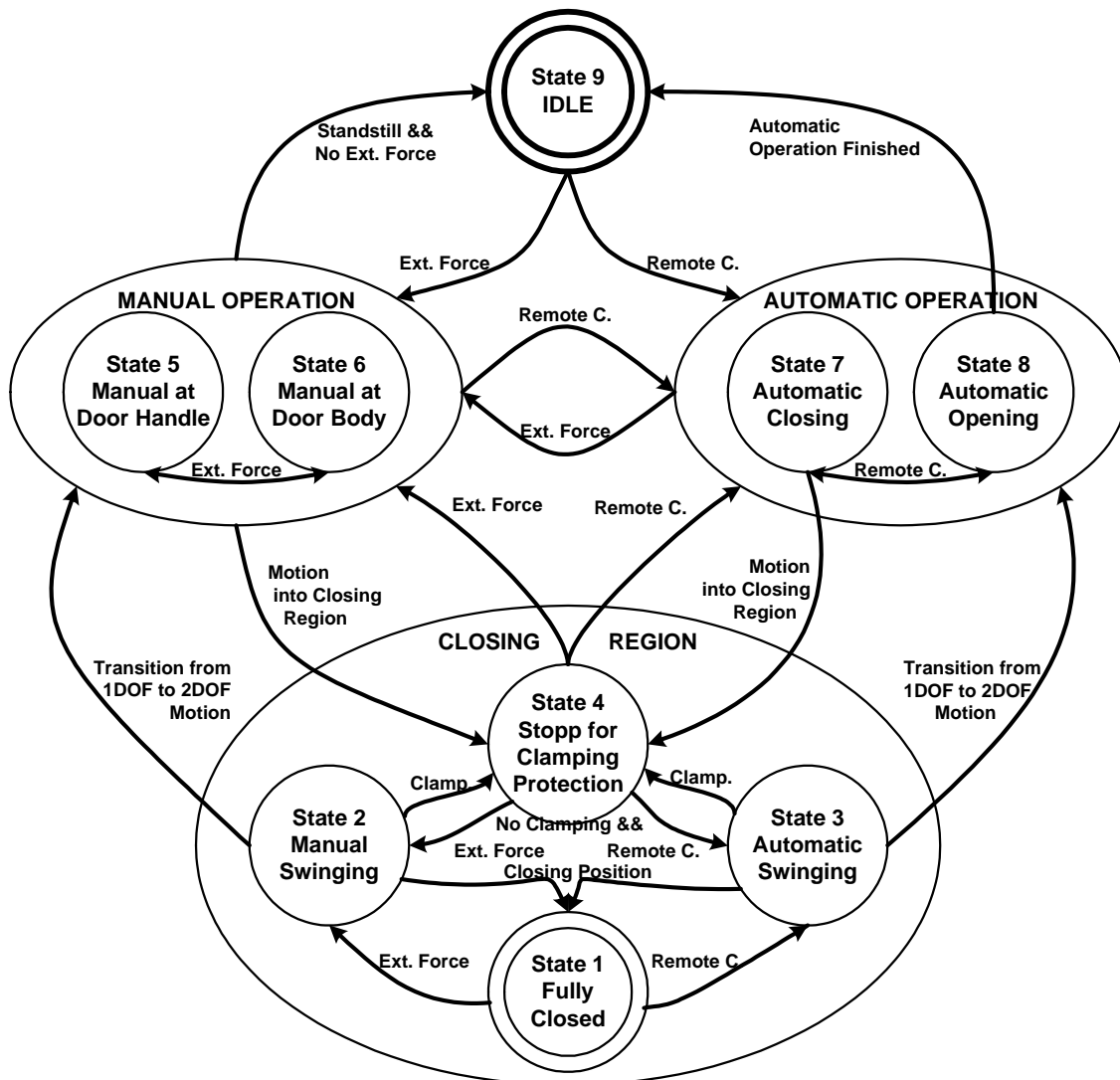


**Figure G.2:** Simplified state machine for the automatic and manual operation of the TLD prototype. Outside the “Closing Region”, which necessitates special precautions such as 1-DOF motion to avoid clamping and self-collisions, the door is either in automatic, manual, or idle operation. The most relevant transitions are triggered by measured external user forces and signals from a remote controller.



**Figure G.3:** Movement of the seat system provided by MiMed (TU München). The seat is used to decrease the level of discomfort during ingress and egress by supporting the desired motion of the driver entering/leaving the car.

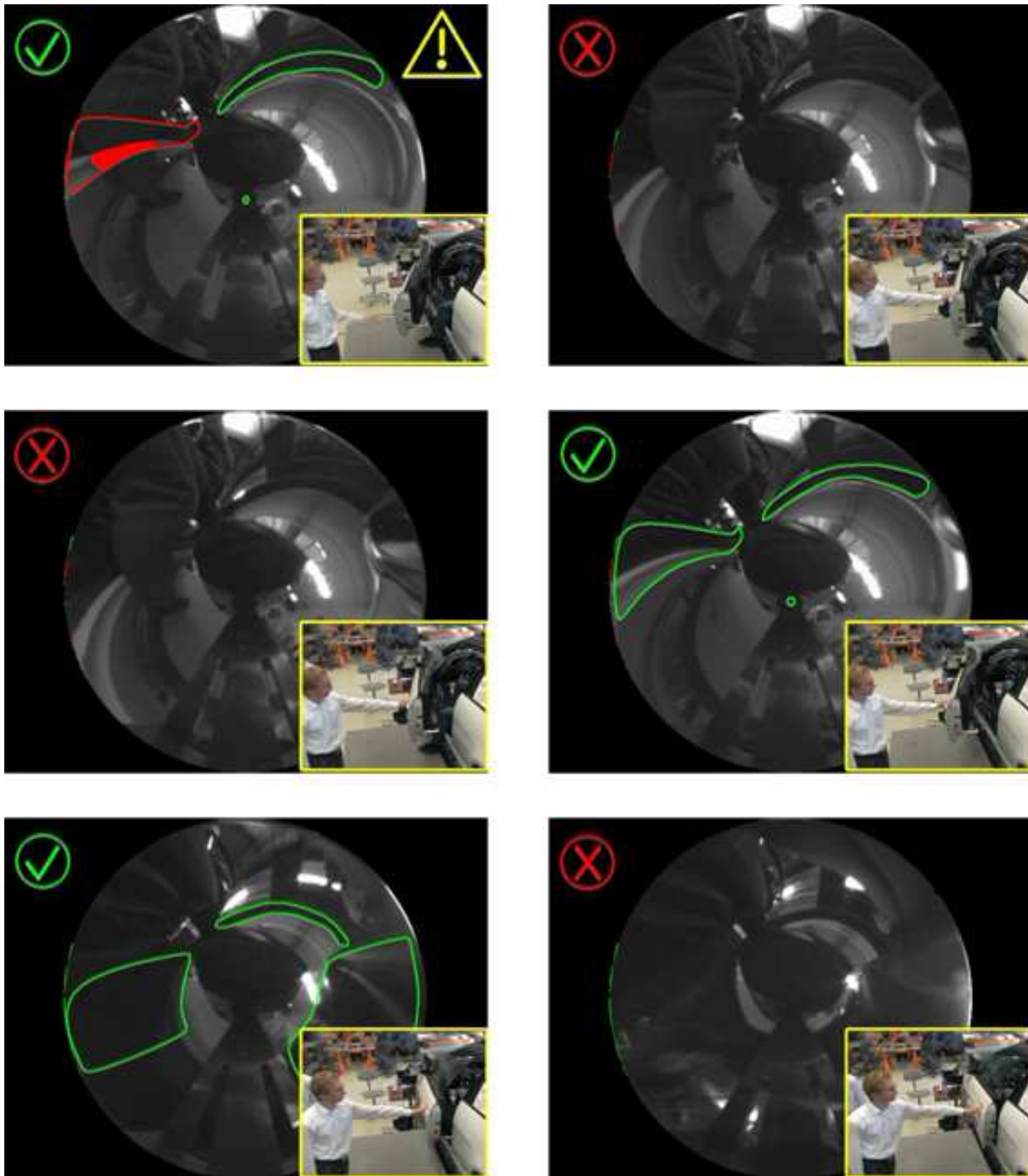


**Figure G.4:** Clamping protection: If the door-frame monitoring system provided by RCS (TU München) detects a partial occlusion, it sets a warning flag in the data packet sent to the door controller which triggers an impediment of closing motions. In the upper left figure, the red frame indicates a clamping threat caused by the driver's foot. The door cannot be closed before the threat ceases to exist.

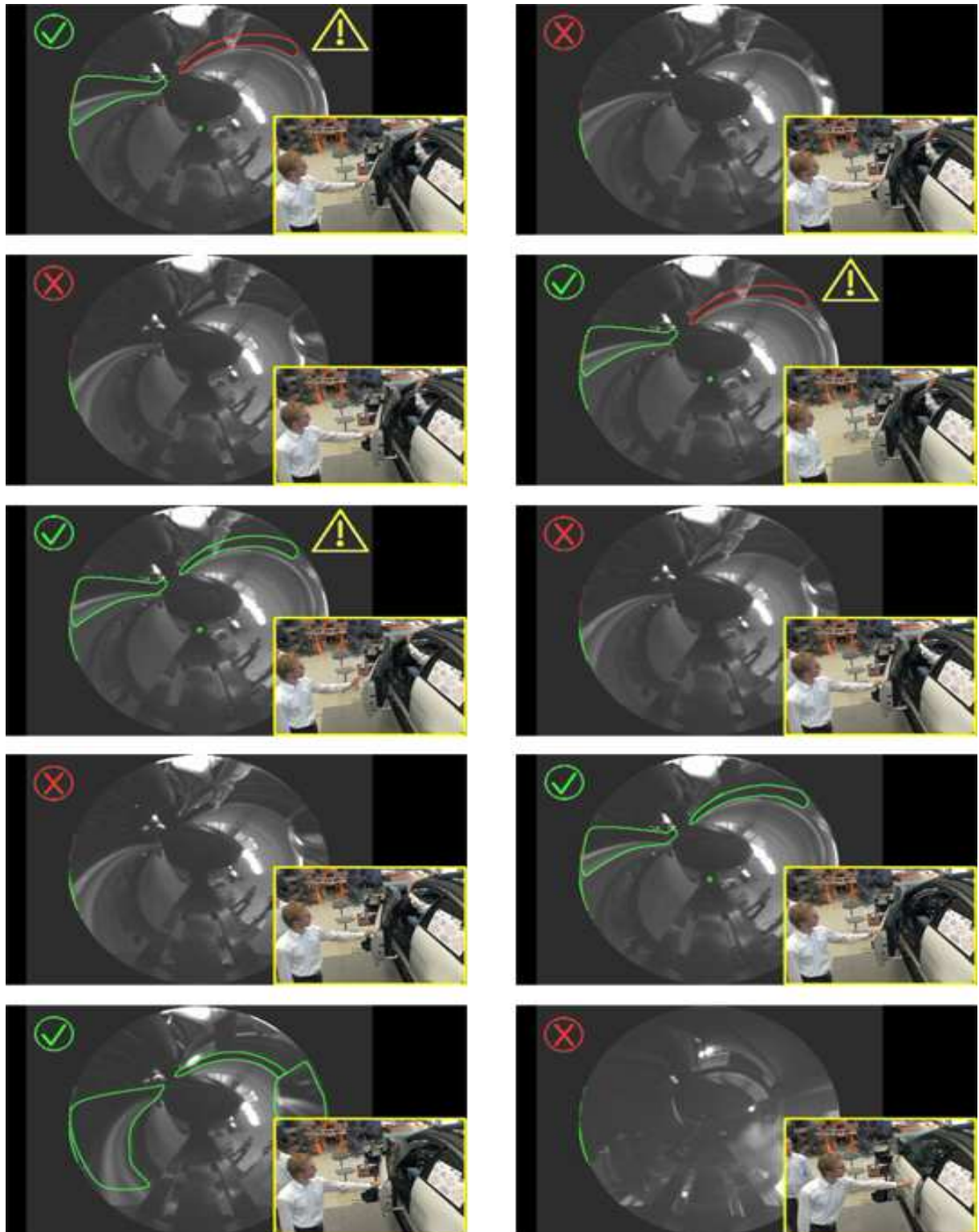


**Figure G.5:** Additional example of the clamping protection described in Fig. G.4: Even a small occlusion as for instance a few fingers is detected, and the door controller effectively counteracts a closing of the door.



**Figure G.6:** Example of the obstacle-detection based adaptive automatic opening: Bounding boxes (blue) are generated for all 3D volume covered by potential obstacles. The effectiveness can be seen from the “tracking” of the dynamically moved obstacle. Based on this 3D data, the path planner and collision avoidance of the door controller provide a collision-free automatic opening of the door.

# Bibliography

- [1] D. Aarno and D. Kragic. Layered HMM for motion intention recognition. In *Proceedings of the IEEE/RSJ International Conference on Intelligent Robots and Systems (IROS 2006)*, October 9 - 15 2006.
- [2] D.A. Abbink and M. Mulder. Exploring the dimensions of haptic feedback support in manual control. *Journal of Computing and Information Science in Engineering*, 9(1):1–10, 2009.
- [3] J.J. Abbott, G.D. Hager, and A.M. Okamura. Steady-hand teleoperation with virtual fixtures. In *Proceedings of the IEEE International Workshop on Robot and Human Interactive Communication*, Millbrae, California, USA, 2003.
- [4] J.J. Abbott and A.M. Okamura. Effects of position quantization and sampling rate on virtual-wall passivity. *IEEE Transactions On Robotics*, 21(5):952–964, 2005.
- [5] A. Abdossalami and S. Sirouspour. Adaptive control for improved transparency in haptic simulations. *IEEE Transactions on Haptics*, 2(1):2–14, 2009.
- [6] R.J. Adams and B. Hannaford. Stable haptic interaction with virtual environments. *IEEE Transactions on Robotics and Automation*, 15(3):465–474, 1999.
- [7] R.J. Adams and B. Hannaford. Control law design for haptic interfaces to virtual reality. *IEEE Transactions on Control Systems Technology*, 10(1):3–13, 2002.
- [8] P. Aigner and B. McCarragher. Shared control framework applied to a robotic aid for the blind. *IEEE Control Systems Magazine*, 19(2):40–46, 1999.
- [9] A. Albu-Schaeffer. *Regelung von Robotern mit elastischen Gelenken am Beispiel der DLR-Leichtbauarme*. PhD thesis, TU München, 2001.
- [10] A. Albu-Schaeffer, C. Ott, and G. Hirzinger. A unified passivity-based control framework for position, torque and impedance control of flexible joint robots. *The International Journal of Robotics Research*, 26(1):23–39, 2007.
- [11] B. Allotta, V. Colla, and G. Bioli. A mechatronic device for simulating push-buttons and knobs. In *1999 IEEE International Conference on Multimedia Computing and Systems*, volume 1, pages 636–642, 1999.
- [12] N.M. Amato and L.K. Dale. Probabilistic roadmap methods are embarrassingly parallel. In *Proceedings of 1999 IEEE International Conference on Robotics and Automation*, volume 1, pages 688–694, 1999.

- [13] M. Ammi and A. Ferreira. Robotic assisted micromanipulation system using virtual fixtures and metaphors. In *Proceedings of the IEEE International Conference on Robotics and Automation (ICRA 2007)*, pages 454–460, 2007.
- [14] H.H. Amor, S. Turki, and T. Soriano. Modelling the behaviour of a mechatronic system in a virtual prototyping environment. In *Enabling Technologies for the New Knowledge Society: ITI 3rd International Conference on Information and Communications Technology*, pages 209–218, 2005.
- [15] J. An and D.-S. Kwon. Modeling of a magnetorheological actuator including magnetic hysteresis. *Journal of Intelligent Material Systems and Structures*, 14:539–602, 2003.
- [16] M. Angerilli, A. Frisoli, F. Salsedo, S. Marcheschi, and M. Bergamasco. Haptic simulation of an automotive manual gearshift. In *Proceedings of the 10th IEEE International Workshop on Robot and Human Interactive Communication*, pages 170–175, 2001.
- [17] H. Apprich. Device for opening and closing a sliding door, in particular for vehicles. EP0900323B1, 2005.
- [18] B. Armstrong-Helouvry and P. Dupont. Friction modeling for control. In *American Control Conference (ACC 1993)*, pages 1905–1909, 1993.
- [19] P. Aschauer and A. Loibl. Fahrzeug, insbesondere Kraftfahrzeug, mit zumindest einer Tür. DE102005010674A1, 2006.
- [20] A. Attridge, M.A. Williams, and C. Tennant. The role of physical modelling in the design verification stage of the automotive NPI process in the premium sector. *International Journal of Automotive Technology and Management*, 7(1):32–54, 2007.
- [21] P. Avss, S. Prasant, and R. Jain. Virtual prototyping increases productivity – a case study. In *International Symposium on VLSI Design, Automation and Test (VLSI-DAT 2009)*, pages 96–101, 2009.
- [22] P.G. Backes and K.S. Tso. Umi: an interactive supervisory and shared control system for telerobotics. In *Proceedings of 1990 IEEE International Conference on Robotics and Automation*, volume 2, pages 1096–1101, 1990.
- [23] K. Basu, J. Prasad, and G. Narayanan. Minimization of torque ripple in pwm ac drives. *IEEE Transactions on Industrial Electronics*, 56(2):553–558, 2009.
- [24] A. Baviskar, J.R. Wagner, D.M. Dawson, D. Braganza, and P. Setlur. An adjustable steer-by-wire haptic-interface tracking controller for ground vehicles. *IEEE Transactions on Vehicular Technology*, 58(2):546–554, 2009.
- [25] M. Beenackers, D. Constantinescu, and M. Steinbuch. Haptic manipulation of virtual linkages with kinematic loops. In *Proceedings of the IEEE/ASME International Conference on Advanced Intelligent Mechatronics (AIM 2007)*, pages 1–6, 2007.

- 
- [26] A. Bernard and A. Fischer. New trends on rapid product development. *Annals of the CIRP*, 51(2):635–652, 2002.
- [27] C. Bernard, S. Bolognani, L. Peretti, and M. Zigliotto. Steering chain hil simulator for steer-by-wire systems. In *12th International Power Electronics and Motion Control Conference (EPE-PEMC 2006)*, pages 1784–1789, 2006.
- [28] M. Bertoluzzo, G. Buja, and R. Menis. Control schemes for steer-by-wire systems. *IEEE Industrial Electronics Magazin*, 1(1):20–27, 2007.
- [29] J. Borenstein and Y. Koren. Real-time obstacle avoidance for fast mobile robots. *IEEE Transactions on Systems, Man, and Cybernetics*, 19(5):1179–1187, 1989.
- [30] P. Bosscher and D. Hedman. Real-time collision avoidance algorithm for robotic manipulators. In *IEEE International Conference on Technologies for Practical Robot Applications (TePRA 2009)*, pages 113–122, 2009.
- [31] M. Breivik and T.I. Fossen. Guidance laws for planar motion control. In *Proceedings of the IEEE Conference on Decision and Control (CDC 2008)*, Cancun, Mexiko, December 2008.
- [32] T.L. Brooks. Telerobotic response requirements. In *IEEE International Conference on Systems, Man and Cybernetics*, pages 113–120, 1990.
- [33] F.P. Brooks Jr. What’s real about virtual reality?’. *IEEE Computer Graphics and Applications*, 19(6):16–27, 1999.
- [34] I. Bukusoglu, C. Basdogan, A. Kiraz, and A. Kurt. Haptic manipulation of microspheres using optical tweezers under the guidance of artificial force fields. *Presence*, 17(4):344–364, 2008.
- [35] G.C. Burdea. Haptic feedback for virtual reality (keynote). In *Proceedings of International Workshop on Virtual Prototyping*, pages 87–96, Laval, France, May 1999.
- [36] G.C. Burdea and P. Coiffet. *Virtual Reality Technology*. Wiley, New York, USA, 1994.
- [37] P. Buttolo, P. Stewart, and A. Marsan. A haptic hybrid controller for virtual prototyping of vehicle mechanisms. In *Proceedings of the 10th Symposium on Haptic Interfaces for Virtual Environment and Teleoperator Systems*, pages 249–254, 2002.
- [38] D. Calisi. Motion planning, reactive methods, and learning techniques for mobile robot navigation, 2010 (accessed May 13, 2010).  
[http://www.dis.uniroma1.it/~dottoratoii/db/relazioni/relaz\\_calisi\\_2.pdf](http://www.dis.uniroma1.it/~dottoratoii/db/relazioni/relaz_calisi_2.pdf).
- [39] S.C. Cannon and G.I. Zahalak. The mechanical behavior of active human skeletal muscle in small oscillations. *Journal of Biomechanics*, 15:111–121, 1982.
- [40] S. Carberry. Techniques for plan recognition. In *User Modeling and User-Adapted Interaction*. Kluwer Academic Publishers, 2001.

- [41] C.R. Carignan and K.R. Cleary. Closed-loop force control for haptic simulation of virtual environments. In *Haptics-e*, volume 1, February 23 2000.
- [42] S. Caselli, M. Reggiani, and M. Mazzoli. Exploiting advanced collision detection libraries in a probabilistic motion planner. In *WSCG*, pages 103–110, 2002.
- [43] D. Challou, D. Boley, M. Gini, and V. Kumar. A parallel formulation of informed randomized search for robot motion planning problems. In *Proceedings of 1995 IEEE International Conference on Robotics and Automation*, volume 1, pages 709–714, 1995.
- [44] D. Challou, M. Gini, V. Kumar, and G. Karypis. Predicting the performance of randomized parallel search: An application to robot motion planning. *Journal of Intelligent and Robotic Systems*, 38:31–53, 2003.
- [45] Y. Chen and T. Lin. Weiterentwicklung und Evaluation einer Sampling-basierten Pfadplanungs-Bibliothek. Interdisciplinary Project, supervised by **M. Strolz**, Institute of Automatic Control Engineering, TU München, 2009.
- [46] C.K. Chua, S.H. Teh, and R.L. Gay. Rapid prototyping versus virtual prototyping in product design and manufacturing. *International Journal of Advanced Manufacturing Technology*, 15:597–603, 1999.
- [47] O.Y. Chuy, Y. Hirata, Zhidong Wang, and K. Kosuge. A control approach based on passive behavior to enhance user interaction. *IEEE Transactions on Robotics*, 23(5):899–908, 2007.
- [48] C.L. Clover. A control-system architecture for robots used to simulate dynamic force and moment interaction between humans and virtual objects. *IEEE Transactions on Systems, Man, and Cybernetics, Part C: Applications and Reviews*, 29(4):481–493, 1999.
- [49] C.L. Clover, G.R. Luecke, J.J. Troy, and W.A. McNeely. Dynamic simulation of virtual mechanisms with haptic feedback using industrial robotics equipment. In *Proceedings of the IEEE International Conference on Robotics and Automation (ICRA 1997)*, volume 1, pages 724–730, 1997.
- [50] J.E. Colgate and J.M. Brown. Factors affecting the z-width of a haptic display. In *Proceedings of the IEEE International Conference on Robotics and Automation (ICRA 1994)*, pages 3205–3210, Los Alamitos, CA, 1994.
- [51] J.E. Colgate and N. Hogan. Robust control of dynamically interacting systems. *International Journal of Control*, 48(1):65 – 88, July 1988.
- [52] M.B. Colton and J.M. Hollerbach. Reality-based haptic force models of buttons and switches. In *Proceedings of the IEEE International Conference on Robotics and Automation (ICRA 2007)*, pages 497–502, 2007.

- 
- [53] D. Constantinescu, S.E. Salcudean, and E.A. Croft. Haptic manipulation of serial-chain virtual mechanisms. *Dynamic Systems, Measurement, and Control*, 128(1):65–74, March 2006.
- [54] R. Cortesao, B. Zenowich, R. Araujo, and W. Townsend. Robotic comanipulation with active impedance control. In *Proceedings of the World Conference on Innovative VR 2009 (WINVR09)*, Chalon-sur-Saône, France, Feb 26-26 2009.
- [55] B. Corteville, E. Aertbelien, H. Bruyninckx, J. De Schutter, and H. Van Brussel. Human-inspired robot assistant for fast point-to-point movements. In E. Aertbelien, editor, *Proceedings of the IEEE International Conference on Robotics and Automation (ICRA 2007)*, pages 3639–3644, 2007.
- [56] D. Cottet. Industry perspective on multi domain simulations and virtual prototyping. In *11th Workshop on Control and Modeling for Power Electronics (COMPEL 2008)*, pages 1–6, 2008.
- [57] E. Coumans. Bullet 2.55 Physics User Manual. Technical report, <http://bulletphysics.com>, 2007.
- [58] F. Dai and M. Goebel. Virtual prototyping - an approach using VR techniques. In *In proceedings of 1994 ASME International Computers in Engineering (CIE) Conference*, pages 311–316, Minneapolis, USA, September 11-14 1994.
- [59] E.B. Dam, M. Koch, and M. Lillholm. Quaternions, interpolation and animation. Technical Report DIKU-TR-98/5, University of Copenhagen, July 1998.
- [60] B.L. Davies, S.J. Harris, W.J. Lin, R.D. Hibberd, R. Middleton, and J.C. Cobb. Active compliance in robotic surgery—the use of force control as a dynamic constraint. *Proceedings of the Institution of Mechanical Engineers, Part H: Journal of Engineering in Medicine*, 211(4):285–292, 1997.
- [61] Defense Modeling and Simulation Office (DMSO). The expanding role of modeling and simulation in the acquisition process. Briefing, p. 12., November 1992.
- [62] E. Demeester, N. Nuttin, D. Vanhooydonck, and H.V. Brussel. Assessing the user’s intent using Bayes’ rule: application to wheelchair control. In *Proceedings of the 1st International Workshop on Advanced in Service Robotics*, pages 117–124, Bardolino, Italy, March 2003.
- [63] R. Diankov. OpenRAVE, 2010 (accessed May 13, 2010). <http://openrave.programmingvision.com/>.
- [64] R. Diankov and J. Kuffner. Openrave: A planning architecture for autonomous robotics.pdf. Technical report, Robotics Institute, Carnegie Mellon University, Pittsburgh, Pennsylvania 15213, 2008.
- [65] N. Diolaiti, G. Niemeyer, F. Barbagli, and J.K. Salisbury. Stability of haptic rendering: Discretization, quantization, time delay, and coulomb effects. *IEEE Transactions on Robotics*, 22(2):256–268, 2006.

- [66] A. Dömel. Entwicklung eines Pfadplaners für einen Virtual Reality-Versuchsstand. Studienarbeit, supervised by **M. Strolz** and K. Klasing, Institute of Automatic Control Engineering, TU München, 2007.
- [67] A. Dömel. Inbetriebnahme, Weiterentwicklung und Evaluation einer Pfadplanungs-Bibliothek an einem VR-Versuchsstand. Interdisciplinary Project, supervised by **M. Strolz**, Institute of Automatic Control Engineering, TU München, 2008.
- [68] Doug Engelbart Institute. Doug's vision highlights, 2010 (accessed May 13, 2010). <http://www.doungengelbart.org/about/vision-highlights.html>.
- [69] P. Drews and M. Weyrich. A system for digital mock-up's and virtual prototype design in industry: 'the virtual workbench'. In *Proceedings of the IEEE International Symposium on Industrial Electronics (ISIE '97)*, volume 3, pages 1292–1296, 1997.
- [70] V. Duchaine and C. Gosselin. Safe, stable and intuitive control for physical human-robot interaction. In *Proceedings of the IEEE International Conference on Robotics and Automation (ICRA 2009)*, pages 3383–3388, 2009.
- [71] Pierre Dupont and Brian Armstrong-Helouvy. Compensation techniques for servos with friction. In *American Control Conference (ACC 1993)*, pages 1915–1919, 1993.
- [72] N. Durlach and A. Mavor. *Virtual Reality and Technological Challenges*. National Academy Press., Washington, D.C, 1995.
- [73] Economic Commission for Europe (ECE). *Uniform Provisions Concerning the Approval of Vehicles with Regard to Door Latches and Door Retention Components*, 1981.
- [74] C. Ehinger. Entwicklung eines VR-Versuchsstands zur Simulation von Fahrzeugtüren. Master's thesis, supervised by **M. Strolz**, Institute of Automatic Control Engineering, TU München, 2008.
- [75] O. Enge. *Analyse und Synthese elektromechanischer Systeme*. PhD thesis, TU Chemnitz, 2005.
- [76] D.C. Engelbart. Augmenting human intellect: A conceptual framework (summary report). Technical report, Stanford Research Institute, 1962.
- [77] D.C. Engelbart. *Vistas in Information Handling*, chapter A Conceptual Framework for the Augmentation of Man's Intellect, pages 1–29. Spartan Books, Washington, D. C., 1963.
- [78] K.S. Eom, I.H. Suh, W.K. Chung, and S.R. Oh. Disturbance observer based force control of robot manipulator without force sensor. In *Proceedings of the IEEE International Conference on Robotics and Automation (ICRA 1998)*, pages 3012–3017, Leuven, Belgium, May 1998.

- 
- [79] S.D. Eppinger and W.P. Seering. Understanding bandwidth limitations in robot force control. In *Proceedings of the IEEE International Conference on Robotics and Automation (ICRA 1987)*, volume 4, pages 904–909, 1987.
- [80] S.D. Eppinger and W.P. Seering. Three dynamic problems in robot force control. *IEEE Transactions on Robotics and Automation*, 8(6):751–758, 1992.
- [81] H. Erdelyi and D. Talaba. Virtual prototyping of a car turn-signal switch using haptic feedback. *Engineering with Computers*, 2009.
- [82] W. Ertel. Or-parallel theorem proving with random competition. In *Proceedings of the International Conference on Logic Programming and Automated Reasoning*, number 624 in Lecture Notes In Computer Science. Springer-Verlag, 1992.
- [83] H. Esen. *Training in Virtual Environments via a Hybrid Dynamic Trainer Model*. PhD thesis, TU München, 2007.
- [84] X. Fan, B.C. Yin, and Y.F. Sun. Yawning detection for monitoring driver fatigue. In *International Conference on Machine Learning and Cybernetics*, volume 2, pages 664–668, 2007.
- [85] Y. Fan. Development and simulation of the open- and closed-loop control of a class of actuated car doors with several degrees-of-freedom. Master’s thesis, supervised by **M. Strolz**, Institute of Automatic Control Engineering, TU München, 2008.
- [86] T. Farkas, A. Hinnerichs, and C. Neumann. A distributed approach for multi-domain simulation of mechatronic systems. In *12th IEEE International Workshop on Future Trends of Distributed Computing Systems (FTDCS '08)*, pages 185–191, 2008.
- [87] M. Fehse. Fahrerassistenzvorrichtung. DE102004005225A1, 2005.
- [88] K. Feldmann, J. Heyer, M. Römer, and A. Kunze, editors. *MID 2006, 6. International Congress Molded Interconnect Devices*. Meisenbach Verlag Bamberg, 2006.
- [89] V. Fernandez, C. Balaguer, D. Blanco, and M.A. Salichs. Active human-mobile manipulator cooperation through intention recognition. In *Proceedings of the IEEE International Conference on Robotics and Automation (ICRA 2001)*, volume 3, pages 2668–2673, 2001.
- [90] G. Ferretti, G.A. Magnani, and P. Rocco. Virtual prototyping of mechatronic systems. *Annual Reviews in Control*, 28:193–206, 2004.
- [91] A. Field. *Discovering Statistics Using SPSS*. Sage Publications Ltd, 2009.
- [92] M. Fischer, C. Richter, S. Braun, D. Hellenbrand, O. Sabbah, C. Scharfenberger, **M. Strolz**, P. Kuhl, and G. Färber. Multidisciplinary development of new door and seat concepts as part of an ergonomic ingress/egress support system. In *FISITA 2008, World Automotive Congress*, Munich, Germany, September 14-19 2008.

- [93] T. Ganz and J. Appel. Manuell betätigtes Antriebssystem für ein motorisch verstellbares Schließteil eines Fahrzeugs. DE19911592A1, 2000.
- [94] A.B. Garcia, R.P. Gocke, and N.P. Johnson. Virtual prototyping: Concept to production. Technical report, Defense Systems Management College Press, Fort Belvoir, USA, 1994.
- [95] H.J. Gevatter and U. Grünhaupt. *Handbuch der Mess- und Automatisierungstechnik in der Produktion*. Springer, Berlin, 2006.
- [96] T. Geyer, G. Papafotiou, and M. Morari. Model predictive direct torque control - Part I: Concept, algorithm and analysis. *IEEE Transactions on Industrial Electronics*, 56(6):1894–1905, 2009.
- [97] T.L. Gibo, L.N. Verner, D.D. Yuh, and A.M. Okamura. Design considerations and human-machine performance of moving virtual fixtures. In *Proceedings of the IEEE International Conference on Robotics and Automation (ICRA 2009)*, Kobe, Japan, May 2009.
- [98] E.G. Gilbert, D.W. Johnson, and S.S Keerthi. A fast procedure for computing the distance between complex objects in three-dimensional space. *IEEE Transactions on Robotics and Automation*, 4(2):193–203, 1988.
- [99] R.B. Gillespie and J.E. Colgate. A survey of multibody dynamics for virtual environments. In *Proceedings of the ASME Dynamic Systems and Control Division*, volume 61, pages 45–54, Dallas, Texas, USA, November 17-18 1997.
- [100] R.B. Gillespie and M. Cutkosky. Interactive dynamics with haptic display. In *Proceedings of the ASME Winter Annual Meeting*, volume 49, pages 65–72, New Orleans, USA, 1993.
- [101] G.D. Glosser and W.S. Newman. The implementation of a natural admittance controller on an industrial manipulator. In *Proceedings of the IEEE International Conference on Robotics and Automation (ICRA 1994)*, volume 2, pages 1209–1215, 1994.
- [102] J. Gonzalez and G. Widmann. Investigations of nonlinearities in the force control of real robots. *IEEE Transactions on Systems, Man, and Cybernetics*, 22(5):1183–1193, 1992.
- [103] J. Gonzalez and G. Widmann. A force commanded impedance control scheme for robots with hard nonlinearities. *IEEE Transactions on Control Systems Technology*, 3(4):398–408, 1995.
- [104] S. Gottschalk, M. Lin, and D. Manocha. OBB-Tree: A hierarchical structure for rapid interference detection. In *In proceedings of SIGGRAPH*, 1996.
- [105] P.G. Griffiths and R.B. Gillespie. Recovering haptic performance by relaxing passivity requirements. In *Proceedings of the Third Joint EuroHaptics Conference and Symposium on Haptic Interfaces for Virtual Environment and Teleoperator Systems (WorldHaptics 2009)*, Salt Lake City, USA, March 2009.

- 
- [106] L. Hagenmayer, P. van den Hurk, S. Nikolaou, and E. Beklaris. *Development and Application of a Universal, Multimodal Hypovigilance-Management-System*, volume 4555/2007 of *Lecture Notes in Computer Science*. Springer, Berlin/Heidelberg, 2007.
- [107] J. Halbritter. Operating device for vehicle door. DE19927871A1, 1999.
- [108] B. Hannaford. A design framework for teleoperators with kinesthetic feedback. *IEEE Transactions on Robotics and Automation*, 5(4):426–434, 1989.
- [109] B. Hannaford and J.-H. Ryu. Time-domain passivity control of haptic interfaces. *IEEE Transactions on Robotics and Automation*, 18(1):1–10, 2002.
- [110] B. Hannaford and J.H. Ryu. Time domain passivity control of haptic interfaces. In *Proceedings of the 2001 IEEE International Conference on Robotics and Automation (ICRA 2001)*, Seoul, Korea, 21-26 May 2001.
- [111] T. Harada, T. Inada, K. Matsumura, N. Kaneda, and O. Michihira. Control device for opening/closing body of vehicle. JP002003206675A, 2003.
- [112] S. G. Hart. NASA-Task Load Index (NASA-TLX); 20 years later. In *Proceedings of the Human Factors and Ergonomics Society 50th Annual Meeting*, pages 904–908, Santa Monica, CA, USA, 2006.
- [113] S. G. Hart and L. E. Stavenland. Development of NASA-TLX (Task Load Index): Results of empirical and theoretical research. In P. A. Hancock and N. Meshkati, editors, *Human Mental Workload*, pages 139–183. Elsevier, 1988.
- [114] M. Hassenzahl. The interplay of beauty, goodness and usability in interactive products. *Human Computer Interaction*, 19:319–349, 2004.
- [115] M. Hassenzahl, M. Burmester, and F. Koller. AttrakDiff: Ein Fragebogen zur Messung wahrgenommener hedonischer und pragmatischer Qualität. In *Tagungsbeiträge der dritten Konferenz Mensch & Computer*, pages 187–196, Stuttgart, January 2003.
- [116] V. Hayward and J.M. Cruz-Hernandez. Parameter sensitivity analysis for design and control of force transmission systems. *ASME Journal of Dynamics Systems, Measurement and Control*, 120(2):241–249, June 1998.
- [117] H.D. Hellige. *Mensch-Computer-Interface. Zur Geschichte und Zukunft der Computerbedienung*, chapter Paradigmenwandel der Computer-Bedienung aus technikhistorischer Perspektive, page 46ff. transcript Verlag, 2008.
- [118] S. Hirche. *Haptic telepresence in packet switched communication networks*. PhD thesis, TU München, 2005.
- [119] A.C. Hoang. Realisierung einer Kollisionsvermeidung für ein VR-System. Studienarbeit, supervised by **M. Strolz**, Institute of Automatic Control Engineering, TU München, 2007.

- [120] N. Hogan. Impedance control: An approach to manipulation. parts 1-3. *J Dyn Syst Measure Control*, 107:1–24, 1985.
- [121] N. Hogan. Controlling impedance at the man/machine interface. In *Proceedings of the IEEE International Conference on Robotics and Automation (ICRA 1989)*, volume 3, pages 1626–1631, 1989.
- [122] A. Holzknecht. Direct drive torque motors for machine tool applications. Technical report, ETEL S.A., 2002.
- [123] K. Huang. Implementierung und Evaluation der Steuerung und Regelung einer Fahrzeugtür mit zwei aktuierten Freiheitsgraden. Master’s thesis, supervised by **M. Strolz**, Institute of Automatic Control Engineering, TU München, 2009.
- [124] IEEE. IEEEXplore digital library, 2010 (accessed May 13, 2010). <http://ieeexplore.ieee.org/>.
- [125] A. Imura, T. Takagi, and T. Yamaguchi. Intention recognition using conceptual fuzzy sets. In *Second IEEE International Conference on Fuzzy Systems, 1993*, volume 2, pages 762–767, 1993.
- [126] The Institute of Measurement and Control. *Guide to the Measurement of Force*, 1998.
- [127] R. Jiang, X. Tian, L. Xie, and Y. Chen. A robot collision avoidance scheme based on the moving obstacle motion prediction. In *ISECS International Colloquium on Computing, Communication, Control, and Management (CCCM '08)*, volume 2, pages 341–345, 2008.
- [128] D.E. Johnson, P. Willemsen, and E. Cohen. A haptic system for virtual prototyping of polygonal models. In *Proceedings of the ASME Design Engineering Technical Conference (DETC 2004)*, Salt Lake City, USA, September 28-October 2 2004.
- [129] L.A. Jones and I.W. Hunter. Differential thresholds for limb movement measured using adaptive techniques. *Perception & Psychophysiology*, 52(4):529–535, 1992.
- [130] P. Jorissen, M. Wijnants, and M. Lamotte. Dynamic interactions in physically realistic collaborative virtual environments. *IEEE Transactions on Visualization and Computer Graphics*, 11(6):649–660, 2005.
- [131] H. Kaneko, T. Arai, K. Inoue, and Y. Mae. Real-time obstacle avoidance for robot arm using collision jacobian. In *Proceedings of the 1999 IEEE/RSJ International Conference on Intelligent Robots and Systems (IROS 99)*, volume 2, pages 617–622, 1999.
- [132] A. Kapoor, M. Li, and R.H. Taylor. A constrained optimization approach to virtual fixtures for multi-handed tasks. In *Proceedings of the 2007 IEEE International Conference on Robotics and Automation*, Orlando, Florida, May 2007.

- 
- [133] L.E. Kavraki, P. Svestka, J.-C. Latombe, and M.H. Overmars. Probabilistic roadmaps for path planning in high-dimensional configuration spaces. *IEEE Transactions on Robotics and Automation*, 12(4):566–580, 1996.
- [134] R.V. Kelly and A.L. Santibanez. *Control of Robot Manipulators in Joint Space*. Springer, 2005.
- [135] M. Kerttula, M. Salmela, and M. Heikkinen. Virtual reality prototyping - a framework for the development of electronics and telecommunication products. In *Proceedings of the 8th IEEE International Workshop on Rapid System Prototyping*, pages 2–11, 1997.
- [136] M. Kerttula and T. Tokkonen. Virtual design of multiengineering electronics systems. *Computer*, 34(11):71–79, 2001.
- [137] O. Khatib. Real-time obstacle avoidance for manipulators and mobile robots. *The International Journal of Robotics Research*, 5(1):90–99, 1986.
- [138] R. Kikuuwe, N. Takesue, and H. Fujimoto. A control framework to generate nonenergy-storing virtual fixtures: Use of simulated plasticity. *IEEE Transactions On Robotics*, 24(4):781–, August 2008.
- [139] T. Kiyoshi and K. Mitsuhiro. Car door opening/closing device. JP09317323A, 1997.
- [140] K. Klasing. Parallelized sampling-based path planning for tree-structured rigid robots. Technical Report TR-LSR-2009-03-01-Klasing, Institute of Automatic Control Engineering, TU München, March 2009.
- [141] K. Klasing. PP, a simple sampling-based path planning library, 2010 (accessed May 13, 2010).  
<http://www.lsr.ei.tum.de/research/software/pp/>.
- [142] J.T. Klosowski. *Efficient Collision Detection for Interactive 3D Graphics and Virtual Environments*. PhD thesis, State University of New York at Stony Brook, 1998.
- [143] M. Kobayashi. Door opening and closing device for vehicle. JP002005226296A, 2005.
- [144] Y. Koren and J. Borenstein. Potential field methods and their inherent limitations for mobile robot navigation. In *Proceedings of the 1991 IEEE International Conference on Robotics and Automation*, pages 1398–1404, 1991.
- [145] J.J. Kuffner and S.M. LaValle. RRT-Connect: An efficient approach to single-query path planning. In *Proceedings of 2000 IEEE International Conference on Robotics and Automation (ICRA 2000)*, volume 2, pages 995–1001, 2000.
- [146] S.M. LaValle. Rapidly-exploring random trees: A new tool for path planning. TR 98-11, Computer Science Dept., Iowa State University, Oct. 1998.
- [147] S.M. LaValle. *Planning Algorithms*. Cambridge University Press, 2006.

- [148] S.M. LaValle. Motion strategy library, 2010 (accessed June 12, 2010). <http://msl.cs.uiuc.edu/msl/>.
- [149] H.N. Le, A.C. Hoang, and H.B. Rached. Entwicklung der Steuerung und Regelung einer intelligenten aktuierten Schwenk-Schiebe-Tür. Interdisciplinary Project, supervised by **M. Strolz**, Institute of Automatic Control Engineering, TU München, 2009.
- [150] K. Lee and D.Y. Lee. Adjusting output-limiter for stable haptic rendering in virtual environments. *IEEE Transactions On Control Systems Technology*, 17(4):768–779, July 2009.
- [151] P.U. Lee, D.C. Ruspini, and O. Khatib. Dynamic simulation of interactive robotic environment. In *Proceedings of the IEEE International Conference on Robotics and Automation (ICRA 1994)*, number 2, pages 1147–1152, 1994.
- [152] S. Lee and H.S. Lee. Intelligent control of manipulators interacting with an uncertain environment based on generalized impedance. In *Proceedings of the 1991 IEEE International Symposium on Intelligent Control*, pages 61–66, 1991.
- [153] B.H. Li, X. Chai, W. Zhu, Y. Di, X. Song, X. Yan, P. Wang, B. Hou, G. Shi, and X. Wang. The recent research on virtual prototyping engineering for complex products. In *Proceedings of the 8th International Conference on Computer Supported Cooperative Work in Design*, volume 2, pages 18–25 Vol.2, 2004.
- [154] M. Li, M. Ishii, and R. H. Taylor. Spatial motion constraints using virtual fixtures generated by anatomy. *IEEE Transactions on Robotics*, 23(1):4–19, 2007.
- [155] S. Li. Monitoring around a vehicle by a spherical image sensor. *IEEE Transactions on Intelligent Transportation Systems*, 7(4):541–550, 2006.
- [156] M.C. Lin and J.F. Canny. A fast algorithm for incremental distance calculation. In *Proceedings of the 1991 IEEE International Conference on Robotics and Automation*, volume 2, pages 1008–1014, 1991.
- [157] M.C. Lin and S. Gottschalk. Collision detection between geometric models: A survey. In *IMA Conference on Mathematics of Surfaces*, 1998.
- [158] Z. Lu and A.A. Goldenberg. Robust impedance control and force regulation: Theory and experiments. *The International Journal of Robotics Research*, 14(3):225–254, 1995.
- [159] R. Lumia, J.C. Fiala, and A.J. Wavering. An architecture to support autonomy, teleoperation, and shared control. In *Proceedings of the 1988 IEEE International Conference on Systems, Man, and Cybernetics*, volume 1, pages 472–476, 1988.
- [160] K.M. Lynch, C. Liu, A.S. Rensen, S. Kim, M. Peshkin, T. Tickel, D. Hannon, and K. Shiels. Motion guides for assisted manipulation. *International Journal of Robotics Research*, 21(1):27–43, 2002.

- 
- [161] W. Ma and P.K. Venuvinod. *Rapid Prototyping: Laser-Based and Other Technologies*. Springer Netherlands, 1 edition, 2003.
- [162] J. Maas and C. Graf. Control schemes for a force-actuated vehicle door assistant. In *Proceedings of the IEEE/ASME International Conference on Advanced Intelligent Mechatronics (AIM 2009)*, pages 1695–1700, 2009.
- [163] J. Maas and S. Kern. Mechatronic vehicle door assistant. In *Proceedings of the IEEE/ASME International Conference on Advanced Intelligent Mechatronics (AIM 2007)*, pages 1–5, 2007.
- [164] J. Maas, R. Kieneke, and C. Graf. Force-actuated vehicle door assistant. In *VDI Mechatronik 2009*, Wiesloch, Germany, May 12-13 2009.
- [165] S.M. Malik, J. Lin, and A.A. Goldenberg. Virtual prototyping for conceptual design of a tracked mobile robot. In *Canadian Conference on Electrical and Computer Engineering (CCECE '06)*, pages 2349–2352, 2006.
- [166] J. Martin and J. Savall. Mechanisms for haptic torque feedback. In *Proceedings of the First Joint EuroHaptics Conference and Symposium on Haptic Interfaces for Virtual Environment and Teleoperator Systems (WorldHaptics 2005)*, 2005.
- [167] L. Martinez-Gomez and T. Fraichard. Collision avoidance in dynamic environments: An ics-based solution and its comparative evaluation. In *Proceedings of the IEEE International Conference on Robotics and Automation (ICRA 2009)*, pages 100–105, 2009.
- [168] A.A. Masoud. Kinodynamic motion planning: A novel type of nonlinear, passive damping forces and advantages. *IEEE Robotics and Automation Magazine*, pages 85–99, March 2010.
- [169] J. Mattingley and S. Boyd. Real-time convex optimization in signal processing. *To Appear In IEEE Signal Processing Magazine, Special Issue On Convex Optimization For Signal Processing, May 2010*, 2010.
- [170] G. Mauter and S. Katzki. The application of operational haptics in automotive engineering. *Global Automotive Manufacturing and Technology*, pages 78–80, 2003.
- [171] A.A. Mezentsev. A methodology of complicated mechanical systems virtual prototyping. In *IEEE International Joint Symposia on Intelligence and Systems*, pages 208–214, 1996.
- [172] B.E. Miller, J.E. Colgate, and R.A. Freeman. Guaranteed stability of haptic systems with nonlinear virtual environments. *IEEE Transactions on Robotics and Automation*, 16(6):712–719, 2000.
- [173] M. Minsky, M. Ouh-Young, O. Steele, F.P. Brooks, and M. Behensky. Feeling and seeing: issues in force display. *Comput. Graph.*, 24(2):235–243, 1990.

- [174] Mitsubishi Electric. V-Clip collision detection library, 2010 (accessed May 13, 2010). <http://www.merl.com/projects/vclip/>.
- [175] M. Montazeri, M. Soleymani, and N. Mehrabi. Application of virtual prototyping for optimization of fuzzy-based active suspension system. In *5th International Symposium on Mechatronics and Its Applications (ISMA 2008)*, pages 1–6, 2008.
- [176] H.P. Moravec and A Elfes. High resolution maps from wide angle sonar. In *ICRA*, pages 116–121, 1985.
- [177] S. Morikawa, T. Senoo, A. Namiki, and M. Ishikawa. Realtime collision avoidance using a robot manipulator with light-weight small high-speed vision systems. In *Proceedings of the IEEE International Conference on Robotics and Automation (ICRA 2007)*, 2007.
- [178] A. Mörtl. Regelkonzepte zur kraftabhängigen Bewegung einer aktuierten Fahrzeugtür. Master’s thesis, supervised by **M. Strolz**, Institute of Automatic Control Engineering, TU München, 2007.
- [179] D.M. Mount. ANN: A library for approximate nearest neighbor searching, 2010 (accessed May 13, 2010). <http://www.cs.umd.edu/~mount/ANN/>.
- [180] D.M. Mount and S. Arya. ANN: A library for approximate nearest neighbor searching. In *Proceedings of Center for Geometric Computing Second Ann. Fall Workshop Computational Geometry*, 1997.
- [181] M+S Mikrotechnik und Sensorik GmbH, Heinrich-Hertz-Straße 8, 07629 Hermsdorf. *Acceleration Transducer 2g BG 2166*.
- [182] Q. Mühlbauer. VR-Simulation und Regelung einer aktuierten Fahrzeugtür. Master’s thesis, supervised by **M. Strolz**, Institute of Automatic Control Engineering, TU München, 2007.
- [183] M. Mulder, D.A. Abbink, and E.R. Boer. The effect of haptic guidance on curve negotiation behavior of young, experienced drivers. In *IEEE International Conference on Systems, Man and Cybernetics (SMC 2008)*, pages 804–809, 2008.
- [184] F.A. Mussa-Ivaldi, N Hogan, and N Bizzi. Neural, mechanical, and geometric factors subserving arm posture in humans. *Journal of Neuroscience*, 5:2732–2743, 1985.
- [185] A. Nahvi, D.D. Nelson, J.M. Hollerbach, and D.E. Johnson. Haptic manipulation of virtual mechanisms from mechanical CAD designs. In *Proceedings of the IEEE International Conference on Robotics and Automation (ICRA 1998)*, volume 1, pages 375–380, 1998.
- [186] G. Narayanan, V.T. Ranganathan, D. Zhao, H.K. Krishnamurthy, and R. Ayyanar. Space vector based hybrid PWM techniques for reduced current ripple. *IEEE Transactions on Industrial Electronics*, 55(4):1614–1627, 2008.

- 
- [187] National Instruments. NI LabVIEW-SolidWorks mechatronics toolkit, 2010 (accessed May 13, 2010).  
<http://zone.ni.com/devzone/cda/tut/p/id/6183>.
- [188] N.N. ColDet 3D collision detection, 2010 (accessed May 13, 2010).  
<http://sourceforge.net/projects/coldet/>.
- [189] N.N. PQP - A proximity query package, 2010 (accessed May 13, 2010).  
<http://gamma.cs.unc.edu/SSV/>.
- [190] N.N. RAPID - Robust and accurate polygon interference detection, 2010 (accessed May 13, 2010).  
<http://gamma.cs.unc.edu/OBB/>.
- [191] N.N. SWIFT++ - Speedy walking via improved feature testing for non-convex objects, 2010 (accessed May 13, 2010).  
<http://gamma.cs.unc.edu/SWIFT++/>.
- [192] N.N. V-COLLIDE, 2010 (accessed May 13, 2010).  
<http://gamma.cs.unc.edu/V-COLLIDE/>.
- [193] D. Odenthal, T. Bünte, H.D. Heitzer, and C. Eicker. How to make steer-by-wire feel like power steering. In *15th Triennial World Congress of the International Federation of Automatic Control*, Barcelona, Spain, 21-26 July 2002.
- [194] K. Ohishi, M. Miyazaki, and M. Fujita. Hybrid control of force and position without force sensor. In *Proceedings of the IEEE International Conference on Industrial Electronics, Control and Instrumentation*, pages 670–675, San Diego, CA, November 1992.
- [195] M.K. O’Malley, A. Gupta, M. Gen, and Y. Li. Shared control in haptic systems for performance enhancement and training. *Journal of Dynamic Systems, Measurement, and Control*, 128(1):75–86, March 2006.
- [196] M.A. Otaduy and M.C. Lin. A modular haptic rendering algorithm for stable and transparent 6-dof manipulation. *IEEE Transactions On Robotics*, 22(4):751–762, 2006.
- [197] S. Ozgoli and D. Taghirad. A survey on the control of flexible joint robots. *Asian Journal of Control*, 8(4):332–344, 2006.
- [198] G. Papafotiou, J. Kley, K. Papadopoulos, P. Bohren, and M. Morari. Model predictive direct torque control - Part II: Implementation and experimental evaluation. *IEEE Transactions on Industrial Electronics*, 56(6):1906–1915, 2009.
- [199] R.P. Paul. *Robot Manipulators*. MIT Press, 1981.
- [200] A. Peer. *Design and Control of Admittance-Type Telemanipulation Systems*. PhD thesis, TU München, 2008.

- [201] Physics Simulation Forum. Bullet physics library, 2010 (accessed May 13, 2010). <http://www.bulletphysics.com/>.
- [202] E. Plaku, K.E. Bekris, B.Y. Chen, A.M. Ladd, and L.E. Kavraki. Sampling-based roadmap of trees for parallel motion planning. *IEEE Transactions on Robotics*, 21(4):597–608, 2005.
- [203] E. Plaku, K.E. Bekris, and L. Kavraki. OOPS for motion planning: An online open-source programming system. In *Proceedings of the IEEE International Conference on Robotics and Automation (ICRA 2007)*, pages 3711–3716, Rome, Italy, 2007.
- [204] E. Plaku and L. Kavraki. OOPSMP: An object-oriented programming system for motion planning, 2010 (accessed June 19, 2010). <http://kavrakilab.org/OOPSMP/index.html>.
- [205] J. Podobnik and M. Munih. Haptic interaction stability with respect to grasp force. *Ieee Transactions On Systems, Man, And Cybernetics - Part C: Applications And Reviews*, 37(6):1214–1222, 2007.
- [206] M.J. Pratt. *Virtual Prototyping - Virtual environments and the product design process*, chapter Virtual prototypes and product models in mechanical engineering. Chapman & Hall, 1995.
- [207] H. Qian and J. DeSchutter. The role of damping and low pass filtering in the stability of discrete time implemented robot force control. In *Proceedings of the 1992 IEEE International Conference on Robotics and Automation*, pages 1368–1373, 1992.
- [208] A. Raabe, S. Hochgurtel, J. Anlauf, and G. Zachmann. Space-efficient fpga-accelerated collision detection for virtual prototyping. In *Proceedings of Design, Automation and Test in Europe (DATE '06)*, volume 2, 2006.
- [209] H.B. Rached. Regelungskonzepte für die Simulation einer aktuierten Fahrzeugtür mit einem Roboterarm. Bachelor Thesis, supervised by **M. Strolz**, Institute of Automatic Control Engineering, TU München, 2008.
- [210] M. Rahmani, W. Hintermaier, R. Mueller-Rathgeber, and E. Steinbach. Error detection capabilities of automotive network technologies and ethernet - a comparative study. In *IEEE Intelligent Vehicles Symposium*, pages 674–679, Istanbul, Turkey, June 2007.
- [211] J. Ren, R.V. Patel, and K.A. McIsaac. Dynamic 3-d virtual fixtures for minimally invasive beating heart procedures. *IEEE Transactions On Medical Imaging*, 27(8):1061, August 2008.
- [212] M. Ren. Weiterentwicklung und Evaluation eines Türsimulators. Master's thesis, supervised by **M. Strolz**, Institute of Automatic Control Engineering, TU München, 2009.

- 
- [213] L.B. Rosenberg. Virtual fixtures: Perceptual tools for telerobotic manipulation. In *1993 IEEE Virtual Reality Annual International Symposium*, pages 76–82, Sept. 1993.
- [214] L.B. Rosenberg. *Virtual Fixtures: Perceptual Overlays Enhance Operator Performance in Telepresence Tasks*. PhD thesis, Dept. Mech. Eng., Stanford University, 1994.
- [215] J.H. Ryu and H. Kim. Virtual environment for developing electronic power steering and steer-by-wire systems. In *Proceedings of the 1999 IEEE/RSJ International Conference on Intelligent Robots and Systems (IROS '99)*, volume 3, pages 1374–1379, 1999.
- [216] J.H. Ryu, D.S. Kwon, and B. Hannaford. Stability guaranteed control: time domain passivity approach. *IEEE Transactions on Control Systems Technology*, 12(6):860–868, 2004.
- [217] V. Santibanez and R. Kelly. Pd control with feedforward compensation for robot manipulators: analysis and experimentation. *Robotica*, 19:11–19, 2001.
- [218] K. Sasajima, K. Nagase, and T. Kuribayashi. Vehicle door operating apparatus. US005804937A, 1998.
- [219] C. Scharfenberger, S. Chakraborty, and G. Farber. Robust image processing for an omnidirectional camera-based smart car door. In *IEEE/ACM/IFIP 7th Workshop on Embedded Systems for Real-Time Multimedia (ESTIMedia 2009)*, pages 106–115, 2009.
- [220] C. Scharfenberger, C. Daniilidis, M. Fischer, D. Hellenbrand, P. Kuhl, C. Richter, O. Sabbah, **M. Strolz**, and G. Färber. Multidisziplinäre Entwicklung von neuen Türkonzepten als ein Teil einer ergonomisch optimierten Ein-/Ausstiegsunterstützung. In *OEM Forum Fahrzeugtüren und -klappen, VDI-Bericht 2064*, 2009.
- [221] D. Schramm, D. Franitza, and W. Lalo. Virtual prototyping and real-time simulation of heavy equipment manipulators including elastic deformations and hydraulics. In *22nd International Symposium on Automation and Robotics in Construction (ISARC 2005)*, Ferrara, Italy, September 11-14 2005.
- [222] P. Schüssler and G. Heim. Stepping out in style - the Opel Meriva door concept. *ATZ - autotechnology*, 10(3):12–17, 2010.
- [223] L. Sciavicco and B. Siciliano. *Modeling and Control of Robot Manipulators*. Springer, 2001.
- [224] T.B. Sheridan. *Telerobotics, Automation, and Human Supervisory Control*. M.I.T. Press, 1992.

- [225] P. Shi, Y. Zhang, and X. Yang. Lower extremity exoskeleton control and stability analysis based on virtual prototyping technique. In *2008 International Conference on Computer Science and Software Engineering*, volume 1, pages 1131–1134, 2008.
- [226] B. Siciliano and O. Khatib, editors. *Springer Handbook of Robotics*. Springer, 2008.
- [227] C. Smith and H.I. Christensen. A minimum jerk predictor for teleoperation with variable time delay. In *IEEE/RSJ International Conference on Intelligent Robots and Systems (IROS 2009)*, pages 5621–5627, 2009.
- [228] P. Smith, M. Shah, and N. da Vitoria Lobo. Determining driver visual attention with one camera. *IEEE Transactions on Intelligent Transportation Systems*, 4(4):205–218, 2003.
- [229] R. Smith. Open dynamics engine, 2010 (accessed May 13, 2010). <http://www.ode.org/>.
- [230] A. Solhjoo. Further development and implementation of the control of a car door with two actuated degrees-of-freedom. Master’s thesis, supervised by **M. Strolz**, Institute of Automatic Control Engineering, TU München, 2009.
- [231] M. Spong. Modeling and control of elastic joint robots. *IEEE Journal of Robotics and Automation*, 3(4):291–300, 1987.
- [232] M. Spong. Variable structure control of flexible joint manipulators. *IEEE Journal of Robotics and Automation*, 3:57–64, 1988.
- [233] M. W. Spong. Motion control of robot manipulators. In W.S. Levine, editor, *The Control Handbook*, pages 1339–1350. CRC Press, Boca Raton, 1996.
- [234] Stabilus. *DORSTOP G2 Stepless Door Positioning System. Customer Satisfaction + Press Releases 2005/2006*, May 2006.
- [235] T. Stadler. Untersuchung und Weiterentwicklung eines Systems zur Regelung von Fahrzeugtüren. Interdisciplinary Project, supervised by **M. Strolz**, Institute of Automatic Control Engineering, TU München, 2009.
- [236] J. Stark. *Product Lifecycle Management: 21st century Paradigm for Product Realisation*. Springer, 1 edition, 2004.
- [237] M. Steele and R.B. Gillespie. Shared control between human and machine: Using a haptic interface to aid in land vehicle guidance. In *Proceedings of the Human Factors and Ergonomics Society 45th Annual Meeting*, pages 1671–1675, 2001.
- [238] **M. Strolz**, C. Ehinger, and M. Buss. Design of a haptic device for the high-fidelity rendering of conventional car doors. In *Proceedings of the 2nd International Conference on Human System Interaction*, Catania, Italy, May 2009.

- 
- [239] **M. Strolz**, A. Mörtl, M. Gräf, and M. Buss. Control of an actuated car door providing outstanding haptic interaction. In *Proceedings of the First Joint EuroHaptics Conference and Symposium on Haptic Interfaces for Virtual Environment and Teleoperator Systems (WorldHaptics 2005)*, Salt Lake City, UT, USA, March 18-20 2009.
- [240] **M. Strolz**, A. Mörtl, M. Gräf, and M. Buss. Development, control, and evaluation of an actuated car door. *IEEE Transactions on Haptics*, 2(3):170–180, 2009.
- [241] **M. Strolz**, Q. Mühlbauer, C. Scharfenberger, G. Färber, and M. Buss. Towards a generic control system for actuated car doors with arbitrary degrees of freedom. In *Proceedings of IEEE Intelligent Vehicles Symposium (IV 2008)*, pages 391–397, Eindhoven, The Netherlands, June 2008.
- [242] **M. Strolz**, M.W. Ueberle, Q. Mühlbauer, and M. Buss. Tür, insbesondere Fahrzeugtür, mit wenigstens zwei kinematischen Freiheitsgraden und Verfahren zu ihrer Betätigung. DE102007062473A1, 2009.
- [243] **M. Strolz**, G. Vasilev, and M. Buss. Sensor system for the determination of the interaction force at a vehicle door. In *Sensoren und Messsysteme 2008, 14. Fachtagung Ludwigsburg, VDI-Berichte 2011*, pages 811–820. VDI-Verlag Düsseldorf, 2008.
- [244] **M. Strolz** and M. Buss. Haptic rendering of actuated mechanisms by active admittance control. In Manuel Ferre, editor, *Haptics: Perception, Devices and Scenarios*, volume 5024 of *LNCS*, pages 712–717. Springer, 2008.
- [245] **M. Strolz** and M. Buss. Tür, insbesondere Fahrzeugtür, und Verfahren zu ihrer Betätigung. DE102007062472A1, 2009.
- [246] I.E. Sutherland. The ultimate display. In *Proceedings of IFIP Congress*, volume 2, pages 506–508, 1965.
- [247] I.E. Sutherland. A head-mounted three-dimensional display. In *Proceedings of AFIPS*, volume 33, pages 757–764, 1968.
- [248] I.E. Sutherland. Computer displays. *Scientific American*, 222:57–81, 1970.
- [249] C. Swindells, K.E. MacLean, and K.S. Booth. Designing for feel: Contrasts between human and automated parametric capture of knob physics. *IEEE Transactions on Haptics*, page Accepted for publication, 2009.
- [250] H.Z. Tan, Shuo Yang, Z. Pizlo, P. Buttolo, and M. Johnston. Manual detection of spatial and temporal torque variation through a rotary switch. *IEEE Transactions on Haptics*, 1(2):96–107, 2008.
- [251] T.J. Tarn. Human/machine sharing control for intelligent mechatronic systems. In *Proceedings of the IEEE/ASME International Conference on Advanced Intelligent Mechatronics (AIM 1997)*, pages 57–, 1997.

- [252] The ViPERS Group. ViPERS - virtual prototyping, 2010 (accessed May 13, 2010). <http://www.kingston.ac.uk/ViPERS/virtualprototyping.htm>.
- [253] N. Tomohiko and S. Hiroyuki. Opening and closing device of door for vehicle. JP05112128A, 1993.
- [254] W. Townsend and J. Salisbury. The effect of coulomb friction and stiction on force control. In *Proceedings of the 1987 IEEE International Conference on Robotics and Automation*, pages 883–889, 1987.
- [255] B. Trefflich. *Videogestützte Überwachung der Fahreraufmerksamkeit und Adaption von Fahrerassistenzsystemen*. PhD thesis, Technischen Universität Ilmenau, 2009.
- [256] S. Trenkel, R. Weller, and G. Zachmann. A benchmarking suite for static collision detection algorithms. In Václav Skala, editor, *International Conference in Central Europe on Computer Graphics, Visualization and Computer Vision (WSCG)*, Plzen, Czech Republic, 29 January–1 February 2007. Union Agency.
- [257] M.W. Ueberle. *Design, Control, and Evaluation of a Family of Kinesthetic Haptic Interfaces*. PhD thesis, TU München, 2006.
- [258] M.W. Ueberle and M. Buss. Control of kinesthetic haptic interfaces. In *Proceedings of the IEEE/RSJ International Conference on Intelligent Robots and Systems (IROS 2004), Workshop on Touch and Haptics*, Sendai, Japan, 2004.
- [259] M.W. Ueberle, N. Mock, and M. Buss. ViSHaRD10, a novel hyper-redundant haptic interface. In *Proceedings of the 12th International Symposium on Haptic Interfaces for Virtual Environment and Teleoperator Systems*, pages 58–65, 27-28 March 2004.
- [260] G. van Bergen. SOLID - Software library for interference detection, 2010 (accessed May 13, 2010). <http://www.win.tue.nl/~gino/solid/index1.html>.
- [261] G. van den Bergen. *Collision Detection in Interactive 3D Environments*. The Morgan Kaufmann Series in Interactive 3D Technology. Morgan Kaufmann, 2003.
- [262] A. Varol, I. Gunev, and C. Basdogan. A virtual reality toolkit for path planning and manipulation at nano-scale. In *Proceedings of the 14th IEEE Symposium on Haptic Interfaces for Virtual Environments and Teleoperator Systems*, pages 485–489, Washington D.C., March 25-27 2006.
- [263] VDI-EKV. *Design methodology for mechatronic systems (VDI-Richtlinie 2206)*, 2004.
- [264] E. Wahlstrom, O. Masoud, and N. Papanikolopoulos. Vision-based methods for driver monitoring. In *Proceedings of Intelligent Transportation Systems*, volume 2, pages 903–908, 2003.

- 
- [265] J. Wang and G. Meng. Magnetorheological fluid devices: Principles, characteristics and applications in mechanical engineering. *Proceedings of the I MECH E / Part L Journal of Materials: Design and Applications*, 215(3):165–174, 2001.
- [266] Z. Wang, Z. Liu, J. Tan, Y. Fu, and C. Wan. A virtual environment simulator for mechanical system dynamics with online interactive control. *Advances in Engineering Software*, 37:631–642, 2006.
- [267] G. Welch and G. Bishop. An introduction to the kalman filter. Technical Report TR 95-041, University of North Carolina at Chapel Hill, July 2006.
- [268] R.M. White. A sensor classification scheme. *IEEE Transactions on Ultrasonics, Ferroelectrics and Frequency Control*, 34(2):124–126, 1987.
- [269] A. Wiehe, S. Kern, and J. Maas. Rotatory MRF-Actuator for an Automotive Door Assistent.pdf. *at - Automatisierungstechnik*, 56(3):155–164, 2008.
- [270] A. Witkin, M. Gleicher, and W. Welch. Interactive dynamics. In *Proceedings of the Symposium on Interactive 3D graphics*, pages 11–21, Snowbird, Utah, United States, 1990. ACM.
- [271] S. Wüst and E. Catrin. Kraftfahrzeug. DE102004027457A1, 2005.
- [272] Y. Yagi, S. Kawato, and S. Tsuji. Collision avoidance using omnidirectional image sensor (copis). In *Proceedings of the IEEE International Conference on Robotics and Automation (ICRA 1991)*, volume 1, pages 910–915, 1991.
- [273] S. Yang, H.Z. Tan, P. Buttolo, M.R. Johnston, and Z. Pizlo. Thresholds for dynamic changes in a rotary switch. In *Proceedings of EuroHaptics 2003*, pages 343–350, 2003.
- [274] X. Yang, T. Mei, M. Luo, and S. Chen. Virtual prototyping of tilting and lifting mechanism in iter tractor. In *International Conference on Information and Automation (ICIA 2008)*, pages 650–655, 2008.
- [275] C. Youngblut, R.E. Johnson, S.H. Nash, S.H. Wienclaw, and C.A. Will. IDA paper P-3186: Review of virtual environment interface technology. Technical report, Institute for Defense Analyses, March 1996.
- [276] W. Yu, R. Dubey, and N. Pernalet. Telemanipulation enhancement through user’s motion intention recognition and fixture assistance. In *Proceedings of the IEEE/RSJ International Conference on Intelligent Robots and Systems (IROS 2004), Workshop on Touch and Haptics*, pages 2235–2240, Sendai, Japan, 2004.
- [277] F. Yun, W. Zheng, T. Jianrong, and W. Changjiang. Positioning and driving virtual prototyping with metaphors in dynamic analysis. *Simulation Modelling Practice and Theory*, 14:527–540, 2006.
- [278] G. Zachmann. *Virtual Reality in Assembly Simulation - Collision Detection, Simulation Algorithms, and Interaction Techniques*. PhD thesis, Technische Universität Darmstadt, 2000.

- [279] G. Zachmann. Optimizing the collision detection pipeline. In *Proceedings of the First International Game Technology Conference (GTEC)*, January 2001.
- [280] N.G. Zamani and J.M. Weaver. *CATIA V5 Tutorials. Mechanism Design & Animation Release 18*. Schroff Development Corporation, 2009.
- [281] F. Zorriassatine, C. Wykes, R. Parkin, and N. Gindy. A survey of virtual prototyping techniques for mechanical product development. *Proceedings of the Institution of Mechanical Engineers, Part B: Journal of Engineering Manufacture*, 217(4):513–530, 2003.